NASA/CR—1998-207406

Combined Numerical/Analytical Perturbation Solutions of the Navier-Stokes Equations for Aerodynamic Ejector/Mixer Nozzle Flows

Lawrence Justin De Chant
Texas A&M University, College Station, Texas

Prepared under Grant NGT–51244

National Aeronautics and
Space Administration

Lewis Research Center

April 1998

Acknowledgments

First and foremost I would like to thank my committee co-chairs: Dr. Malcolm J. Andrews and Dr. Jerald A. Caton for their technical support, encouragement and advice. This research would not have been possible without them and I cannot thank them both enough. Special thanks to Dr. Caton for his patience and help in dealing with the administrative and contractual obligations associated with this project. I would like to thank and recognize the support received from the NASA Lewis Research Center, Propulsion System Analysis Office (formerly the Aero-propulsion Analysis Office) staff and management, who provided the principal funding for this work through a series of NASA Graduate Student Researchers Programs (NGSRP) scholarships and grant NAG3–1512. Special thanks to Dr. Francis J. Montegani of the NASA Lewis University Programs Office for his support and Dr. John K. Lytle for sponsoring the original grant NAG3–1512. A special debt of gratitude to Jonathan A. Seidel and Shari-Beth Nadell: Jon who has supported this work from its initial inception till now and Shari, who has (patiently) worked to integrate these tools into NASA and industry codes. Thanks guys, it's been a long time in coming. Thanks also to the NASA co-op students, Marc Tattar, John Harper and Darryl Whitlow whose summer research helped support my own. Thanks to Joe Holcomb, Dean Schrage and Paul Barnhart of NYMA Corp. for help through the technical phases of this research.

Available from

NASA Center for Aerospace Information
7121 Standard Drive
Hanover, MD 21076
Price Code: A10

National Technical Information Service
5287 Port Royal Road
Springfield, VA 22100
Price Code: A10

ABSTRACT

Combined Numerical/Analytical Perturbation Solutions of the Navier-Stokes Equations for Aerodynamic Ejector/Mixer Nozzle Flows.

Lawrence Justin De Chant
Texas A&M University, College Station, Texas 77843
Principle investigators: Dr. Malcolm J. Andrews
Dr. Jerald A. Caton

Submitted to the Office of University Programs of
the NASA Lewis Research Center
in partial fulfillment of the requirements of the

NASA Graduate Researchers Program and Grant NGT-51244

In spite of rapid advances in both scalar and parallel computational tools, the large number of variables involved in both design and inverse problems make the use of sophisticated fluid flow models impractical. With this restriction, it is concluded that an important family of methods for mathematical/computational development are reduced or approximate fluid flow models.

In this study a combined perturbation/numerical modeling methodology is developed which provides a rigorously derived family of solutions. The mathematical model is computationally more efficient than classical boundary layer but provides important two-dimensional information not available using quasi-1-d approaches. An additional strength of the current methodology is its ability to locally predict static pressure fields in a manner analogous to more sophisticated parabolized Navier Stokes (PNS) formulations. To resolve singular behavior, the model utilizes classical analytical solution techniques. Hence, analytical methods have been combined with efficient numerical methods to yield an efficient hybrid fluid flow model.

In particular, the main objective of this research has been to develop a system of analytical and numerical ejector/mixer nozzle models, which require minimal empirical input. A computer code, DREA Differential Reduced Ejector/mixer Analysis has been developed with the ability to run sufficiently fast so that it may be used either as a subroutine or called by an design optimization routine. Models are of direct use to the High Speed Civil Transport Program (a joint government/industry project seeking to develop an economically viable U.S. commercial supersonic transport vehicle) and are currently being adopted by both NASA and industry.

Experimental validation of these models is provided by comparison to results obtained from open literature and Limited Exclusive Right Distribution (LERD) sources, as well as dedicated experiments performed at Texas A&M. These experiments have been performed using a hydraulic/gas flow analog. Results of comparisons of DREA computations with experimental data, which include entrainment, thrust, and local profile information, are overall good. Computational time studies indicate that DREA provides considerably more information at a lower computational cost than contemporary ejector nozzle design models. Finally, physical limitations of the method, deviations from experimental data, potential improvements and alternative formulations are described.

This report represents closure to the NASA Graduate Researchers Program and Grant NGT-51244. Versions of the DREA code and a user's guide may be obtained from the NASA Lewis Research Center grant monitor:

Shari Nadell
Mail Location 77-2
NASA Lewis Research Center
21000 Brookpark Road
Cleveland, OH 44135

nadell@lerc.nasa.gov
(216) 977-7035

Additionally, a related, but more theoretically detailed discussion of this research is contained in the dissertation by the author entitled:

Combined Numerical/Analytical Perturbation Solutions of the Navier-Stokes Equations
for Aerodynamic Ejector/Mixer Nozzle Flows.

Texas A&M University, May 1997

which may be obtained:

UMI Dissertation Services
A Bell & Howell Company
300 N. Zeeb Road, Ann Arbor, Michigan 48106
1-800-521-0600

ACKNOWLEDGMENTS

First and foremost I would like to thank my committee co-chairs: Dr. Malcolm J. Andrews and Dr. Jerald A. Caton for their technical support, encouragement and advice. This research would not have been possible without them and I cannot thank them both enough. Special thanks to Dr. Caton for his patience and help in dealing with the administrative and contractual obligations associated with this project.

I would like to thank and recognize the support received from the NASA Lewis Research Center, Propulsion System Analysis Office (formerly the Aeropropulsion Analysis Office) staff and management, who provided the principal funding for this work through a series of NASA Graduate Student Researchers Programs (NGSRP) scholarships and grant NAG3-1512. Special thanks to Dr. Francis J. Montegani of the NASA Lewis University Programs Office for his support and Dr. John K. Lytle for sponsoring the original grant NAG3-1512.

A special debt of gratitude to Jonathan A. Seidel and Shari-Beth Nadell: Jon who has supported this work from its initial inception till now and Shari, who has (patiently) worked to integrate these tools into NASA and industry codes. Thanks guys, it's been a long time in coming. Thanks also to the NASA co-op students, Marc Tattar, John Harper and Darryl Whitlow whose summer research helped support my own. Thanks to Joe Holcomb, Dean Schrage and Paul Barnhart of NYMA Corp. for help through the technical phases of this research.

(This page intentionally left blank.)

TABLE OF CONTENTS

LIST OF FIGURES

LIST OF TABLES

(This page intentionally left blank.)

NOMENCLATURE

a	speed of sound
a*	dimensionless locally defined turbulence constant
A	cross-sectional area, lower band in block tridiagonal system
B	middle band in block tridiagonal system
c	constant
C	upper band in block tridiagonal system
C_p	constant pressure heat capacity
C_0	full momentum inversion parameter; $(\rho u^2+p)^2/(\rho u H \rho u)$
C_{0m}, $C_{0,mod}$	modified momentum inversion parameter; $(\rho u^2+\omega p)^2/(\rho u H \rho u)$
C_δ	spreading rate constant
CFG	Gross thrust coefficient, $[\rho u^2 A+(p-p_\infty)]/(m_1 V_{ideal,1})$
d	constant, right hand side vector in block tridiagonal system
D	diffusion constant
erf(x)	error function
f	functional value
F	first derivative
Fr	Froude Number; $V/(gh)^{1/2G}$
g	gravitational constant
G	momentum flux; ρu^2+p
G_{mod}	modified momentum flux, $\rho u^2+\omega p$
h	channel height, enthalpy, water depth
h_0	lobe to lobe, y direction distance
h_s	splitter plate height
i	streamwise direction differencing knot subscript, imaginary unit, $i^2=-1$
j	cross-stream direction differencing knot subscript
k	locally defined turbulence constant; wave number, $2\pi/\lambda$; thermal conductivity, $2/(u_{near}+u_{far})$
H	total enthalpy
l	full mixing layer thickness
L	streamwise length scale
M	Mach number
M_c	Convective Mach Number; $(U_1-U_2)/2a$
m	mass flow rate
MAR	Mixer Area Ratio; $A_3/(A_1+A_2)$
N	saturation time constant, maximum number of terms
O	order of magnitude
p	static pressure
P	total pressure
Pr	Prandtl number, $\mu C_p/k$
Q	volumetric flow rate
r	radial coordinate, recovery factor
R	ideal gas constant
Re	Reynolds number
Re_{vort}	vortical Reynolds number, $\Gamma/U\lambda$
s	temporal amplification factor, similarity parameter, t-kx
S	second derivative
SAR	Suppresser Area Ratio; $A_3/A_{primary,throat}$
t	time
tanh(x)	hyperbolic tangent function
T	temperature

u	streamwise velocity
U	free stream or velocity
v	cross-stream velocity
V	total velocity
x	streamwise coordinate
x_c	first minimum, near field far field match point
y	cross-stream coordinate
z	bi-normal stream coordinate
z_0	lobe width at y=0.

Greek

α_0	defined proportionality constants, $\lambda=\alpha_0\delta$
Δ	change, grid spacing
ε	small perturbation term; velocity perturbation parameter, $U_{10}-U_{20})/(U_{10}+U_{20})$
ε_G	momentum flux perturbation parameter, $(G_{10}-G_{20})/(G_{10}+G_{20})$
β	$(M^2-1)^{1/2}$; $\Delta tD/\Delta^2 y$.
β_0	local constant
δ	half mixing layer thickness function
∇	gradient operator
γ	ratio of specific heats
Γ	vortical mixer lobe circulation
κ	wall turbulence (von Karman constant) 0.4
λ	wavelength, vortical wavelength
ω	Vigneron (1978) parameter; $\gamma M^2/[1+(\gamma-1)M^2]$
ϕ	conservative flux, perturbation velocity potential, function value
Φ	velocity potential
ν	kinematic viscosity
μ	dynamic viscosity, Mach angle
ρ	density
τ	"e" folding time, shear stress
φ	amplitude
σ	tension parameter, empirical turbulence constant (free jet)
η	turbulent similarity parameter
ξ	interface height, dimensionless interface amplitude, $(\beta_{1s})^2[1-U_1/U_{1s}]$, similarity variable

Subscripts

1,2	primary and secondary streams, perturbation level
10, 20	primary and secondary stream initial condition
3	exit stream
0	stagnation or reservoir condition, perturbation level
acoustic	acoustic quantity
an	analytical
ave	average condition
b.l.	boundary layer method approximated value
c, crit	critical, convective
eff	effective state
e, exit	nozzle exit conditions

friction	frictional quantity
far	far field quantity
inc	incompressible
ideal	ideal, typically isentropic expansion
G	momentum flux quantity
mix	mixing layer quantity
near	near field quantity
num	numerical
s	streamline condition
throat	nozzle throat conditions
turb	turbulent quantity
vort	vortical quantity
wall	wall value
∞	ambient, free stream conditions
θ	polar quantity

Superscripts

'	(prime) small perturbation, ordinary derivative, unsteady turbulent fluctuation
-	(bar) mean value, local definition, vector
*	dimensionless or scaled quantity
n	iteration counter

(This page intentionally left blank.)

1. INTRODUCTION

1.1 Objectives and summary

In spite of the rapid advances in both scalar and parallel computational tools, the large number and breadth of variables involved in both design and inverse problems make the use of sophisticated and even relatively simple (parabolized or boundary layer) fluid flow models impractical. With this restriction, it may be concluded that an important family of methods for mathematical/computational development are reduced or approximate models. In this study a combined perturbation/numerical modeling methodology is developed which will provide a rigorously derived hierarchy of solutions. These solutions are characterized by varying levels of complexity versus analytical fidelity. Additionally, the solutions to these models utilize analytical solutions to resolve singular behavior as required. Hence, classical methods are to be combined with efficient numerical methods to yield an efficient and original class of fluid flow models.

In particular, the main objective of this research is to develop a system of analytical and numerical ejector/mixer nozzle models, which require minimal empirical input. A code, DREA Differential Reduced Ejector/mixer Analysis has been written with the ability to run sufficiently fast such that it may be used either as a subroutine or called by an design optimization routine. Models are of direct use to the High Speed Civil Transport Program and are in the process of being adopted by both NASA and industry. Experimental validation of these models is provided by comparison to results obtained from the literature, industry proprietary data, as well as, a dedicated experiment performed at Texas A&M. These experiments have been performed using a hydraulic/gas flow analog model and provide information about the inviscid mixing interface structure.

Since this reduced/approximate approach is applicable to a wide range of fluid flow problems, an additional family of test problems described in a preliminary manner, come from geophysical fluid dynamics. These problems directly influenced the linearization and solution methods applied to the main aerodynamic problem.

1.2 Motivation

1.2.1 Ejector nozzles

As indicated in the summary, the basic physical problem of interest in this project is the mixing and operation of ejector-mixer nozzles. Although the physics of ejector nozzles is described in greater detail subsequently, it is useful to define the type of devices that are of interest. An ejector is a relatively simple, passive mixing/pumping device which serves to entrain (or pump) fluid from a secondary stream, mix it with a primary, high energy stream; thus obtaining a mixed (and potentially uniform) exit stream of greater mass flow. This process is shown schematically in Figure 1.1.

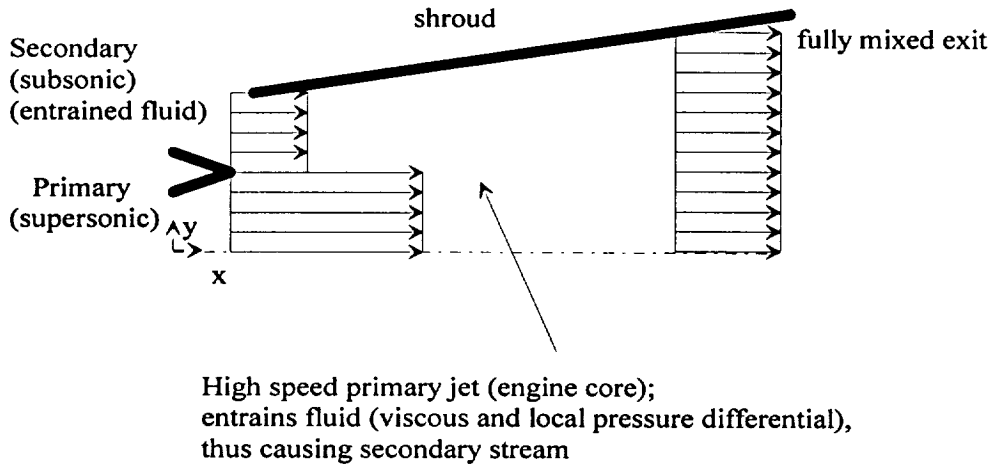

FIGURE 1.1 Schematic of ejector nozzle operation.

The concept underlying the use ejector/mixer nozzles for aerodynamic applications is driven by two conflicting design requirements. One is to reduce takeoff noise to an acceptable level, while the other is to maintain a predetermined gross thrust. The conflicting requirements of this problem are revealed by examining the relationship for acoustic power (a measure of noise) (Lighthill (1952) (1961), (1963) and Curle (1961)).

$$P_{acoustic} \propto V^N \tag{1.1}$$

where N is an exponent varying between 3-8 and V is an ideal exhaust velocity. The smaller value of N corresponds to a fully supersonic jet, while the larger value is that of a fully subsonic jet. Though acoustic measurements are notoriously complex, industry and NASA designs tend to based upon the larger values of N. An alternative to this relationship which indicates this design relationship compares exhaust velocity versus sideline noise is presented in Figure 1.2.

Also presented in Figure 1.2, is the maximum sideline noise threshold labeled FAR36 Stage 3, which is a regulation for the maximum "airport" noise to be accepted. Clearly, noise is strongly dependent on jet exit velocity.

Thrust on the other hand may be estimated by the ideal thrust momentum relationship:

$$F = \dot{m} V \tag{1.2}$$

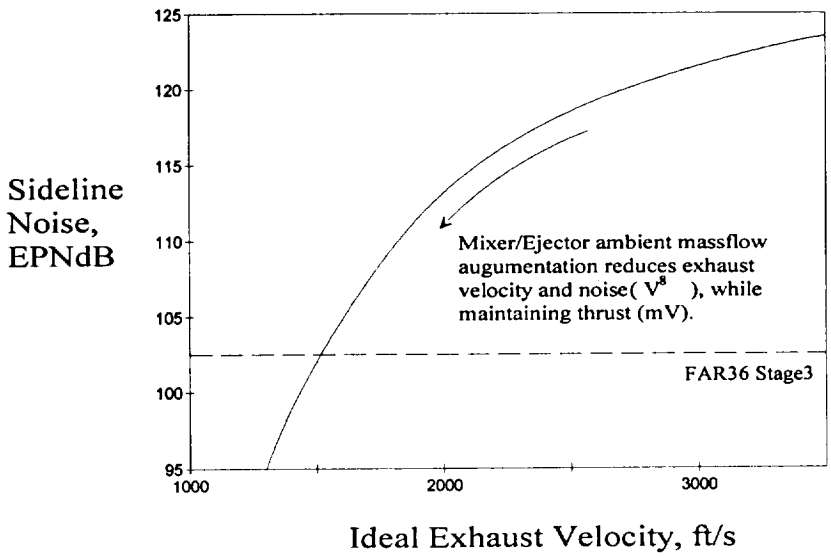

FIGURE 1.2 Side line noise versus ideal exhaust velocity and design threshold for supersonic transport concept.

Now, if thrust is to be maximized and we must reduce exit jet velocity to a minimum, the only term available to control is the mass flow rate of the propulsion system. Hence the objective here is to efficiently maximize the flow rate. Ejector nozzles, since they are an elegant passive device, have the potential for providing this mass flow augmentation in a very efficient manner. The desired modification of the flow field by use of an ejector/mixer nozzle is shown graphically in Figure 1.3.

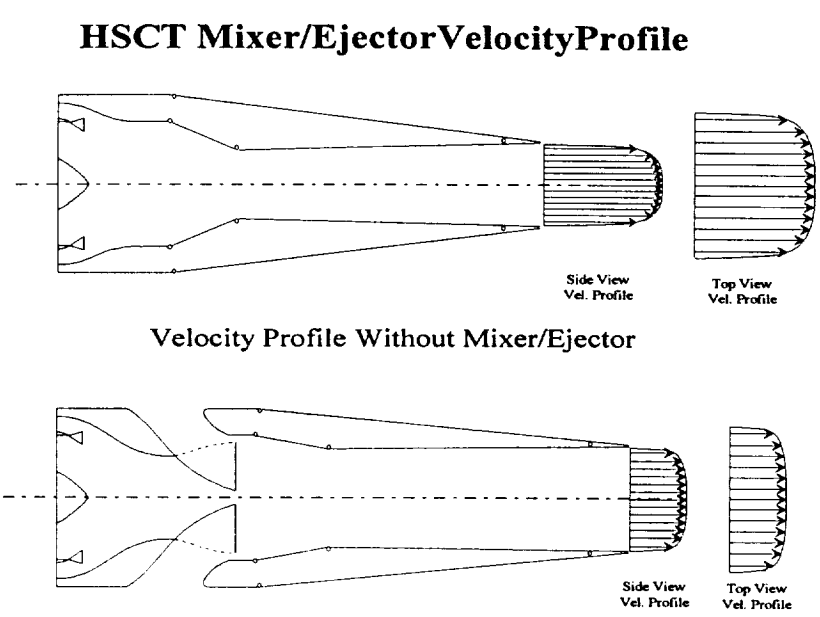

FIGURE 1.3 General comparison of exit velocity field untreated by ejector versus treated by ejector.

1.2.2 Installation and basic flight hardware

From the above application, it is apparent, that the ejector nozzle is to be inserted in the engine/cycle flow path to entrain additional mass. As such the ejector is installed in the flow path after the engine core as shown in Figure 1.4.

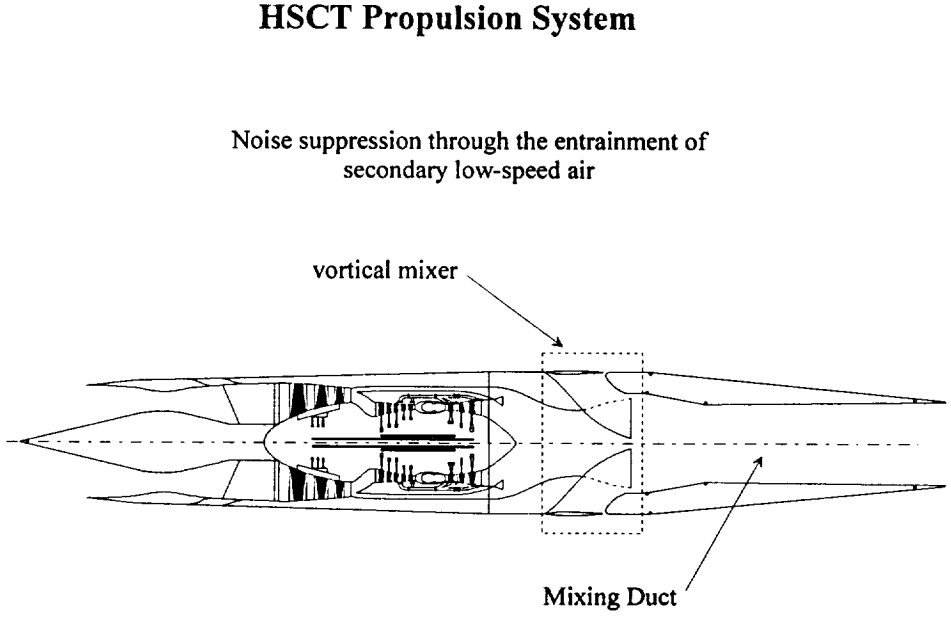

FIGURE 1.4 Engine cycle and ejector mixer concept installation.

The close analogy between an engine concept fitted with an ejector and a high bypass turbofan is to be noted (Morrison (1996)). In fact, one might consider a turbofan to be a forced pumping, poorly mixed, i.e. unshrouded ejector. Also, the terminology "ejector/mixer" nozzle refers to two concepts:

1. Ejector implies entrainment of fluid from ambient conditions. In our work the ejector nozzle refers to the overall system. This includes a set of inlets and chutes (shown in cross Section in Figure 1.5) and a "mixing duct"
2. The mixer refers to the convoluted splitter plate system. Of course, the goal of the complex lobing is to enhance the mixing and entrainment of the flow

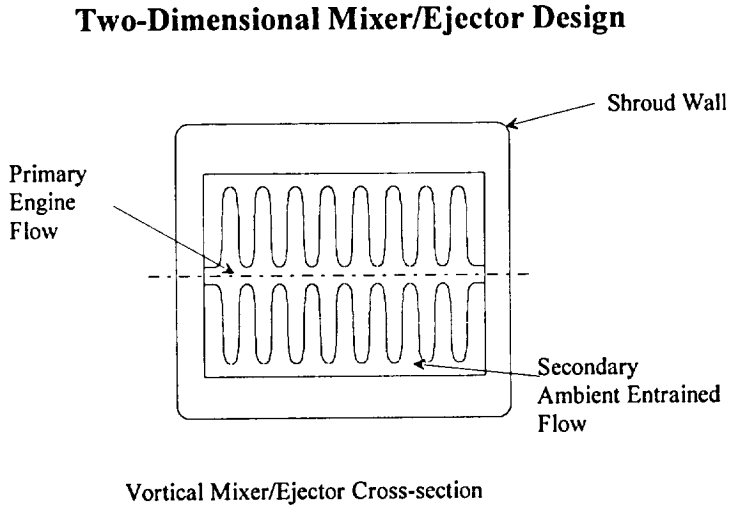

FIGURE 1.5 Cross section of mixer/ejector nozzle system showing convoluted splitter plate of mixer.

1.3 Literature Review

Ejector/mixer nozzles have been used for industrial (mixing, jet pump) and aerodynamic (noise suppression, thrust augmentation) applications for many years. An example of this is an atomizer, a simple entrainment device used to produce a fine aerosol or mist. As such a significant body of theoretical, computational and experimental literature exists for these devices. Consider the bibliography of over 1600 papers related to ejector research compiled by Porter and Squyers (1978) before 1978. A portion of this basic literature is described to show that intermediate level models (more powerful than control volume analyses, and less costly than computational simulations) are needed. Then, current models and research that have been developed to fill this gap are compared.

The simplest modeling approach to ejector/mixer nozzle formulation involves using simple 1-d, or lumped parameter control volume formulations. An incomplete list of workers who have developed this type of analysis include: Presz et al. (1986) and (1990) as well as Braden et al. (1982), Alperin and Wu (1983a) and (1983b), Addy et al. (1981), Quinn (1973), Dutton and Carroll (1988) and (1988), Keenan et al. (1950), and Ginoux (1972). Alternative viewpoints, for example the lifting surface analogy of Bevilaqua (1978), have also been developed. Distinguished from the basic mixing analysis, which predicts ideally mixed, 1-d exit conditions are the supersonic ejector models (downstream flow does not influence inlet conditions), discussed initially by Fabri and Siestrunck (1958), which predict secondary inlet conditions for this problem. Most other

workers in this flow regime have followed this approach, e.g. Addy et al. (1981) and Dutton and Carroll (1986). Many of these workers have provided experimental measurements for basic 1-d quantities such as entrainment, thrust etc. Abe et al. (1992), Chandrasekhara et. al. (1991), Fernando and Menon (1993), Goebel and Dutton (1991), and Yang et al. (1985) provide experimental results useful for simple (planar shear layer) mixing flow and ejector studies. An alternative formulation, De Chant (1993), provides estimates of design information (geometry and operating conditions) using a similar integral approach.

Unfortunately, none of the control volume based approaches can make any meaningful prediction about the streamwise length required to achieve a desired level of mixing. This length or equivalently rate of mixing is necessary for any aerospace application where length required for mixing translates directly to weight, a critical flight design constraint. To obtain this information, more complete mathematical models are needed. Early models employed boundary layer or 2-d, inviscid (method of characteristics) formulations to provide this type of information. These models require that the primary stream be supersonic. Examples of inviscid methods (corrected integral with boundary layer losses) include Chow and Addy (1964) and Chow and Yeh (1965). Boundary layer formulations include the studies by Gilbert and Hill (1973) and Hedges and Hill (1974a) and (1974b). These method-of-characteristics and boundary layer models provide considerably more information than their integral, 1-d counterparts, though again, at much greater computational cost. The work developed here provides a model of intermediate complexity, more powerful than the control volume formulations, yet simpler (and in several ways more general) than the either the inviscid computations or the boundary layer methods.

The previous paragraph emphasized the need to minimize the mixing length of ejector/mixer nozzle for aerodynamic applications. One of the methods currently being used to improve the mixing performance of ejector mixer nozzles involves replacing the straight splitter plate by a convoluted or "chuted" mixer plate. This has the effect of inducing streamwise vorticity in the flow and accelerating the mixing rate. Here also, a large number of experimental and computational studies have been performed. Since the flow is rather complex, full Navier-Stokes simulations have been typically used to simulate these flows. Again a partial list of experimental and full simulations include: Presz et al. (1986), (1987a), (1987b), Skebe et al. (1988a), Lord et al. (1990), Tillman et al. (1992), Povinelli et al. (1980), Malecki and Lord (1990), Debonis (1992), Barber and Anderson (1991), Barber et al. (1988), Keith et al. (1993), Abdol-Hamid et al. (1993), Booher et al. (1993), Qui (1992), Elliott et al. (1992), Tew (1992) and O'Sullivan (1993). Strictly experimental results include: Paterson (1984), Werle and Paterson (1987), Skebe et al. (1988b), Koutomos and McGuirk (1989), Manning (1991) and McCormick (1992). Although the simulations and, by their very nature, experiments are potentially excellent representations of full scale ejector mixers, the results are far too expensive in terms of cost, manpower and expertise to interact directly with design or inverse design computations.

Alternatives to the previous research methods, include this study, a code developed at MIT, Fung (1995), as well a code developed by Boeing and Clark (1995) are compared in Table 1.1. As can be seen from Table 1.1, the DREA code provides a significant improvement over the other current models, all of which have been developed to fill the need for a fast, yet sufficiently powerful computational model.

Criterion	DREA (Texas A&M)	Fung (MIT)	Clark (CFA)
Vortical Mixing	yes; analytically based turbulence model	yes, piecewise model and scaling functions	no, multiple lobe only
governing equations	simplified 2-d, conservative	scaling law	1-d
primitive variable profiles	yes	no	two stream model
empiricism	limited	moderate ("scaling" constants)	limited (unknown)
compressible	expressly developed for compressible flow	1-d and extensions	1-d and extensions
internal shock /choke structure	yes; Fabri-choke and back pressure limited	no, pumping only	current version no
computational speed (suitable for preliminary design/optimization)	fast (user may choose control volume and/or mixing)	fast	fast
experimental validation	yes, literature, proprietary data and experiments	yes, literature and experiments	yes, experiments
publications	journal articles, conference papers, dissertation and reports	thesis, conference papers	conference papers (main code proprietary)
status availability	preliminary summer 1996, fully tested and documented 05-97	complete	complete

TABLE 1.1 Comparison of ejector-mixer models suitable for preliminary design/optimization.

Analytical solution methods, numerical differencing and solution algorithms, and formal perturbation methods will be used thorough out this project. No attempt is made to give a formal historical literature development of these methods since they are truly subjects unto themselves. However, the fundamental and relevant references are provided as we develop our specific problem.

1.4 Mathematical framework

This section describes the overall mathematical framework for the ejector problem. The requirements for the analysis are presented first. Then the basic perturbation hierarchy, which is used to develop the systems of governing equations, is described.

1.4.1 Overall analysis

The model developed here describes an analysis code, i.e. one for which geometry and operating conditions have been specified. Performance characteristics (thrust, noise, degree of mixing, and pumping) are predicted in a very efficient manner by this code. Ultimately, this type of tool may be used to generate off line performance information in the form of "ejector" maps, which are tabular list of performance characteristics. It is also sufficiently computationally efficient to be run in a "real time" fashion. Table 1.2 presents the requirements of this analysis follow:

Computational efficiency	Hierarchy of complexity	Minimum of empiricism	Experimentally validated	Documentation
Reduced equation formulation	Formal perturbation	First principle methods	Literature and dedicated experiment	journal, dissertation, reports

TABLE 1.2 Requirements for computational simulation tool.

The efficiency of this method also permits the realistic use of this analysis code as the "base solver" for an iterative, inverse design analysis. In this problem, geometric and operating conditions are parametrically adjusted to meet a series of overall design constraints. This inverse design methodology can be quite efficient, especially if a reasonable first iteration estimate is available. A simplified method that may be used to estimate operating and geometric parameters has been developed by De Chant (1993). Hence, there is an overall family of codes that provide a useful preliminary design capability for the design and implementation of ejector nozzles.

1.4.2 Formal perturbation hierarchy

As implied in the previous section, one of the main strengths of the overall modeling methodology is development of a formal perturbation hierarchy. This type of expansion method permits us to "apriori" estimate the error associated with a particular approximation, as well as, formulate corrections to the approximation. Of course, approximate methods in fluid mechanic have been well developed over the years. For example considering steady, viscous problems only, consider the hierarchy Anderson et al. (1984) and Anderson (1989):

Perturbation Method/Approximation	Comments:
Integral/Control volume (.i.e. 1-d or quasi-1-d)	Satisfy integral forms of conservation equations. Cannot predict local values.
Current DREA model O(1) equation system	Parabolic in terms of conservative flux quantities. primitive quantities: u, v, p, ρ, M, locally predicted. PNS subsonic pressure approximation
Boundary layer	Parabolic in terms of u, v for all flows; p(x), thin layer, p(x) must be specified by an auxiliary relationship
Viscous-shock layer	Parabolic for supersonic flow; u, v, p(x) specified by auxiliary relationship, p(x,y) specified by inviscid y-momentum; PNS (Vigneron et al (1978)) subsonic pressure approximation.
Parabolized Navier-Stokes	Parabolic (in space) for supersonic flow, elliptic subsonic regions; u, v, p(x), p(x,y) Viscous y-momentum. PNS subsonic pressure approximation
Full Navier-Stokes Analysis	Parabolic-hyperbolic, fully viscous equations. Always solved using unsteady or iterative method.

TABLE 1.3 Comparison of classical and current approximation methods in fluid dynamics.

Each level has certain strengths and weaknesses associated with it. Complexity and cost increase at an extraordinary rate as we work our way from down Table 1.3.

The work described in this section is to develop a system of partial differential equations describing viscous mixing. Expansions that are less complex than the boundary layer family but provide more information (local mixing field) than the integral methods are of special interest in this study. Like a quasi-1-d model, though, it is desirable to retain (at least approximately) the local prediction of static pressure, rather than the external imposition of a pressure field, predicted either using free stream information or through a global mass conservation constraint, as would be done for a classical boundary layer analysis. As is shown in Section 2, this local pressure prediction requirement adds considerably to the complexity of the model.

The fundamental governing equations for this project (lowest order system) are developed in this section and higher order expressions are deferred to Appendix A.

To this end, the development begins by considering compressible, two-dimensional Reynolds equations Anderson et al. (1984) or White (1991). Note that the turbulent Prandtl number has been assumed to be close to unity, hence dissipation terms in the energy equation, may be neglected. Due to the high Reynolds number asymptotic nature of these equations, the molecular viscosity and the molecular Reynolds numbers are ignored (See Schlichting (1979) or Tennekes and Lumley (1972)). The resulting equations are:

x-momentum:

$$\frac{\partial}{\partial x}(\rho u^2) + \frac{\partial}{\partial y}(\rho uv) + \frac{\partial p}{\partial x} = -\frac{\partial}{\partial y}(\rho u'v') - \frac{\partial}{\partial x}(\rho u'u') \tag{1.3}$$

y-momentum:

$$\frac{\partial}{\partial x}(\rho uv) + \frac{\partial}{\partial y}(\rho v^2) + \frac{\partial p}{\partial y} = -\frac{\partial}{\partial x}(\rho u'v') - \frac{\partial}{\partial y}(\rho v'v') \tag{1.4}$$

energy:

$$\frac{\partial}{\partial x}(\rho uH) + \frac{\partial}{\partial y}(\rho vH) = -\frac{\partial}{\partial y}(\rho v'H') - \frac{\partial}{\partial x}(\rho u'H') \tag{1.5}$$

and continuity:

$$\frac{\partial}{\partial x}(\rho u) + \frac{\partial}{\partial y}(\rho v) = 0 \tag{1.6}$$

To proceed with the analysis, it is recognized that when non-dimensionalized, there are a number of "small terms" inherent to the governing equations. They come from both the magnitude of the dependent and independent variables. The flux difference between streams is relatively small, as is the mixing layer thickness compared to the streamwise distance. Formally stated this yields:

$$\varepsilon = \frac{(U_{10} - U_{20})}{(U_{10} + U_{20})} \approx \varepsilon_G = \frac{(G_{10} - G_{20})}{(G_{10} + G_{20})} \approx \frac{\delta_{mix}}{L} \tag{1.7}$$

where δ_{mix} refers to the mixing layer thickness and $G=\rho u^2+p$. It should be noted that $\varepsilon \approx \varepsilon_G$ may not be small for all cases. Indeed $\varepsilon \approx \varepsilon_G = 1$ in the free jet limit. In spite of this, the governing equations will be shown to provide reasonable results despite the fact they may be "formally tenuous" approximations. Support for effectiveness of the free jet limiting case may be found in Schlichting (1979).

Though it has not explicitly stated at this point, this expansion parameter ε which is valid for turbulent flow will have a form analogous to that of Ting (1959), who studied laminar mixing between two streams. Of course the essential stretching transformation, as well as, the Poincare' expansion methods are fundamental to virtually all perturbation (especially singular perturbation) approximations. Nayfeh (1973), Kevorkian and Cole (1981), Van Dyke (1975) and Cole and Cook (1986) provide developments for a wide range of classical problems where regular and singular perturbation methods have been applied.

It may be noted, that the finite or bounded form of internal ejector flow makes the classical definition and then "patching" of inner and outer solutions problematic for the problem developed here. As such, stretching transformations are used to develop a solution valid through out the ejector flow field.

Since it is necessary to derive differential equations that can "see" or resolve the mixing layer itself, it will be necessary to rescale (stretch) the cross-stream or "y" coordinate:

$$x \approx O(1) \quad y \equiv \varepsilon^{\frac{1}{2}} y^* \quad \frac{\partial}{\partial y} \equiv \frac{1}{\varepsilon^{\frac{1}{2}}} \frac{\partial}{\partial y^*} \tag{1.8}$$

This is, of course, the classical boundary layer scaling as introduced by Van Dyke (1975). The selection to rescale the cross-stream variable to permit resolution of the mixing layer is the connection between the partial differential equation based models and the simple control volume based models. Literally if it is assumed that for the integral analysis that the cross-stream scale is O(1) all "viscous" terms on the right hand side are lost, governing equations revert to the control volume formulations.

Proceeding with the scaled problem, we further estimate the magnitude of the Reynolds stress terms. This starts, by considering the Boussinesque approximation (introduction of an effective turbulent viscosity (Tennekes and Lumley (1972), Hinze (1959) or Rodi (1993)) for the streamwise momentum flux: $(\rho u^2)'v'$ (Schlichting (1979) and Tennekes and Lumley (1972)):

$$G'v' = (\rho uu)'v' \approx -\nu^*_{eff\,G} \frac{\varepsilon_G}{\varepsilon^{\frac{1}{2}}} \frac{\partial}{\partial y^*} (\rho u^{2^*}) \tag{1.9}$$

This quantity is chosen since the streamwise momentum flux is a conservative value, rather than simply velocity, which is a primitive variable. This choice of variables helps to overcome one of the main objections raised to using mixing length based algebraic turbulence models, which do not even conserve momentum (Tennekes and Lumley (1972)). To apply this to our problem, the momentum flux transport must be must related to the transport of velocity fluctuations by turbulence, i.e. $\rho u'v'$ by introducing the definition:

$$\rho u'v' \equiv \frac{(\rho uu)'v'}{u} = -\frac{\nu^{*}_{eff\,G}}{u}\frac{\varepsilon_G}{\varepsilon^{\frac{1}{2}}}\frac{\partial}{\partial y^{*}}(\rho u^{2^{*}}) \tag{1.10}$$

This is considered to be an acceptable approximation, since the effective viscosity closure is a definition already. To apply this equation, we must linearize terms like:

$$\frac{1}{u} = \frac{1}{U\left[u_0^{*} + u_1^{*}\varepsilon^{\frac{1}{2}} + \ldots\right]} \tag{1.11}$$

where $U=1/2(U_{10}+U_{20})$ Since, u_0^{*} is our O(1) approximation, it will be acceptable, to O(1), to write:

$$\frac{1}{u} = \frac{1}{U}\left[1 - u_1^{*}\varepsilon^{\frac{1}{2}} + \ldots\right] \tag{1.12}$$

Hence our O(1) approximation for the Reynolds stress must be:

$$\rho u'v' \approx -\left(\frac{\nu_{eff}}{U}\right)^{*}_{G}\frac{\varepsilon_G}{\varepsilon^{\frac{1}{2}}}\frac{\partial}{\partial y^{*}}(\rho u^{2^{*}}) + \ldots \tag{1.13}$$

The physical basis for this scaling and the turbulence model values, such as, ν_{eff}/U, are discussed in Section 2.5.

Using equation (1.13) and invoking the additional well founded approximation that the turbulent Reynolds number Pr_t=O(1), the Reynolds transport of total enthalpy is written:

$$\rho H'v' \approx -\frac{1}{\mathrm{Pr}_t}\left(\frac{\nu_{eff}}{U}\right)^{*}_{G}\frac{\varepsilon_G}{\varepsilon^{\frac{1}{2}}}\frac{\partial}{\partial y^{*}}(\rho u H^{*}) \tag{1.14}$$

At this point the perturbation expansions for the various variables are introduced. The streamwise variables are simply expanded:

$$\rho f^{*} = \rho f_0^{*} + \rho f_1^{*}\varepsilon^{\frac{1}{2}} + \rho f_2^{*}\varepsilon + \ldots \qquad f^{*} \equiv u^{*},\ H^{*}$$

$$g = g_0^{*} + g_1^{*}\varepsilon^{\frac{1}{2}} + g_2^{*}\varepsilon + \ldots \qquad g^{*} \equiv p^{*},\ u^{*},\ H^{*} \tag{1.15}$$

The expansion of the cross-steam flux and velocity take more care. It is expected, that for our basically parallel flow that the cross stream velocity, v, is very small O(ε). The cross stream mass flux, ρv, is also small, but to conserve mass is an order of magnitude larger $O(\varepsilon^{1/2})$. With these estimates, the cross-stream mass flux and velocity are written:

$$\rho v^* = \rho v_0^* \varepsilon^{\frac{1}{2}} + \rho v_1^* \varepsilon + \ldots$$

$$v^* = v^*{}_0 \varepsilon + v_1^* \varepsilon^{\frac{3}{2}} + v_2^* \varepsilon^2 + \ldots \tag{1.16}$$

Using these expansions and estimates available, it is possible to scale the dependent variables, substitute the expansions and collect terms. Performing these operations, the two lowest order systems are obtained. The lowest order, O(1), system (which is of most particular interest) is a simple set of parabolic "mixing" equations. Most of the analysis in the dissertation will focus on the analysis of these equations. The second system will be recognized to be a linear formulation of the classical boundary layer equations. See Appendix A. Hence as desired, this expansion has yielded a set of governing equations of lessor complexity than even the classical boundary equations:

x-momentum:

$$\frac{\partial}{\partial x}(\rho u_0^* u_0^* + p_0^*) = \frac{\partial}{\partial y^*}\left[\left(\frac{\nu_{eff}}{U}\right)^* \frac{\varepsilon_G}{\varepsilon} \frac{\partial}{\partial y^*}(\rho u_0^* u_0^*)\right] \tag{1.17}$$

y-momentum:

$$\frac{\partial p_0^*}{\partial y^*} = 0 \tag{1.18}$$

energy:

$$\frac{\partial}{\partial x}(\rho u_0^* H_0^*) = \frac{\partial}{\partial y^*}\left[\frac{1}{Pr_t}\left(\frac{\nu_{eff}}{U}\right)^* \frac{\varepsilon_G}{\varepsilon} \frac{\partial}{\partial y^*}(\rho u_0^* H_0^*)\right] \tag{1.19}$$

and mass conservation:

$$\frac{\partial}{\partial x}(\rho u_0^*) + \frac{\partial}{\partial y^*}(\rho v_0^*) = 0 \tag{1.20}$$

This is the O(1) system, that is solved. As it is written, it is not possible proceed, since the last term in equation (1.20) is not closed. To solve this system it is necessary to approximate the cross-steam mass flux term:

$$\rho v_0^{\bullet} \varepsilon^{\frac{1}{2}} \approx -\frac{1}{Sc_t}\left(\frac{\nu_{eff}}{U}\right)_G^{\bullet} \frac{\varepsilon_G}{\varepsilon^{\frac{1}{2}}} \frac{\partial}{\partial y^{\bullet}}(\rho u_0^{\bullet}) \tag{1.21}$$

Which is merely a linearization of our Reynolds stress closure.

One more convenient change may be made. Since the cross-stream pressure gradient $\partial p/\partial y \approx O(\varepsilon)^{1/2}$, we can add this term to the right hand side of the streamwise momentum equation thus yielding:

$$\frac{\partial}{\partial x}(\rho u_0^{\bullet} u_0^{\bullet} + p_0^{\bullet}) = \frac{\partial}{\partial y^{\bullet}}\left[\left(\frac{\nu_{eff}}{U}\right)_G^{\bullet} \frac{\varepsilon_G}{\varepsilon} \frac{\partial}{\partial y^{\bullet}}(\rho u_0^{\bullet} u_0^{\bullet} + p^{\bullet}{}_0)\right] \tag{1.22}$$

Finally, a state equation is included, which for our uses is an ideal (and thermally perfect) gas law. Combining this with the definition of total enthalpy and retaining first order terms yields:

$$p_0 = \frac{\gamma - 1}{\gamma}\left[\rho H_0 - \frac{1}{2}\rho u_0 u_0\right] \tag{1.23}$$

Though, the solution is actually formed in terms of alternative variables it is desirable to perform an equation count shown in Table 1.4.

Equations	Unknowns
momentum, equation (1.17 or 1.22)	u_0
energy; equation (1.19)	H_0 or T_0
mass; equation (1.20)	p_0
mixing relationship closure; equation (1.21)	v_0
state; equation (1.23)	ρ_0
Total=5	Total=5

TABLE 1.4 Equation versus unknown count for O(1) equation system.

It is worth noting, that this solution set, equations (1.17)-(1.22), is not merely linearized boundary layer, since the static pressure p_0 participates directly in the solution procedure. In a classical internal boundary layer solution, on the other hand, the pressure is strictly a function of x, i.e. p=p(x). This permits the estimation of p(x) by demanding that global mass conservation be observed, i.e. total mass= $\int \rho u dy$. Our method, alternatively, is more closely related to local, 1-d and quasi-1-d compressible modeling relationships. The benefit to us, is the maintenance of a strong thermodynamic coupling between variables and the ability to predict p(x,y) on a local basis. That on a local basis p(x,y) may show strong variations both streamwise and across the mixing layer, seems to contradict the y-momentum equation. To satisfy this equation it is formally required to model equations for matching inlet pressure. In reality, though, we will often need to model problems with large static pressure imbalances. Apparently, due to the local pressure computations, our equations still provide a useful model even in these situations. Classical boundary layer could never achieve this, since p=p(x) only. Other quantities, such as, Mach number and total pressure are supplemented by their own specific definitions.

It has been stated that equations (1.17)-(1.22) are not a straight forward linearization of the boundary layer equations. The basis for this statement comes from the fact, that linearizations were developed using an alternative transformation (the use of the conservative fluxes, ρu^2+p, ρuH and ρu) rather than primitive variables. Other examples of the use of a transformation and subsequent linearization for incompressible and compressible boundary layer flows is the classical von Mises Transformation (Schlicting (1979), Von Karman and Tsein, (1938) Schetz and Jannone (1965)). We remark that Schetz and Jannone (1965) compare primitive variable linearization versus von Mises transformation and linearization and conclude the latter method is superior for a wide range of flows. This studiy helped to motivate our use of the conservative flux transformation and linearization employed in this study.

Before closing the perturbation development is worth describing the system of equations consistent with treating the cross-stream or "y" variable as O(1). As indicated earlier, they take the form:

$$\frac{\partial}{\partial x}(\rho u_0^{\bullet} u_0^{\bullet} + p_0^{\bullet}) = 0$$

$$\frac{\partial}{\partial x}(\rho_0 u_0^{\bullet} H_0^{\bullet}) = 0 \tag{1.24}$$

$$\frac{\partial}{\partial x}(\rho u_0^{\bullet}) = 0$$

which is precisely what is to be expected. Integration of these relationships provides no information as to the streamwise length scale. These are literally control volume formulations. Though control volume formulations provide no streamwise mixing length scale, we will use control volume and integral methods to estimate initial conditions for the mixing portion of the code. These analyses are described in detail in section. This completes the formal perturbation development of the systems of equations used in this project

1.5 Basic physical problem

This section describes the basic physical arrangement of the ejector/mixer problem. Though ejectors have already been described briefly, it is the goal of this section to concentrate upon the physics and variety of flow characteristics. An ejector is a relatively simple, passive mixing/pumping device that serves to entrain (or pump) fluid from a secondary stream, mix it with a primary, high energy stream; thus obtaining a mixed (and potentially uniform) exit stream of greater mass flow. The additional mass entrainment is cause by two major effects: (1) inviscid pressure imbalance, which literally sucks fluid into the stream from the secondary inlet and (2) an effective viscous component, which drags fluid in from the secondary inlet.

It is necessary to be somewhat careful in the use of these two end member decompositions, in that through the momentum equation, pressure and effective viscous terms are coupled. Therefore, in reality, no simple decomposition is appropriate. This coupling of mixing and pressure will become apparent as the pumping computation methodology is developed in detail. Additionally, we need to define "effective viscous" components of the entrainment as terms which are caused by turbulent mixing effects. These effects are typically estimated using the concept of a turbulent viscosity, but are really strong, non-linear fluctuation type terms, i.e. u'v' terms and have no relationship to molecular viscosity. Though molecular viscosity is certainly present in any physical flow, the Reynolds number is assumed to be large enough such that molecular viscosity effects are wholly negligible, since they are multiplied by terms like $1/Re_{mol.,visc.}$

An interesting limiting case of the pumping computation is the free 2-d jet. This would be the case for an ejector where the area ratio $A_2/A_1 \rightarrow \infty$. In this limit, the pressure balancing control volume concept that would be applied is not suitable. There the entrainment is truly due to local effective viscous (turbulent) interaction. Following Schlichting (1979) the local self similar velocity relationship for a two-dimensional turbulent jet is quoted:

$$u = \frac{\sqrt{3}}{2}\left(\frac{k\sigma}{x}\right)^{\frac{1}{2}}\left(1 - \tanh^2 \eta\right) \quad \eta \equiv \sigma\frac{y}{x} \tag{1.25}$$

where k is the net momentum flux, $\int u^2 dy$ and σ is an empirical turbulence constant, i.e. $1/\sigma \propto \nu_{eff}$. Now, to compute the mass flow rate entrained we integrate over the flow field, to obtain:

$$Q = \frac{\sqrt{3}}{2}\left(\frac{kx}{\sigma}\right)^{\frac{1}{2}} \int_0^{\infty} \left(1 - \tanh^2 \eta\right) d\eta = \frac{\sqrt{3}}{2}\left(\frac{kx}{\sigma}\right)^{\frac{1}{2}} \tag{1.26}$$

From this equation, it is apparent that entrainment increases as we proceed from the origin. To our dissatisfaction, it is noted that this flow rate integral has entirely neglected the contribution of the primary stream! This failure is due to the fact, that for our case with its infinite secondary area, the flow rate from the primary is negligible. This emphasizes the limitation of the free jet approximation for use in finite ejectors. Ejectors are finite devices. Integral quantities may not be estimated using infinite space methods. Hence the proper use control volume methods is to predict entrainment and thrust. As a side note, though, it may be noted that locally non-integral quantities such as velocity etc. can be acceptably modeled using infinite method if we are far from confining walls.

Depending upon the operation of the ejector net thrust may also increase. As indicated previously, it is the ability to maintain (or even improve) thrust, while reducing the exit velocity which is fundamental to the application for high speed civil transport aircraft.

Since ejectors involve the mixing of two streams of fluid which (for compressible gas flows) may be either supersonic or subsonic, several possible flow types or flow regimes may exist. These flow regimes are strongly characterized by the extent of supersonic or subsonic flow. This is directly related to the physics of subsonic versus supersonic flow.

Supersonic flow is properly modeled using a parabolic-hyperbolic equation set. The need for a hyperbolic system stems from the fact, that due to the supersonic nature of the flow, information or disturbances, are convected downstream more rapidly than can be transmitted upstream by molecular interaction (i.e. speed of sound). Hence, there is no chance of sending any information upstream. As one would expect form the mathematical classification, (parabolic-hyperbolic) flows of this type are dependent solely on their initial conditions. In contrast, the convective speed of a subsonic flow field is less that the molecular signal propagation velocity, i.e. speed of sound. As such, downstream signals can eventually propagate back upstream. Here, the flow field and even the initial conditions depend upon the downstream conditions. The modeling equations for this case are parabolic-elliptic.

Ultimately simplified equations that have a single character, i.e. parabolic are developed. We will, however, supplement this parabolic system, by initial conditions which (depending on the flow regime) will respect the potential for downstream dependence or downstream independence. It is apparent, that all of the problems of interest will virtually always contain some region of subsonic flow; forcing us to respect some form of a downstream constraint.

The first flow that is considered is a supersonic inlet, which has a sufficiently large back pressure (i.e. ambient pressure) to cause the supersonic primary stream to go through a family of oblique shocks, ultimately terminating in a strong normal shock. This is illustrated in Figure 1.6. In Section 2 an approximate criterion for the critical exit pressure needed to cause this shock is developed. With this "shock down" the exit flow is fully subsonic. As such, the local pressure must match the external giving a constraint that is used to estimate the secondary entrainment. This is also developed in detail in Section 2.

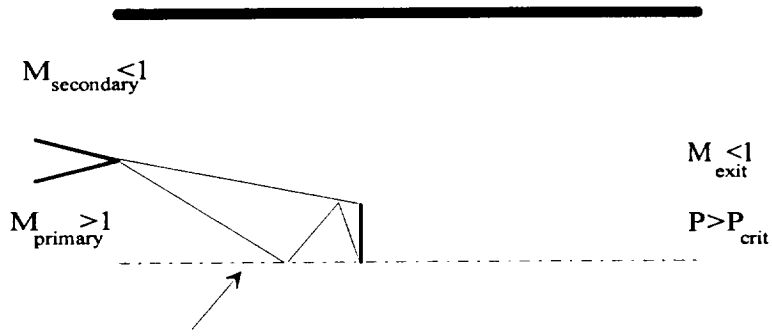

FIGURE 1.6 Ejector nozzle in subsonic (back pressure dependent mode) with shock down of primary stream.

This shock down criterion is dependent upon complete mixing between the two streams. The complete mixing assumption is reasonable for a long ejector, but unrealistic for many short shroud ejectors. Often, due to insufficient mixing, two distinct streams exit the ejector: one supersonic and one subsonic. See Figure 1.7. For this type of flow, though, the secondary entrainment is dominated by the exit pressure because it is subsonic. When this occurs, the entrainment should be predicted, as before, on the basis of the exit pressure.

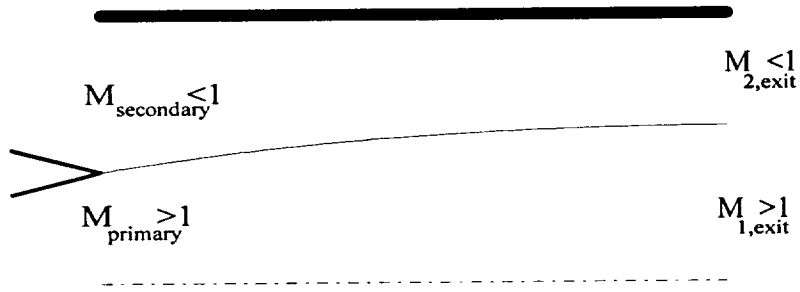

FIGURE 1.7 Ejector nozzle in back pressure dependent mode due to poorly mixed secondary stream.

Finally, for sufficiently low back pressure, the flow is fully supersonic at the exit plane. This situation may occur if the primary stream accelerates (expands) while the secondary stream (also expands) but chokes. As shown in Figure 1.8 this expansion/choking phenomenon causes the streamlines separating the two flows to form an aerodynamic or Fabri (Fabri and Seistrunk (1958)) choke. Clearly then the exit stream is supersonic, and as such, is independent of the back pressure. The local effect of the subsonic stream does, though, influence the secondary entrainment. The information, though, that is sent into the secondary inlet is no longer a pressure constraint, but the fact that the flow has choked. An entrainment model based upon this scenario is developed in Section 2.

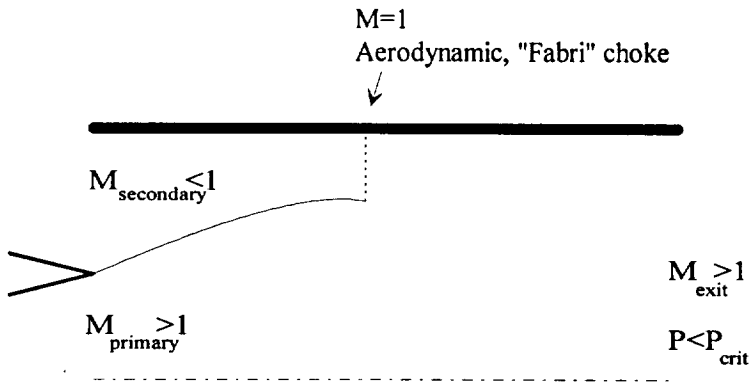

FIGURE 1.8 Ejector nozzle in back pressure independent mode, exhibiting aerodynamic or Fabri choke.

Finally a special case of the aerodynamic choking phenomenon occurs when the choke forms within the secondary inlet itself. This situation is called saturated supersonic flow and is represented by Figure 1.9.

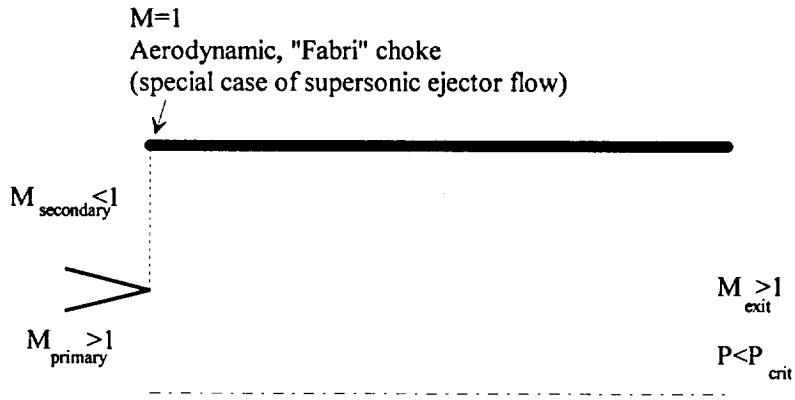

FIGURE 1.9 Ejector nozzle in back pressure independent mode. Aerochoke in secondary inlet causing classical "supersonic saturated" operation.

As one would expect, this flow is completely specified by upstream conditions, with no chance of any downstream influence.

Due to the possibility of mixed or transonic flow fields, ejector nozzles have a rich physical and mathematical character. In Section 2 analytical and numerical models to deal with this varied character are developed. In Section 5 long-term solutions to problems, which may be directly traced to the multiple regime flow, fields that we have just discussed are developed.

2. THEORETICAL DEVELOPMENT

2.1 Overall solution methodology

The modeling algorithm developed in this study is conveniently divided into several modules or components. These modules are combined to approximate the flow structure of the ejector. Although the ejector is an integrated device (secondary stream inlet static conditions are flow dependent for any degree of subsonic flow, i.e. elliptic flow, in the secondary inlet stream) it is far more efficient to model this dependency in a decoupled fashion. This decomposition is acceptable, since the secondary stream conditions are in a large sense governed by inviscid phenomena. Hence, the secondary stream pumping may be estimated using ideal relationships, (though we have introduced modifications to account for mixing losses and the effects of incomplete mixing on the initial conditions). These methods are described in Section 2.2. The actual turbulent mixing region is model using a single pass, parabolic marching method, which provides flow field/mixing information and a more complete estimate of two and three dimensional effects within the mixing section of the ejector and are developed in Section 2.4. Consider the "flow chart" description of these modules and this iterative solution. Additionally, the possibility of an inverse design iterative loop is shown, though this level of iteration is not within the scope of the current project.

*Part of the data reported in this section is reprinted with permission from Interface Wavelength between supersonic jets and subsonic flowfields. by De Chant, L. J. Seidel, J. A. and Andrews, M. J. 1996. *AIAA Journal.* 34, 1946-1948.

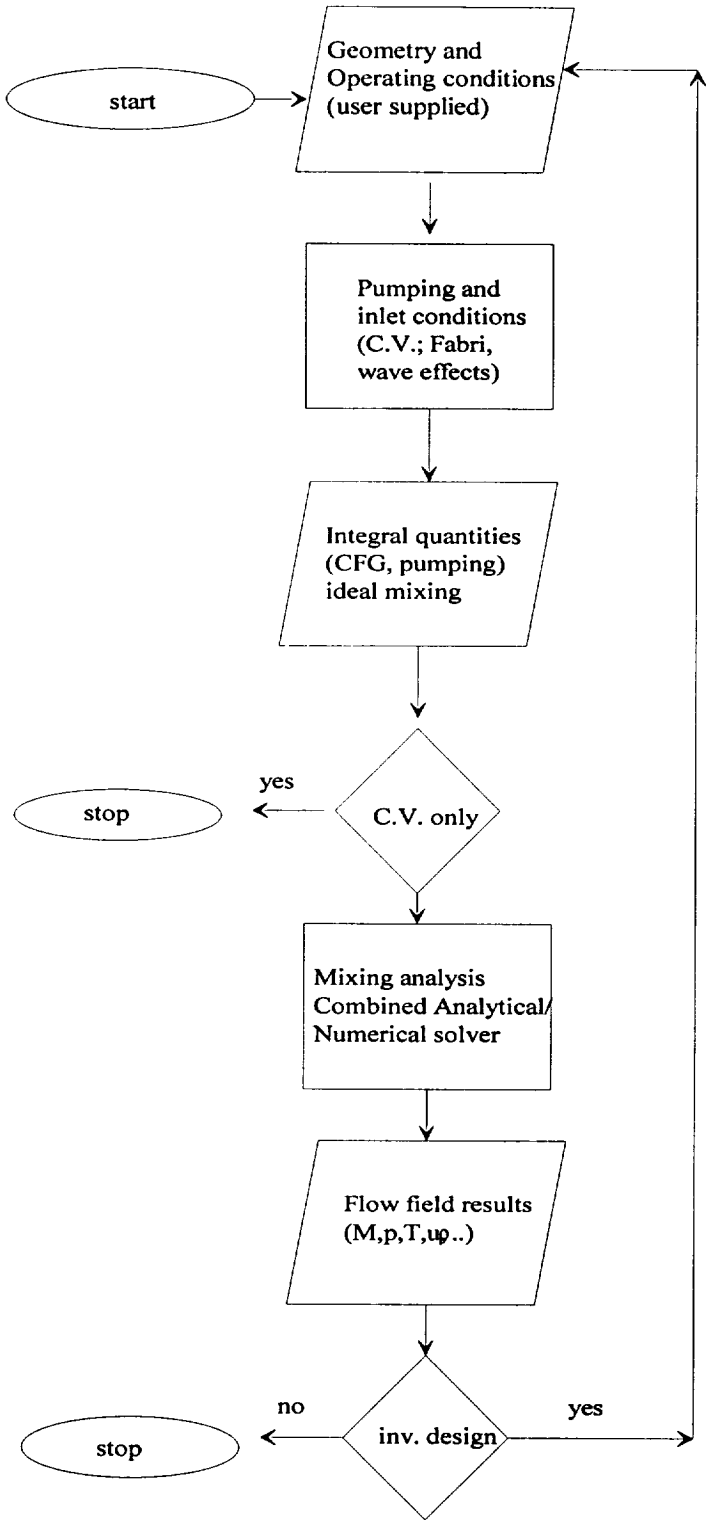

FIGURE 2.1 Flow chart of overall computational method.

As indicated by the flow chart, Figure 2.1, estimates of inlet conditions are principally, for the secondary stream flow. Further, since the parabolic marching technique which models the mixing portion of the flow is steady (single pass marching), but typically must model transonic flow fields, the extent of regions of supersonic or subsonic flow must be estimated. This task is performed using modifications of classical, inviscid slipline analyses, and is described in the Section 2.3. Then the mathematics and numerics of the rest of the flow chart are developed, which is principally the mixing algorithm portion and the associated turbulence model, in the remainder of Section 2 and Section 3.

2.2 1-d Control volume analyses

In this section a classical, 1-d, compressible, control volume based, mixer/ejector analysis is implemented. The basic mixing analysis consists of 1-d, conservation equations with upstream conditions fully specified and "mixed" or downstream conditions to be computed. Although simple, this model provides useful insight into the mixing process. However, the ejector mode of operation, in which the secondary stream static conditions are specified by downstream conditions, is not as clearly defined. Two possible modeling techniques for the ejector mode of operation are discussed and compared: Fabri choke analysis, (Fabri and Siestrunck (1958) or Addy et al. (1981)) which are back pressure independent flows and the use of a subsonic downstream pressure condition for back pressure dependent flow (Addy et al. (1981)). As implied by their descriptions, the choice of the proper modeling technique is determined by the back pressure conditions.

2.2.1 Introduction to control volume methodologies

One-dimensional or control volume mixing analyses (Alperin and Wu, (1983), Addy et al. (1981), Dutton and Carroll, (1986) and (1988)) provide simple, but relatively accurate predictions of mixer/ejector operation. However, the basic integral formulations do not permit prediction of non-ideal behavior, nor do they provide any information concerning the rate of streamwise mixing or streamwise length scales. This, of course, provides the impetus for the mixing flow modeling portion of this code. Although the integral relationships are contained implicitly in the differential method, it is convenient to have access to these solutions. In fact, the control volume solutions may be seen as a "zeroth" order solution or boundary conditions for the higher order models and, more importantly, provide a method to predict the initial conditions for the partial differential equations based mixing model.

This section seeks to describe the basics of 1-d mixing analyses. The ejector mode of operation, and its associated closure methods, are then discussed. The analyses associated with these closure methods, or boundary conditions, are derived. Finally, the analysis is verified by comparisons to available experimental data.

2.2.2 Mixer/ejector formulation

Since ejector flow modeling may be considered an extension of simple mixing, we begin by considering 1-d control volume conservation equations. See Figure 2.2. A number of assumptions are implicit in these relationships:

(1) The entrance and exit flow fields are locally one-dimensional. When describing the exit location, this is a "fully mixed" assumption. Although, this is the most restrictive assumption of this analysis, it is shown that this model still provides good comparison to experimental data. This assumption is relaxed in Section 2.2.6.
(2) Thermally perfect gases are assumed throughout, as well as, ideal gas behavior.

With the application of these restrictions, the conservation equations may be written:

$$\dot{m}_1 + \dot{m}_2 = \dot{m}_3 \equiv w \tag{2.1}$$

$$\dot{m}_1 u_1 + p_1 A_1 + \dot{m}_2 u_2 + p_2 A_2 + \int_{A_1+A_2}^{A_3} p dA = \dot{m}_3 u_3 + p_3 A_3 \equiv p_{mom} \tag{2.2}$$

and

$$\dot{m}_1 T_{01} + \dot{m}_2 T_{02} = \dot{m}_3 T_{03} \equiv E \tag{2.3}$$

where the subscripts, "1", "2" and "3" refer to the primary, secondary and exit locations, respectively.

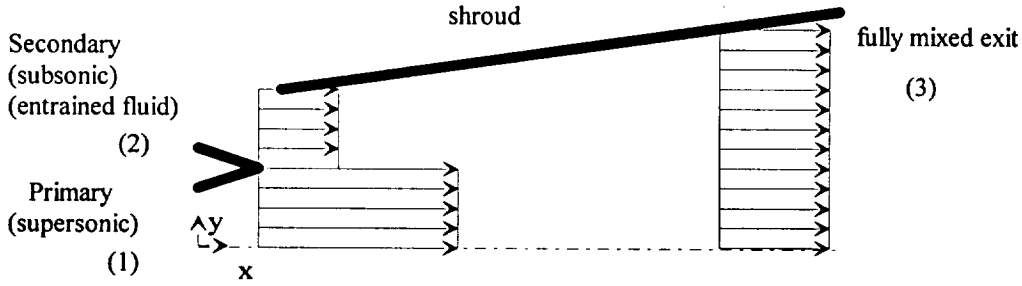

FIGURE 2.2 Control volume analysis and control surface definitions.

The integral term in the momentum equation (2.2), is closed in an approximate manner by the relationship:

$$\int_{A_1+A+2}^{A_3} p dA \approx \frac{1}{2}[p_3 + (p_1 A_1 + p_2 A_2)/(A_1 + A_2)][A_1 + A_2 - A_3] \tag{2.4}$$

The implications and restrictions of this approximate closure are discussed in, De Chant (1993).

For simple mixing, all upstream quantities are specified. Thus with addition of state, and constant heat capacity thermodynamic definitions the above equations may be solved for the downstream unknowns. In particular, the above relationships in terms of the mixed Mach number, for M_3:

$$[(1 - G/2)\gamma^2 + \gamma\frac{G}{2}] M_3^4 + [\gamma(\frac{A_1 + A_2}{A_3} + 1) - G\gamma] M_3^2 + \frac{1}{4}(\frac{A_1 + A_2}{A_3} + 1)^2 = 0 \tag{2.5}$$

where

$$G \equiv \frac{p_{mom}^{\ 2}}{REw} \tag{2.6}$$

Equation (2.5), has two roots, in terms of M_3^2. One root corresponds to a supersonic solution, while the other root denotes subsonic flow that would result if the supersonic flow passed through a normal shock. We note that with specification of the exit Mach number, M_3, all other static and stagnation quantities are available to us by back substitution.

The solution in equation (2.5), also provides the essential formulation for ejector flows, in which all conditions for the primary stream are specified, while only the total conditions, P_{02} and T_{02}, are specified for the secondary stream. To apply the simple mixing analysis all the conditions in the secondary stream must be specified. This is accomplished by invoking a downstream constraint that implicitly defines the secondary stream static quantities. A discussion concerning the physical and mathematical modeling of this constraint is provided here.

The modeling of ejector flows may be made more concrete by counting equations and unknowns as presented in Table 2.1.

Unknowns	equations
secondary Mach number, M_2	momentum conservation
exit Mach number, M_3	energy conservation
exit velocity, u_3	mass conservation
exit pressure, p_3	exit constraint
exit density, ρ_3	Mach number definition
exit temperature, T_3	state
total=6	total=6

TABLE 2.1 Control volume analysis equation versus unknown counts.

The specification of the downstream condition or constraint requires discussion of the physics of ejector flow. Three possible cases or flow regimes may be identified. These cases are (i) "mixed" flow or subsonic flow, (ii) supersonic flow and, (iii) a subset of supersonic flow denoted supersonic saturated flow. These regimes are considered in detail:

(i) "mixed" or subsonic flow. In this case, the secondary stream is fully subsonic. The appropriate downstream boundary condition or constraint is:

$$p_3 = p_{exit} \equiv p_\infty$$

This is a classical condition for 1-d, subsonic nozzle flow. The actual computations are performed by guessing the secondary Mach number, computing the downstream pressure, and correcting M_2 until the downstream pressure satisfies the above constraint.

(ii) supersonic flow. As the name implies, at the fully mixed flow, exit location, the flow is supersonic. Thus, the secondary stream must accelerate from subsonic flow to supersonic flow. The transonic point in this flow is often termed an "aerodynamic throat". Closure is obtained by noting

that the flow upstream of the aerodynamic choke is dominated by inviscid phenomenon. This provides the basis for the Fabri choke formulation, which is discussed in detail later. We note that this constraint leads to under-expanded or over-expanded nozzle operation.

(iii) saturated supersonic flow. This regime denotes a choked secondary stream, with the choke occurring in the "mouth" of the secondary stream, at location (2). For this flow, specification of the secondary Mach number by a downstream constraint is trivial, since (M_2=1).

The above discussion shows that supersonic flow in an ejector requires further consideration. Before proceeding, it is worthwhile to note that qualitatively, subsonic (mixed) flow regimes may be expected for high static back pressure and supersonic or even saturated supersonic flow for lower back pressures. In practical ejector operation, flight from sea level to high altitude with ejector deployed is possible, as such, it is necessary to be able to model both back pressure dependent and back pressure independent flow regimes.

2.2.3 Back pressure dominated flow

As indicated previously back pressure dependent flow is characterized by a fully subsonic secondary stream. This is in accord with our understanding of steady supersonic/subsonic flow, since only for a subsonic flow is it possible for a downstream signal (back pressure level) to be sent upstream to modify the secondary inlet flow static conditions. Within the assumptions of classical one-dimensional control volume modeling, it is clear that the ejector closure for this problem is the downstream boundary condition: $p_3=p_{exit}=p_{amb.}$

2.2.4 Back pressure independent flow (Fabri-choke)

Two possible supersonic flow regimes have been discussed supersonic flow and supersonic saturated flow. Since supersonic saturated flow is a relatively simple mixing process, it is not discussed further. Instead, the closure for supersonic flow, the Fabri or aerodynamic choke analysis is presented.

Consider Figure 2.3 illustrating the development and location of an aerodynamic choke.

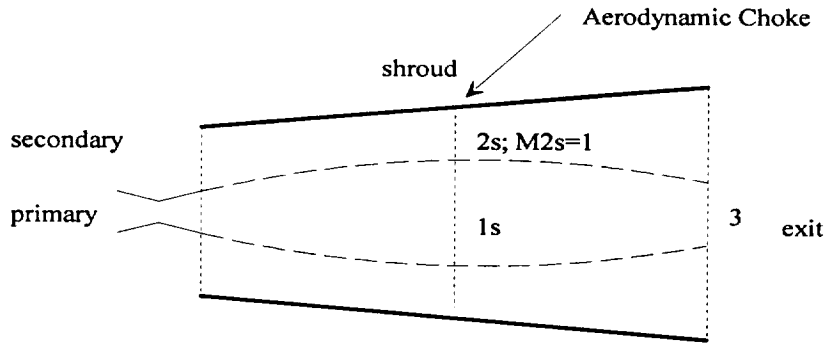

FIGURE 2.3 Aerodynamic/Fabri choke analysis definitions.

Aerodynamic or Fabri choking analysis has been discussed by several workers, Fabri, (1958) and Addy et al. (1981). The analysis involves invoking a new control surface located at the secondary stream aerodynamic choking point. See Figure 2.3. Additional assumptions include: the streams remain separate, so there is no mixing and the flow is isentropic for each stream. Neither assumption is exactly true, but assuming the choke occurs relatively close to the primary and secondary inlets and that the flow is primarily inviscid, this is an

appropriate analysis. These assumptions may be poor for a forced ejector where mixing enhancement is desired. To overcome some of these limitations, we have developed a loss mechanism (in terms of total pressure and total temperature) to account for the interaction between the two streams. This loss model closure is also presented in Section 2.2.6.

Considering the modeling in detail and with reference to Figure 2.3, four (4) unknown quantities may be identified:

$$A_{2s},\ A_{1s},\ M_2,\ M_{1s}$$

The related equations are:

$$\frac{A_2}{A_{2s}} = \frac{1}{M_2}\left[\frac{2}{\gamma+1}\left(1+\frac{\gamma-1}{2}M_2^2\right)\right]^{\frac{\gamma+1}{2(\gamma-1)}} \tag{2.7}$$

$$\frac{A_1}{A_{1s}} = \frac{M_{1s}}{M_1}\left[\frac{1+\frac{\gamma-1}{2}M_1^2}{1+\frac{\gamma-1}{2}M_{1s}^2}\right]^{\frac{\gamma+1}{2(\gamma-1)}} \tag{2.8}$$

the so called Mach number area relationships (isentropic mass conservation), (Anderson (1985)). The equation set is completed with a constant area ejector cross-sectional area definition:

$$A_{2s} + A_{1s} = A_3 = const. \tag{2.9}$$

and the isentropic momentum equation.

$$p_1 A_1[1+\gamma M_1^2] + p_2 A_2[1+\gamma M_2^2] = p_{2s} A_{2s}[1+\gamma M_{2s}^2] + p_{1s} A_{1s}[1+\gamma M_{1s}^2] \tag{2.10}$$

The static pressure may be related to the total pressure using:

$$p = p_0\left[1+\frac{\gamma-1}{2}M^2\right]^{\frac{\gamma}{1-\gamma}} \tag{2.11}$$

These (4) equations may be solved to provide a direct value for the secondary stream inlet Mach number M_2. Thus, with the secondary static quantity, M_2, specified the flow now acts like other mixing flows, where all quantities upstream are specified and the downstream (mixed) values are computed.

Equation (2.9) has implied that the ejector is locally constant area, with this area based upon the inlet values. This statement is equivalent to restricting the location of the aerodynamic choke close to the inlet plane. This is a reasonable first approximation for two reasons:

(1) The cross-sectional area for typical designs is approximately constant, i.e. Mixer Area Ratio, MAR≅1.
(2) The Fabri analysis as developed here is locally isentropic. This would not be true for a long mixing section. Ultimately methods for estimating the aerodynamic choke location in the next section, as well as the losses incurred reaching that point are discussed.

Clearly, to effectively validate this type of analysis comparison to experimental data is necessary. To start, we begin with both constant area and variable area, supersonic ejector experiments from Addy et al. (1981). These are fully supersonic cases and are modeled using the Fabri choke method. Results are presented in Figure 2.4 and Figure 2.5.

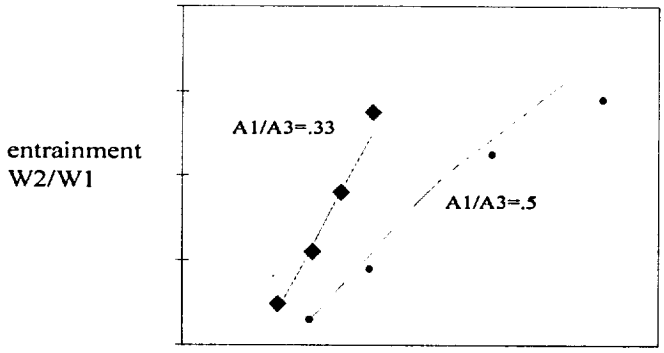

Constant Area Ejector Flow. Data from Addy et al. (1981).
Conditions: M1=2.5, T01/T02=1., NPR=5.

FIGURE 2.4 Comparison of Fabri choke model entrainment predictions to experimental data.

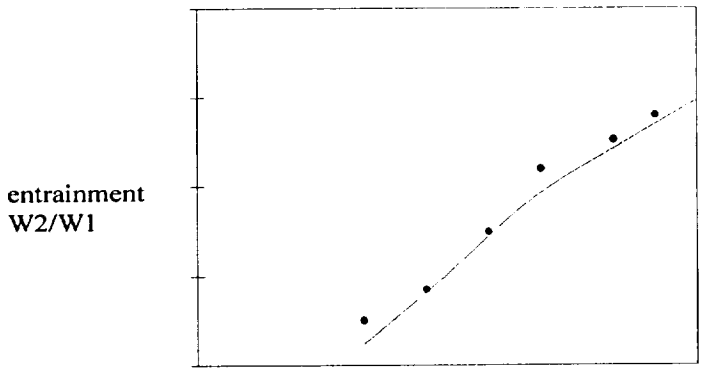

Variable Area Ejector Flow. Data fromAddy et al. (1981).
Conditions: M1=2.5, A1/A3=0.814, A2/A3=0.764, NPR=5.

FIGURE 2.5 Comparison of Fabri choke model entrainment predictions to experimental data.

The comparison with experimental data is shown to be good for a range of operating conditions. In spite of the fact, that these ejectors are simple slot ejectors that would not be typically used for a practical aeropropulsion design, they do provide confidence, that the simple control volume models are providing useful information.

2.2.5 Critical back pressure computation and subsonic flow limiting conditions

Sections 2.2.3 and 2.24 have developed two basic possible ejector flow problems, namely, back pressure constrained and back pressure unconstrained flows. These two flow regimes have significantly different modeling methods associated with them. Although the distinction that two flow problems exist is clear, at no point did we discuss how one chooses, "apriori", which is the appropriate model. In this section an approximate model to choose the appropriate flow regime is discussed. In addition to the supersonic/subsonic regime transition there are a series of constraints imposed upon the subsonic operation of the ejector. Attempting to operate outside of these constraints will cause DREA to fail due to physical reasons. As such, it is of considerable interest to provide an analysis to delineate these operational regions. Though it is beyond the scope of this study to develop operational maps, one of the constraints is modeled and results are compared to DREA to show that convergence failure of DREA is indeed associated with one of the physical constraints.

The choice of the proper condition is dependent, as one would expect, upon the back pressure or exit pressure level that the ejector senses. The task here is to develop a value for the exit pressure that separates the back pressure dependent regime from the back pressure independent regime. This value is termed as the critical back pressure or p_{crit}. The computation of this value follows. Referring to Figure 2.6, we consider the combined model.

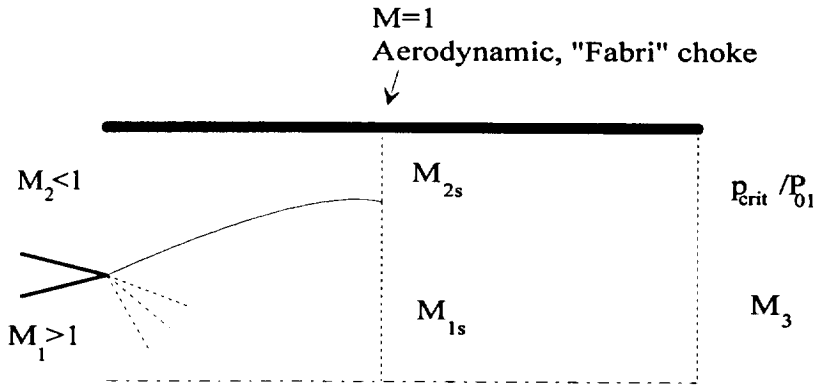

FIGURE 2.6 Critical back pressure analysis method definitions.

The first portion of the model involves the Fabri limited flow. The solution for this problem (which have been described in section 2.2.4) are the conditions associated with supersonic flow and choking in the secondary stream. Hence, if it were possible to estimate the exit conditions associated with this flow, then we would know the critical back pressure level. If the exit back pressure level is below p_{crit}, then the Fabri-choke is the correct solution. If, on the other hand, the back pressure level is greater than p_{crit} then the flow is not properly modeled using Fabri theory and should be modeled using the back pressure dependent model. This criterion is summarized in Table 2.2.

$(\frac{p_e}{p_{01}}) \leq (\frac{p_{crit}}{p_{01}})$	Back pressure independent flow Section 2.2.4
$(\frac{p_e}{p_{01}}) > (\frac{p_{crit}}{p_{01}})$	Back pressure dependent flow Section 2.2.3

TABLE 2.2 Critical back pressure criteria.

From Table 2.2, it is apparent that the key parameter is the value of p_{crit}/p_{01}. We may compute this value by reformulating the classical 1-d conservation relationships shown in section 2.2.3. These are repeated for convenience:

$$\dot{m}_{1s} + \dot{m}_{2s} = \dot{m}_3 \tag{2.12}$$

$$\dot{m}_{1s}u_{1s} + p_{1s}A_{1s} + \dot{m}_{2s}u_{2s} + p_{2s}A_{2s} = \dot{m}_3 u_3 + p_3 A_3 \tag{2.13}$$

$$\dot{m}_{1s}T_{01s} + \dot{m}_{2s}T_{02s} = \dot{m}_3 T_{03} \tag{2.14}$$

and the exit pressure definition:

$$p_3 = p_e \tag{2.15}$$

Combining these relationships to obtain a relationship in terms of M_{1s}, M_{2s}, and the critical pressure ratio p_{crit}/p_{01}. Details for this reduction are presented in Appendix B. The resulting non-linear, algebraic equation may be written:

$$(1+\frac{\gamma-1}{2}M_{1s})^{\frac{\gamma}{1-\gamma}}(1+\gamma M_{1s}^2)+(\frac{p_{02}}{p_{01}})(\frac{A_2}{A_1})(1+\frac{\gamma-1}{2}M_{2s})^{\frac{\gamma}{1-\gamma}}(1+\gamma M_{2s}^2)-$$

$$[\frac{\gamma}{\gamma-1}(\frac{p_e}{p_{01}})^2+\frac{2\gamma^2}{\gamma-1}*$$

$$[M_{1s}^2(1+\frac{\gamma-1}{2}M_{1s}^2)^{\frac{\gamma+1}{1-\gamma}}+M_{1s}M_{2s}(\frac{p_{01}}{p_{02}})(\frac{A_2}{A_1})(\frac{T_{01}}{T_{02}})^{\frac{1}{2}}(1+\frac{T_{01}}{T_{02}})* \tag{2.16}$$

$$(1+\frac{\gamma-1}{2}M_{1s}^2)^{\frac{\gamma+1}{2(1-\gamma)}}(1+\frac{\gamma-1}{2}M_{2s}^2)^{\frac{\gamma+1}{2(1-\gamma)}}+$$

$$M_{2s}^2(\frac{p_{02}}{p_{01}})^2(\frac{A_2}{A_1})^2(1+\frac{\gamma-1}{2}M_{2s})^{\frac{\gamma+1}{1-\gamma}}]^{\frac{1}{2}}]+\frac{1}{\gamma-1}(\frac{p_e}{p_{01}})(\frac{A_3}{A_1})=0$$

Equation (2.16) relates the critical pressure ratio p_{crit}/p_{01} to the aerodynamic choke quantities, A_{1s}, M_{1s}, A_{2s} and M_{2s}. Solution of these relationships is relatively straight forward, in that, p_{crit}/p_{01} is decoupled from the Fabri analyses, permitting solution of the Fabri problem and inversion (using a single variable non-linear equation solver) to compute the critical pressure ratio.

At this point the limiting flow field conditions for subsonic mixing are discussed. The meaning of a "limiting" subsonic flow in this application describes flow fields for which the intended ejector operation; i.e. primary stream flow inducing secondary entrainment, thereby, satisfying the downstream pressure constraint fails. It is possible to identify three possible limiting subsonic limiting flow situations:

1. Incipient reverse flow into the secondary inlet.
2. Choked flow in the secondary inlet.
3. Choked flow in the exit mixing stream.

These three cases are illustrated in Figure 2.7:

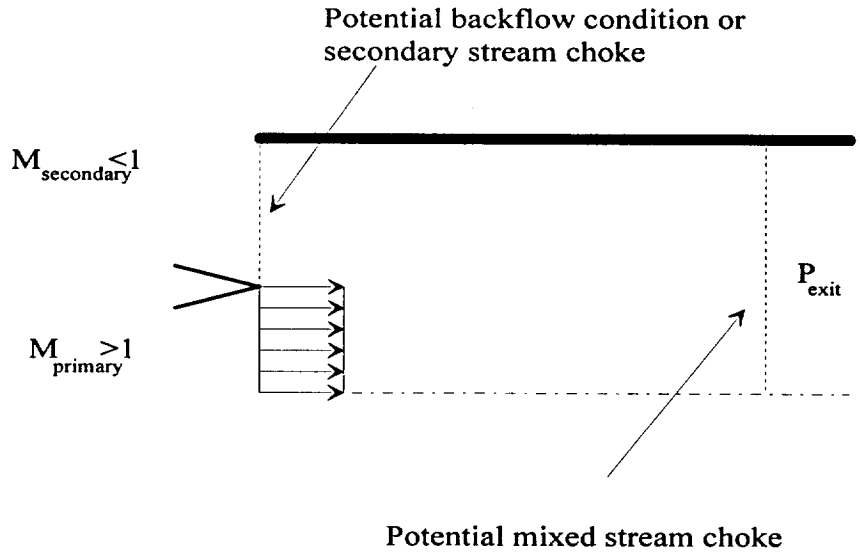

FIGURE 2.7 Limiting subsonic flow fields.

Our task is to determine upper and lower bounds on $(P_{02}/P_{01})(A_2/A_1)$, such that there is sufficient secondary pressure to prevent back flow, without inducing secondary inlet choking or exit stream choking. Hence an estimate for $(P_{02}/P_{01})(A_2/A_1)_{crit}$ which is used to delimit various flow regimes is developed. The details of this procedure are described in Appendix B.

2.2.6 Non-ideal entrainment/pumping

The requirement that we must model non-ideal pumping effects is central to our understanding of ejector flows. The need for this type of modeling comes from the simplified treatment of entrainment or pumping employed in this project. In the previous models we introduced quasi-one-dimensional assumptions or isentropic restrictions. Of course real, turbulent mixing flows are strongly influenced by multi-dimensional effects, as well as, irreversible losses (heat transfer and viscous dissipation). In this section, reduced complexity closure or feedback mechanisms that model these non-ideal effects are developed. Non-ideal pumping effects, just as inviscid pumping modeling itself, may be conveniently divided into two problems: back pressure dependent pumping and back pressure independent flow.

The closure for the back pressure dependent non-ideal pumping problem is dependent upon correctly modeling the multi-dimensional form of the exit pressure matching constraint. This is performed by generalizing the pressure constraint. It is extended by computing the integral average after the pressure has been corrected for viscous and multi-dimensional effects. Consider the relationship with "n" as the known iterative level (from the viscous mixing code output) and "n+1" as the unknown iterative level:

$$p_{exit}^{n+1} = p_{ave}^{n} = \int_0^1 p^n \, dA \tag{2.17}$$

Clearly, for a well mixed flow, the only non-ideal effect which will be recovered is the pressure loss effect due to friction and heat transfer. Fortunately, it is possible to develop an estimate of the average exit pressure without the burden of solving the full mixing equations for each pass. This deviation from ideal pumping is presented in Figure 2.8:

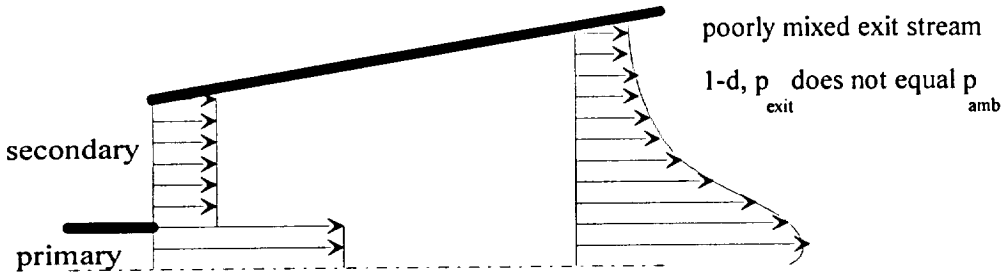

FIGURE 2.8 Back pressure dependent non-ideal flow definitions.

Back pressure independent pumping which was modeled by ideal (isentropic, quasi-one-dimensional) Fabri choke theory must also be corrected for multi-dimensional effects as well as frictional and heat transfer effects. As in the back pressure dependent case, we estimate the amount of irreversibility and deviation from one-dimensional theory by using result from the viscous mixing code. These losses are presented in Figure 2.9.

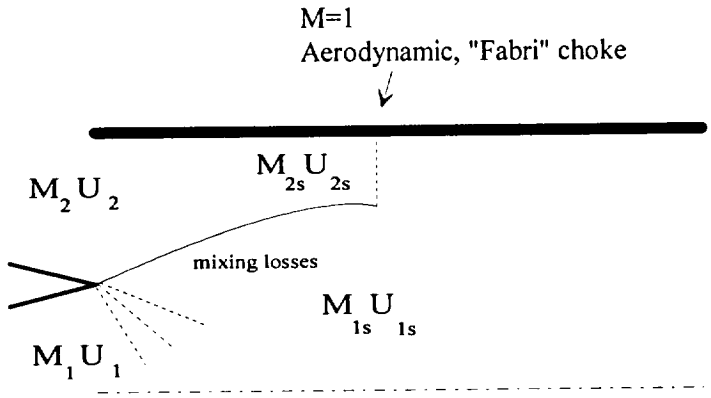

FIGURE 2.9 Back pressure independent loss definitions.

Saying this in functional form, we write:

$$\left(\frac{w_2}{w_1}\right)^{n+1} = \left(\frac{w_2}{w_1}\right)\left[\left(\frac{P_{01s}}{P_{01}}\right)^n_{ave}, \left(\frac{P_{02s}}{P_{02}}\right)^n_{ave}, \left(\frac{T_{01s}}{T_{01}}\right)^n_{ave}, \left(\frac{T_{02s}}{T_{02}}\right)^n_{ave}\right] \tag{2.18}$$

Now, to compute averaged pressure ratios and temperature ratios, we average using the expected relationship:

$$\left(\frac{F_{0is}}{F_{0i}}\right)^{n+1}_{ave} = \frac{1}{A^n_{is}} \int_0^{A^n_{is}} F_i^n(x,y)\,dA \tag{2.19}$$

Hence, the back pressure independent flow problem is closed, as well. Again, our goal is to develop models that do not require the solution of the full mixing equations and subsequent averaging.

The description of the algorithm above provides us with a methodology for computing the losses expected for the Fabri or aerodynamic choking problem, as shown in Figure 2.7. Some objections to this overall approach of averaging the viscous flow field must be considered:

1. a fully 2-d viscous solution is used to correct the quasi-1-d Fabri solution. This model fidelity inconsistency needs to be addressed. In other words, do we need to compute an expensive, 2-d flow field to estimate a 1-d quantity?
2. from preliminary experimental evidence, the effects of total pressure loss and heat transfer are expected to be small. Thus, the use of an expensive globally iterative algorithm may not be justified.

With these objections in mind, the need for a simplified method for the estimation of the loss becomes apparent.

2.2.6.1 Back pressure dependent regime loss/heat transfer model

As described in section 2.2.3, pumping for the subsonic problem is modeled by demanding conformance to the 1-d/average exit static pressure condition:

$$p^n_{ave} = \int_0^l p^n \, dA \quad \Rightarrow \quad F = p^n_{ave} - p_{exit,amb.} \tag{2.20}$$

Since the model already iteratively matches $p_{exit}=p_{ambient}$ assuming complete mixing, what remains to be computed, is a correction for the profile. This is especially important for mixing processes where significant regions of supersonic flow may exist:

In this type of problem or in a shock down problem, the lack of mixing will strongly influence the average pressure field and thereby the entrainment. In contrast, the entrainment for a fully subsonic ejector will be significantly less sensitive to the degree of mixing. As such, we will always model fully subsonic ejectors using the ideal mixing approximation.

Returning to flows with significant regions of sub sonic flow, i.e. $M_1>1$, we consider how the exit static pressure profile may be estimated. This could be done by integrating the profiles provided by the full mixing equations, but as pointed out, this is computationally prohibitively expensive. Consider alternatively the development of an approximate differential equation written for the average pressure. We start by defining the dimensional relationship (essentially a finite difference approximation):

$$\frac{dp_{ave}}{dx} = \frac{p_{ave,3} - p_{ave}}{L_{char.mix}} \qquad p_{ave} \equiv \int_0^l p \, dA \tag{2.21}$$

where $L_{char.\,mix}$ is a length characteristic of the mixing and $p_{ave,3}$ is the ideally fully mixed value. Clearly for a very long ejector, the average pressure must asymptotically approach this value. As is shown in section 2.4., it is reasonable to associate this length scale with:

$$\frac{1}{L_{char.mix}} \approx \frac{\nu_{eff}}{U_{ave}} \frac{\partial^2}{\partial y^2} \approx \frac{\nu_{eff}}{U_{ave}} \frac{1}{H^2} \tag{2.22}$$

Non-dimensionalizing and substituting into the previous equation yields our final differential equation and the initial condition:

$$\frac{dp_{ave}}{dx} = a^{*}x(p_{ave,3} - p_{ave}) \qquad p_{ave}(0) = p_1 h_s + (1 - h_s)p_2 \tag{2.23}$$

where a*x is the dimensionless effective turbulent viscosity. This is a linear differential equation which is easily solved to yield:

$$\frac{p_{ave}}{p_{ave,3}} = 1 + [\frac{p_{ave}(0)}{p_{ave,3}} - 1]\exp(-\frac{a^{*}x^2}{2}) \qquad p_{ave}(0) = p_1 h_s + (1 - h_s)p_2 \tag{2.24}$$

With this solution, it is possible to estimate the effect of mixedness upon the secondary properties. Since now the exit constraint takes the form:

$$F = p^{n}{}_{ave}(L_{shroud}) - p_{exit,amb} = p^{n}{}_{ave,3}[\frac{p^{n}{}_{ave}}{p_{ave,3}}(L_{shroud})] - p_{exit,amb} \tag{2.25}$$

Equation (2.25) drives towards zero at convergence.

Entrainment or pumping is a strong function of the shroud length. A poorly mixed problem will not satisfy the 1-d exit constraint, and will fail to give a reasonable estimate of pumping. We note that pumping will still occur, by a viscous, jet like entrainment, but this limiting effect is not modeled here. This is not a critical limitation, since any practically designed ejector will seek to maximize mixing, typically by using a complex, lobed mixer.

2.2.6.2 Back pressure independent regime loss/heat transfer model

A model based upon extensions of the inviscid analyses developed previously for back pressure independent flows (to include loss terms) and approximations of the more complete mixing model are presented here. The solution procedure may be stated as:

- estimate the choke location
- compute the asymptotic or fully mixed losses, which will be needed for the loss differential equation
- estimate the turbulent viscosity, which is also fundamental to the loss equation
- solve the loss differential equations
- substitute the loss terms into the extended Fabri choke equations.

Since this is a rather complex problem, a useful way to visualize this progression is to write the functional forms of these equations with their variable dependencies. Further, due to the simplifying assumptions applied to the associated differential equations, this model is completely algebraic. As such, we may solve it with any one of our non-linear inversion algorithms. See Section 3 for a discussion of nonlinear equation solution algorithms. Consider then the vector equation written in functional terms:

$$\left.\begin{array}{c} X_c(M_1, M_{1s}, T_{01s}, T_{01}, H_s) \\ T_{0,\infty} = T_{0,\infty}(P_{01}, P_{02}, T_{01}, T_{02}, M_1, M_2, A_1, A_2) \\ M_3 = M_3(P_{01}, P_{02}, T_{01}, T_{02}, M_1, M_2, A_1, A_2) \\ P_{0,\infty} = P_{0,\infty}(P_{01}, P_{02}, T_{01}, T_{02}, M_1, M_2, A_1, A_2, M_3) \\ a^* = a^*(P_{01}, P_{02}, T_{01}, T_{02}, M_1, M_2, A_1, A_2) \\ P_{01s} = P_{01s}(P_{01}, P_{02}, P_{0,\infty}, a^*, X_c) \\ P_{02s} = P_{02s}(P_{01}, P_{02}, P_{0,\infty}, a^*, X_c) \\ T_{01s} = T_{01s}(T_{01}, T_{02}, T_{0,\infty}, a^*, X_c) \\ T_{02s} = T_{02s}(T_{01}, T_{02}, T_{0,\infty}, a^*, X_c) \\ mass\ (P_{01}, P_{02}, P_{01s}, P_{02s}, T_{01}, T_{02}, T_{01s}, T_{02s}, M_1, M_2, M_{1s}, M_{2s}, A_1, A_2) \\ momentum\ (P_{01}, P_{02}, P_{01s}, P_{02s}, T_{01}, T_{02}, T_{01s}, T_{02s}, M_1, M_2, M_{1s}, M_{2s}, A_1, A_2) \end{array}\right\} = \bar{0} \quad (2.26)$$

and the (11) unknowns:

$$\left(X_c \quad T_{0,\infty} \quad M_3 \quad P_{0,\infty} \quad a^* \quad P_{01s} \quad P_{02s} \quad T_{01s} \quad T_{02s} \quad M_{1s} \quad M_2\right)^T \quad (2.27)$$

Solution of these equations is simplified by the fact that the first nine equations in the system may be written explicitly. Thus, although this system is formally an eleven equation system, it may be solved using a two variable inversion. Broyden's method is used here (Burden and Faires (1993)). Also see Section 3.

The "workhorse" analysis in the above system, are the mixing equations for the total pressures and temperatures. All the analyses have been taken from previous sections (either with some simplification or with extensions). Since these governing ordinary differential equations are new, their development is outlined here. This starts with the "model" equations for mixing of any scalar quantity. The notation, ϕ is chosen to emphasize the analogy with the main governing equations:

$$U_{ave}\frac{d\phi_1}{dx} = \frac{kx}{H}(\phi_1 - \phi_\infty) \quad (2.28)$$

$$U_{ave}\frac{d\phi_2}{dx} = \frac{kx}{H}(\phi_2 - \phi_\infty) \quad (2.29)$$

where "kx" represents ν_{eff} the turbulence model and ϕ_∞ is the asymptotic fully mixed value. The subscripts, of course, refer to the appropriate stream. Non-dimensionalizing yields:

$$\frac{d\phi_1}{dx} = a^* x(\phi_1 - \phi_\infty) \quad (2.30)$$

$$\frac{d\phi_2}{dx} = a^* x(\phi_2 - \phi_\infty) \tag{2.31}$$

Since these equations are linear, they may be immediately solved. It is interesting, though, to subtract these equations to yield:

$$\frac{d(\phi_1 - \phi_2)}{dx} = -a^* x(\phi_1 - \phi_2) \tag{2.32}$$

In this form the mixing form of these equations is more apparent.

Solving equations (2.32) and (2.33) provides estimates of the total conditions within a stream at any place in the flow field. Consider the general solution:

$$\phi_i(x) = \phi_\infty + (\phi_i(0) - \phi_\infty)e^{-\frac{a^* x^2}{2}} \tag{2.33}$$

Thus we have access to the total quantities (P_{01s}, P_{02s}, T_{01s}, T_{02s}) at any point in the flow field. Although this methodology is rather simple, it does contain both an approximation to the turbulent mixing, as well as, the loss mechanism through the asymptotic value.

The Fabri governing equations must be extended to include the loss terms as computed above. This is a straightforward derivation where loss terms are now retained. Consider the extended equation for mass conservation:

$$\begin{aligned}
&\left(\frac{M_1}{M_{1s}}\right)\left(\frac{1+\frac{\gamma-1}{2}M_{1s}^2}{1+\frac{\gamma-1}{2}M_1^2}\right)^{\frac{\gamma+1}{2(\gamma-1)}}\left(\frac{P_{01}}{P_{01s}}\right)\left(\frac{T_{01}}{T_{01s}}\right)^{\frac{1}{2}} + \\
&+\left(\frac{A_2}{A_1}\right)\left(\frac{M_2}{M_{2s}}\right)\left(\frac{1+\frac{\gamma-1}{2}M_{2s}^2}{1+\frac{\gamma-1}{2}M_2^2}\right)^{\frac{\gamma+1}{2(\gamma-1)}}\left(\frac{P_{02}}{P_{02s}}\right)\left(\frac{T_{02}}{T_{02s}}\right)^{\frac{1}{2}} = 1+\left(\frac{A_2}{A_1}\right)
\end{aligned} \tag{2.34}$$

and the global momentum equation:

$$\left(\frac{M_1}{M_{1s}}\right)\left(\frac{1+\frac{\gamma-1}{2}M_{1s}^2}{1+\frac{\gamma-1}{2}M_1^2}\right)^{\frac{\gamma+1}{2(\gamma-1)}}(1+\frac{\gamma-1}{2}M_{1s}^2)^{\frac{\gamma}{1-\gamma}}(1+\gamma M_{1s}^2)\left(\frac{P_{01}}{P_{01s}}\right)^{\frac{1-\gamma}{\gamma}}\left(\frac{T_{01}}{T_{01s}}\right)^{\frac{1}{2}}+$$

$$\left(\frac{A_2}{A_1}\right)\left(\frac{P_{02}}{P_{01}}\right)M_2\left(\frac{\frac{2}{\gamma+1}}{1+\frac{\gamma-1}{2}M_2^2}\right)^{\frac{\gamma+1}{2(\gamma-1)}}(\frac{\gamma+1}{2})^{\frac{\gamma}{1-\gamma}}(1+\gamma)\left(\frac{P_{01}}{P_{01s}}\right)^{\frac{1-\gamma}{\gamma}}\left(\frac{T_{01}}{T_{01s}}\right)^{\frac{1}{2}}= \tag{2.35}$$

$$=(1+\gamma M_1^2)(1+\frac{\gamma-1}{2}M_1^2)^{\frac{\gamma}{1-\gamma}}+(\frac{A_2}{A_1})(\frac{P_{02}}{P_{01}})(1+\gamma M_2^2)(1+\frac{\gamma-1}{2}M_2^2)^{\frac{\gamma}{1-\gamma}}$$

The extension terms are apparent in these equations as well as the closures (P_{01s}, P_{02s}, T_{01s}, T_{02s}) which were described previously.

The above paragraphs provide a description of the algorithm that is to be used to model the form of non-ideal mixing effects on the pumping. This provides us information on the flow rate and hence, other static quantities. Unfortunately, the above equations do not give us any idea of the convergence rate of the method or conditions under which convergence (or divergence) might be expected. Of course, we can make some estimates of these effects by referring to general fixed point iterative methods ((Johnson and Riess (1982) or Gerald (1980)). Some areas that might be considered include:

1. General fixed point convergence rate linear
2. General fixed point convergence rate criterion
3. methods to improve convergence rates (such as Aitkens method (Johnson and Riess (1982)) etc.

Fortunately, since the model was described by the reduced set of equations, the convergence rate is the same as Broyden's method, which is superlinear.

2.3 Inviscid flow field analysis

As indicated, the viscous mixing region solver is a steady state, single pass marching algorithm. Although the basic mixing process is formulated in terms of conservative flux quantities (mass flux, momentum flux and energy flux) which are Mach number invariant, the local primitive variables, such as, velocity, temperature, static and total pressure, density and Mach number are certainly subsonic/supersonic dependent. Since the supersonic or back pressure independent ejector problem, is by its very nature, a transonic flow; delineation of regions of supersonic or subsonic flow must be provided for the mixing code primitive variable inversion analysis. Estimates of the flow regime are supplied using a set of extended, classical inviscid, supersonic/subsonic slipline interaction algorithms. These are described in this subsection.

2.3.1 Slipline interface analysis

Considering the most general problem, we note that a supersonic gas jet issuing into a co-flowing medium has an almost periodic structure for small stream pressure variations. In this section, formulas that describe the periodicity and wavelength of the slipline are developed for two-dimensional and axi-symmetric, supersonic-subsonic jets. Classical inlet and streamline perturbation solution methodologies are limited to small stream pressure imbalances. To increase the range of validity of the streamline perturbation solution, a modified

strained coordinate technique is introduced that shows good comparison with experimental data over the Mach number and pressure ratio p_1/p_2 range of 1.2-4.0 and 1.0-20.0, respectively. This more general relationship provides a limiting form of a supersonic ejector flow field, since the location of the first maximum expansion corresponds to the location of the aero-dynamic or Fabri-choke analyzed in the previous section.

An early class of models for free jet flows were developed by Prandtl (1904) and later by Pai (1952) and (1954) based upon perturbations about the inlet quantities, i.e. $u=U_i+u_i'$. Although straightforward to use, these models have restrictive assumptions and yield relatively poor results. An improvement was made by Pack (1950) who used a perturbation about the velocity field at the slipline. This model shows significantly better comparison with experimental data but is still only valid for small pressure ratios between the jet and ambient flows.

In this section, the fundamental equations are merely quoted. The derivations are deferred to Appendix C. The appendix starts by briefly describing the models of Pai and Pack for reference use. Then, a modification to the streamline perturbation model is derived using a strained coordinate technique that extends the range of application to larger pressure ratios for jet flows. A comparison is performed to evaluate the new model for available large pressure ratio free jet experiments. Having helped establish the validity of the relationships for free jets, their use for the ejector flows is developed.

The principle parameter is discussed is x_c, which is the location of the first minimum in the expansion/compression system resulting in the flow. This value for both axi-symmetric and two dimensional flows is described by the equations below:

•axi-symmetric:

$$\frac{x_c}{2} = 1.22\beta_{eff} - .22\beta_{1s} \equiv 1.22(1+\frac{1}{2}\bar{\xi_m^2})\beta_{1s} - .22\beta_{1s} \tag{2.36}$$

•two-dimensional:

$$\frac{x_c}{2} = 2\beta_{eff} - \beta_{1s} \equiv 2(1+\frac{1}{2}\bar{\xi_m^2})\beta_{1s} - \beta_{1s} \tag{2.37}$$

where $\beta_{1s}=(M_{1s}^2-1)^{1/2}$ and $\xi=\beta_{1s}^2[1-U_1/U_{1s}]$. Equations (2.38) and (2.39) are the final modified solutions for the critical slipline location. These relationships with the lowest order terms based upon control volume theory comprise our solution for the location of the first minimum of the slipline. By symmetry, half this distance is the local maximum of the primary expansion and corresponds to the location of the Fabri-choke. Results are presented in Figure 2.10. Further comparisons are presented in De Chant (1996).

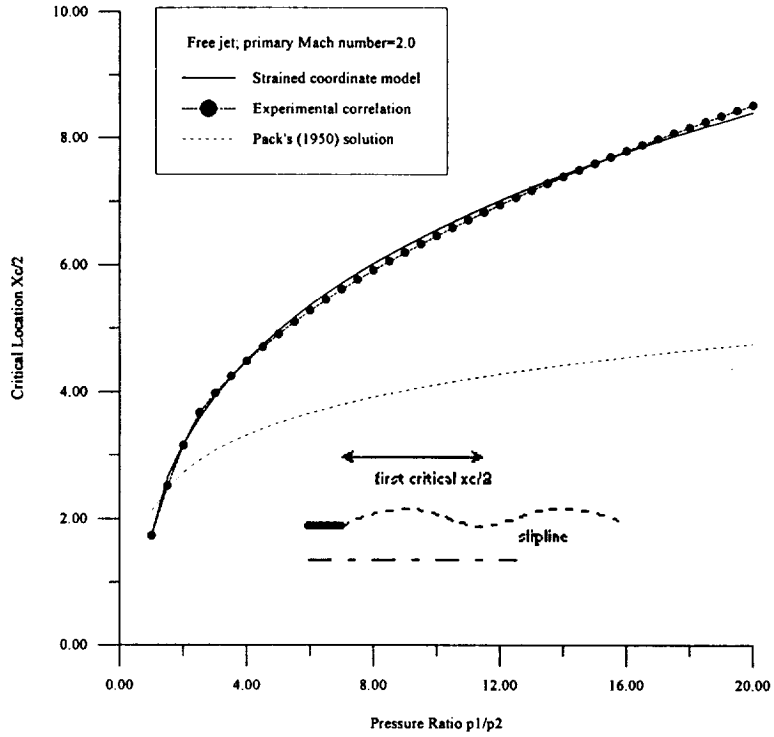

FIGURE 2.10 Comparison of new strained coordinate analysis interface geometry (first critical) location, x_c with inlet perturbation and experimental correlation of Love (1959).

A simple linearized, potential flow model for unconfined/free jet, axi-symmetric and two-dimensional flows has been developed based upon a strained coordinate extension to Pack's (1905) streamline or slipline perturbation.

This analysis provides analytically based estimates of the slipline geometry for co-flowing supersonic and subsonic streams. The slipline is described by the wavelength or the streamwise location of the first minimum of slipline displacement. Free jet data was used to test this model and compare with other classical relationships.

2.3.2 Confined flow modifications

The prediction of the critical location or wavelength for unconfined flows developed here provides a limiting case estimate for ejector flows which are important for aerodynamic and industrial applications. Additionally, this model provides information about the efflux of a supersonic jet, which is important for aerodynamic noise generation problems. Of course, though, ejector/mixer nozzles are by their very nature confined or internal flow problems. As such, modifications to the basic inviscid flow analyses are necessary. This modification takes the form of estimating the base flow quantities in a different manner. Consider the expansion

$$\frac{u}{U_{ls}} = 1 + \frac{\partial \phi}{\partial x}\varepsilon + \qquad \varepsilon \equiv (1 - \frac{U_l}{U_{ls}}) \tag{2.38}$$

where, U_{1s}, is the velocity at the interface. Note the local definition of ϕ, which here represents a small disturbance velocity potential.

As explained in Appendix C, the slipline velocity U_{1s}, was estimated using a simple static pressure matching methodology for the free jet problem. To account for the internal flow effects, though, it is necessary to apply a control volume methodology. Consider the two fundamental problems for an internal flow problem:

(1) Large area ratio, unknowns: M_{1s}, M_{2s}, U_{1s}
(2) Small area ratio (Fabri problem), unknowns: M_{1s}, M_2, U_{1s}

The necessity for two problem closures needs to be explained. The conditions for a free jet, are based solely upon local static pressure matching. Consequently, problems for $A_2/A_1 >> 1$ are analyzed using static pressure and mass conservation. Unfortunately, the local 1-d control volume assumptions are poor approximations for sufficiently small area ratio's, A_2/A_1,. Therefore, this approximation cannot be expected to apply for $A_2/A_1 \approx 1$, and hence provide an alternative formulation.

Starting with mass conservation which is common to both problems, we write:

$$\left(\frac{M_1}{M_{1s}}\right)\left(\frac{1+\frac{\gamma-1}{2}M_{1s}^2}{1+\frac{\gamma-1}{2}M_1^2}\right)^{\frac{\gamma+1}{2(\gamma-1)}} + \left(\frac{A_2}{A_1}\right)\left(\frac{M_2}{M_{2s}}\right)\left(\frac{1+\frac{\gamma-1}{2}M_{2s}^2}{1+\frac{\gamma-1}{2}M_2^2}\right)^{\frac{\gamma+1}{2(\gamma-1)}} = 1+\left(\frac{A_2}{A_1}\right) \tag{2.39}$$

and static pressure matching which is used for large area ratio problems $A_2/A_1 >> 1$

$$\left(\frac{P_{01}}{P_{02}}\right) = \left(\frac{1+\frac{\gamma-1}{2}M_{1s}^2}{1+\frac{\gamma-1}{2}M_{2s}^2}\right)^{\frac{\gamma}{\gamma-1}} \tag{2.40}$$

or the global momentum equation used for, $A_2/A_1 \approx 1$.

$$\left(\frac{M_1}{M_{1s}}\right)\left(\frac{1+\frac{\gamma-1}{2}M_{1s}^2}{1+\frac{\gamma-1}{2}M_1^2}\right)^{\frac{\gamma+1}{2(\gamma-1)}}\left(1+\frac{\gamma-1}{2}M_{1s}^2\right)^{\frac{\gamma}{1-\gamma}}(1+\gamma M_{1s}^2)+$$

$$\left(\frac{A_2}{A_1}\right)\left(\frac{P_{02}}{P_{01}}\right)M_2\left(\frac{\frac{2}{\gamma+1}}{1+\frac{\gamma-1}{2}M_2^2}\right)^{\frac{\gamma+1}{2(\gamma-1)}}\left(\frac{\gamma+1}{2}\right)^{\frac{\gamma}{1-\gamma}}(1+\gamma)= \tag{2.41}$$

$$=(1+\gamma M_1^2)\left(1+\frac{\gamma-1}{2}M_1^2\right)^{\frac{\gamma}{1-\gamma}}+\left(\frac{A_2}{A_1}\right)\left(\frac{P_{02}}{P_{01}}\right)(1+\gamma M_2^2)\left(1+\frac{\gamma-1}{2}M_2^2\right)^{\frac{\gamma}{1-\gamma}}$$

These relationships provide closure for the internal flow Mach numbers and area ratios.

Since the flow is locally assumed to be isentropic, it is possible to compute the slipline velocity:

$$\frac{U_1}{U_{1s}}=\frac{M_1}{M_{1s}}\left(\frac{1+\frac{\gamma-1}{2}M_{1s}^2}{1+\frac{\gamma-1}{2}M_1^2}\right)^{\frac{1}{2}} \tag{2.42}$$

Contained as a degenerate case is the free jet solution:

$$M_{1s}^2=\frac{2}{\gamma-1}\left[\left(1+\frac{\gamma-1}{2}M_1^2\right)\left(\frac{p_1}{p_2}\right)^{\frac{\gamma-1}{\gamma}}-1\right] \tag{2.43}$$

With these low order forms available the analysis proceeds in a straightforward manner, namely solving x_c and the Fabri choke location using equations (2.36) or (2.37).

2.4 Parabolic mixing flow analysis

The second major portion of the flow chart, Figure 2.1 considered is the turbulent compressible mixing analysis. In this section the character and solution of the mixing governing relationships which were developed in Section 1 are discussed.

2.4.1 Conservation form mixing differential equations

A reduced set of partial differential equations was derived in Section 1, i.e. equations (1.19), (1.20) and (1.22). They are a decoupled set of parabolic, scalar, heat equations. Equations (1.19), (1.20) and (1.22) may be placed in a simpler, "canonical" form. Next, numerical and classical analytical solution methods are developed and the inherent limitations of both methods are discussed. Finally an alternative to these solely numerical or analytical solution methods which combines the best features of both numerical and analytical methods is described.

2.4.2 Solution of mixing partial differential equations

From the previous section, the governing equations may be approximately written for the conservation quantities in terms of the general linear parabolic equation:

$$\frac{\partial \phi}{\partial x} = a(x)\frac{\partial^2 \phi}{\partial y^2} = a^* x \frac{\partial^2 \phi}{\partial y^2} \tag{2.44}$$

with the boundary conditions:

$$\frac{\partial \phi(x,0)}{\partial y} = \frac{\partial \phi(x,1)}{\partial y} = 0 \tag{2.45}$$

with the initial condition:

$$\phi(0,y) = \begin{pmatrix} \phi_{10} & 0 \le y \le h_s \\ \phi_{20} & h_s < y \le 1 \end{pmatrix} \tag{2.46}$$

and ϕ is defined by:

$$\phi(x,y) \equiv \begin{pmatrix} \rho u^2 + p \\ \rho u H \\ \rho u \end{pmatrix} \tag{2.47}$$

The complex turbulence model $(\nu_{eff}/U)\varepsilon_G/\varepsilon$ has been replaced by some function a(x). This functional closure will be described in detail in Section 2.5. Additionally, the "*" superscript and the "0" subscript denoting a dimensionless quantity and level within the perturbation expansion, respectively, have been suppressed for simplicity.

For our turbulence model it will appropriate to make an additional local assumption, that the function a(x) may be approximated by the linear function $a(x)=a^{\bullet} x$. This will give us an analogous formulation to that of Reichardt. See Schlichting (1979). The choice of the locally linear functional form is justified by our development of the near field turbulence model. Again, this assumption will be justified in Section 2.5.

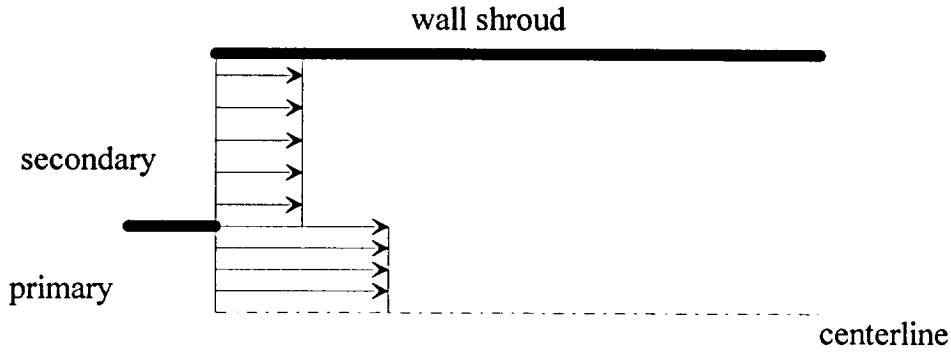

FIGURE 2.11 Mixing analysis singularity definitions.

The above governing equation with associated boundary and initial conditions are on the surface a relatively trivial set of equations. As we shall see, though, the discontinuous nature of the initial condition, as shown in Figure 2.11, will cause considerable difficulties both for numerical and analytical solutions. With this in mind, it will be of interest to "naively" solve the governing equation. It is linear so one may immediately write an analytical solution. The straightforward eigenfunction expansion (Haberman (1983)) solution is:

$$\phi(x,y) = \bar{\phi} + \frac{2}{\pi}(\phi_{10} - \phi_{20}) \sum_{n=1}^{\infty} \frac{1}{n} \sin(n\pi h_s) \cos(n\pi y) e^{-a^{\bullet}(n\pi)^2 \frac{x^2}{2}} \tag{2.48}$$

where:

$$\bar{\phi} = \phi_{10} h_s + (1 - h_s)\phi_{20} \equiv 1 \tag{2.49}$$

This equation is formally an exact solution to equations (2.46)-(2.50). Unfortunately, this equation is very slow to converge for x<<1, indeed truncation error is on the order of O(1/n), and the solution suffers from Gibb's jump departures (Haberman (1983) and Weinberger (1965)). Unfortunately, x<<1 is precisely where good converge is necessary since the concentration in this project is on short shroud ejectors.

Since the eigenfunction expansion (Fourier series) method is both inefficient and yields very poor results, alternative methods must be considered. The most obvious solution from the standpoint of efficiency is to apply a strictly numerical solution. Early in this work, a high accuracy ($O(\Delta y^4)$, $O(\Delta x^2)$) numerical solver based upon a variable step, compact differencing scheme (Kreiss differencing) in the cross-stream and variable step, fully implicit differencing in the streamwise direction, was applied to this problem. This model is described in detail in Section 3. Although, the solver which achieves 4th order accuracy on three-point support by simultaneously computing the function, and two derivatives, was of high accuracy, it could not in general, resolve the discontinuous nature of the input profile. This limitation was shown clearly when the divergence theorem constraint, i.e. mass conservation which demands:

$$\int_0^1 \phi(x,y)dy = 1 \tag{2.50}$$

Unfortunately, this constraint was not properly honored by the strictly numerical solver due to the singular behavior near the step input. Clearly a methodology which is not even conservative is unacceptable.

The poor performance of the strictly numerical model may be analyzed further. Though Section 3 describes the compact (spline-on-spline method) in detail, it is useful to discuss the truncation error briefly here. Considering the implicit relationship governing the second derivatives we find the error terms:

$$error = \frac{1}{60}(\Delta_{j+1}\Delta_j(\Delta_{j+1} - \Delta_j))\phi^{(4)} + O(\Delta^4)\phi^{(6)} \tag{2.51}$$

which is formally fourth order for constant grid spacing. Unfortunately for very rapid changes in ϕ, the high order derivatives, such as, $\phi^{(6)}$ are very large. In fact they may be as large as $O(1/\Delta^4)$ which would yield a very poor solution with errors O(1)! Indeed, this was observed.

Clearly, naive analytical solution or numerical solution of this problem will lead to poor performance. What is requires is an analysis capable of dealing with extremely rapidly changing functions. Fortunately a solution method from classical analysis is available which is based upon distribution theory rather than continuous functions. This is the method of Green's function expansions. We may actually, more usefully derive the solution using a cosine transform, i.e. even function, semi-infinite Fourier transform and the method of images (Haberman (1983), Churchill and Brown (1978)). The result, which is merely quoted here, is derived in Appendix D.

$$\phi_{an} = \frac{1}{2}(\phi_{10} - \phi_{20})\sum_{-\infty}^{\infty}\left[erf\left(\frac{y + h_s - 2n}{(2a^*)^{\frac{1}{2}}x}\right) - erf\left(\frac{y - h_s - 2n}{(2a^*)^{\frac{1}{2}}x}\right)\right] + \phi_{20} \tag{2.52}$$

Note, that for x<<1 this relationship recovers the step input. The solution could have also been derived directly using infinite space Green's functions and the method of images (Haberman (1983)).

Although the above relationship is exact, and does not suffer from the near field (small "x") limitations that the eigenfunction expansion solution did, it is still in the form of an infinite series. It may be noted that, in the near field, the solution converges extremely quickly. This is desirable since most of our interest is in the near field. Although short shroud ejectors are of interest in this study, it is necessary to be able model far field behavior using a reasonable number of terms in the series. A method, which invokes the best features of the analytical near field expansion and an efficient finite difference approximation, is developed subsequently.

It is important to quantitatively estimate the number of terms required to satisfy the governing equation to some pre-determined level. This knowledge will make it possible to balance our numerical effort against the analytical effort, since a combined problem is ultimately to be solved. This may be done most conveniently by considering the derivative of the flux at the wall, i.e. $\partial\phi/\partial y$. In particular, it will be useful to consider the size of a single term in the Green's function expansion. The choice of using the boundary condition as an indicator of convergence, is especially appropriate, in that the Green's function expansion is very accurate near the step function (Haberman (1983)), with reduced accuracy far from the singularity. Hence a boundary condition is a reasonable requirement used to estimate convergence rate. The single term is written:

$$\frac{\partial \phi_{an}}{\partial y} = \frac{1}{2}\frac{(\phi_{10}-\phi_{20})}{(2a^*)^{\frac{1}{2}}x}\left[\exp -\left(\frac{y+h_s-2n}{(2a^*)^{\frac{1}{2}}x}\right) - \exp -\left(\frac{y-h_s-2n}{(2a^*)^{\frac{1}{2}}x}\right)\right] \tag{2.53}$$

Selecting y=1 and concentrating on the rate of exponential decay (for the first term in the above equation), and solving for n yields:

$$n = \frac{1}{2}\left(1+h_s+(2a^*)^{\frac{1}{2}}x\left\{-\ln\left[\frac{2(2a^*)^{\frac{1}{2}}x\dfrac{\partial \phi_{an}}{\partial y}}{(\phi_{10}-\phi_{20})}\right]\right\}^{\frac{1}{2}}\right) \tag{2.54}$$

This gives us an estimate of the required to obtained a pre-specified error for $\partial\phi/\partial y$. Two trends may be observed:

1. As x or a^* increases, the required number of series terms, "n" required will increase and
2. As the difference in initial condition ϕ_{10}-ϕ_{20} increases, the required number of terms will also increase.

Numerical experimentation, shows that a maximum number (even for very long ducts) of terms in the Green's function expansion is always less than six. This is acceptable, since the problem is solved using a hybrid numerical/analytical method, where the series truncation error is corrected by invoking a numerical/analytical decomposed problem. Again, hybrid method is described subsequently.

A combined numerical and analytical solution of the problem is easily effected, since the governing equation (2.47) is linear. Consider the decomposition:

$$\phi(x,y) = \phi_{an}(x,y) + \phi_{num}(x,y) \tag{2.55}$$

with the governing equation:

$$\frac{\partial \phi_{num}}{\partial x} = a(x)\frac{\partial^2 \phi_{num}}{\partial y^2} = a^* x\frac{\partial^2 \phi_{num}}{\partial y^2} \tag{2.56}$$

with the new boundary conditions:

$$\frac{\partial_{num}\phi(x,0)}{\partial y} = -\frac{\partial_{an}\phi(x,0)}{\partial y} \qquad \frac{\partial_{num}(x,1)}{\partial y} = -\frac{\partial_{an}\phi(x,1)}{\partial y} \tag{2.57}$$

and the new initial condition:

$$\phi_{num}(0,y) = 0 \tag{2.58}$$

The overall solution is then, of course the sum of the two functions. Notice, that the new numerical initial condition equation (2.58) is essentially trivially, and very easily represented numerically.

Before concluding the mixing analysis, it is worth noting, that the singularity that is shown in Figure 2.11 is caused by our mathematical representation of the near field conditions. Physical, a discontinuous initial profile cannot exits in the presence of physical viscosity. In reality, the flow has wall boundary layers and a "blunt" tip zone (and therefore, a locally subsonic elliptic region) very near the splitter plate as shown in Figure 2.12.

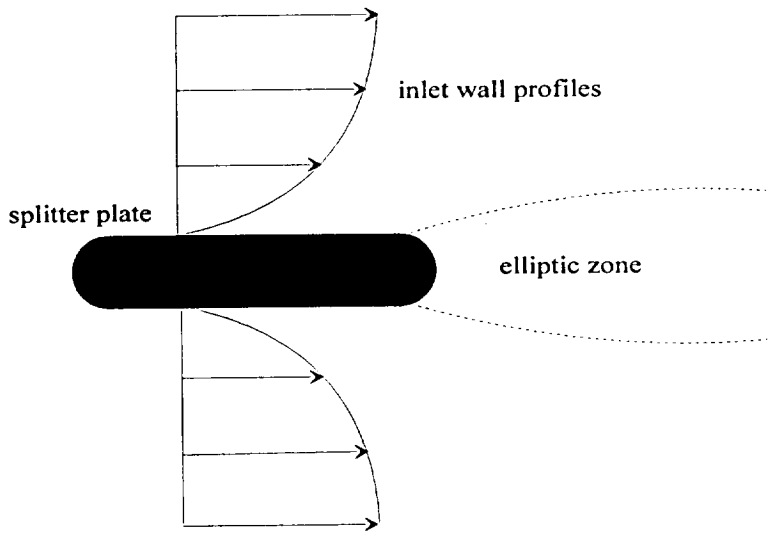

FIGURE 2.12 Details of the physical flow field near the splitter plate.

We chose not to attempt to model these effects for the following reasons:

1. Inlet conditions are complex and difficult to model at the level of fidelity which the mixing model has been developed for. Additionally more information than will ever be known at the initial design level would be required to properly model the inlet flow. Figure 2.12 is clearly reminiscent of classical "triple deck" theory (Van Dyke (1975)), with all the attendant theoretical and analytical complexities associated with that work.
2. It is our intention to connect this mixing model to thermodynamic design codes, for which profile information is not known, whereas 1-d inlet information certainly is.
3. Modeling of the near field would require an expensive elliptic methodology, completely inappropriate for the model that is developed in this study.

For these reasons, the decision has been made to model a virtually (and mathematically exactly) an input step discontinuity. This is effectively a Heaviside step input (Haberman (1983)). The purpose of this paragraph, though, is to state that the inlet discontinuity is a modeling feature. Colloquially stated, physical fluid flows are "smart enough" to prevent the existence of singular behavior, we have introduced this idealization for the reasons stated above.

2.4.3 Primitive variable decoding algorithm

In this section, the inversion of conservative flux quantities, φ, to "primitive" variable such as velocity, pressure, temperature, density, Mach number etc. is developed.

2.4.3.1 Complete inversion

The solver described in the previous section is written strictly in terms of the conservative flux quantities:

$$\phi(x,y) \equiv \begin{pmatrix} \rho u^2 + p \\ \rho u H \\ \rho u \end{pmatrix} \tag{2.63}$$

To convert, these fluxes into primitive variables, such as (M, u, p, T, ρ), a local one-dimensional approximation is applied combined with the definitions of the fluxes themselves to compute the primitive variables. Consider, for example, the velocity may be recovered from the flux values using:

$$F(u) \equiv \frac{\gamma+1}{2\gamma}[\rho u(x,y)](u)^2 - [(\rho u^2 + p)(x,y)]u + \frac{\gamma-1}{\gamma}[\rho u H(x,y)] = 0 \tag{2.64}$$

A somewhat more convenient form for analytical purposes of equation (72), which is in terms of the conservative fluxes and the Mach number, may be written:

$$\left(\gamma^2 - \frac{\gamma^2}{2}C_0\right)M^4 + \left(2\gamma - \frac{\gamma^2}{\gamma-1}C_0\right)M^2 + 1 = 0 \quad C_0 \equiv \frac{(\rho u^2 + p)^2}{(\rho u)(\rho u H)} \tag{2.65}$$

These equations contain a considerable amount of physics. The two roots of the quadratic equation (in terms of M^2) correspond to supersonic and subsonic solutions for the ejector flow field. Hence, at every point in the flow field, the two basic ejector solutions are contained. One can also show that where the flow is choked, M=1, implies a single solution. This corresponds to a zero discriminant in equation (2.64) or (2.65). The choice of the appropriate solution is determined by inviscid flow field solver, which locates the Fabri-choke and the subsonic/supersonic interface. The very close correspondence to shock capturing methods used for Inviscid Euler type solvers (Anderson et al. (1984)) should also be noted. With this similarity in mind, it is apparent, that this equation has strong normal shock solutions embedded within it. This is consistent with our ejector analysis, which for negligible secondary flow must recover the classical-one-dimensional normal shock relationships.

Although equation (2.65) provides a method for recovering primitive quantities from the conservative fluxes, for the steady, viscous problem with embedded subsonic regions, this formulation is not without problems. This problem becomes clear if one considers Figure 2.13:

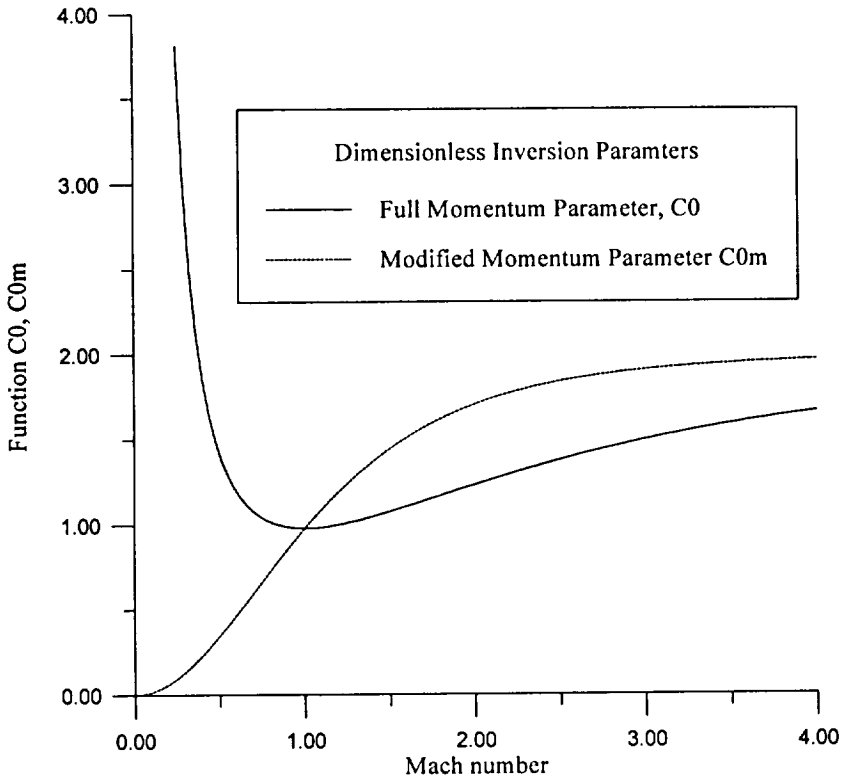

FIGURE 2.13 Characteristics of complete and modified primitive variable inversion relationships.

From Figure 2.13, the double valued nature of the function C_0 is apparent. Recall that C_0 is the dimensionless ratio used in equation (2.65). As the graph implies, it can also be written solely as a function of Mach number:

$$C_0 \equiv \frac{\gamma-1}{\gamma^2}\frac{\left[\gamma M^2+1\right]^2}{M^2\left(1+\frac{\gamma-1}{2}M^2\right)} \tag{2.66}$$

which is merely equation (2.65) rewritten. This double valued nature, although physically significant in the streamwise direction (normal shock down shock or Fabri expansion) causes considerable trouble in the cross-stream, or "y" direction for mixed supersonic/subsonic flow fields.

Consider the mixing of low speed (large C_0) subsonic fluid (subsonic branch) fluid with supersonic fluid. Mixing causes a decrease in C_0 in the subsonic region which, correctly, decodes as an increasing Mach number. Unfortunately, this large value of C_0 will also increase the C_0 within the supersonic portion of the mixing zone (the flux quantities are monatomic and hence the value of C_0 is also). This incorrectly decodes as an increasing Mach number on the supersonic branch! This is represented in Figure 2.14.

This cannot be correct since the Mach number must monatomically decrease from supersonic to subsonic. Other primitive quantities are similarly effected, including local static pressure spikes.

What has happened? The "failure" of the model is caused by the singular behavior of the inversion function for M<<1, or incompressible flow. Equation (2.66) is not bounded for M→0, which in turn is a remnant of the fact that the state equation and the incompressible assumption

$$p = \rho RT \quad \rho = const. \tag{2.67}$$

cannot simultaneously hold. Of course, for a single regime, i.e. fully subsonic or fully supersonic flow, the singularity is irrelevant except for M=0, exactly. Hirsch (1988) and Anderson et al. (1984) also discuss a related issue, though, this is more of a question of computational expense when applying compressible flow algorithms to virtually incompressible problems.

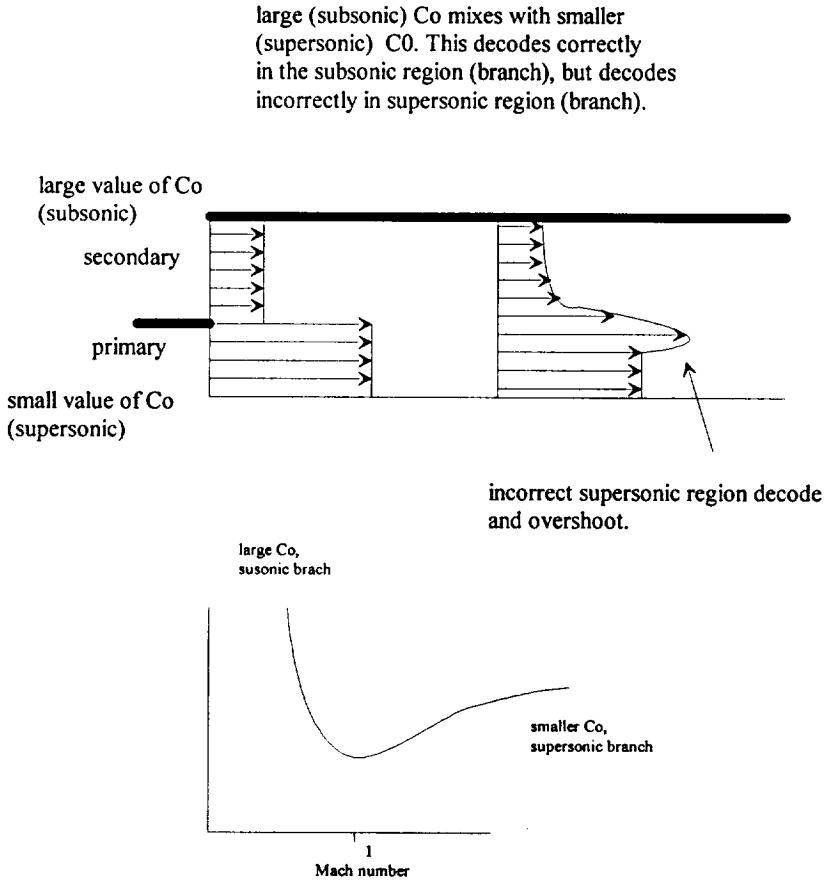

FIGURE 2.14 Primitive variable inversion failure for mixing transonic flow fields.

The problem encountered here is closely related to the departure solution phenomenon encountered for mixed subsonic and supersonic flow fields when solved by single pass parabolic Navier-Stokes solvers (Anderson et al. (1984)). In this type of primitive variable formulation, elliptic influences of the subsonic pressure field cause the development of negative eigenvalues and hence poorly posed, and unphysical solutions. These take the form of unphysical pressure fields. It was hoped, by the author, that this problem would have been eliminated in this study, by the choice of conservative variables, since the scalar eigenvalues of (2.44) a simple heat equation are indeed positive, but at a cost of a non-physical inversion.

2.4.3.2. A model problem for primitive variable inversion

Since the inversion problem is so closely related to the ill-posed behavior exhibited by space marching version of the parabolized Navier-Stokes equations (Anderson et al. (1984) or Vigneron et al. (1978)), it is useful to explore the use of transformations and subsequent inversion further. An appropriate way to do this is to consider a model equation (which is closely related to our problem). Consider the equation:

$$\left[1-\frac{1}{M^2}\right]\frac{\partial M}{\partial x}=\frac{\nu_{eff}}{U}\frac{\partial^2 M}{\partial y^2} \tag{2.68}$$

This is a scalar analogue to equations (2.44)-(2.47). Equation (2.68) exhibits two regimes a supersonic regime ($M\geq 1$) and a subsonic regime ($M\leq 1$). Examination of the lead coefficients indicate that equation (2.68) will not yield a physical relationship for the subsonic region, since this would imply, that initial conditions would grow in an unbounded fashion as the solution marches forward in space, i.e. a negative eigenvalue. Alternatively stated, for subsonic flow with local linearization the "viscosity"

$$\left[1-\frac{1}{M^2}\right]^{-1}\frac{\nu_{eff}}{U}\leq 0 \tag{2.69}$$

would be negative! This is contrary to our physical understanding of diffusive phenomena. Looking at a flux vector in this case "Mach flux" in the cross stream direction:

$$q_M=-\left[1-\frac{1}{M^2}\right]^{-1}\frac{\nu_{eff}}{U}\frac{\partial M}{\partial y} \tag{2.70}$$

would lead to the conclusion, that Mach number increases from low potential to high.. This would violate the second law of thermodynamics.

Since it is apparent, that the current formulation leads to unacceptable behavior for subsonic flow, it is necessary to consider alternatives. The alternative developed in this study was the recasting of equation (2.68) into conservation form, and the approximate modification of the viscous term. This lead to:

$$\frac{\partial}{\partial x}\left[M+\frac{1}{M}\right]=\frac{\nu_{eff}}{U}\frac{\partial^2}{\partial y^2}\left[M+\frac{1}{M}\right] \tag{2.71}$$

In this form, the governing equation is unquestionably well posed at least with respect to the linear diffusion of $M+1/M=G_{model}$. This modification is closely analogous to our linearization as shown by equation (2.44). Indeed by using the diffusion (or mixing) equation to predict G_{model} at all points in the flow field, a model inversion polynomial (analogous to equation (2.47)) may be formed:

$$G_{model} = M + \frac{1}{M} \qquad M = \frac{G_{model} \pm \left[G^2_{model} - 4\right]^{\frac{1}{2}}}{2} \tag{2.72}$$

which has the desired two roots corresponding to subsonic and supersonic shock phenomena. Unfortunately, though, well posed in terms of the linear diffusion operator and retaining shock phenomena does not imply well posed in a physical sense. This failure of the transformation becomes apparent when one considers a plot of G_{model} with respect to M. Once again this is analogous to Figure 2.13.

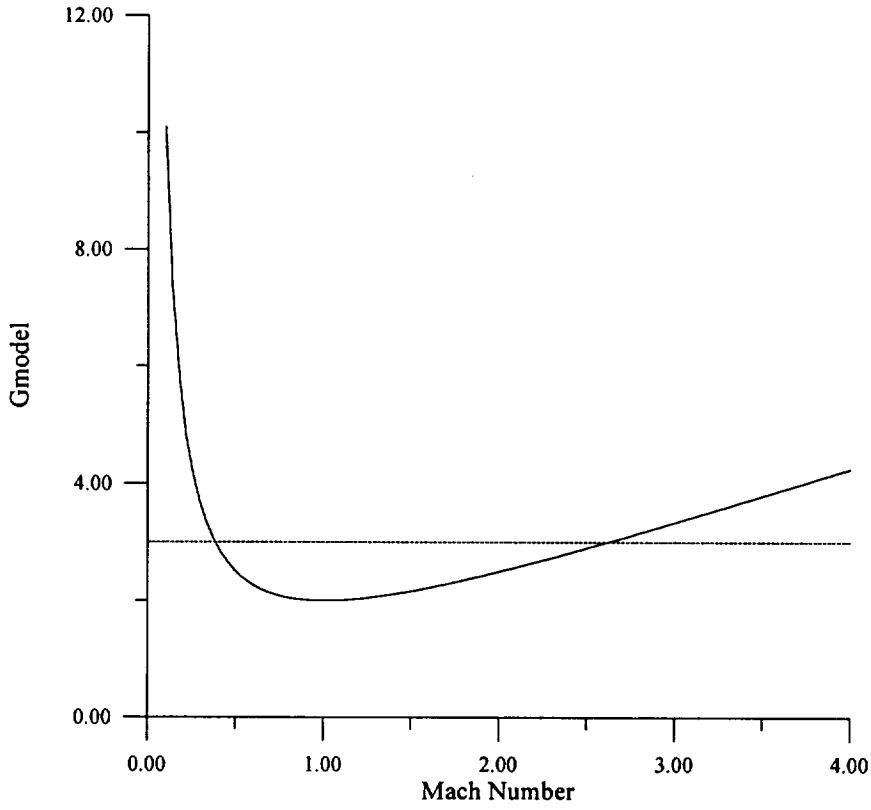

FIGURE 2.15 Characteristic inversion relationship for model problem.

From Figure 2.15 and motivated by our previous discussion, the limitation inherent with change of variables may be discussed. A special, but insightful problem is illustrated in the Figure 2.15. Here a subsonic Mach field left branch is mixed with a supersonic Mach field, right branch. If the case, where G_{model} is exactly the same, denote by the dashed line, is chosen we have the situation where G_{model} is constant, i.e. no mixing and yet in the untransformed problem we have a subsonic/supersonic mixing problem! Clearly, the transformation has failed to honor the monatomic behavior of the mixing problem. This is because the nonlinear transformation is double valued. It is apparent, that a double valued function will not satisfy the physical requirements needed for a monatomic mixing problem. This can be reinforced if one considers the G_{model} flux vector:

$$q_G = -\frac{\nu_{eff}}{U}\frac{\partial G_{model}}{\partial y} = -\left[1 - \frac{1}{M^2}\right]^{-1}\frac{\nu_{eff}}{U}\frac{\partial M}{\partial y} \tag{2.73}$$

So, in summary, the transformation yields a well posed diffusive problem in terms of G_{model}, but this does not guarantee a well posed formulation in terms of the primitive variables. Clearly, a non-linear transformation does not eliminate the difficult problem of modeling viscous, transonic flows using space marching methods. In passing it may be noted, that a potential solution to this dilemma is the introduction of an unsteady term, effectively modifying the form of the governing equation:

$$\frac{\partial M}{\partial t} + \left[1 - \frac{1}{M^2}\right]\frac{\partial M}{\partial x} = \frac{\nu_{eff}}{U}\frac{\partial^2 M}{\partial y^2} \tag{2.74}$$

Equation (2.74) is effectively, a hyperbolic-parabolic equation. It would require multiple pass relaxation to drive to a steady state; a highly inefficient procedure relative to single pass space marching. It is not clear, that even this formulation will lead to a well posed problem.

The basis for this concern comes from a simple analysis of this problem. One may linearize, equation (2.74), and solve by using separation of variables and the method of characteristics. The most important result of this analysis, is that for a supersonic problem the characteristic of the hyperbolic portion will take the form:

$$x = [1 - \frac{1}{M^2}]t + c_0 \qquad [1 - \frac{1}{M^2}] \geq 0 \tag{2.75}$$

This is a right running wave in the x-t plane. As per our intuition, signals (or initial condition information) are sent from upstream to down stream. Thus, this problem is considered to be well posed.

Alternatively, considering the subsonic problem, we must write:

$$x = -[1 - \frac{1}{M^2}]t + c_0 \qquad [1 - \frac{1}{M^2}] \leq 0 \tag{2.76}$$

which is viewed as a left running wave in the x-t plane. This type of propagation does not follow our intuition, in that it demands that the initial condition information be propagated downstream to upstream. Hence, under these conditions the inlet conditions (initial conditions) propagate right out of the solution domain. This is a consequence of the elliptic-like behavior (for a true elliptic problem, one would expect to have imaginary characteristics) where downstream influences propagate back upstream. This limitation is a direct consequence of treating the pressure term as a part of the flow field for subsonic regions. See Lighthill (1953) for a related discussion.

The solution to this problem used for parabolized Navier-Stokes (PNS) flows is to approximately, restrict the size of the static pressure gradient within the subsonic region. (For the model equation, this requires neglecting the 1/M term within the subsonic region of the flow. Fortunately this is a much better physical approximation for the real problem) This has the effect of modifying the non-linear function to be a single valued relationship. One the most successful methods was pioneered by (Vigneron et al. (1978)). By analogy with this work, a variation of this method has been applied to this analysis to define a new inversion technique that is viable for mixed flows. This method is developed subsequently.

2.4.3.3 Modified inversion

The modified inversion method requires limiting the size of the static pressure term in the inversion method of equations (2.65) and (2.66), within the subsonic region only. Hence, the momentum flux is modified:

$$G_{\text{mod}} \equiv \rho u^2 + \omega p \qquad \omega \equiv \frac{\gamma M^2}{1+(\gamma-1)M^2} \tag{2.77}$$

where, ω, is the "Vigneron" parameter (Vigneron et al. (1978)). The form of the parameter, ω, applicable for simple mixing flows is derived in Appendix E. Forming the analogous non-dimensional parameter to equation (2.66) yields:

$$C_{0m} \equiv \frac{(\rho u^2 + \omega p)^2}{(\rho u)(\rho u H)} = 4(\gamma-1)\frac{M^2\left(1+\frac{\gamma-1}{2}M^2\right)}{\left(1+(\gamma-1)M^2\right)} \tag{2.78}$$

and the corresponding inversion polynomial:

$$(\gamma-1)[(\gamma-1)-\frac{1}{2\widetilde{C}_{0m}}]M^4 + [2(\gamma-1)-\frac{1}{\widetilde{C}_{0m}}]M^2 + 1 = 0$$

$$\widetilde{C}_{0m} \equiv \frac{C_{0m}}{4(\gamma-1)} \tag{2.79}$$

Plotting equation (2.79) in the Figure 2.13, repeated here as Figure 2.16:

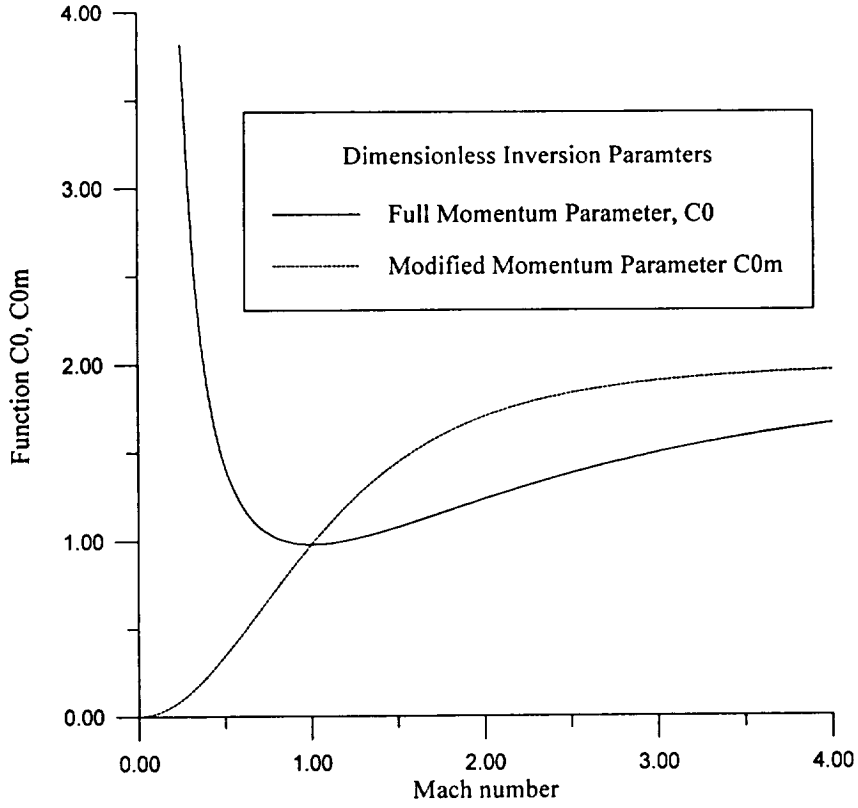

FIGURE 2.16 Characteristics of complete and modified primitive variable inversion relationships.

and observation of the form of the equation indicates that the this dimensionless parameter and the resulting inversion relationship are bounded for M→0. Further, the inversion is single valued and will prevent the unphysical behavior exhibit previously. This type of formulation will be used to model mixing flows. For this parameter to be available throughout the flow field requires that a new differential equation in terms of the modified momentum flux also be satisfied. Hence for mixed flows the vector of conservation quantities is now:

$$\phi(x,y) \equiv \begin{pmatrix} \rho u^2 + p \\ \rho u H \\ \rho u \\ \rho u^2 + \omega p \end{pmatrix} \tag{2.80}$$

For ejector flows, where the subsonic stream must accelerate, a slight modification of this model is necessary. This is due to the fact that the subsonic stream must be able to accelerate (due to the Fabri or aerodynamic choking phenomenon) to supersonic speed. Within the scope of one-d flow and the single valued inversion that has been developed, it is not possible to achieve this acceleration. The approximation introduced by the modification cannot be valid beyond the sonic point. The momentum field approximation, equation (2.77), must be relaxed and the complete momentum field is applied, for supersonic regions of the flow field. This is possible, since the governing equation for the complete momentum, ρu^2+p, is also solved. Hence it is "blended" into the flow field. This blending is accomplished using the function:

$$G_{eff} \equiv \left[1 - \tanh\left(\frac{x}{2x_c}\right)^2\right] G_{\text{mod}} + \tanh\left(\frac{x}{2x_c}\right)^2 G \tag{2.81}$$

where $G=\rho u^2+p$ and $G_{eff}=\rho u^2+\omega p$. This function is constructed to smoothly introduce the full momentum G. Indeed for $x>>x_c/2$, the choke location; G is completely recovered. Although the function is empirical, the basis for it is consistent with the first order approximations needed to model transonic flow using steady, marching equations.

Another closure that may be used at the Fabri choke point is to merely "jump" the solution to supersonic and complete inversion. This has been done successfully for several test cases and is described in Section 5. The inherent limitation in the governing equations, i.e. that wave phenomenon such as expansion and compression wave are not modeled is discussed in Section 5 also.

2.4.3.4 Flow regime and thermodynamic restrictions

Due to the existence of two possible solutions corresponding to supersonic and subsonic flows, determination of the locally appropriate solution type is critical. Actually the use of the modified pressure field, somewhat circumvents this problem, in that the modified inversion is single valued. Even with this modification, though, it is necessary to determine which flow field regions will be considered supersonic, since we always use the unmodified inversion method for supersonic regions (just like the classical space marching PNS problem) and use the modified pressure field only in the subsonic region. As such, the first situation: a supersonic and subsonic stream interacting due to turbulent mixing is considered.

Determination of flow field type for the mixed problem proceeds by considering the required value for the dimensionless parameters, C_0 and $C_{0,mod}$. Due to the formulation chosen, at the transonic point, these two relationships have the same value. This in fact, gives us the critical value for C_0 and $C_{0,mod}$:

$$C_0(M=1) = C_{0,\text{mod}}(M=1) = \frac{2(\gamma^2-1)}{\gamma^2} \tag{2.82}$$

This intersection point is shown clearly in Figure 2.16. Equation (2.82) is utilized by choosing a subsonic solution for (and the modified inversion polynomial) $C_{0,mod} \le C_{0,mod}(M=1)$. Conversely, one must choose the supersonic solution (and full inversion polynomial), for $C_{0,mod} \ge C_{0,mod}(M=1)$.

In addition to mixing of two streams, it is necessary to be able to identify thermodynamic restrictions placed upon both fully supersonic flow and fully subsonic flows. For these types of flow fields, the complete inversion polynomial is used. To understand the limitations on C_0 we may refer to Figure 2.16 or examine the solution types possible for equation (2.65), repeated here:

$$\left(\gamma^2 - \frac{\gamma^2}{2}C_0\right)M^4 + \left(2\gamma - \frac{\gamma^2}{\gamma-1}C_0\right)M^2 + 1 = 0 \quad C_0 \equiv \frac{\left(\rho u^2 + p\right)^2}{(\rho u)(\rho u H)} \tag{2.65}$$

This second degree polynomial, in terms of M^2, has the classical restrictions on the number of roots that are solutions which can be ascertained by applying Descartes Rule of Signs (Johnson and Riess (1982)). Here, we are looking for sign changes in the polynomial coefficients, indicating the existence of the number of solutions. Considering the restrictions for supersonic solutions, the demand can be made, that two possible solutions

(supersonic and the potential to shock down to subsonic flow) must exist. For two solution types it is necessary that two sign changes occur or that:

$$\left(\gamma^2 - \frac{\gamma^2}{2}C_0\right) \geq 0 \quad \Rightarrow C_0 \leq 2$$

$$\left(2\gamma - \frac{\gamma^2}{\gamma - 1}C_0\right) \leq 0 \quad \Rightarrow C_0 \geq \frac{2(\gamma - 1)}{\gamma} \tag{2.83}$$

The first condition is meaningful, the second condition is not permitted, since the minimum value for C_0, occurs for $C_0 \geq 2(\gamma^2\text{-}1)/\gamma^2$. Hence, it is apparent that for two solutions to exist, which imply supersonic flow, with the potential to shock down to subsonic flow, we must bound C_0, as follows: $2(\gamma^2\text{-}1)/\gamma^2 \leq C_0 < 2$. The use of this relationship is a criterion for determining the feasibility of fully supersonic flow. It can be seen graphically that indeed this must be the case, by referring to Figure 2.16.

Fully, subsonic flow, on the other hand, is less encumbered. Here, it is necessary to demand only a single change in sign of the relevant polynomial. With this restriction it is possible to require that the first term:

$$\left(\gamma^2 - \frac{\gamma^2}{2}C_0\right) \leq 0 \quad \Rightarrow C_0 \geq 2 \tag{2.84}$$

There is no upper bound on this branch, in that the subsonic branch is not well defined as $M \rightarrow 0$.

Summarizing the results of this section, a family of restrictions for the local inversion polynomials, which are in turn related to the local flow field conditions have been presented, as presented in Table 2.3.

Flow Field Type	Restriction upon $C_0 = \frac{(\rho u^2 + p)^2}{(\rho u)(\rho u H)}$
Mixed, supersonic/subsonic (i.e. transonic)	$C_{0,mod} \leq \frac{2(\gamma^2 - 1)}{\gamma^2} \Rightarrow$ subsonic
Fully supersonic	$2(\gamma^2-1)/\gamma^2 \leq C_0 < 2$
Fully subsonic	$C_0 \geq 2$

TABLE 2.3 Thermodynamic restrictions upon flow regime for the complete inversion relationship.

2.4.4 Quasi-1-d extensions

Although the above analysis is exact for 1-d flow fields, it is necessary to correct the problem for quasi-one-d flows caused by variable area shrouds, such as shown in Figure 2.17:

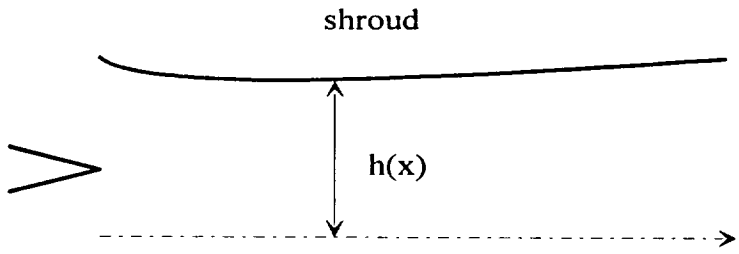

FIGURE 2.17 Variable area shroud geometry definitions.

To perform this correction two strategies are employed:

- Modification of the partial differential equation
- local quasi-1-d modifications to the local inversion scheme

The first modification involves scaling the dependent variable ϕ by h(x). Performing this substitution, the governing equation takes the form:

$$\frac{\partial \phi}{\partial x} = a(x)\frac{\partial^2 \phi}{\partial y^2} + \frac{h'(x)}{h(x)}\phi \tag{2.85}$$

The new term added here has the same structure as a quasi-1-d approximation. This term modifies the distribution of the conservative quantities, but it does nothing for local inversion process. Alternatively stated, the inversion from flux quantities to thermodynamic quantities is independent of changes of area. As an alternative to this situation, we consider the local control volume:

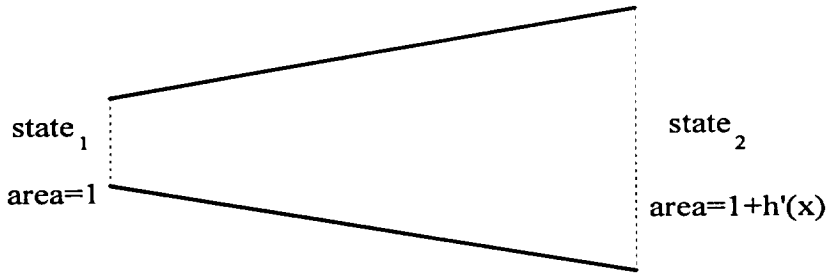

FIGURE 2.18 Variable area thermodynamic inversion method modification definitions.

Our task is to define a local process which takes the unmodified primitive quantity (M, p, T, u, ρ) as it is predicted by the decoding algorithm (state 1), and then execute an isentropic variable area expansion or compression to yield (state 2). For example, consider the Mach number predicted to be M_1 using the decoding algorithm. Now, applying the Mach number area expansion using:

$$\frac{1}{1+h'(x)} \equiv \frac{A_1}{A_2} = \frac{M_2}{M_1}\left[\frac{1+\frac{\gamma-1}{2}M_1^2}{1+\frac{\gamma-1}{2}M_2^2}\right]^{\frac{\gamma+1}{2(\gamma-1)}} \tag{2.86}$$

yields, M_2 the local Mach number with variable area shroud effects. Additional isentropic corrections are available for all static quantities using a similar control volume. Additional corrections are applied to the pressure term for very low Mach number flows, which are not uniformly retained by the isentropic model. This takes the form of modeling static pressure for low subsonic Mach numbers with a relationship of the form:

$$p = P_0 - \frac{1}{2}\rho u^2[1+\frac{1}{4}M^2+\ldots \tag{2.87}$$

Which is a compressible Bernoulli's type relationship.

2.5 Turbulence model

The basic turbulence model developed for this research is an extended, algebraic model loosely based upon Prantl's second hypothesis for turbulent free jet and mixing layer type flows. There is stronger relationship with the model proposed by Reichardt, as described in Schlichting (1979). This is a form of the classical self similar analysis described by Tennekes and Lumley (1972). The range of extensions to this model is rather considerable. They include:

(1) Formulation in terms of flux quantities, rather than primitive variables
(2) Near field analytical estimation of mixing constants and relationship to free shear layer mixing problems.
(3) Analytical prediction of incompressible mixing layer growth rates using a non-linear stability analogy.
(4) Semi-analytical estimation of compressibility effects upon mixing layer growth rates using a compressible vortex sheet model and non-linear stability analog.
(5) Far field or boundary dominated mixing effects.
(6) Vortical, 3-d, mixing enhancements due to the streamwise vorticity induced by lobed ejector/mixer nozzle configurations.

As can be seen, the turbulence model for this flow is a considerable portion of the overall development problem.

Tennekes and Lumley (1972) use the concept of self preservation or invariance to motivate their discussion on free shear layers (jets, mixing layers and wakes). The mathematical description for this type of "rule" would be termed "self similarity". Our development proceeds from a somewhat different direction without explicitly invoking self-preservation or invariance. Nonetheless, the analysis developed in this study recovers these classical results, as indeed it must. When working with algebraic formulations, one of the few "fundamental principles" one can use to try to understand turbulent flow is self preservation or invariance.

To avoid confusion, it should be emphasized that even though the turbulence model and governing mixing equations may be considered mathematically self-similar, the bounded internal flow that characterizes ejectors cannot be self similar due the existence of the boundaries themselves. This is the reason that it was not possible to solve the governing equations using some form of a similarity or Boltzmann (Bear(1972)) type variable. The fact that the local mixing behavior will be modeled using equations that are consistent with self similarity or self preservation is not at all inconsistent with this fact, since locally, the effect of the wall boundaries cannot be "sensed."

2.5.1 Two-dimensional mixing layer model

The basic two-dimensional shear layer model is described in this section. As indicated the basic model is an algebraic formulation in terms of an effective viscosity. Starting with the basic "near field" (boundaries are not yet important in this region of the flow) differential equation, a relationship may be drawn between the effective viscosity and the thickness of the mixing layer. The result of this is the elementary turbulence model:

$$\left(\frac{\nu_{eff}}{U}\right)_G = \frac{x}{2\eta_\infty^2}\left(\frac{\delta}{x}\right)^2 \varepsilon_G \qquad \eta_\infty \equiv erf^{-1}(0.99) \approx 1.82 \tag{2.88}$$

which is derived by analytically solving the partial differential equation:

$$\frac{\partial G'}{\partial x} = k\varepsilon_G \frac{\partial^2 G'}{\partial y^2} \qquad \left(\frac{\nu_{eff}}{U}\right)_G \equiv k\varepsilon_G$$

$$\varepsilon_G \equiv \frac{G_{10} - G_{20}}{G_{10} + G_{20}} \quad G = \overline{G} + G' \tag{2.89}$$

for a mixing layer with a 0.99 mixing thickness definition, i.e. $G(-\delta)=G_1$, $G(\delta)=G_2$. It is possible to formalize the method by solving this equation:

$$\phi = \overline{\phi} - \frac{1}{2}(\phi_{10} - \phi_{20})erf\left(\eta^*\right) \tag{2.90}$$

Evaluating this equation at $y=\pm\delta$ and subtracting yields:

$$\begin{aligned} 0.99\phi_{10} &= \overline{\phi} + \frac{1}{2}(\phi_{10} - \phi_{20})erf\left(\eta^*_\infty\right) \\ -0.99\phi_{20} &= \overline{\phi} - \frac{1}{2}(\phi_{10} - \phi_{20})erf\left(\eta^*_\infty\right) \\ \hline 0.99 \quad &= \qquad\qquad erf\left(\eta^*_\infty\right) \end{aligned} \tag{2.91}$$

from which one derives:

$$\eta^*_\infty \equiv erf^{-1}(0.99) \approx 1.82 \tag{2.92}$$

Finally, decomposing, η_∞ yields:

$$\left(\eta^*_\infty\right)^2 \equiv \left(\frac{\delta}{x}\right)^2 \frac{1}{2k\varepsilon_G} = (1.82)^2 \tag{2.93}$$

which provides the desired relationship between the effective viscosity and δ/x, the mixing layer spreading rate:

$$k\varepsilon_G = \frac{1}{2}\frac{x}{\left(\eta^*_\infty\right)^2}\left(\frac{\delta}{x}\right)^2 \tag{2.94}$$

It is clear from equation (2.94) that prediction of the turbulent viscosity is directly related to estimation (or empirical measurement) of the shear layer thickness, δ. A turbulent Reynolds number may also be written for

this problem. As indicated previously, the turbulent viscosity may be used to model heat transfer (energy transport) and mass transport by definition of appropriate turbulent Prandtl and Schmidt numbers (White (1991) or Williams (1988)).

Recall, that the basic equations were perturbed using $\varepsilon=(U_{10}-U_{20})/(U_{10}+U_{20})$. The above analysis for the effective viscosity was based upon ε_G. Though, we expect these small parameters to be of the same order of magnitude, it is possible to write the effect upon the turbulence model, which accounts for the $\varepsilon_G/\varepsilon$ in the momentum equation (1.22):

$$\frac{\partial}{\partial x}(\rho u^2 + p) = \left(\frac{\nu_{eff}}{U}\right)^*_G \left(\frac{\varepsilon_G}{\varepsilon}\right) \frac{\partial^2}{\partial y^{*2}}(\rho u^2 + p) \tag{2.95}$$

where from definition we write:

$$\left(\frac{\varepsilon_G}{\varepsilon}\right) = \left(\frac{G_{10} - G_{20}}{G_{10} + G_{20}}\right)\left(\frac{U_{10} + U_{20}}{U_{10} - U_{20}}\right) \approx 1 \tag{2.96}$$

It is not necessary to assume that the momentum scale and velocity scale ratio are O(1), i.e. $\varepsilon_G/\varepsilon \approx O(1)$. Since for any problem, ε_G and ε are both known, these scales are included in our analysis.

Now for clarity, the closure approximations from Section 1 are repeated:

$$\rho u'v' = -\left(\frac{\nu_{eff}}{U}\right)^*_G \frac{\varepsilon_G}{\varepsilon^{\frac{1}{2}}} \frac{\partial}{\partial y^*}(\rho u^2 + p) \tag{1.13}$$

and the turbulent energy closure:

$$\rho H'v' = -\left(\frac{\nu_{eff}}{U}\right)^*_G \frac{1}{\mathrm{Pr}_t} \frac{\varepsilon_G}{\varepsilon^{\frac{1}{2}}} \frac{\partial(\rho u H)}{\partial y^*} \tag{1.14}$$

and the turbulent mass term:

$$\rho v' = -\left(\frac{\nu_{eff}}{U}\right)^*_G \frac{1}{Sc_t} \frac{\varepsilon_G}{\varepsilon^{\frac{1}{2}}} \frac{\partial(\rho u)}{\partial y^*} \tag{1.21}$$

Clearly, to complete the mixing model, an analysis is needed to predict $(\nu_{eff}/U)^*$ and therefore δ/x. This development performed in the next section.

2.5.1.1 Kelvin-Helmholtz instability

Although the above equations relate spreading rate to the turbulent viscosity, it still relies on predictions of the shear layer spreading rate, δ/x. These predictions may be supplied using the classical, incompressible closure:

$$\delta = C_\delta \frac{(U_1 - U_2)}{(U_1 + U_2)} x \tag{2.97}$$

Physically, the spreading rate or mixing layer thickness may be defined by Figure 2.19.

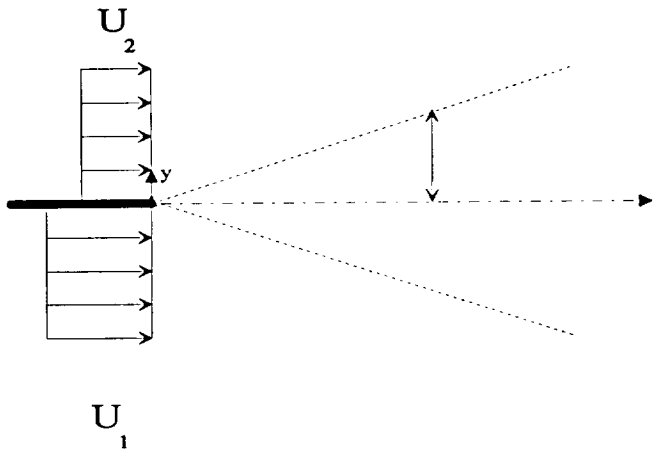

FIGURE 2.19 Shear/mixing layer definitions.

Though most work has developed this form using empirical or semi-empirical methods, here, a more formal theory based upon non-linear stability methods is developed here. We believe that this is viable, since the spreading rate for incompressible, turbulent mixing layers may be classically analyzed using dimensional reasoning and the concept of shear layer self-preservation, Tennekes and Lumley (1972), show that spreading rate, $\delta' \equiv d\delta/dx$, is a constant, hence, δ/x, is a constant as well. The goal of this section then is to predict, δ/x, for compressible and incompressible flows using a simple, yet analytically based method.

It should be stated, however, that this work is not by any means the final say in predictive models for 2-d mixing layers. This field has very significant depth and breadth. Methods to study this problem range from basic dimensional reasoning to direct simulation. It is claimed, though, that this analysis provides a structured basis for predicting the form of the spreading rate, as well as, yielding deriving a compressibility correction to the above spreading rate equation. Additionally, the analytical basis of the prediction is desirable, in that, the ejector/mixer design problem is considerably more complex than the simple two-dimensional, incompressible, semi-infinite shear layer described by equation (2.94). As such, any method developed here must be generalizable to more complex configurations.

A scaling model is developed for the growth rate of 2-D, compressible turbulent mixing layers. The basis of the development is the use of a time scale for growth of a dominant wavelength that is obtained using a nonlinear saturation time relationship with a temporal amplification factor obtained from quasi-unsteady, linear theory. The analysis extends to compressible flows by combining an unsteady, linear, vortex sheet

amplification factor and the same nonlinear theory. Results for compressible growth rates are in good agreement with experimental measurements and are expressed in terms of a convective Mach number.

What is perhaps most striking about turbulent, free shear layers is the remarkable degree of repeatable, large scale structures exhibited in their growth and development. This structure is well documented in the work of Papamoschou and Roshko (1988) and Brown and Roshko (1974). Tam and Chen (1979); Morris, et al. (1990) and Liou and Morris (1992) have attributed the appearance of well-defined large scale or coherent structures in the fully developed turbulence to the relatively well understood, deterministic, growth of small initial disturbances, which are often modeled by linear and nonlinear small disturbance theory. They have connected instability wave theory to fully developed turbulence and their results are in reasonable agreement with the experimental data. However, these analyses are complex and require a numerical computation of linear disturbance growth rates from an Orr-Sommerfeld equation or the inviscid Rayleigh equation, as well as the computation of eigenfunctions or amplitudes from an auxiliary relationship, most usually some form of the turbulent kinetic energy equation. These wave solutions are then related to turbulence using a superposition technique or a hypothesized closure. The method used here relates to the previous works but with a simpler scaling relationship. It is shown that the result is a model for the turbulent spreading rate that agrees with the data and lends itself to a generalized approach. A similar direct relationship between small disturbance growth rates and turbulent spreading rates is discussed by Lu and Lele (1994), however, they only provide a limited justification and model development.

The present model combines the temporal amplification factor (Drazin and Reid (1981)) and the concept of a nonlinear e-folding time (Youngs (1984), Andrews(1993)) to yield an estimate of the time required for the growth of the dominant wavelength. This temporal/spectral growth rate relationship is converted to a spatial estimate of the growth of mixing layer structures that determines the mixing layer spreading rate. The result of the analysis is a mathematical formulation for the mixing layer spreading rate that extends to compressible flows.

2.5.1.2 Linking linear stability with fully developed turbulence

Introducing an analogy with Morris, et al. (1990) turbulent fluctuations are related to linear disturbance amplification factors, s and $\tilde{\xi}$ as:

$$u' \equiv s\tilde{\xi}e^{\frac{sx}{U}} \quad ; \quad u' \equiv \beta_0 s\tilde{\xi}e^{\frac{sx}{U}} \tag{2.98}$$

$$u \equiv U + u' \ , \ v \equiv v' \ , \ U \equiv \frac{1}{2}(U_1 + U_2)$$

The constant, β_0, is to be determined later. The close relationship between the turbulent fluctuation closure in equation (2.97) and the linear disturbance theory developed in the next paragraph is deliberate.

The amplification rate, s, for a 2-D, incompressible, vortex sheet mixing layer may be obtained using perturbation potentials (Drazin and Reed (1981)) as:

$$s = -\frac{(U_1 + U_2)ki}{2} \pm \frac{k(U_1 - U_2)}{2} \tag{2.99}$$

Equation (2.99) shows that this flow is unconditionally unstable for any finite velocity difference.

With the small disturbance amplification rate available, the sizes of the turbulent fluctuations are determined using Equation (2.96). The closure given by equation (2.97) has two unknowns: the amplitude constant β_0 and the wave number k. The wave number k has dimension 1/length, however, a free shear layer has no defined length dimension except for the mixing layer thickness, δ. Thus the following relationship for the wavenumber is proposed:

$$k = \frac{2\pi}{\lambda} = \frac{2\pi}{\alpha_0 \delta} \tag{2.100}$$

where α_0 is a proportionality constant which is discussed later.

Specification of the wavenumber using the shear layer thickness is a key assumption of the present analysis, and may be motivated by considering the approximate rapid deformation (Arpaci and Larsen (1984)) simplification of the turbulent kinetic energy equation:

$$U\frac{\partial}{\partial x}\left(\frac{1}{2}u'u'\right) = -u'v'\frac{U}{\delta} \tag{2.101}$$

where $\Delta U=(U_1-U_2)/2$. Since equation (2.100) is in terms of the turbulent fluctuations, equations (2.97)-(2.101) may be combined to yield an ordinary differential equation for $\delta(x)$:

$$\frac{d}{dx}\left(k^2 e^{\frac{k\Delta U}{U}x}\right) = -2\beta_0 \frac{k^2}{\delta}\frac{\Delta U}{U} e^{\frac{k\Delta U}{U}x} \qquad k \equiv \frac{2\pi}{\alpha_0 \delta} \tag{2.102}$$

For analytical purposes, equation (2.102) is a complex nonlinear differential equation that cannot be directly solved. The complexity may be overcome if a suitable particular solution can be identified. From dimensional reasoning, the mixing layer width takes the functional form $\delta \propto x$. If the functional form of δ and k has been correctly postulated, equation (2.102) should collapse to an algebraic relationship between constants. Making the substitution:

$$\delta \equiv C_\delta \frac{\Delta U}{U} x \tag{2.103}$$

into equation (2.101), gives:

$$\beta_0 = C_\delta \tag{2.104}$$

Thus, the turbulent fluctuation and wave number closures, equations (2.97) and (2.103), are particular solutions of the turbulent kinetic energy equation. Equation (2.103) indicates that the magnitude of the cross-stream fluctuation, β_0 , is related to the shear layer spreading rate. This is plausible because cross-stream fluctuations should scale according to the only available cross-stream length scale δ.

The result in equation (2.104) indicates a strong connection between turbulent kinetic fluctuations and small disturbance stability theory. Further, the structure of the previous equations developed using dimensional considerations, has been shown to be correct. To close these equations, the constants α_0 and C_σ are evaluated in the next section.

2.5.1.3 Non-linear scaling model

The previous section showed that the equations describing the shear layer spreading rate satisfy the turbulent kinetic energy equation if an appropriate wave number closure is applied. The dimensional reasoning that provided an appropriate closure for the wave number also suggests that the development of large scale, coherent structures in these flows does not require the solution of the previous equations. Instead, a model for shear layer growth rate is derived by recognizing that the fundamental time and length scales are contained within the linear theory and the overall convective frame of reference. The benefit of this type of analysis is that the spreading rate function can be obtained for a very general class of problems without the burden of directly solving a more complete set of equations, such as the boundary layer or Navier Stokes equations.

Starting with the linear stability growth rate, equation (2.99), the e-folding time scale governing the growth of disturbances in the flow is $1/s_r$. N multiples of the e-folding time, is the time required for the dominant wavelength, λ_d, to appear. A constant of N for different wavelengths implies a coherency between the developing large scale flow structures that arises through the saturation of the amplitude growth rate of instabilities. These concepts are related to the buoyancy driven mixing flow and jet break up models empirically developed by Youngs (1984) and Andrews (1993), respectively. From a survey of experimental data, they estimated that $N \approx 9-10$.

The e-folding time is obtained from the real part of equation (2.99) as:

$$\tau_d \approx \frac{1}{s_r} = \frac{2}{k_d (U_1 - U_2)} \tag{2.105}$$

Similarities between supersonic and subsonic amplification factors mean it is not necessary to explicitly differentiate between supersonic and subsonic factors. Taking td=Ntd and further introducing the wave number definition k=2p/ld yields:

$$L = t_d U = \frac{\alpha l}{2\pi} \frac{2N}{U_1 - U_2} \frac{1}{2}(U_1 + U_2) \tag{2.106}$$

Introducing equation (2.105) into equation (2.106) and solving for δ/L yields:

$$\frac{l}{L} \equiv 2\delta' = \frac{2\pi}{\alpha N} \frac{(U_1 - U_2)}{(U_1 + U_2)} \tag{2.107}$$

Equation (2.107) provides a formula for the spreading rate of a 2-D incompressible shear layer.

Although equation (2.107) represents a complete relationship for the spreading rate, the wave number closure constant, α_0, has not been determined. No additional relationships are available to provide an exact determination of α_0. An estimate of α_0 can be ascertained by considering the saturation length scale, $L_{sat} \equiv L$. This length scale was previously estimated as $L=NU/s_r$ to arrive at equation (2.106). If it is recognized that the available local length scale in a shear flow is δ, then equation (2.107) may be written:

$$L \approx N\delta \approx \frac{\alpha_0 \delta}{2\pi} \frac{N}{U_1 - U_2}(U_1 + U_2) \tag{2.108}$$

Dividing both sides of equation (2.108) by $N\delta$ yields:

$$1 = \frac{\alpha_0}{2\pi} \frac{1}{U_1 - U_2}(U_1 + U_2) \tag{2.109}$$

which should be considered an order of magnitude relationship rather than a strict equality.

Now, if we recognize that the velocity ratio terms in equation (2.109) are bounded:

$$\leq \frac{(U_1 + U_2)}{U_1 - U_2} \leq \infty \tag{2.110}$$

Thus, for equation (2.109) to hold the term $\alpha_0/2\pi$ must be bounded by:

$$0 \leq \frac{\alpha_0}{2\pi} \leq 1 \quad \Rightarrow \quad 0 \leq \alpha_0 \leq 2\pi \tag{2.111}$$

This is still a wide bound. However, α_0 is expected to be a universal constant, virtually independent of initial conditions and flow conditions, and so may also be estimated from experimental measurements. Additionally empirical measurements indicate that α_0 will be O(1), so that the lower bound, i.e. $\alpha_0=0$ will never occur. Following Andrews (1993), and inspection of the experimental photography of Brown and Roshko (1974), an average wavelength versus amplitude ratio of the largest scales was measured. This is done by measuring the streamwise length between any repeating portion of the large scale structures. This length is then scaled by the local mixing layer half width giving the ratio λ/δ. This ratio is observed to be approximately 4.0, hence from equation (5), $\alpha_0=\lambda/\delta=4$. This value is used in the current work and is within the upper and lower bound of equation (2.111). We note with some satisfaction that the arithmetic average between the upper and lower bound, $\alpha_0=\pi$ is within about 20% of the experimentally measured value $\alpha_0=4$.

Equation (2.107) may be re-written:

$$2\delta = \frac{1}{2}\frac{\pi}{N}\frac{(U_1 - U_2)}{\frac{1}{2}(U_1 + U_2)} \tag{2.112}$$

so that Papamoschou and Roshko's (1988) constant density form of the convective velocity $U=U_c=(U_1+U_2)/2$ is apparent. Equation (2.112) reproduces the functional form of the incompressible spreading rate functions given by Papamoschou and Roshko (1988), Brown and Roshko (1974) and Abramovich (1963) as:

$$2\delta = C_\delta \frac{U_1 - U_2}{\frac{1}{2}(U_1 + U_2)} \tag{2.113}$$

The result of equation (31), yields a prediction of $C_\delta=\pi/2N$. Table 2.4 favorably compares this analytical predicted value with other values.

2.5.1.4 Compressibility effects upon turbulent mixing

In this section, the effect of compressibility on the spreading rate of the shear layer is discussed. It is our desire to use the same type of analytically based formulation as developed previously. Then an approximate extension the mixing layer relationship, which was used to relate the turbulent viscosity to the spreading rate, to handle turbulent flow.

	Analytical $C_\delta=\pi/2N$ $\alpha_0=4$	Brown and Roshko (1974)	Papamoschou and Roshko (1988)	Langely Curve
C_δ N=10	0.16	0.19	0.17	0.14
relative error		17.3%	7.6%	14.3%
C_δ , N=9	0.17	0.19	0.17	0.14
relative error		10.5%	0.0%	21.4%

TABLE 2.4 Proportionality constant, C_δ, for incompressible mixing layer spreading rate.

To relax the limitations of the quasi-steady theory used to compute the mixing layer relationship, the complete unsteady potential equations are considered (Pai (1959)):

$$\frac{M_i^2}{U_i^2}\left[\frac{\partial^2\phi_i}{\partial t^2} + 2U_i\frac{\partial^2\phi_i}{\partial x \partial t}\right] = -\beta_i^2\frac{\partial^2\phi_i}{\partial x^2} + \frac{\partial^2\phi_i}{\partial y^2} \tag{2.114}$$

The form of the incompressible solution suggests a normal mode solution and interface disturbance of the form (Drazin and Reid (1981)):

$$\phi_i = \tilde{\phi}_j(y)\, e^{ik(x-Ut)+st} \qquad \xi = \tilde{\xi}_j\, e^{ik(x-Ut)+st} \tag{2.115}$$

A Galilean transformation has been made using the average velocity $U=(U_1+U_2)/2$. This transformation affects the phase speed, but not the temporal growth rate s. Following the method of normal modes the functions described by equation (2.115) are substituted into equation (2.114) and the resulting boundary value problem is solved. Applying far field boundary conditions, the interface kinematic relationship and the compressible form of the pressure matching condition yields the dispersion relationship:

$$\frac{(s+ik\Delta U)^2}{a_1^2\sigma_1} = -\frac{(s-ik\Delta U)^2}{a_2^2\sigma_2} \quad ; \quad \sigma_i \equiv k\left(1-\frac{1}{a_i^2}\left(\pm\Delta u-\frac{is}{k}\right)^2\right)^{\frac{1}{2}} \tag{2.116}$$

where $\Delta U=(U_1-U_2)/2$. Miles (1958) solved equation (2.116) for "s" as:

$$s = -aki\left[M_c^2+1-(4M_c^2+1)^{\frac{1}{2}}\right]^{\frac{1}{2}} \quad , \quad M_c \equiv \frac{(U_1-U_2)}{2a} \tag{2.117}$$

We note, that this is a constant temperature solution. We may approximately relax the constant temperature restriction by introducing the correction term into (2.118) to yield:

$$s = -a\left(\frac{T_{01}}{T_{02}}\right)^{\frac{1}{2}} ki\left[M_c^2+1-(4M_c^2+1)^{\frac{1}{2}}\right]^{\frac{1}{2}} \quad , \quad M_c \equiv \frac{(U_1-U_2)}{2a} \tag{2.118}$$

The explicit relation for the temporal growth rate, equation (2.117), is used to find the fully turbulent spreading rate using the same coherency concepts developed previously, giving:

$$\frac{\delta}{L} = a\frac{\pi}{2\alpha_0 NU}\left[(4M_c^2+1)^{\frac{1}{2}}-M_c^2-1\right]^{\frac{1}{2}} \tag{2.119}$$

Equation (2.119) is normalized by the incompressible solution, equation (2.113), to give a compressibility correction:

$$\frac{\delta'}{\delta'_{inc}} = \frac{\left[(4M_c^2+1)^{\frac{1}{2}}-M_c^2-1\right]^{\frac{1}{2}}}{M_c} \tag{2.120}$$

This compressibility correction is for the spreading rate of 2-D mixing layers. It is dependent on the convective Mach number, M_c. Later, it is shown to be consistent with the experimental work of Papamoschou and Roshko (1988) and others.

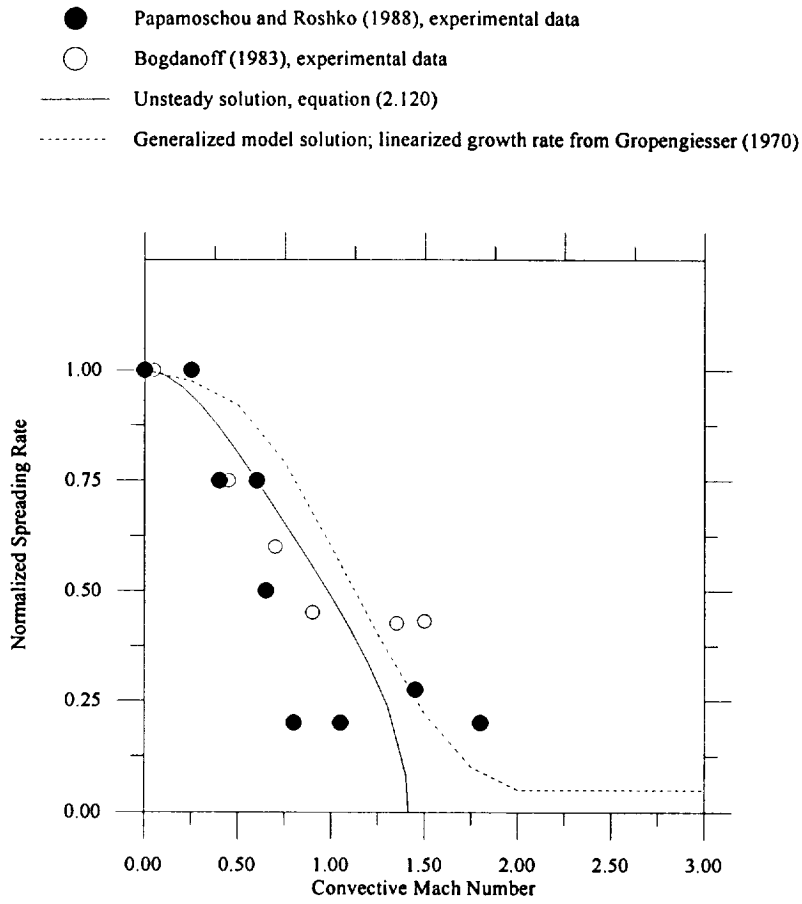

FIGURE 2.20 Normalized spreading rate comparison of theory to experiments.

Though, the formulation presented in Figure 2.20 is not valid for convective Mach number greater than $\sqrt{2}$ a simple piecewise construction has proven to be effective. This has been the methodology chosen by us to correct for the effects of compressible flow on turbulent mixing. To extend the model for these convective Mach numbers, we employ a piecewise constant extension to apply the solution for $M_c > \sqrt{2}$.

This analysis has done an adequate job in estimating the effect of compressibility upon the mixing layer thickness. This is the most important effect. A secondary effect of compressibility is to modify the mixing relationship used to relate the velocity mixing layer thickness to the momentum mixing layer thickness.

It is appropriate to move away from the incompressible equation (2.94) and consider the more general equation:

$$\rho \frac{\partial \phi'}{\partial x} = \varepsilon_\phi \frac{\partial}{\partial y}\left(\rho_0 k x \frac{\partial \phi'}{\partial y}\right) \qquad \varepsilon_G \equiv \frac{\phi_{10} - \phi_{20}}{\phi_{10} + \phi_{20}} \quad \phi = \overline{\phi} + \phi' \tag{2.121}$$

In this relationship, it is necessary to include the effect of the variable density term on the left hand side. To do this a modification of the Lee -Dorodnitsyn transformation:

$$\eta^* = \frac{\int_0^{y^*} \rho dy^*}{\rho_0 x} \tag{2.122}$$

is introduced, where y^* is our "stretched variable $y^*=\varepsilon y$. Employing this new similarity variable, will modify the governing equation to take the form:

$$\frac{d}{d\eta^*}\left(\frac{\rho}{\rho_0}\frac{d\phi'}{d\eta^*}\right) + \eta^*(k)^{-1}\frac{d\phi'}{d\eta^*} \tag{2.123}$$

Unfortunately, at this point it is not possible proceed without information concerning ρ/ρ_0. This is formally possible to model, by solving the energy equation or applying some kind of particular energy integral (Crocco-Busemann). Instead, we will "freeze" the parameter ρ/ρ_0. This term is then carried through the analysis and evaluated it at the appropriate time. Though this is by no means rigorous, it should capture the gross effects pressure gradient (at least better than linearizing at this point). Following this strategy, the above equation is solved to yield:

$$\phi = 1 + \varepsilon\, erf\left[\left(\frac{\rho}{\rho_0}k\right)^{\frac{1}{2}}\eta^*\right] \tag{2.124}$$

Following the same strategy used in the incompressible development, the solution is matched to the 0.99% free stream (unmixed) conditions. This defines δ the mixing layer half thickness. Applying this analysis yield the dimensionless number:

$$\eta^*_\infty = 1.82\frac{4}{\left[\left(\frac{\rho_1}{\rho_0}\right)^{\frac{1}{2}} + \left(\frac{\rho_2}{\rho_0}\right)^{\frac{1}{2}}\right]^2} \tag{2.125}$$

Which clearly collapses back to the incompressible value for constant density flows. This is consistent with our previous formulation.

2.5.5 Far field "boundary dominated" effects

The previously described turbulence model is based upon free shear (semi-infinite) flow domains. Clearly, this type of model is valid for an internal flow for short shroud mixing problems. To extend the previously

developed concepts, in a rigorous manner the spreading rate function is modified by invoking the turbulence kinetic energy equation:

$$U\frac{\partial k}{\partial x} = \upsilon_{eff}\left(\frac{\partial u}{\partial y}\right)^2 - C_d\frac{k^{\frac{3}{2}}}{l} \tag{2.126}$$

where the terms refer to: [transport]=[production]-[dissipation] (Arpaci and Larsen (1984)). By introducing the approximate closures: $k=(\Delta u\delta^*)^2$, $\delta^*=\delta/H$, $\nu_{turb}= \delta\Delta u$ and $l=H$, we may write:

$$\frac{d\delta}{dx} = C_\delta\varepsilon(1-\delta^{*2}) \quad \Rightarrow \quad \frac{\delta}{x} = \frac{\tanh(\varepsilon C_\delta x)}{x} \tag{2.127}$$

The solution of this elementary Riccati equation (Boyce and DiPrima (1965)) provides a limiting value to growth of the mixing layer thickness, i.e. $\delta_{max}<1$.

One limitation to this formulation, however, is that as $x\rightarrow\infty$, the $\delta/x\rightarrow 0$. This is an artifact of the derivation, since ν_{eff}/U_0 was derived based upon a near field (no wall influence relationship), i.e. equation (2.89). As such, we cannot expect the turbulence model developed here to be valid for very large values. It is possible to estimate the estimate the size of these large values by considering the streamwise value for which $\tanh(C_\delta x_{max})=0.99$. Solving for x_{max} yields:

$$x_{\max} = \frac{1}{C_\delta\varepsilon}\tanh^{-1}(0.99) >> 1 \tag{2.128}$$

Since this study is concerned principally with short shroud aerodynamic ejectors and the acceptable streamwise length is on the order of $15/\varepsilon$, this is seen to be a minor limitation.

2.5.6 Vortical mixing enhancements

Mixing within the ejector shroud is the key to satisfying noise constraints for high speed civil transport problems. Obtaining this mixing within a sufficiently short streamwise distance, which implies a short and therefore small weight penalty, is a key technology for the high speed civil transport program. Methods to obtain this goal involve the distortion of the splitter plate into a form that enhances mixing. This type of corrugated splitter plate is illustrated in the Figure 2.21:

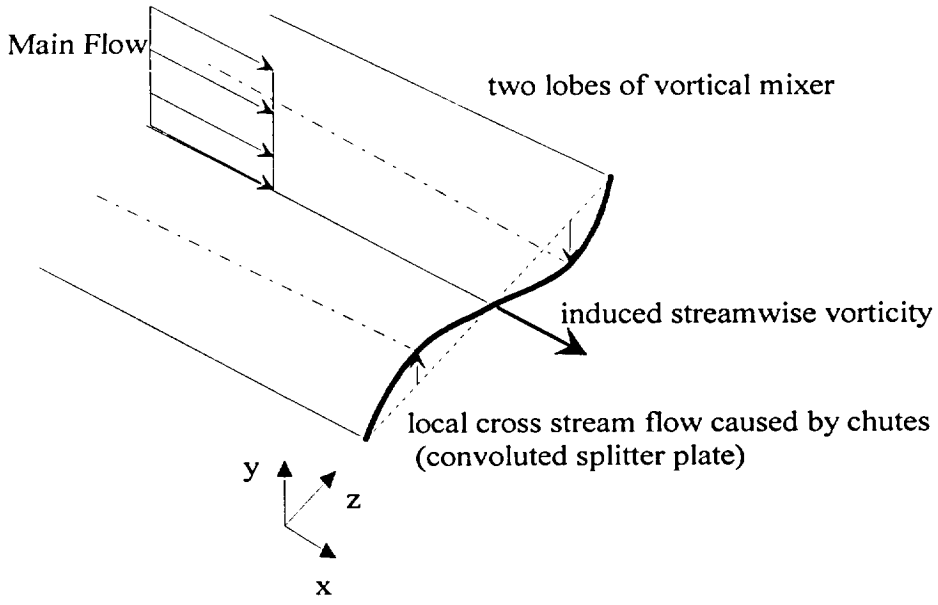

FIGURE 2.21 General vortical flow field definitions.

For a practical vortical mixer, these corrugations are greatly exaggerated and are often referred to as chutes.

The basic mixing enhancement mechanism caused by the introduction of convolutions is the formation of a rotational or vortical component. The axis of the resultant velocity vector is in the streamwise direction (or "x" direction); hence the rotational distortion is referred to as streamwise vorticity. The effect upon the fluid of the streamwise vorticity is the dramatic elongation of the interface i.e. mixing layer, which separates the two flows. This elongation and ultimate distortion of the mixing layer interface dramatically increases the "effective" two-dimensional mixing layer.

Since the model developed here is a strictly two dimensional approximation the introduction of this inclusion of the inherently three dimensional effects of vortical mixing would seem to be beyond the reach of this model. Fortunately, though, the three dimensional effects of vortical mixing can be mapped into an effective 2-d mixing layer. Our strategy to do this, is to model and predict the three dimensional interface elongation and distortion, then to use this solution to enhance the 2-d shear layer. Effectively, we are decoupling the 2-d mixing layer from the three-dimensional roll up. Though only a hypothesis, it seems to be a valid approach as discussed by Qui (1996), Fung (1996) and Marble (1985). Additionally, to introduce a model of greater complexity, would be to invalidate the scope of our current work which is a preliminary design tool.

The task, then is to develop a relatively simple model which predicts the behavior of the kinematic interface (or slipline) between the two mixing stream. Clearly, this roll up or twisting cannot proceed indefinitely. Ultimately, the interface must interfere with itself and with adjacent (and counter-rotating vortical cells. At this point, turbulent diffusive effects dominate and the roll up structures collapse onto themselves. This increase of interface, followed by a collapse mechanism, brings to mind an analogy with water waves breaking on a beach. The water wave surface or interface grows in an inviscid manner. Eventually, though, this growth steepens to a point where the wave can no longer hold itself. (and actually would become double valued). To prevent this double valued effect it is necessary introduce the concept of a normal shock or discontinuity. In reality of course, this breaking wave and discontinuity cannot occur without local smoothing due to viscosity. The mechanism described is one classically modeled by a Burgers equation (Anderson et al. (1984) or Logan (1987)).

Our modeling of the vortical mixing phenomenon uses the above breaking wave solution as an analogy. Proceeding, the governing equation for the interface problem is written (Drazin and Reid (1981)):

$$\cos\theta V_\theta = U_0 \frac{\partial \xi}{\partial x} - \sin\theta V_\theta \frac{\partial \xi}{\partial z} \tag{2.129}$$

where V_θ is the local rotational velocity caused by the streamwise vorticity. Geometry for this flow is shown in Figure 2.22.

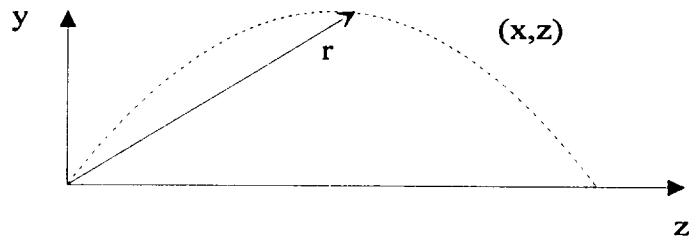

FIGURE 2.22 Vortical flow interface distortion definitions.

Now, very early in the flow, i.e. close to the splitter plate, where $\theta<<1$, the kinematic equation reduces to:

$$V_\theta = U_0 \frac{\partial \xi}{\partial x} \tag{2.130}$$

Integrating and replacing V_θ by an inviscid, point vortex solution, $V_\theta=\Gamma/2\pi r$, yields:

$$\xi_{near} = \frac{1}{U_0}\frac{\Gamma}{2\pi r}x \tag{2.131}$$

which is valid in the "near field". This relationship is approximate, in that near field roll up does not act like a simple vortex, hence we generalize:

$$\xi_{near} = \frac{C_{inv,vort}}{U_0}\frac{\Gamma}{2\pi r}x \tag{2.132}$$

where $C_{inv,vort}$ is a semi-empirical constant which takes the approximate value of about two.

Farther downstream, where interference effects will begin to dominate, it is no longer possible to utilize the near field solution. Here, we make a far field approximation valid for $\pi/2<\theta<2\pi$:

$$\cos\theta \approx -\frac{\xi}{z_0} \quad \sin\theta \approx -\frac{\xi}{z_0} \tag{2.133}$$

Substituting into the interface equation yields:

$$-\frac{\xi}{z_0} V_{\theta,i} = U_\theta \frac{\partial \xi}{\partial x} + \frac{\xi}{z_0} V_{\theta,i} \frac{\partial \xi}{\partial z} \tag{2.134}$$

This equation is a damped non-linear wave (Logan (1978)). It is necessary to be able to model the left hand side of this equation. To do this a Reynolds stress analogy is applied, yielding:

$$-\frac{\xi}{z_0} V_{\theta,i} \approx \nu_{eff,vort} \frac{\partial^2 \xi}{\partial z^2} \tag{2.135}$$

The effective, vortical kinematic viscosity will be estimated later. Accepting this new closure, equation (2.129) may be rewritten:

$$U_\theta \frac{\partial \xi}{\partial x} + \frac{\xi}{z_0} V_{\theta,i} \frac{\partial \xi}{\partial z} = \nu_{eff,vort} \frac{\partial^2 \xi}{\partial z^2} \tag{2.136}$$

This is a classical Burgers equation.

Solution of the Burgers equation, given sufficiently simple boundary conditions turns out to be straightforward. To illustrate this, we consider a canonical problem of the form:

$$\frac{\partial u}{\partial t} + u\frac{\partial u}{\partial x} = \nu \frac{\partial^2 u}{\partial x^2} \tag{2.137}$$

where, u, represents any general scalar variable. Now if we have the boundary conditions: $u(-\infty)=u_{near}$ and $u(\infty)=u_{far}$,, presented in Figure 2.23.

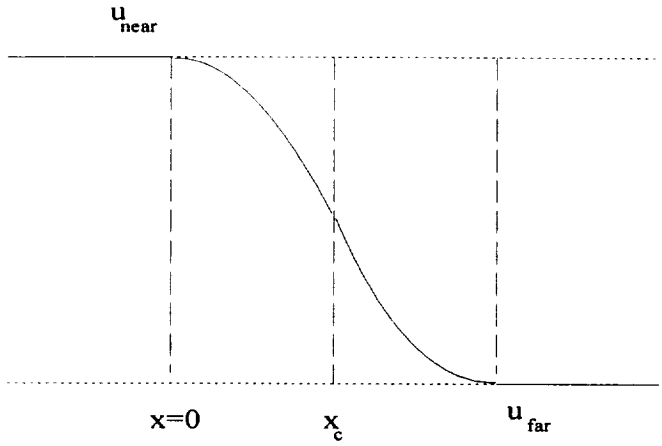

FIGURE 2.23 Breaking wave analogy model for vortical flow definitions.

It may be noted, that for these boundary conditions to make sense for our physical problem, that we must translate the problem downstream some amount x_c. See Figure 2.23. With these conditions, a traveling wave solution is possible, hence we search for a traveling wave similarity solution of the form:

$$u(x,t) = f(t - kx) \equiv f(s) \tag{2.138}$$

where k is computed as a part of the solution. Substituting yields the ordinary differential equation:

$$f' - kff' = \nu k^2 f'' \tag{2.139}$$

Integrating this equation twice and applying the associated boundary conditions yields:

$$u = \frac{u_{near} + u_{far} e^{\alpha s}}{1 + e^{\alpha s}} \qquad \alpha = \frac{(u_{near} - u_{far})}{2\nu k} \tag{2.140}$$

From the far field conditions, we obtain, $k=2/(u_{near}+u_{far})$.

From the above equation, we can return to the actual physical problem by noting, $x-x_c=z_0/V_{\theta,i}\, z$, $t=x/U_0$, $\nu=\nu_{eff,vort}\,(z_0/V_{\theta,i})^2$ and $u=\xi$. With these conditions the above equation becomes:

$$\xi = \frac{\xi_{near} + \xi_{far} e^{\alpha s}}{1 + e^{\alpha s}} \qquad \alpha s = \frac{1}{4} \frac{(\xi_{near} - \xi_{far})(\xi_{near} + \xi_{far}) v^2{}_{\theta,i}}{\nu_{eff,vort} z^2{}_0} \frac{(x - x_c)}{U_0} \tag{2.141}$$

It is helpful to associate the unknown x_c, with a "shock location," a location of rapid collapse of our vortical system. The shock location is found by noting that at x=0, $\xi \cong 0.99\xi_{near}$. It is worth noting the similarity with a 99% boundary layer thickness definition. If this is the case, it is possible to write the non-linear equation:

$$0.99\xi_{near} = \frac{\xi_{near} + \xi_{far} e^{\alpha s_c}}{1 + e^{\alpha s_c}} \qquad \alpha s = -\frac{1}{4}\frac{x_c}{U_0}\frac{(\xi_{near} - \xi_{far})(\xi_{near} + \xi_{far})v^2{}_{\theta,i}}{\nu_{eff,vort} z^2{}_0} \tag{2.142}$$

Which is a non-linear equation for x_c.

To proceed, it is necessary to associate the near field ξ_{near} constant, with our near field solution:

$$\xi_{near} = \frac{1}{U_0}\frac{\Gamma}{2\pi r}x \tag{2.143}$$

It is worth commenting that although the above analysis required a constant near field solution, we have approximately extended the analysis to include the variable function. If the previous analysis is to be suitable, it is certainly not possible to merely substitute the previous equation into our shock layer computations. Instead it is necessary to define a maximum value for equation (2.413). This maximum is related to the early linear growth phase, followed by the shock decay. This maximum is denoted as ξ_{max}.

$$x_c = -4\frac{U_0 \nu_{eff,vort} z^2{}_0}{(\xi_{\max} - \xi_{far})(\xi_{\max} + \xi_{far})v^2{}_{\theta,i}} \ln\left[\frac{0.01\xi_{\max}}{0.99\xi_{\max} - \xi_{far}}\right] \tag{2.144}$$

It is necessary to further, modify the initial interface function to include the additional surface area associated with the corrugations of the mixing layer. This will occur even in the absence of vortical mixing, i.e. Γ=0. This initial interface length will ultimately be damped out by viscous/turbulent mixing. To account for this effect we include an exponential decay term, which scales according to turbulent mixing only. Writing this additional interface length term:

$$\xi_{initial} = \xi(0) e^{-\frac{1}{2}\frac{\nu_{turb}}{U_0}\left(\frac{x}{\lambda}\right)^2} \tag{2.145}$$

Finally, the far field solution, is characterized by no stretching of the interface, hence ξ_{far}=0. Clearly, this will simplify the previous equations dramatically.

The above relationships contain the unknown ξ_{max}. This unknown is associated with our critical location formula, equation (2.144). It is now necessary to compute ξ_{max}, and x_c. This may be achieved if we consider the shock location and breaking phenomenon, to be a patching between an initial solution (our near field equation) and the far field. For a steep shock front, this is a reasonable approximation. Mathematically, this patching takes the form:

$$\xi_{\max} = C_{inv,vort}\frac{v_{\theta,i}}{U_0}x_c \tag{2.146}$$

where equation (2.144) has been rewritten:

$$x_c = 18.38 \frac{U_0 \nu_{eff,vort} z^2{}_0}{\xi_{max}{}^2 \nu^2{}_{\theta,i}} \tag{2.147}$$

Solving for ξ_{max} yields:

$$\xi_{max}{}^3 = 18.38 C_{inv,vort} \frac{\nu_{eff,vort} z^2{}_0}{\nu^2{}_{\theta,i}} \tag{2.148}$$

To complete the solution, it is necessary to model the effective vortical viscosity term. We choose to use the average velocity and the initial lobe heights as relevant length and velocity scales; $\nu_{eff,vortical}=C_0U_0z_0$. C_0 is a semi-empirical constant related to the number of vortical rotations that we might expect before collapse of the defined interface structure. It's value is approximately 16.-32. With this closure, it is possible to write the maximum interface height in a standard non-dimensional form:

$$\frac{\xi_{max}}{\lambda} = \left[\frac{C_{inv,vort}}{2} 18.38 \left(\frac{U_0 \lambda}{\Gamma} \right) \right]^{\frac{1}{3}} \tag{2.149}$$

This non-dimensional form is significant, in that this relationship between interface maximum distortion and vortical Reynolds number ($Re_{vort}=\Gamma/U_0\lambda$), has been observed from the full Navier-Stokes, computational experiments of Elliott et al. (1992) and Fung (1995), as the appropriate scaling law for strong vorticity flows. We have grossly reproduced a composite of their figures, to exemplify this relationship. This is presented in Figure 2.24:

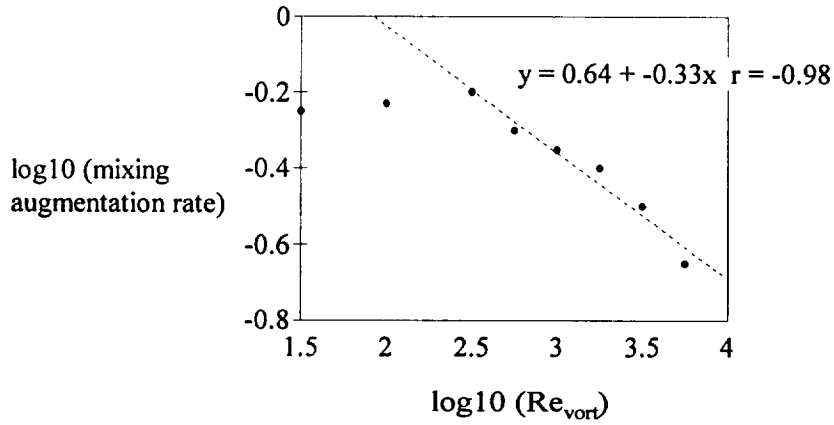

FIGURE 2.24 Scaling law from the Navier Stokes computations of Qui as reported by Elliott et al. (1992) and Fung (1995).

In our work, of course, the mixing augmentation rate is associated with ξ_{max}/λ. Hence from equation (2.149) it is apparent that we have reproduced the high vortical Reynolds number regime functional

relationship, i.e. the power of -1/3. It is gratifying, that our coarse, analogy based model has recovered this dependence.

At this point, our development of the function describing the shape of the interface separating the two streams is complete. It is necessary, to estimate the surface area of an elemental strip of the vortically mixed interface surface. This is formally done by computing an integral of the form:

$$\frac{dS}{dx} = \int 1 + \left[\left(\xi(x,z) \right)^2 \right]^{\frac{1}{2}} dz \tag{2.150}$$

Since the interface function is essential only a function of x, the integral may be approximated on a per lobe basis:

$$\frac{1}{\lambda}\frac{dS}{dx} = \frac{dS^*}{dx} = \left[1 + \left(\xi(x,z) \right)^2 \right]^{\frac{1}{2}} \tag{2.151}$$

As a summary, it is desirable to collect the pieces of our analysis which consist of the:

- -the interface growth and decay
- -shock location and initial maximum
- -and the initial interface function.

Combining one obtains the final relationship:

$$\frac{dS^*}{dx} = \left[1 + \left(\frac{\frac{4}{\pi}t^* + \xi_0(x)}{1 + \exp\left(\left[110.98 \left(\frac{\Gamma}{U\lambda} \right) t^* \right]^{\frac{1}{3}} + \ln(0.01) \right)} \right)^2 \right]^{\frac{1}{2}} \tag{2.152}$$

$$t^* \equiv \left(\frac{\Gamma}{U\lambda} \right)\left(\frac{x}{\lambda} \right) = Re_{vort}\left(\frac{x}{\lambda} \right)$$

where:

$\xi_0(x)$ = Additional surface area length due to splitter plate corrugations
λ = lobe wavelength
Γ = streamwise vorticity circulation
h_0 = total height of offset
$C_{vort,inv}$ = 2.0

as, shown in Figure 2.25. The initial wave length relationship takes the form:

$$\xi_0(x) = \xi'(0) e^{-\frac{1}{2}\frac{v_{turb}}{U_0}\left(\frac{x}{\lambda}\right)^2} \approx \pi\left(\frac{h_0}{\lambda}\right) \exp\left[-8\alpha\left(\frac{x}{\lambda}\right)^2\right] \tag{2.153}$$

where, this α:

$$\alpha \equiv 0.1543\left(C_\delta\right)^2 \left(\frac{1 - \frac{u_{20}}{u_{10}}}{1 + \frac{u_{20}}{u_{10}}}\right) \tag{2.154}$$

which may be recognized to be an incompressible simplification of the mixing layer growth rate equations.

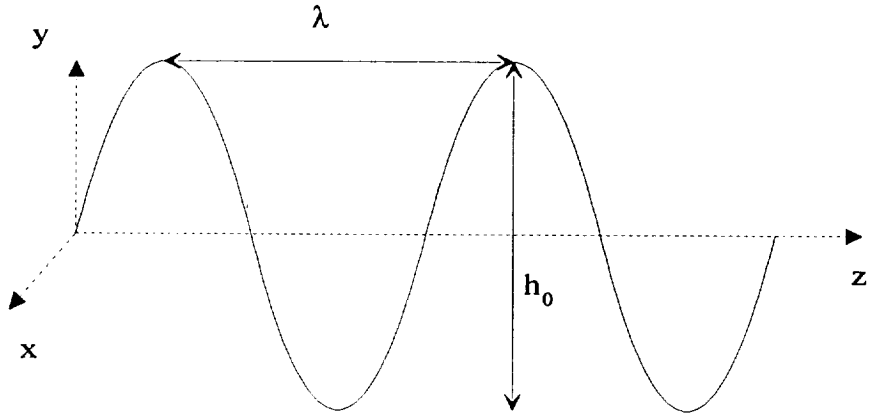

FIGURE 2.25 Vortical flow geometry input parameter definitions.

Finally, to close the above relationships, the vortical circulation, Γ, or more importantly it's non-dimensional form, must be estimated. The vortical Reynolds number Re_{vort} is related to the chute geometry using the inviscid/continuity relationship of Skebe and Barber (1988):

$$\mathrm{Re}_{vort}\left(\frac{\lambda}{h_0}\right) = 2\left[\frac{U_{10}\tan\alpha_1 + U_{20}\tan\alpha_2}{U_{10} + U_{20}}\right] \tag{2.155}$$

This is the major effect of vortical mixing. We also hypothesize an additional effect upon the 2-d shear layer thickness δ. It is expected that the addition of streamwise vorticity in addition to causing greater surface area will be to increase the spanwise vortical effects. The "equivalence" of this effect to the streamwise vorticity is motivated by considering a 3-d vortex sheet equation:

$$\frac{M_i^2}{U_i^2}\left[\frac{\partial^2\phi_i}{\partial t^2}+2U_i\frac{\partial^2\phi_i}{\partial x\partial t}+2V_{z,i}\frac{\partial^2\phi_i}{\partial z\partial t}\right]=$$

$$=(1-M_i^2)\frac{\partial^2\phi_i}{\partial x^2}+(1-M_{z,i}^2)\frac{\partial^2\phi_i}{\partial z^2}-2U_i V_{z,i}\frac{\partial^2\phi_i}{\partial z^2}+\frac{\partial^2\phi_i}{\partial y^2} \tag{2.156}$$

To compute the unsteady growth rate as in Section 2.5.4 it is necessary to introduce a normal mode solution that takes the form:

$$\phi_i=\tilde{\phi}_j(y)\,e^{ik(x+lz-Ut)+st} \qquad \xi=\tilde{\xi}_j\,e^{ik(x+lz-Ut)+st} \tag{2.157}$$

Where l, is a dimensionless wave number for disturbances in the z direction. At this point, one can perform virtually the same analysis as in Section 2.5.4 to obtain:

$$\frac{\left[s+ik(\Delta U+\Delta V_z l)\right]^2}{a_1^2\sigma_1}=-\frac{\left[s-ik(\Delta U+\Delta V_z l)\right]^2}{a_2^2\sigma_2} \tag{2.158}$$

From this equation, the "equivalence" of disturbances due to shear, whether due to the mixing layer, ΔU, or due to vortical effects, ΔV_z is apparent at least within the scope of the vortex sheet formulation.

Physically, it is possible to use a schematic of a single vortex and the hypothesized equivalent forms to help motivate the previous mathematical structure as shown in Figure 2.26:

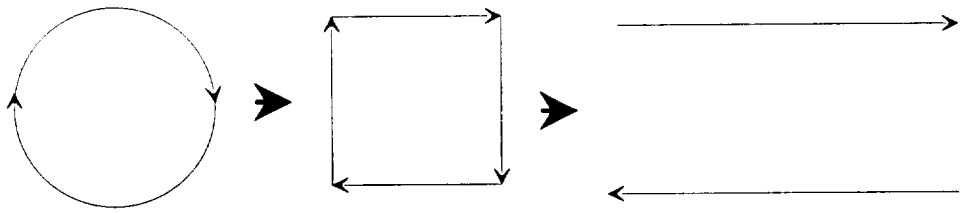

FIGURE 2.26 Mixing layer enhancement due to vortical interaction model.

Using the development, we estimate $V_z=2U_{ave}Re_{vort}$. This approximation is used to both modify the convective Mach number, as well as modify the expected closure for δ. Finally, we state that this modification goes along with at least the authors intuition, that vortical enhancement is not merely the wrapping and distorting of a 2-d mixing layer sheet, but that the growth rate of the sheet, i.e. $\delta(x,z)$, is modified by the vortical enhancement.

2.6 Wall friction and heat transfer

To develop a complete simulation tool the effects of friction and heat transfer are included in the analysis in an approximate manner. This takes the form of assessing compressible, turbulent skin friction and (through

Reynolds analogy) heat transfer losses. These are reflected in the governing equations through a wall loss term:

$$\frac{\partial G_{wall}}{\partial y} = \frac{\partial (\rho u^2 + p)_{wall}}{\partial y} = \frac{\frac{1}{2}\rho_{ave} u_{ave}^2 C_f}{h(x)} \tag{2.159}$$

The skin friction closure is compute through a locally fully-developed, locally adiabatic, internal skin friction relationship developed by De Chant (1993). This implicit relationship takes the form:

$$\frac{\sqrt{2}}{C_f^{1/2}} \frac{\arcsin(1-a^2)^{1/2}}{a} = \frac{1}{\kappa}\ln\left(\mathrm{Re}_h C_f^{1/2}\right) + \frac{1}{\kappa}\left(\frac{\sqrt{2}}{2}(1-a^2)^{\frac{1}{2}(1+2\omega)}\right) + (B - \frac{1}{\kappa}) + \tag{2.160}$$

$$-\frac{1}{\kappa}\ln\left(1 + 0.3(\frac{\kappa}{h})\mathrm{Re}_h C_f^{1/2}(1-a^2)^{\frac{1}{2}(1+2\omega)}\right)$$

where:

$$a^2 = r\frac{\gamma - 1}{2} M_{ave}^2 \frac{T_{ave}}{T_{wall}} \tag{2.161}$$

and $Re_h=Uh/\nu_{wall}$, B=5.5, κ=0.4, ω=0.76, the power law exponent for the air viscosity and r=recovery factor and for turbulent flow, this takes the form: $r=Pr^{1/3}$ (White (1974)).

2.7 Theoretical conclusions

This section has described and developed the mathematical models used to provide an ejector mixer-nozzle analytical tool. At this point, it is worth summarizing. Section 1, provided the basic conservation equations using formal perturbations methods. Section 2, developed the initial condition models, a combined numerical/analytical decomposition solution method and the necessary turbulent closure. Coming up are Section 3, discussing numerical methods, and Section 4, which outlines "in house" experiments associated with the ejector. Finally, Section 5 compares the model to experimental results and provides conclusions and recommendations.

3. NUMERICAL METHODS

Section 3 discusses the numerical methods used to solve the governing equations developed in the previous section. Since a heavy emphasis has been placed upon analytical developments, these models are relatively simple. In spite of this simplicity there are some relevant and interesting here, especially, the higher order differential equations solver.

3.1 Introduction and motivation

Implicit finite difference relationships and their use in solving 1-d parabolic partial differential equations are developed and discussed. Differencing methods of this form have high accuracy in terms of truncation error, while requiring limited support. This type of formulation has been applied to a high efficiency, combined analytical/numerical fluid flow model. Since the flow model has been derived such that a relatively simple, linear, scalar parabolic equation governs the flow; it is appropriate to develop the numerical methods for a general, scalar heat equation. Methods to resolve initial condition singularities in the physical problem are discussed. The streamwise marching portion of this problem is differenced using both Crank-Nicolson and a three point backward fully implicit method. Stability of the implicit finite difference/Crank-Nicolson method is analyzed using von Nuemann's method. Heuristic extensions are drawn for the three point backward approach. A brief discussion of the method for inversion of the linear system characterizing the implicit difference methods is also included. Finally a comparison of strengths and weaknesses and recommendations for further research for implicit differencing method are presented.

Hirsch (1988) defines implicit finite difference formulas as expressions where derivatives at different mesh points appear simultaneously. Relationships of this form have high accuracy in terms of truncation error, while only requiring limited support. For this reason, this type of formulation is rather attractive for our actual research problem, namely, a high efficiency, combined analytical/numerical fluid flow model. The model has been derived such that a relatively simple, linear, scalar heat equation governs the flow. It is then appropriate to develop the numerical methods for a scalar heat equation. The marching portion of this problem is differenced using relatively standard techniques. Both Crank-Nicolson and a three point backward fully implicit method have been employed. These methods have a lower order truncation error, but are A-stable as defined by Ferziger (1981). A further rational beyond stability concerns for the combined approach of high accuracy differencing in the cross stream (spatial) coordinate and lower accuracy in the streamwise (effective temporal) coordinate is that the physical problem has very rapid changes in the cross-stream direction (the actual initial condition is modeled as a Heaviside step function) and relatively gentle changes in the streamwise direction.

An outline of our discussion:

- Derivation and general discussion of a variable step, compact, implicit finite difference algorithm applied to a general, linear heat equation. Relationships to other methods are also considered.
- Resolution of singular behavior: tension spline bases and analytical decomposition.
- Conservative (finite volume) implicit differences.
- Streamwise differencing and von Neumann stability analysis of a heat equation.
- Block tridiagonal matrix solution algorithm.

Having described the numerical methodology, some recommendations on current and future uses of these techniques as wazzu compared to other methods are made.

3.2 A variable step compact implicit finite difference algorithm

As indicated in the introduction, Hirsch (1988) defines implicit finite difference formulas as expressions where derivatives at different mesh points appear simultaneously. These methods have high accuracy with limited, here three point, support. Many methods and associated terminologies have be used to derive implicit formulas

for derivatives, including compact methods Kreiss (1973) and Hirsch (1975), spline methods, Rubin and Khosla (1977), and Mehrstellen or Hermitian for their relationship to Hermitian finite elements, Collatz (1966). As pointed out by Hirsch (1988) or Peyret and Taylor (1984), formulas of this type may be systematically developed using Taylor series methods. This approach is followed, except it is generalized to variable grid spacing.

Considering only the right hand side portion of the linear, 1-d, constant coefficient, parabolic partial differential equation

$$\frac{\partial \phi}{\partial x} = a\frac{\partial^2 \phi}{\partial y^2} + b\frac{\partial \phi}{\partial y} + c\phi + d \tag{3.1}$$

implicit formulas for the "y" derivative terms on a variable grid spacing are developed for some function f (where clearly f≡ϕ). Referring to Figure 3.1 the variable grid is defined.

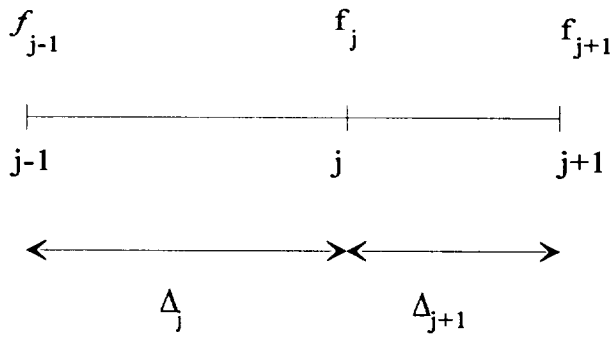

FIGURE 3.1 Variable grid definitions.

Beginning by writing the Taylor series expansion for f'':

$$f''_{j-1} = f''_j - \Delta_j f'''_j + \frac{1}{2}\Delta^2_j f^{(4)}_j - \frac{1}{6}\Delta^3_j f^{(5)}_j + \frac{1}{24}\Delta^4_j f^{(6)}_j + O(\Delta)^5 \tag{3.2}$$

$$f''_{j+1} = f''_j + \Delta_{j+1} f'''_j + \frac{1}{2}\Delta^2_{j+1} f^{(4)}_j + \frac{1}{6}\Delta^3_{j+1} f^{(5)}_j + \frac{1}{24}\Delta^4_{j+1} f^{(6)}_j + O(\Delta)^5 \tag{3.3}$$

Combining terms in equations (3.2) and (3.3), yields:

$$\frac{\Delta_{j+1}f'_j+\Delta_j f'_{j+1}}{\Delta_{j+1}+\Delta_j} = f'_j+\frac{1}{2}\Delta_j\Delta_{j+1}f^{(4)}_j+\frac{1}{6}\Delta_j\Delta_{j+1}(\Delta_{j+1}-\Delta_j)f^{(5)}_j+$$

$$+O(\Delta)^4 \tag{3.4}$$

Now, it is desired to eliminate the second order term, to yield a higher order relationship. Consider the function f, expanded in Taylor series:

$$f_{j-1} = f_j-\Delta_j f'_j+\frac{1}{2}\Delta^2_j f''_j-\frac{1}{6}\Delta^3_j f'''_j+\frac{1}{24}\Delta^4_j f^{(4)}_j-\frac{1}{120}\Delta^5_j f^{(5)}_j+$$

$$+O(\Delta)^6 \tag{3.5}$$

$$f_{j+1} = f_j+\Delta_j f'_j+\frac{1}{2}\Delta^2_j f''_j+\frac{1}{6}\Delta^3_j f'''_j+\frac{1}{24}\Delta^4_j f^{(4)}_j+\frac{1}{120}\Delta^5_j f^{(5)}_j+$$

$$+O(\Delta)^6 \tag{3.6}$$

Equations (3.5) and (3.6) are combined to yield the term:

$$\frac{\Delta^3_j f_{j+1}-\left(\Delta^3_j+\Delta^3_{j+1}\right)\Delta f_j+\Delta^3_j f_{j-1}}{\Delta^2_{j+1}\Delta^2_j(\Delta_{j+1}+\Delta_j)} = \frac{2\left(\Delta^2_j-\Delta^2_{j+1}\right)}{\Delta_j\Delta_{j+1}}f'+f''_j+\frac{1}{12}\Delta_j\Delta_{j+1}f^{(4)}_j+$$

$$+\frac{1}{60}\Delta_j\Delta_{j+1}(\Delta_{j+1}-\Delta_j)f^{(5)}_j+O(\Delta)^4 \tag{3.7}$$

and rewriting equation (3.4) to eliminate the second order term in (3.7):

$$\frac{1}{12}\Delta_j\Delta_{j+1}f^{(4)}_j = \frac{1}{6}\frac{\Delta_{j+1}f'_j-(\Delta_{j+1}+\Delta_j)f'_j+\Delta_j f'_{j+1}}{\Delta_{j+1}+\Delta_j}-\frac{1}{36}\Delta_j\Delta_{j+1}(\Delta_{j+1}-\Delta_j)f^{(5)}_j+$$

$$+O(\Delta)^4 \tag{3.8}$$

combining terms and simplifying yields the implicit relationship for the second derivatives:

$$\frac{1}{12}\left[\Delta_{j+1}f''_{j-1}+5(\Delta_{j+1}+\Delta_j)f''_j+\Delta_j f''_{j+1}\right]+\frac{\left(\Delta^2_j-\Delta^2_{j+1}\right)}{\Delta_j\Delta_{j+1}}f'=$$

$$=\frac{\Delta^3_j f_{j+1}-\left(\Delta^3_j+\Delta^3_{j+1}\right)f_j+\Delta^3_j f_{j-1}}{\Delta^2_{j+1}\Delta^2_j}+\frac{1}{180}\Delta_j\Delta_{j+1}(\Delta_{j+1}-\Delta_j)f^{(5)}_j+O(\Delta)^4 \tag{3.9}$$

Equation (3.9) is our implicit relationship for the second derivatives for a variable grid. It involves function values as well as first and second derivatives. This structure poses no major problem, since the solution methods presented here do not require an explicit formulation, but will solve the resulting implicit system simultaneously. The accuracy of equation (3.9) is formally third order for variable grid problems, but for gentle grid changes acts more like a fourth order method. This same claim is made for variable space problems (though explicit) by Ferziger (1981) and is consistent with our experience. For constant grid spacings, the classical implicit formula for the second derivatives is obtained:

$$\frac{1}{12}\left[f''_{j-1}+10f''_j+f''_{j+1}\right]=\frac{f_{j+1}-2f_j+f_{j-1}}{\Delta^2}+O(\Delta)^4 \tag{3.10}$$

In an analogous manner, the variable grid spacing implicit formula for the first derivatives is derived, to yield:

$$\frac{1}{6}\left[\Delta_{j+1}f'_{j-1}+2(\Delta_{j+1}+\Delta_j)f'_j+\Delta_j f'_{j+1}\right]=\frac{\Delta^2_j f_{j+1}+\left(\Delta^2_j-\Delta^2_{j+1}\right)\Delta f_j-\Delta^2_j f_{j-1}}{2\Delta_{j+1}\Delta_j}+$$

$$+O(\Delta)^4 \tag{3.11}$$

which also reduces to the expected constant grid first derivative implicit formula:

$$\frac{1}{6}\left[f'_{j-1}+4f'_j+f'_{j+1}\right]=\frac{f_{j+1}-f_{j-1}}{2\Delta}+O(\Delta)^4 \tag{3.12}$$

Equations (3.9) and (3.11) are the implicit relationships used in our analysis.

As indicated, they are a of an overall system. This system may be more clearly discussed by introducing the new variables: ϕ functional value, F=first derivative and S=second derivative. Hence, re-writing equations (3.1), (3.9) and (3.11) in terms of these new variable yields the system:

$$\frac{\partial\phi_j}{\partial x}=aS_j+bF_j+c\phi_j+d \tag{3.13}$$

$$\frac{1}{12}\left[\Delta_{j+1}S_{j-1}+5(\Delta_{j+1}+\Delta_j)S_j+\Delta_j S_{j+1}\right]+\frac{\left(\Delta^2{}_j-\Delta^2{}_{j+1}\right)}{\Delta_j\Delta_{j+1}}F_j=$$
$$=\frac{\Delta^3{}_j\phi_{j+1}-\left(\Delta^3{}_j+\Delta^3{}_{j+1}\right)\Delta\phi_j+\Delta^3{}_j\phi_{j-1}}{\Delta^2{}_{j+1}\Delta^2{}_j}+\frac{1}{180}\Delta_j\Delta_{j+1}(\Delta_{j+1}-\Delta_j)\phi^{(5)}{}_j+O(\Delta)^4 \tag{3.14}$$

$$\frac{1}{6}\left[\Delta_{j+1}F_{j-1}+2(\Delta_{j+1}+\Delta_j)F_j+\Delta_j F_{j+1}\right]=\frac{\Delta^2{}_j\phi_{j+1}+\left(\Delta^2{}_j-\Delta^2{}_{j+1}\right)\phi_j-\Delta^2{}_j\phi_{j-1}}{2\Delta_{j+1}\Delta_j}+$$
$$+O(\Delta)^4 \tag{3.15}$$

It may be noted that the streamwise derivative, i.e. $\partial/\partial x$ has not been treated yet. A discussion of this discretization is postponed until later.

From equations (3.13), (3.14) and (3.15), the three equations needed to close the three unknown functions are available. Further, at any marching (streamwise) plane the matrix structure of the system is block tridiagonal since the support was three point. Inversion of block tridiagonal systems is described in Section 3.5.

The above governing difference equations are applied to any interior point within the flow. Appropriate boundary conditions are required. Following Hirsch (1975) the question is posed: what is the maximum accuracy one can ask for at any boundary point (necessarily involving only two adjacent grid points) and any combination of function, first and second derivatives? The answer is the relationship:

$$\phi_j-\phi_{j+1}+\frac{\Delta_{j+1}}{2}\left[F_j+F_{j+1}\right]+\frac{\Delta_{j+1}{}^2}{12}\left[S_j-S_{j+1}\right]+O(\Delta)^4=0 \tag{3.16}$$

with an analogous relationship at the other boundary. Equation (3.16) is also obtained using splines by Rubin and Khosla (1977). Equation (3.16) supplemented by equation (3.13) and the boundary type: e.g. $\phi_j=0$ for Dirichlet or $F_j=0$ for Nuemann boundary conditions. (These equations are the required three equations in three unknowns at the wall node). The benefit of this closure is that it avoids the boundary condition problem faced by five point support difference techniques, which typically must resort to a locally lower order method near the boundary.

Realizing, that partial differential equations may be analyzed using many different methods, it would be useful to summarize alternative techniques. These are presented in Table 3.1. The basis function is used as a key parameter separating them. Comments on the strengths and weaknesses of methods are provided in the conclusions:

Method	Basis Function
finite difference	polynomial (local)
implicit finite difference	polynomial in terms of function and derivatives; (global)
traditional Galerkin	polynomial (global)
finite element	polynomial (local)
spectral	trigonometric or Chebyshev (global)

TABLE 3.1 Numerical solution methods for partial differential equations.

3.3 Resolution of singular behavior: tension spline bases and analytical decomposition

In the following sections, the initial condition singularity that was developed previously is now discussed with respect to differencing methods. Numerical methods, which are intended to better resolve the rapid changes in the initial condition, are discussed. Then the numerical/analytical decomposition is described for completeness.

3.3.1 Flow singularities and analytical methods

The idea behind deriving implicit equations based upon tension splines was motivated by the singular nature of the initial condition for the physical problem that is fundamental to this project. The step function initial condition is shown in Figure 3.2:

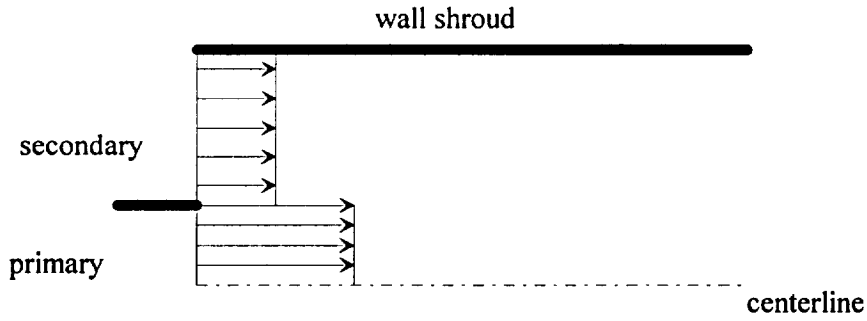

FIGURE 3.2 Schematic of flow initial conditions.

Additionally, governing equations for this problem may be approximately written for the conservation quantities in terms of the general linear parabolic equation:

$$\frac{\partial \phi}{\partial x} = a(x)\frac{\partial^2 \phi}{\partial y^2} \tag{3.17}$$

with the boundary conditions:

$$\frac{\partial \phi(x,0)}{\partial y} = \frac{\partial \phi(x,1)}{\partial y} = 0 \tag{3.18}$$

with the initial condition:

$$\phi(0,y) = \begin{pmatrix} \phi_{10} & 0 \le y \le h_s \\ \phi_{20} & h_s < y \le 1 \end{pmatrix} \tag{3.19}$$

and ϕ is defined by:

$$\phi(x,y) \equiv \begin{pmatrix} \rho u^2 + p \\ \rho u H \\ \rho u \end{pmatrix} \tag{3.20}$$

which are the flow quantities. These are, of course, the canonical forms of our mixing equations described in section 2. Here they may be considered any scalar simple equation. As before, it will be appropriate to make the local assumption, that the function a(x) may be approximated by the linear function $a(x)=\dot{a}\,x$.

As illustrated the flow is discontinuous at the interface between the primary and secondary streams. It was felt that a tension spline might provide a more satisfactory resolution of the initial condition, since tension splines are purposely designed to zones of large curvature. In fact for a very large tensioning parameter, σ, the tension spline acts like a linear (i.e. "connect the dots") basis. Unfortunately, though this spline showed improvement, it still did not resolve the input condition adequately. Further, large values for σ, cause degradation of the truncation error order.

As indicated in Section 2 the poor performance of the strictly numerical model may be analyzed further. Upon considering the implicit relationship governing the second derivatives, equation (3.9), the error term is found to be:

$$error = +\frac{1}{180}\Delta_j \Delta_{j+1}(\Delta_{j+1} - \Delta_j) f^{(5)}{}_j + O(\Delta)^4 f^{(6)} \tag{3.21}$$

which is formally fourth order for constant grid spacing. Unfortunately for very rapid changes in f, the high order derivatives, such as, $f^{(5)}$, $f^{(6)}$ are very large. In fact they may be as large as $O(1/\Delta)^4$ which would yield a very poor solution with errors O(1).

Further, this deficiency was shown clearly when the divergence theorem constraint, i.e. mass conservation which demands:

$$\int_0^1 \phi(x,y)dy = 1 \tag{3.22}$$

was considered. Unfortunately, this constraint was not properly honored by the strictly numerical solver due to the singular behavior near the step input. Physically, failure to observe the mass constraint is not acceptable. Ultimately, it became clear that the only possible way to appropriately deal with this singularity was introduce a local analytical solution that models the discontinuity. Examples of the use of basis or trial function (Galerkin terminology) come from Fletcher (1984) as well as others. Other examples of local treatment of rapidly varying functions near singularities include: steady state well functions used to resolve local radial well behavior in petroleum field simulation, Ewing (1983) and the use of "wall functions" to resolve local, near wall shear stress and velocity, for turbulent, viscous flow, Anderson et al. (1984). In the problem considered, here instead of developing a local special differencing method and blending it back into the overall system , the linearity of the governing equation itself was used to perform a global decomposition.

This global decomposition begins by recognizing the requirement for an analysis capable of dealing with extremely rapidly changing functions. Fortunately a solution method from classical analysis is available which is based upon distribution theory rather than continuous functions, described previously in Section 2 and repeated for convenience.

$$\phi_{an} = \frac{1}{2}(\phi_{10} - \phi_{20}) \sum_{-\infty}^{\infty} \left[erf\left(\frac{y + h_s - 2n}{(2a^*)^{\frac{1}{2}} x} \right) - erf\left(\frac{y - h_s - 2n}{(2a^*)^{\frac{1}{2}} x} \right) \right] + \phi_{20} \tag{3.23}$$

It is important to note, that for x<<1 this relationship recovers the step input. In passing it may be noted, that a straight forward eigenfunction solution may be written:

$$\phi(x, y) = \bar{\phi} + \frac{2}{\pi}(\phi_{10} - \phi_{20}) \sum_{n=1}^{\infty} \frac{1}{n} \sin(n\pi h_s) \cos(n\pi y) e^{-a^*(n\pi)^2 \frac{x^2}{2}} \tag{3.24}$$

where:

$$\bar{\phi} = \phi_{10} h_s + (1 - h_s)\phi_{20} \equiv 1$$

As pointed out previously, Equation (3.24) is formally an exact solution to our governing equation. Unfortunately, this equation is very slow to converge for x<<1, O(1/n), and suffers from Gibb's jump departures. Worse, x<<1 is precisely where it is desired to obtain good converge since this is a region of great interest in the physical problem.

Although equation (3.23) is exact, and does not suffer from the near field (small "x") limitations that the eigenfunction expansion solution, equation (3.23), did, it is still in the form of an infinite series. Note that in the near field, the solution converges extremely quickly. What is proposed and actually implemented is a combined numerical and analytical solution of the problem. Since it is linear this is easily effected. Consider the decomposition:

$$\phi(x, y) = \phi_{an}(x, y) + \phi_{num}(x, y) \tag{3.25}$$

with the governing equation:

$$\frac{\partial \phi_{num}}{\partial x} = a(x)\frac{\partial_{num}{}^2 \phi}{\partial y^2} \approx a^* x \frac{\partial_{num}{}^2 \phi}{\partial y^2} \tag{3.26}$$

with the new boundary conditions:

$$\frac{\partial_{num}\phi(x,0)}{\partial y} = -\frac{\partial_{an}\phi(x,0)}{\partial y} \qquad \frac{\partial_{num}(x,1)}{\partial y} = -\frac{\partial_{an}\phi(x,1)}{\partial y} \tag{3.27}$$

and the new initial condition:

$$\phi_{num}(0,y) = 0 \tag{3.28}$$

The overall solution is then, the sum of the two functions.

It may be noted, that a "patched" combination of the Green's function expansion solution, equation (3.23) (useful in the near field), and the eigenfunction expansion solution (3.24) might provide a useful and efficient solution method valid in both near and far fields. This question is somewhat irrelevant for the 1-d scalar problems described here, since the numerical portion of numerical/analytical global decomposition is relatively inexpensive. On the other hand, when considering a 3-d mixing scheme (See Section 5.), numerical inversion may become significantly more expensive, thus making fully analytical solution more competitive.

3.4 Streamwise differencing and von Neumann stability analysis

The previous derivations have concentrated on cross-stream, "y" direction differencing. In this section the streamwise "x" discretization is discussed. Two methods, a completely implicit three point difference operator and a two point, semi-implicit, Crank-Nicolson operator, are considered. Then the more restrictive operator (the two point, Crank-Nicolson method) is tested for stability using the von Neumann method.

3.4.1 Streamwise differencing

Two different streamwise discretization methods are discussed. Consider first; the computational molecule for the second order, 3 point backward, fully implicit operator (which was ultimately the method of choice) presented in Figure 3.4:

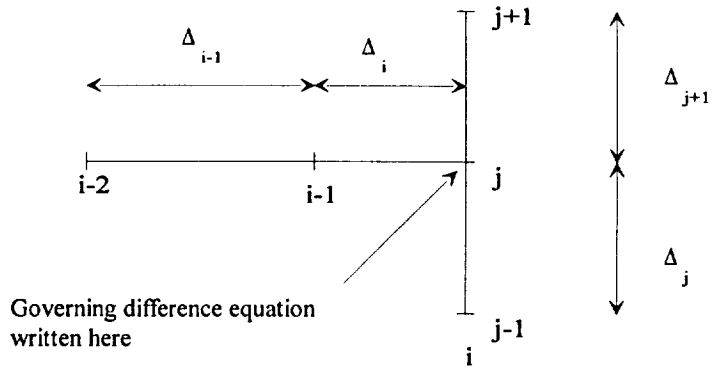

FIGURE 3.3 Computational molecule for the three point backward discretization method.

From Figure 3.4 it should be noted, that the "i" level is where the viscous, right-hand side of the governing equation, equation (3.1) is written. Figure 3.4 indicates that a variable grid, variable in the marching or "x" coordinate has been used. In a well-known way (we actually used Taylor series), the variable step formula for the streamwise derivative may be written:

$$f'_i = \frac{\Delta_{i-1}\left[2\Delta_i + \Delta_{i-1}\right] f_i - \left[\Delta_i + \Delta_{i-1}\right]^2 f_{i-1} + \Delta^2_i f_{i-2}}{\Delta_i \Delta_{i-1}\left[\Delta_i + \Delta_{i-1}\right]} + O(\Delta)^2 \tag{3.29}$$

and for constant grid spacing recovers the 3-point backward formula:

$$f'_i = \frac{3f_i - 4f_{i-1} + f_{i-2}}{2\Delta} + O(\Delta)^2 \tag{3.30}$$

With equation (3.29), the equation set (3.13), (3.14) and (3.15) is fully discretized. Rewriting (3.13) with double subscripts (i=streamwise, j=cross-stream).

$$\frac{\partial \phi_{i,j}}{\partial x} \equiv \frac{\Delta_{i-1}\left[2\Delta_i + \Delta_{i-1}\right]\phi_{i,j} - \left[\Delta_i + \Delta_{i-1}\right]^2 \phi_{i-1,j} + \Delta^2_i \phi_{i-2,j}}{\Delta_i \Delta_{i-1}\left[\Delta_i + \Delta_{i-1}\right]} =$$

$$= aS_{i,j} + bF_{i,j} + c\phi_{i,j} + d \tag{3.31}$$

This is completes the computational set actually used in this work. One objection to the three point backward formulation is that it is not self starting, since 2 levels of information are required to begin the marching procedure. Actually, this is not a major difficulty, since the near field expansion equation (3.23) is very accurate in the near field even for a small number of terms.

From the above derivations, it is apparent, that the method that is applied has a truncation error $O(\Delta^2{}_i \Delta^{3\text{-}4}{}_j)$. Our motivation to use a lower order method is a consideration of stability limitations. A multistep, (Adams, Adams-Moulton) (Ferziger 1981) or predictor corrector method, i.e. of the Runge-Kutta methods

could have been used to gain higher marching accuracy. It was felt, though, that this trade of higher order accuracy would come at an unacceptable limitation in stability.

3.5 Block tridiagonal matrix solution algorithm

The implicit method that has been described requires the solution of a system of block (at minimum [3x3], and possibly more if there is a system of equations or non-linearity) tridiagonal linear equations. The matrix structure for this type of system may be conveniently described:

$$\begin{bmatrix} [B]^1 & [C]^1 & 0 & 0 & 0 \\ [A]^2 & [B]^2 & [C]^2 & 0 & 0 \\ 0 & \cdot & \cdot & \cdot & 0 \\ 0 & 0 & [A]^{N-1} & [B]^{N-1} & [C]^{N-1} \\ 0 & 0 & 0 & [A]^N & [B]^N \end{bmatrix} \begin{bmatrix} x^1 \\ x^2 \\ \cdot \\ x^{N-1} \\ x^N \end{bmatrix} = \begin{bmatrix} d^1 \\ d^2 \\ \cdot \\ d^{N-1} \\ d^N \end{bmatrix} \tag{3.32}$$

where the [A], [B] and [C] terms are [3x3] submatrices and the x and d terms are [3x1] vectors. The x vector would be associated: $x=[\phi,F,S]^T$. This matrix may be inverted in an efficient manner. Routines are provided by many workers, for example, Anderson et al. (1984).

A simple way to understand the block tridiagonal algorithm is to merely generalize the scalar LU factorization method. This generalization is described by:

$$[B]^i = [B]^{i-1} - [A]^i \left\{ [B]^{i-1} \right\}^{-1} [C]^{i-1} \tag{3.33}$$

$$d^i = d^{i-1} - [A]^i \left\{ [B]^{i-1} \right\}^{-1} d^{i-1} \tag{3.34}$$

for i=1,2,3...N. At i=N the back substitution is begun:

$$x = \left\{ [B]^N \right\}^{-1} d^N \tag{3.35}$$

and :

$$x^i = \left\{ [B]^i \right\}^{-1} \left\{ d^N - [C]^i x^{i+1} \right\} \tag{3.36}$$

where i=N-1,N-2,...1.

The above is a summary of the algorithm that are used to invert the block system described by equation (3.32). It should be noted that we would never compute the inverse of the partitioned matrices such as described in the above algorithm, instead one would always set up an equivalent problem, i.e.:

$$x = \left\{[B]^N\right\}^{-1} d^N \quad \Leftrightarrow \quad [B]^N x^N = d^N \tag{3.37}$$

where the linear system would be solved using Gauss elimination with partial pivoting.

This completes the summary of our block tridiagonal solver. Because this type of matrix inversion has the capability of simultaneously solving coupled systems of discretized (on a three point basis) equations, it has proven very useful in a number of (personally developed) problems. In addition to the implicit formulation described here, the block inversion method has been used as the base linear solver in a relatively complex, multispecies combustion modeling problem. This combustion problem exhibits strong coupling and non-linearity. Quasi-linearization and use of the block tridiagonal inversion method provided a workable solver, while decoupled scalar methods failed. For coupled marching problems, this seems to be an excellent matrix inversion method.

3.6 Conclusions and recommendations for discretization methods

This report has sought to describe the discretization using implicit finite difference methods and the numerical solution for a scalar, parabolic, linear partial differential equation. The areas described include:

1. Derivation of a variable step, compact, implicit finite difference algorithm applied to a general, linear heat equation. Relationships to other methods are also considered.
2. Resolution of singular behavior using analytical decomposition
3. streamwise differencing.
4. Block tridiagonal matrix solution algorithm.

Many of the areas analyzed above were explored to try to develop methods that satisfied necessary constraints in the face of singular behavior. The linearity of this problem permitted the use of a relatively elegant and computationally successful decomposition to eliminate the singularity caused by the initial conditions.

Since the ultimate intent of the underlying research has not been to make explore solution methods, but to provide a computational fluid dynamic tool, little numerical experimentation has been performed. Certainly, though, considerable experience was obtained in deriving and implementing these methods. Extending the table given by Fletcher (1984) using our experience, strengths and weaknesses of comparable methods are summarized below:

Attribute\Method	Explicit finite difference	implicit finite difference (compact)	Finite Element	Spectral
Trial Solution	local	"pseudo" global; Roach (1972)	local	global
Ease of coding	very good	good	good	fair
flexibility (geometric description etc.)	good	good	very good	fair
accuracy per unknown	fair	good	good	very good
computational efficiency	good	good	good	very good
boundary conditions	good, low order, fair, higher order	very good	good	very good for simple conditions
Matrix inversion	very good, low order good, higher order	very good, block inversion	good	very good, FFT
Main strengths	economy and ease of coding	high order accuracy with minimal support	flexible geometry	high accuracy
Main Weaknesses	extension to higher order boundary conditions	coupled formulation and inversion	complexity, extension to non-linear problems	Geometric inflexibility, complexity

TABLE 3.2 Comparison of discretization methods.

Table 3.2 provides a brief and perhaps somewhat prejudiced comparison of partial differential equation numerical solution methods. Newer methods, such as those based on wavelets, have not been included, since the author has very little knowledge of them. Other more classical methods, such as, traditional Galerkin methods, have not been directly included. Traditional Galerkin methods tend to be very poorly posed for simple polynomial (non-orthogonal) bases. Choosing a more suitable basis, such as, Chebyshev polynomials is leading us back to spectral and pseudo-spectral problems.

With the limitations in the report in mind, the author concludes, that implicit or compact differencing methods offer an improvement in accuracy over simple explicit finite difference or finite element methods. They are far more useful than higher order explicit methods, i.e. five and seven point support methods, due to the superior treatment of boundary conditions. It is the authors opinion that implicit methods offer a method of intermediate complexity and utility between explicit finite element and finite difference methods and spectral

methods. Streamwise (temporal) differencing using the three point backward method provides a fully implicit method while preserving second order accuracy. The choice of lower order with respect to truncation error compared to stability restrictions seems to be appropriate. Numerical experiments described in Section 5 will also help justify the use of a lower order differencing scheme used in the streamwise direction, due to relatively gentle changes in the direction.

Though significant recommendations for further work are made in Section 5, it is be useful to make some comments on area for further research concentrating on numerical methods here. Probably the biggest area of concern, is the development of compact formulas and methods which satisfy the conservation or control volume constraint. Equations (3.38) and (3.39) represent initial progress towards this work. Stability limitations for higher order methods, both streamwise and cross-stream, remain of interest. Exploration of methods based on Richardson extrapolation, predictor correctors or Gear's methods; Ferziger (1981) may be of use for streamwise (temporal) differencing. Resolution of singularities, which was the driver behind much of the theoretical work presented here, remains critical. Finally, handling of nonlinearities in a manner that takes advantage of the higher order differencing, i.e. quasi-linearization with iteration, needs to be addressed.

3.7 Nonlinear equation solvers

The majority of the closed form solutions developed previously are written implicitly in the form of a system of governing algebraic equations. As such, they often need to be inverted to yield appropriate variables. In this section the solvers used to invert these problems are briefly discussed. The methods employed:

Problem	Method	Comments	Use in DREA	variable
Scalar	Bisection	Linear convergence, robust	rarely used	
	Secant	Superlinear Convergence, may fail to converge	Slipline static pressure matching; pressure constrained entrainment	M_{1s}; M_2
System	Gradient	Linear convergence, robust	rarely used	
	Broyden	Superlinear Convergence, may fail to converge.	Fabri choke, critical back pressure	M_{1s}, M_2; M_{1s}, p_{crit}/p_{01}

TABLE 3.3 Comparison of non-linear equation numerical solution methods.

Although, Table 3.3 indicates, that several of the methods are "robust" while others may fail to converge, experience indicates that the faster converging methods (superlinear) are to be preferred. Convergence failure is more related to physics, i.e. no solution exists, than it is to numerical inversion.

Since there has been little original development or modification to these solvers we refer the reader to the excellent references by Johnson and Riess (1982) for the scalar secant method and Burden and Faires (1993) for the Broyden method for descriptions of their development.

3.8 Variable grid Simpson's rule integration

As the DREA suite of codes have been developed, the need to be able to obtain an integral average value of any quantity across the mixing duct has been apparent. A clear example of this need is the computation of the integral constraint (repeated here for convenience):

$$\int_0^l \phi(x,y)dy = 1 \tag{3.38}$$

The quadrature method chosen must:

1. retain formal fourth order accuracy, to be consistent with the fourth order accurate difference formulation incorporated previously, and
2. be valid on a variable grid.

To satisfy these two requirements the most obvious choice is a variable step Newton-Cotes formula. One that will obtain the fourth order accuracy desired is a variable step Simpson rule quadrature formula. This type of formula is easily derived in principle, but is rather tedious to implement. As such, the development method is merely outlined here. We may start by defining the variable grid with the now known function f, as shown in Figure 3.3.

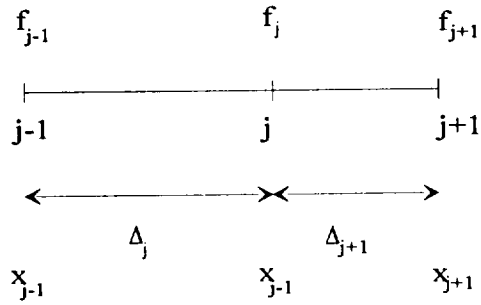

FIGURE 3.4 Variable grid definitions.

To proceed, one next fits a Lagrange interpolating polynomial (Ferziger (1981)) through these three nodal points. This yields:

$$f(x) = \frac{(x_i - x)(x_{j+1} - x)}{\Delta_j(\Delta_{j+1} + \Delta_j)} f_{i-1} - \frac{(x_{i-1} - x)(x_{j+1} - x)}{\Delta_{j+1}\Delta_j} f_j + \frac{(x_{i+1} - x)(x_j - x)}{\Delta_{j+1}(\Delta_{j+1} + \Delta_j)} f_{j+1} \tag{3.39}$$

At this point it is possible to integrate, f(x) between x_{j-1} and x_{j+1} to obtain a rather cumbersome quadrature formula.

$$\int_{x_{j-1}}^{x_{j+1}} f(x)dx = f(\Delta_j, \Delta_{j+1}, f_{i-1}, f_j, f_{j+1}) \tag{3.40}$$

It can be shown that for constant grid spacing, this equation reduces to the expected "1/3" Simpson rule (Ferziger (1981)). The net integral is then the summation of the intervals covering the range of integration.

This formulation is poorly posed however, if the number of intervals chosen is odd. In this case it is formally necessary to go to the extent to derive an equivalent variable step 3/8 Simpson rule formula, which is even more tedious. The development is identical, except the quadrature stencil now involves four point support (and three panels), fit a Lagrangian cubic and proceed as before. A tedious procedure to implement but not conceptually difficult.

Before concluding the formal discussion of integration methods, it is worth noting that since this methodology was based upon local polynomial curve fitting (i.e. Lagrange polynomials), the resulting quadrature formula is a very poor estimate in regions where the gradient is large. Indeed, this situation can and does occur in our flow field near the Heaviside step function inputs. As a bound on this error, consider the error associated with a 1/3 Simpson rule on a constant grid:

$$e_{simpson} = -\frac{f^{(4)}(\eta)}{90}\Delta^5 \tag{3.41}$$

Clearly, in regions where $f^{(4)}$, i.e. the fourth derivative is large the error will be very large.

In Section 5 it is shown that the integral constraint, as computed using our quadrature formula, is indeed a very poor estimate of the actual constraint near the singularity, for this reason. Clearly, the appropriate way to resolve this situation would be to introduce a combined numerical analytical quadrature formula. Fortunately, however, local integrations near the singularity are not of great interest. As such, it is acceptable to ignore this problem. This completes our discussion of the numerical solution methodologies.

4. EXPERIMENTAL METHODS

In this section, inviscid, confined supersonic and subsonic stream interactions are studied using a hydraulic analog experiment. Specifically, the length of the first minimum location of the slipline is measured. Reasonable agreement is shown between a theoretical model and analog measurements. A method for extending the isentropic limited hydraulic analogy to model these inherently non-isentropic flows is also developed. This work is intended to aid in the general understanding of aerodynamic ejector/mixer nozzle operation, as well as, providing data for confined expansion compression surface

4.1 Introduction

Though free jets provide a useful limiting form of the ejector flow, the effect of confinement on the flow field is important. Thus measurements confined jet interactions provide data to validate the models developed in Section 2.3.2. Additionally, delineation of the inviscid flow field structure within an ejector nozzle has design implications for acoustic, structural, fluid mechanic reasons.

In this portion of our study, a hydraulic analog/gas flow model of a 2-d ejector is used principally to locate and understand the structure of the inviscid multiple stream flow (principally the location of the aerodynamic choke). Figure 4.1 shows photographs of the hydraulic analog ejector model and slipline structure. As a basis for analytical comparison, formulas that describe wavelength of the slipline are developed for confined two-dimensional and axi-symmetric, supersonic-subsonic jets in De Chant et al. (1996) and Appendix C. Modifications have been made to this solution to extend its validity to include internal flows (De Chant et al. (1997)). This more general relationship provides internal flow field information for a supersonic ejector flow field, since the location of the first maximum expansion, approximately corresponds to the location of the aerodynamic or Fabri-choke, Fabri and Siestrunck (1958) or Addy et al. (1981).

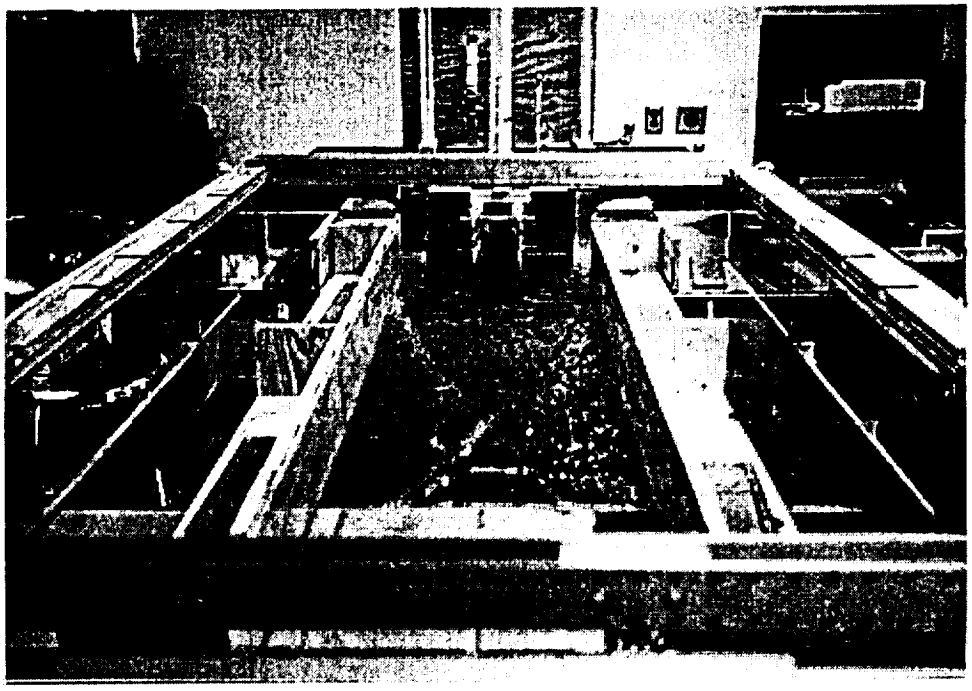

FIGURE 4.1 Water table analogy and expansion/compression structure.

In general, a formal mathematical analogy between two physical systems may be drawn whenever the non-dimensional governing equations and boundary conditions for the systems are equivalent. Examples for the Laplace equation include: electrostatic, membrane, Heleshaw and others (Bear (1972)). The inherent weaknesses of these methods are increased uncertainty due to additional theoretical basis. The analog discussed in this paper is a hydraulic analogy between gas flow and hydraulic flows. An analogy exists between thin, horizontal flow water under the influence of gravity and 2-d compressible, potential gas flows and this analogy has been utilized by a number of workers. Prieswerk (1940) performed some of the first practical studies using the analogy. Later workers include Shapiro (1954), Loh (1959) and (1969) and more recently, Pal and Bose (1993).

Normal shock waves are approximately modeled by hydraulic jump phenomenon (Loh (1969)). The classical limitation for the hydraulic analogy, namely an effective specific heat ratio, γ=2, is less restrictive if the analogy is used to verify an analytical tool for which it is possible to specify any convenient specific heat ratio.

Gas Flow	Hydraulic Flow	Implication
$\frac{T_0}{T} = 1 + \frac{\gamma - 1}{2} M^2$	$\frac{h_0}{h} = 1 + \frac{1}{2} Fr$	$\frac{T_0}{T} = \frac{h_0}{h} \;;\; \gamma = 2$
$\frac{\partial(\rho u)}{\partial x} + \frac{\partial(\rho v)}{\partial y} = 0$	$\frac{\partial(hu)}{\partial x} + \frac{\partial(hv)}{\partial y} = 0$	$M^2 = Fr^2 \;;\; \frac{\rho_0}{\rho} = \frac{h_0}{h}$
$\frac{p_0}{p} = \frac{\rho_0}{\rho} \frac{T_0}{T}$		$\frac{p_0}{p} = \left(\frac{h_0}{h}\right)^2$

TABLE 4.1 Summary of hydraulic analogy.

The key strength of analog methods is that they are less expensive relative to "full scale" measurements, in terms of, money, time and expertise. Table 4.1 is a summary of the relationships that may be drawn between the hydraulic and the analogous gas flow.

4.2 Experimental facilities

Practical application of the hydraulic analog is dependent upon the availability of a facilities where a thin hydraulic flows of water under the surface of gravity may be obtained, as well, as studied and measured. The Emil Buehler Aerodynamic Analog (EBAA) in the Mechanical Engineering Department at Texas A&M

University provides such a facility. Figure 4.2 provides a schematic of this facility. Detailed descriptions of the facility are provided by Felling (1992) and Lawton (1989).

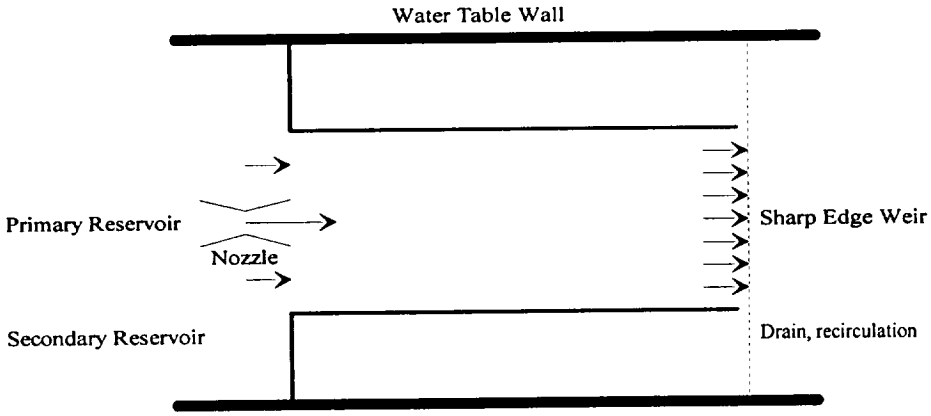

FIGURE 4.2 A schematic representation of the water table apparatus.

The basic flow components include:

- Pump
- Primary and secondary reservoirs with flow rate measurement
- Primary CD nozzle, and contoured secondary inlets
- Ejector model test section
- Return reservoir

Originally, the EBAA facility was designed for single stream flows, Felling (1992). The EBAA facility was used with modifications to permit multiple stream flow rate measurement. A two stream manifold and gate valve array used in previous work was modified. The manifold, flow measurement, and piping array provided the basic source or reservoirs for the two streams. The large size of the EBAA reservoir provides very clean uniform flow for the secondary stream. The primary reservoir due to its smaller size has both a perforated "T" fitting and a series of three honeycomb screens to reduce primary reservoir turbulence.

The EBAA facility was used with modifications to permit multiple stream flow rate measurement. A two stream manifold and gate valve array used in previous work was modified. These modifications included the installation of three Omega rotameter flow measurement devices. Specifications include:

1. Primary Stream: Single, 60 GPM Rotameter, Model FL75K, 2.5% full scale, 0.5% repeatability.
2. Secondary Stream: Double 30 GPM Rotameters, Model FLD, 2.5% full scale, 0.5% repeatability.

With primary and secondary reservoirs available, the two streams are mixed in a manner that simulates the ejector arrangement. Starting with the primary reservoir, a minimum length, converging-diverging nozzle was designed using the method of characteristics, see Shapiro (1953) and Anderson (1985), modified for hydraulic flows. The minimum length nozzle, Anderson (1985), accelerates the flow using a single "sharp" edged Prandtl-Meyer expansion. The exit flow is straightened using appropriately designed nozzle walls. These walls were designed using a graphical form of the method of characteristics method. Prandtl-Meyer expansion tables for heat capacity ratio γ=2.0, required to satisfy the analogy, were generated and used in this computation. The nozzle throat was chosen to be 7.62 cm (3.0 in.) wide. For the design exit mach number, M=2.0, and throat, a nozzle contour was developed. The graphical value of the exit area 11.43 cm (4.5 in.)

compares well with the one dimensional value of 10.97 cm (4.25 in.) computed from the one-dimensional Mach number area relationship (isentropic mass conservation, γ=2.0)

$$\frac{A_{exit}}{A_{throat}} = \frac{1}{M_e}\left[\frac{2}{3}(1+\frac{1}{2}(M_e)^2)\right]^{\frac{3}{2}} \tag{4.1}$$

Comparing the graphical versus analytical exit area, the relative error here is approximately 6.0%. The subsonic (or subcritical) section of the flow was designed using large radius, smooth entrance inlets. The importance of large diameter inlets is emphasized by White (1986). The same type of inlet is used in the secondary flow field to minimize head losses. The two streams are brought together at the nozzle splitter plates, which are 0.3175 cm (0.125 in.) in thickness. The splitter plates induce local wakes, but these are small relative to the inviscid phenomenon of interest and may be neglected.

The primary stream Mach/Froude number is a key parameter needed to model the inviscid interactions. It may be measured by employing the local Bernoulli relationship written between the primary reservoir and the primary nozzle exit plane:

$$h_0 = h + \frac{1}{2}\frac{u^2}{g} \qquad Fr \equiv \frac{u}{(gh)^{\frac{1}{2}}} = [2(\frac{h_0}{h} - 1)]^{\frac{1}{2}} \tag{4.2}$$

This measurement requires measurement of the local water height. As indicated in Shapiro (1954), these measurements may be made most conveniently using a needle probe arrangement. A simple, but effective, measurement tool consists of a beam (concrete level) with a pin probe (modified combination square, accuracy: ±0.08 cm, ±0.0313 inches). More recently, Pal and Bose (1993) have used a flow visualization method to measure water depth. Though, this method has the advantage of being non-intrusive, it is not practical to apply to the two stream problem studied here due to significant three-dimensional disturbances inherent in a mixing flow. The pin probe introduces an additional degree of error, but remains the most practical and direct method for estimating local Froude numbers in the mixing flow.

The location of the interface, may be readily observed by the marked change in water height at the interface. As seen from Figure 4.1, the interface is relatively well defined since it is caused by a rapid transition from supercritical flow (Fr>1) to subcritical flow (Fr<1). Length was measured using the same beam and probe arrangement. Though the interface has small scale unsteadiness, it is of sufficiently small amplitude, less than 5% of the total inviscid structure length, and sufficiently high frequency, that an observer takes a "naturally" time averaged reading.

4.3 Theoretical model and extensions of the hydraulic analogy

This section summarizes the analytical model described in Section 2 and Appendix C, which is used to predict the geometry (length of first critical) of supersonic/subsonic confined and unconfined jets. These models provide a basis to understand the analog measurements. Then, the limitation of the hydraulic analogy in multiple stream flows is discussed and modifications to the analogy are developed using first order analytical arguments.

4.3.1 Interface slipline geometry (first critical location)

Following (De Chant et al. 1996) and Appendix C, relationships describing the slipline interface between a supersonic flow and subsonic flow free jet flow are merely quoted. The principle parameter is discussed is $x_c/2$ which is the dimensionless location of the first minimum in the expansion/compression system resulting in the flow. See Figure 4.3. This value for both axi-symmetric and two dimensional flows is described by the equations below:

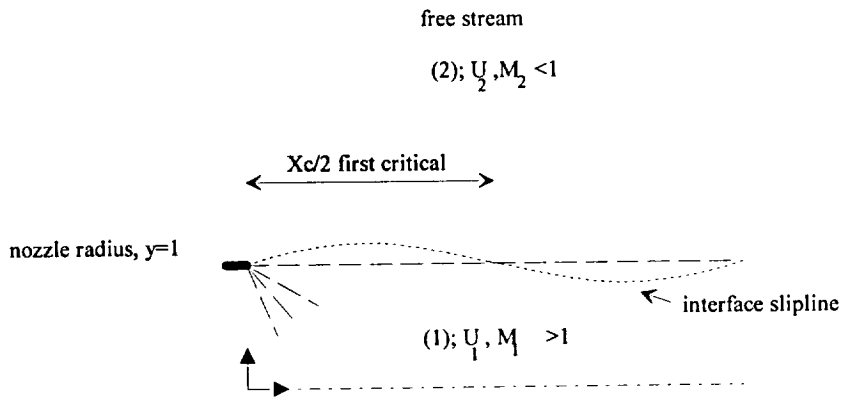

FIGURE 4.3 A schematic of the free jet problem geometry and definitions.

•axi-symmetric:

$$\frac{x_c}{2} = 1.22\beta_{eff} - .22\beta_{1s} \equiv 1.22(1 + \frac{1}{2}\xi_m^{\frac{1}{2}})\beta_{1s} - .22\beta_{1s} \tag{4.3}$$

•two-dimensional:

$$\frac{x_c}{2} = 2\beta_{eff} - \beta_{1s} \equiv 2(1 + \frac{1}{2}\xi_m^{\frac{1}{2}})\beta_{1s} - \beta_{1s} \tag{4.4}$$

where $\beta_{1s}=(M_{1s}^2-1)^{1/2}$ and $\xi_m=(\beta_{1s})^2[1-U_1/U_{1s}]$. Equations (4.3) and (4.4) are the final modified solutions for the critical slipline location. These relationships with the lowest order terms, i.e. β_{1s}, U_{1s}, based upon local static pressure matching for free jet problems and a modified method internal flow control volume theory, comprise our solution for the location of the first minimum of the slipline. By symmetry, half this distance is approximately the local maximum of the primary expansion and corresponds to the location of Fabri's aerodynamic choke. Of course, only the 2-d formula is useful here since the analog is strictly valid for 2-d.

4.3.2 Confined flow modifications

Ejector/mixer nozzles are by their very nature confined or internal flow problems as indicated by Figure 4.4.

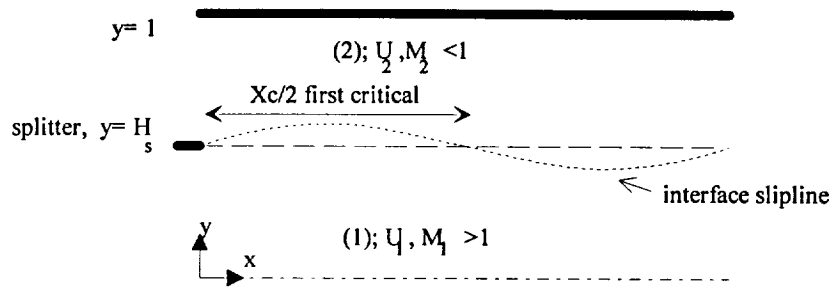

FIGURE 4.4 Description of the internal/ejector flow geometry and definitions.

As such, modifications to the basic inviscid flow analyses of Section 2.3.1 are necessary. This modification takes the form of estimating the base flow or lowest order quantities in a different manner. Consider the expansion

$$\frac{u}{U_{1s}} = 1 + \frac{\partial \phi}{\partial x}\varepsilon + \qquad \varepsilon \equiv (1 - \frac{U_1}{U_{1s}}) \tag{4.5}$$

where, U_{1s}, is the velocity at the interface. In De Chant et al. (1996) the slipline velocity, U_{1s}, was estimated using a static pressure matching methodology. To account for the internal flow effects in the current paper, it will be necessary to fall back on a more complete control volume methodology. Consider the two basic problems for an internal flow problem:

(1) Large area ratio, unknowns: M_{1s}, M_{2s}, U_{1s}
(2) Small area ratio (Fabri problem), unknowns: M_{1s}, M_2, U_{1s}

It is reasonable to expect, that two closures might be necessary to model large area ratio and small area ratio problems, in that, the limiting case of an infinite secondary flow field (free jet) cannot be analyzed at all using control volume methods. For a free jet, conditions are based solely upon local static pressure matching. This statement justifies the two modeling procedures: large area ratio problems are analyzed using static pressure and mass conservation, while for A_2/A_1 on the order of one, both mass and momentum conservation must be demanded. For a choked secondary stream, M_{2s}=1, this becomes Fabri's problem. Analytical details of this work are provided by De Chant et al. (1997), and Section 2.3.2.

4.3.3 Multiple stream extensions and limitations of hydraulic/gas flow analogy

The hydraulic analogy as described in the introduction has been written for a single stream of water or gas. In this section, the analog is approximately extended to be capable of multiple stream flow simulation. This is done by first developing the classical analog with particular attention to restrictive assumptions. Then by examining a multiple stream flow the single stream limitation of the analog will be demonstrated. To overcome this limitation an approximate correction is introduced. The importance of this approximation is determined by comparison to experimental results.

To understand the formal limitation of single stream, isentropic flow, the basic hydraulic/gas flow analogy is developed here. Consider the conservation equations for the two systems compared in Table 4.2.

Conservation Equation	Hydraulic	Aerodynamic
mass	$\nabla \bullet (\frac{\rho}{\rho_0}\frac{u}{u_0}) = 0$	$\nabla \bullet (\frac{h}{h_0}\frac{u}{u_o}) = 0$
energy	$\frac{h_0}{h} = 1 + \frac{1}{2}Fr^2$	$\frac{T_0}{T} = 1 + \frac{\gamma - 1}{2}M^2$
momentum	$\frac{1}{2} = (\frac{1}{2} + Fr^2)(\frac{h}{h_0})^2$	$\frac{1}{\gamma} = (\frac{1}{\gamma} + M^2)(\frac{\rho}{\rho_0})(\frac{T}{T_0})$

TABLE 4.2 Governing equations for hydraulic analog.

Finally, although it has no counterpart in hydraulic flows, the state equation for the aerodynamic gas flow is written:

$$\frac{p}{p_0} = \frac{\rho}{\rho_0}\frac{T}{T_0} \tag{4.7}$$

The relationships in Table 4.2 and equation (4.7) must be satisfied if an analogy is to exist between hydraulic and aerodynamic gas flows. By inspection, all these relationships may be simultaneously satisfied if one demands:

$$\gamma = 2 \quad \frac{\rho}{\rho_0} = \frac{T}{T_0} = \frac{h}{h_0} \tag{4.8}$$

By either state or momentum it is necessary to write:

$$\frac{p}{p_0} = (\frac{h}{h_0})^2 \tag{4.9}$$

It should be noted, though, that this relationship is equivalent to invoking an isentropic assumption with γ=2. It is apparent, that the isentropic assumption will limit the validity of the hydraulic analogy for any flow in which isentropic conditions are not well approximated.

To emphasize this limitation, consider the case of two streams of different total conditions separated by a vortex sheet or slipline. By the definition, for a slipline to exist, the local static pressure is matched. Thus for two streams at a slipline, we may write:

$$P_{1s} = P_{01}[1 + \frac{\gamma - 1}{2}M_1^2]^{\frac{\gamma}{1-\gamma}} = P_{2s} = P_{02}[1 + \frac{\gamma - 1}{2}M_2^2]^{\frac{\gamma}{1-\gamma}} \tag{4.10}$$

Eliminating the static pressure and introducing the definition of total temperature yields:

$$\frac{P_{02}}{P_{01}} = \left[\frac{T_{1s}}{T_{2s}}\right]^{\frac{\gamma}{\gamma-1}} \left[\frac{T_{02}}{T_{01}}\right]^{\frac{\gamma}{\gamma-1}} \tag{4.11}$$

Now, alternatively, consider the total pressure definition required to satisfy the analogy:

$$\frac{P_{02}}{P_{01}} = \left[\frac{T_{02}}{T_{01}}\right]^{\frac{\gamma}{\gamma-1}} \tag{4.12}$$

Hence, it is clear that except for the case of precisely matched static conditions (which is the trivial case of a single stream) that the hydraulic analog cannot precisely represent multiple stream flows. Our task is then to develop an extension to the hydraulic analogy that better represents these flows.

4.3.4 An extended water table closure model

The previous relationship, equation (4.12), indicates that the hydraulic analogy requires an isentropic relationship between the streams to be strictly valid. The definition of the total pressure at the interface described by equation (4.10) could be directly used, but it is in terms of the local interface static temperature ratio (and by analogy the local interface water height) which is difficult to measure. To understand this limitation from another point of view, a more physically based equation relating the total pressure jump to the total temperature using a local particular energy integral is developed.

The closure relationship may be developed by considering Crocco's law, White (1974), a particular energy integral, valid for small pressure gradient and Prandtl number equal to one:

$$dT_0 = \frac{T_{01} - T_{02}}{u_1 - u_2} du \tag{4.13}$$

and the definition of total temperature:

$$\frac{dT_0}{T} = \frac{dT}{T} + (\gamma - 1) M^2 \frac{du}{u} \tag{4.14}$$

Solving for the static temperature yields:

$$-\frac{dT}{T} = \left[\left(\frac{T_0}{T_{01} - T_{02}}\right)\left(\frac{u_1 - u_2}{u_0}\right) - \left(1 + \frac{\gamma - 1}{2} M^2\right)\right] \frac{dT_0}{T_0} \tag{4.15}$$

The product term in the brackets may be simplified by assuming that:

$$\left(\frac{1 + \frac{T_{02}}{T_{01}}}{1 - \frac{T_{02}}{T_{01}}}\right)\left(\frac{1 - \frac{u_2}{u_1}}{1 + \frac{u_2}{u_1}}\right) \approx 1 \tag{4.16}$$

which is true for large variations in total temperature and interface velocity. These are precisely the type of flow conditions where the isentropic assumption needed by the analogy is at its weakest. Using a locally constant Mach number i.e. average between streams permits integration of equation (4.15) to yield:

$$\frac{T_1 S}{T_2 S} = \left(\frac{T_{02}}{T_{01}}\right)^{\left[\frac{1}{2}(\gamma-1)M_{ave}^2-1\right]} \tag{4.17}$$

Note that for incompressible flow $M_{ave}=0$, that the proper limit is obtained:

$$\frac{T_{1s}}{T_{2s}} = \left(\frac{T_{02}}{T_{01}}\right)^{-1} = \frac{T_{01}}{T_{02}} \tag{4.18}$$

Hence, the approximate relationship for the total pressure in terms of the stream total temperatures valid for multiple stream flows is obtained:

$$\frac{P_{02}}{P_{01}} = \left(\frac{T_{02}}{T_{01}}\right)^{\left[\frac{\gamma}{\gamma-1}\right]\left[1+\frac{1}{2}(\gamma-1)M_{ave}^2-1\right]} \tag{4.19}$$

Simplifying the exponent of equation (4.19), yields:

$$\frac{\gamma}{\gamma-1}\left[\frac{(\gamma-1)}{2}M_{ave}^{\ 2}\right] = \frac{\gamma}{2}M_{ave}^{\ 2} \tag{4.20}$$

The classical analogy, though, requires that equation (4.20) take the constant value of two. From equation (4.19) it is clear that satisfaction of analogy for multiple stream flows is Mach (or Froude) number dependent. It is our conclusion that in air, where $\gamma=1.4$, that only for an interface Mach number of:

$$M_{ave} \approx \left(\frac{4}{\gamma}\right)^{\frac{1}{2}} \approx 1.69 \tag{4.21}$$

can the analogy be expected to hold for non-isentropic flows. Additionally, since it has been shown that for multiple stream flows, the exponent in the pressure relationship is Mach number dependent, slight modification of the exponent in the classical closure i.e. $2\rightarrow 2\pm\varepsilon$, with ε a small correction term, may be expected to extend the validity of the model. To satisfy the other relationships in the analogy, $\gamma=2.0$, should be used for all computations. This would yield an average Mach number value:

$$M_{ave} \approx \left(\frac{4}{2}\right)^{\frac{1}{2}} \approx 1.4142 \tag{4.22}$$

Ultimately, as long as, either equation (4.19) or (4.20) is approximately satisfied, the analogy can be expected to provide reasonable results even for multiple stream interactions.

Later in Section 4.4, the validity of this correction strategy is ascertained by comparison of the analog data for a case where $M_1=2$ and the secondary stream chokes. For this flow, the correction factor, ε, may be estimated. Neglecting the acceleration of the primary stream, but recognizing that the secondary stream is sonic yields a local average Mach/Froude number, $M_{ave}\cong(2.0+1.0)/2=1.5$. To approximately satisfy equation (4.22) and, more importantly match the estimated local Mach/Froude number, the classical exponent value of two is modified $2\rightarrow 2\pm\varepsilon$, with $\varepsilon=1/8$. From equation (4.22) this would yield an average Mach number $M_{ave}=[(2.125)^2/2]^{0.5}=1.5026$. As will be seen, this correction term provides a slight improvement to the model for multiple stream flows. A summary of the basis and form of this correction is provided in Table 4.3.

Gas Flow	Hydraulic Analog	Extended Analog ($M_{ave}=1.5$)
$\frac{P_{02}}{P_{01}}=\left(\frac{T_1}{T_2}\right)^{\frac{\gamma}{\gamma-1}}\left(\frac{T_{02}}{T_{01}}\right)^{\frac{\gamma}{\gamma-1}}$	$\frac{P_{02}}{P_{01}}=\left(\frac{h_{02}}{h_{01}}\right)^{2} \quad \gamma=2$	$\frac{P_{02}}{P_{01}}=\left(\frac{h_{02}}{h_{01}}\right)^{2+\varepsilon} \quad \varepsilon\approx\frac{1}{8}$

TABLE 4.3 Extended hydraulic analogy.

4.3.5 Error and error propagation for the hydraulic analogy

The previously developed analyses have essentially assumed that the flow of water in the hydraulic analogy is a 1-d, frictionless flow. Three dimensionality and frictional losses are significant for the two stream mixing problem described here. As a way to understand the effect that losses have upon the analogy consider the Froude (or by analogy Mach) number computation:

$$Fr=\left(\frac{2(\frac{h_0}{h}-1)}{1+f_{friction}}\right)^{\frac{1}{2}} \tag{4.23}$$

As shown in equation (4.23), friction has the effect of reducing the actual Mach number. Off setting this reduction is the presence of local three-dimensional effects and turbulence caused by the rapid acceleration of the flow through the nozzle. Biasing is also possible in the nozzle design or fabrication. Measurements of the exit Mach number for 20 separate cases using the pin probe and beam arrangement and equation (3) yield an average exit Mach/Froude number of 2.09, a relative error of 4.5%.

An additional source of uncertainty comes from the actual measurement of the Froude number. As a way to quantify this error and its propagation, consider the uncertainty analysis method of Kline and McClintock (1953). For our problem, it is sufficient to consider the Froude or Mach number squared relationship:

$$Fr^2\equiv\frac{u^2}{gh}=[2(\frac{h_0}{h}-1)] \tag{4.24}$$

Now, since both h_0 and h are directly measured, using the pin probe apparatus, the partial derivatives of the two measured quantities, h_0 and h are computed:

$$\frac{\partial Fr^2}{\partial h_0} = \frac{2}{h} \qquad \frac{\partial Fr^2}{\partial h} = -2\left(\frac{h_0}{h}\right)\frac{1}{h} \tag{4.25}$$

Introducing the ratios $\Delta h_0/h_0$ and $\Delta h_0/h_0$ where the Δh is the error associated with the pin probe measurement, squaring, summing and taking the root yields the propagated uncertainty:

$$\omega_{Fr}^2 = 2\left(\frac{h_0}{h_1}\right)\left[\left(\frac{\Delta h_0}{h_0}\right)^2 + \left(\frac{\Delta h}{h}\right)^2\right]^{\frac{1}{2}} \tag{4.26}$$

The errors associated with the two measurements for a representative case are:

- primary reservoir value: $\Delta h_0/h_0$=0.031(inches)/3.0 inches=0.01
- secondary reservoir value $\Delta h/h$=0.031 inches/1.0 inches=0.031

Substituting these values into equation (4.26) yields a value for the Kline-McClintock uncertainty of approximately ω_{Fr}^2=20%. This value gives a rather pessimistic estimate of the error associated with the measurement of the Mach number in the primary stream. The actual error is probably considerably smaller, as indicated by the small relative error 4.5% shown for the primary Mach number.

The good comparison between aerodynamic theory and the hydraulic analogy experiment demonstrate that the hydraulic analogy may provide a viable method for making quantitative measurements in support of numerical and analytical modeling efforts. Additionally, the rather generous error bound from the Kline-McClintock theory is shown to be just that, a pessimistic upper bound on the error.

4.4 Results; analog versus theoretical results and repeatability

The fundamental result for this problem is the measurement of the critical location, x_c, of the slipline. Results for two cases are presented in Figures 4.5 and 4.6. The relevant operating conditions for these cases are summarized in Table 4.4:

case	Primary Mach No., M_1	Secondary Mach No. , M_2	Area Ratio: A_2/A_1
1	2.0	negligible	9.60
2	2.0	negligible	3.235

TABLE 4.4 Operating conditions for slipline geometry measurement.

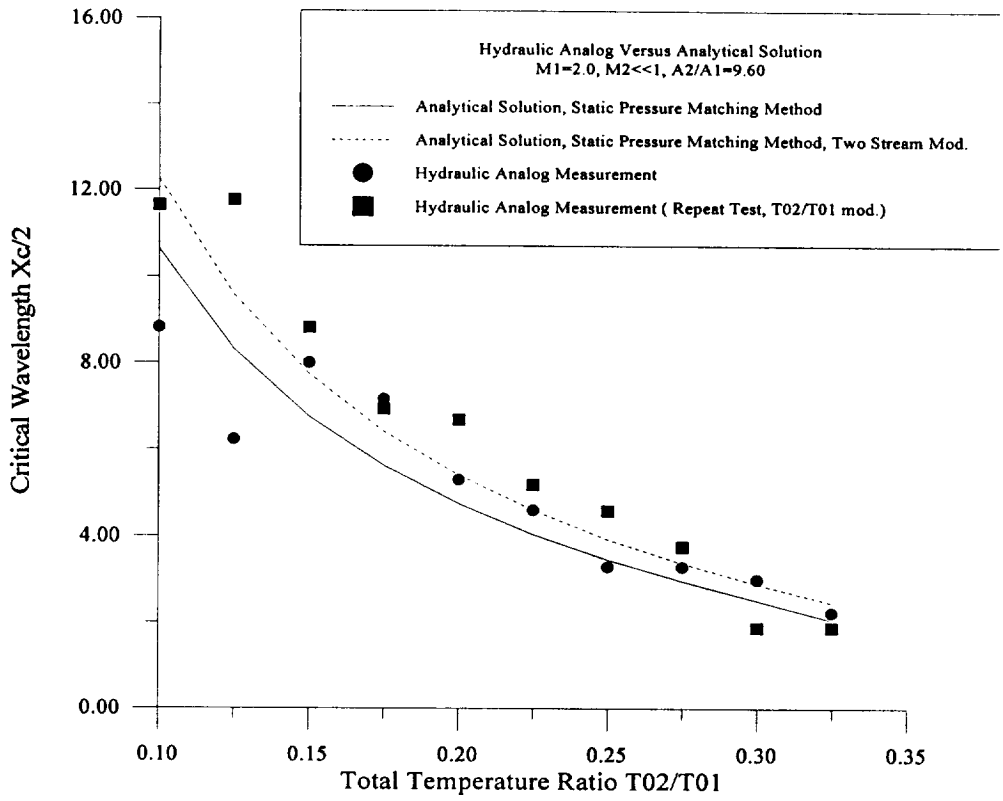

FIGURE 4.5 Comparison of experimental and model critical interface lengths, for A_2/A_1=9.60.

Since both of the area ratios for the problems measured are relatively large, the closure model chosen is the large area ratio static pressure matching method, i.e. equation (2.40). Analog measurements have been consistently reduced using the extended model. Both the unmodified model and the extended model have been used to provide total pressure ratio input values into the control volume method. Additionally, a series of repeatability test were run, using dimensional water height combinations to yield the same reservoir ratio's, to assess the effect of actual water heights upon the measurements. A significant, but acceptable, amount of error is introduced by varying this ratio, especially for significant differences in reservoir height, i.e. T_{02}/T_{01} small. For these cases, three-dimensional effects are very pronounced. Though not presented here, repeatability using similar reservoir ratios, but rerunning the overall experiment, is excellent.

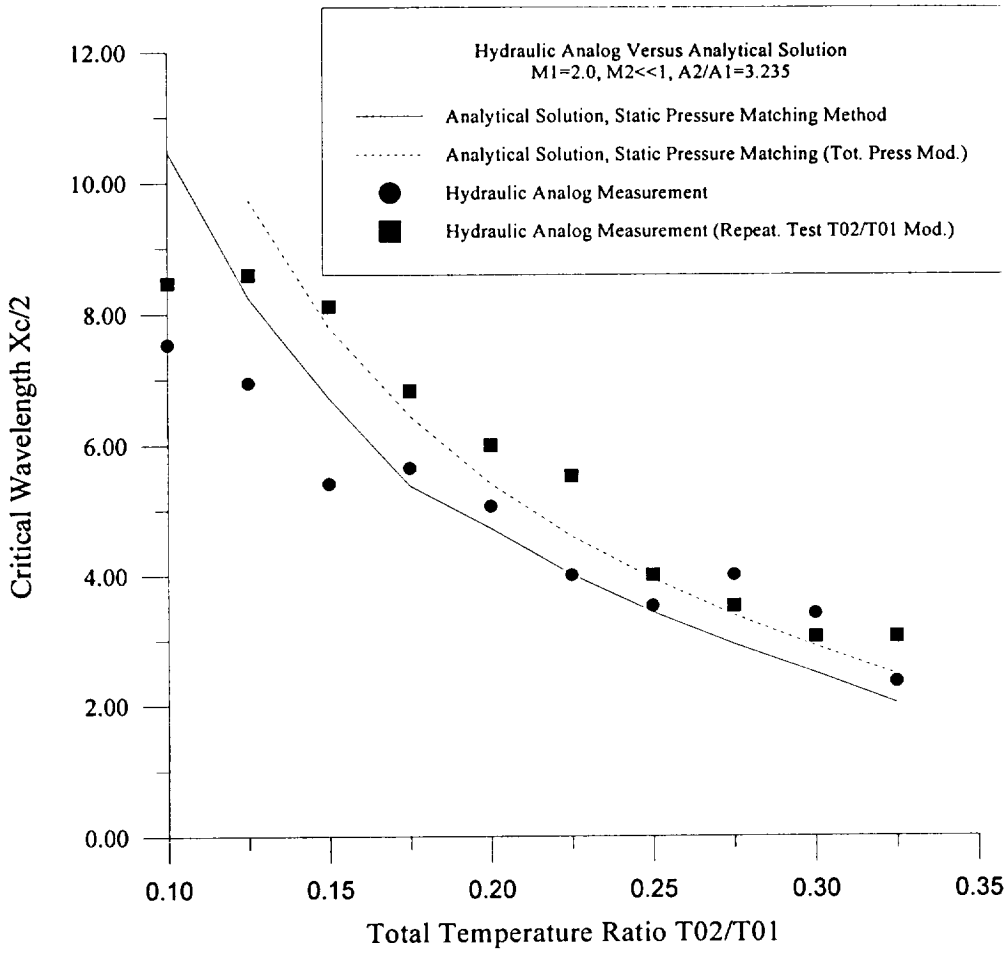

FIGURE 4.6 Comparison of experimental and model critical interface lengths, for A_2/A_1=3.235.

A series of general conclusions may be drawn from the Figures 4.5 and 4.6.

- The theoretical model, De Chant et al. (1996) and Section 2.3.1., provides reasonable agreement with the analog measurements. This good agreement gives confidence in the simple model described previously. Alternatively, the analog provides a reasonable simulation of inviscid gas flow phenomenon including the choking phenomenon characteristic of supersonic nozzle flow.
- The hydraulic analog provides an inexpensive, adequately repeatable model for studying inviscid, multiple stream flows.

The simple correction model, i.e. modification of the total pressure ratio term $2\rightarrow 2\pm\varepsilon$, with $\varepsilon=1/8$, provides moderate improvement for the analytical model.

4.5 Experimental conclusions

Inviscid, confined supersonic and subsonic stream interactions have been studied using an experimental hydraulic analog model, as well as, an approximate, perturbation theoretical model. Specifically, the first critical location of the slipline is considered. Reasonable agreement is shown between the theoretical model and analog measurements, hence helping to validate the concepts developed in Section 2. Additionally, a method for extending the isentropic analogy to model these inherently non-

isentropic flows was discussed. This work was of considerable use in extending our understanding of aerodynamic mixer ejector nozzle operation.

5. RESULTS AND CONCLUSIONS

5.1 Results

This section compares the computational methods developed previously to experimental measurements. Given the wide range of approximations inherent in this modeling effort, this type of comparison is absolutely mandatory. Since many of the supporting analyses have been partially validated along the way, the overall computational code, DREA is compared in detail. Included in these results are:

- flow conservation and grid independence studies
- integral quantities: pumping/entrainment and CFG
- local quantities: streamwise and cross-stream profiles of Mach number, velocity, and static pressure. Additionally, we present limited contour information to get a view of the overall ejector phenomenon.

It should be pointed out, that results are virtually always computed and presented in dimensionless form. The input files use dimensional quantities only to ease interfacing with existing codes. Spatial position, x and y are scaled by the inlet centerline to shroud distance:

$$x_{non-diim} = \frac{x}{h(0)} \quad y_{non-\dim} = \frac{y}{h(0)} \tag{5.1}$$

where h(0) is the inlet shroud to centerline distance as shown in Figure 5.1.

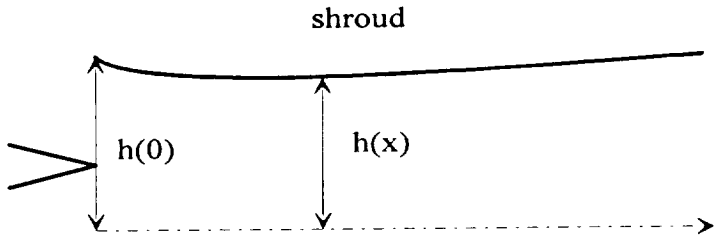

FIGURE 5.1 Definition of non-dimensionalization quantities.

Additionally, the dependent variables, both conservative and primitive variables, are scaled by the inlet mixing plane, area averaged conditions. These conditions are chosen, since they are readily available. In other words:

$$f_{non-\dim}(x,y) = \frac{f(x,y)}{f_{ave}} = \frac{f(x,y)}{f_{10}A_{10} + f_{20}A_{20}}\left(A_{10} + A_{20}\right) \tag{5.2}$$

Note that the "non-dim" subscript is virtually always suppressed.

5.1.1 Flow conservation and grid independence studies

In this section, some computational aspects of our simulation are considered. Here, we are principally concerned with the numerical accuracy of our simulation. To ascertain numerical errors, concentration is placed upon, the momentum flux, $G=\rho u^2+p$ (which is conservative) for a simple subsonic flow problem with a constant area shroud. Our interest is in the degree to which the integral constraint will be satisfied:

$$\int_0^1 \phi(x,y)dy = 1 \tag{5.3}$$

where, $\varphi=G$. The degree to which the constraint is satisfied is dependent upon several factors that are presented in Table 5.1:

solution portion	dependency	comments
numerical solution	Δy (j_{max}) and Δx (i_{max})	truncation errors in streamwise and cross-stream direction
analytical solution	n_{max}	number of terms in Green's function expansion
numerical integration	Δy (j_{max})	cannot resolve near field singularity
shroud geometry	number of wall points and length	second order

TABLE 5.1 Sources of numerical and truncation error for integral constraint.

We start by considering a subsonic, constant area shroud problem the size of the constraint, again which must equal one, for a basic $j_{max}=20$ and $i_{max}=30$. As is clearly shown in Figure 5.2 (and accentuated by the logarithmic scales), the near field value of the constraint, is poorly predicted.

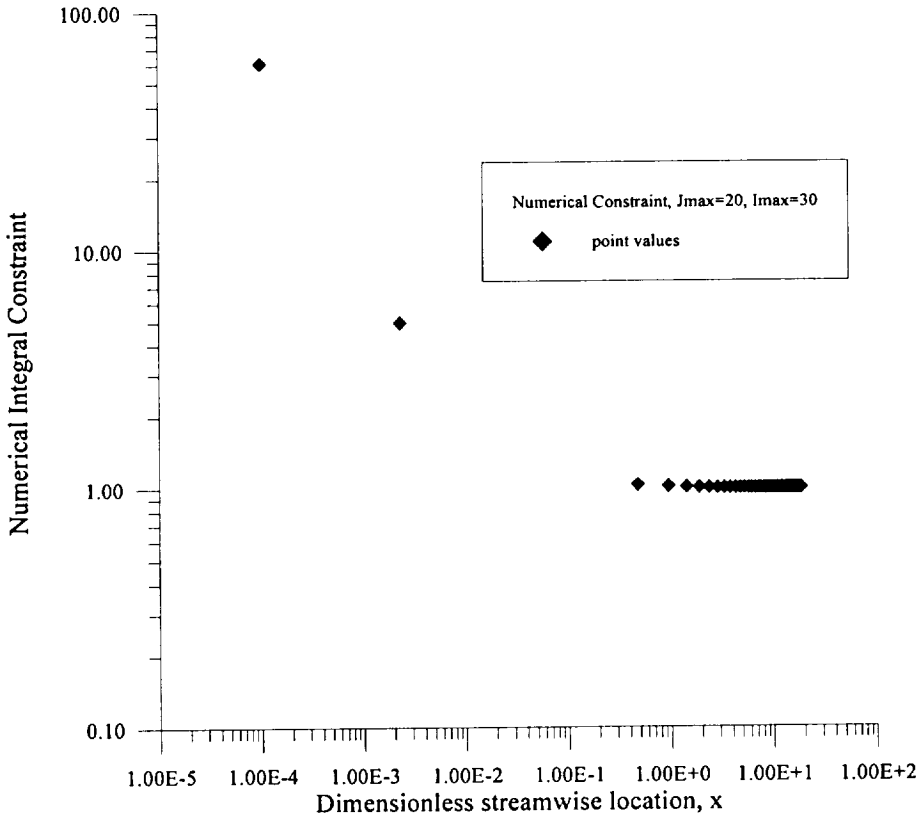

FIGURE 5.2 Values of the integral constraint at various streamwise locations.

This failure is directly related to the inability of the polynomial based, variable step integration routine, which is incapable of resolving the near field singularity. This limitation is exactly analogous to the inability to resolve the near field "Heaviside" step function using solely numerical means. This limitation is somewhat irrelevant, in that in a very short distance, the solution recovers the desired constraint value. Further, it should be emphasized, that the quadrature method is in error; not the underlying functional values at the knots, since these values were computed using our combined analytical/numerical method which is capable of resolving the singular behavior.

Due to the fact, that the integration routine cannot be used in the near field it would be more sensible to consider the degree of error, as a function of grid parameters, in the constraint at the exit of the flow.

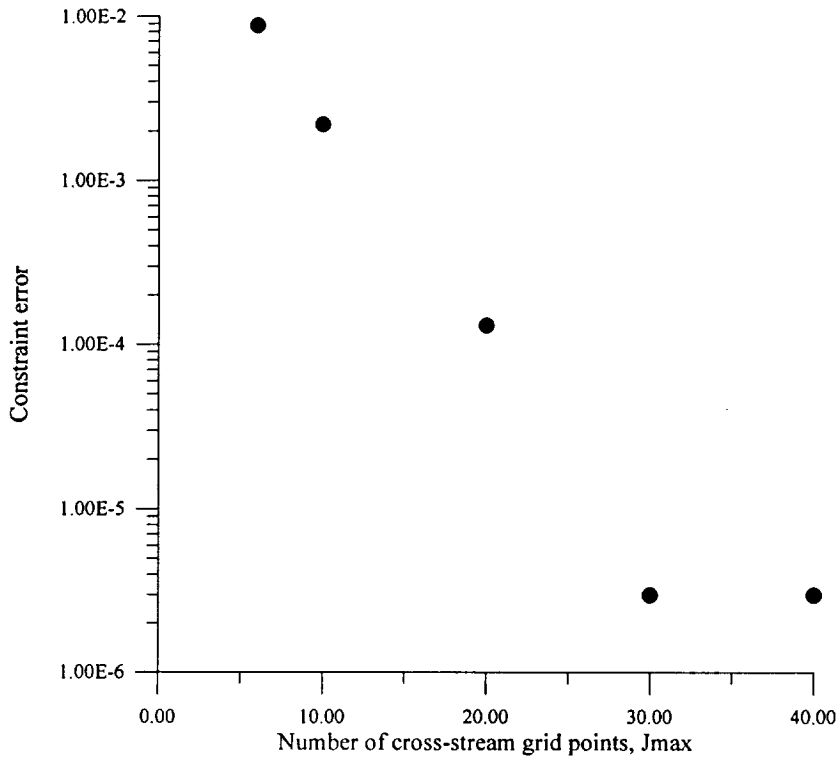

FIGURE 5.3 Relative error in satisfaction of integral constraint versus number of cross stream grid points evaluated at ejector exit plane for a subsonic ejector.

As can be seen from Figure 5.3 the expected grid dependence is observed. The numerical error, does indeed does drive to a maximum (where round off issues may become important, more likely, though, the definition of the shroud geometry which uses a cubic spline basis is the key limitation). Additionally, a simple regression of the linear (on a logarithmic plot) portion of this plot, Figure 5.4:

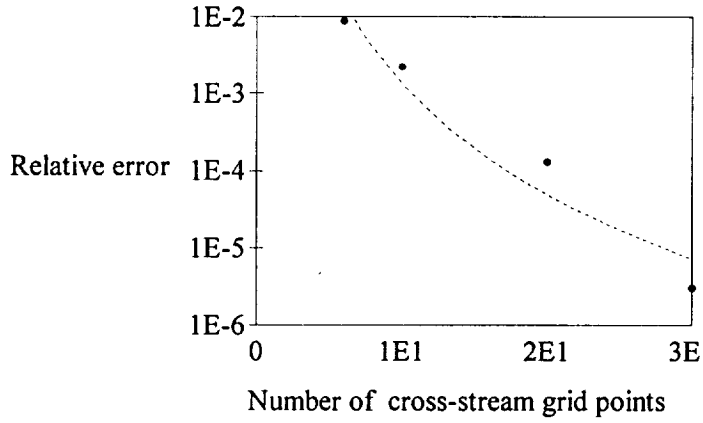

FIGURE 5.4 A regression fit of relative error versus number of cross-stream grid points at the exit plane which demonstrates 4th order accuracy for a subsonic ejector.

clearly indicates the fourth order (exponent=-4.77; actually almost fifth order) dependency of the constraint upon the number of cross stream grid points. It is shown, that the numerical portion of the code is contributing very little error. Most of the error in this problems is being generated due to the integration routine itself.

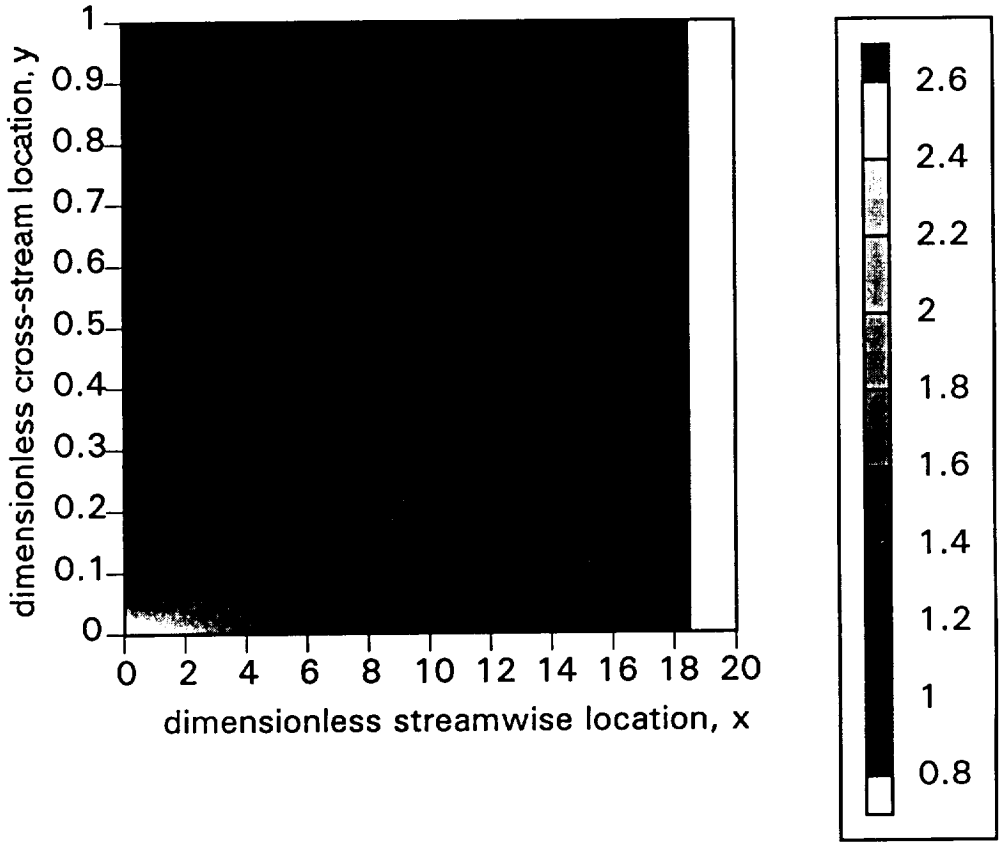

FIGURE 5.5 Contour plot of momentum conservation term, G, demonstrating rapid cross stream variation and gentle streamwise variation for a subsonic constant area ejector.

Performing the same type of computations, except now holding the cross-stream coordinate constant and considering the effect of the streamwise coordinate shows the insensitivity of the modeling to streamwise gradients. This is of little surprise, in that, the most significant changes occur in the cross stream direction. Recall that it was indicated in Section 3 that this was the basis for accepting a method which is 4th order in the cross-stream and only 2nd order in the streamwise direction. Additionally, the numerical portion of the solution is virtually negligible for this problem. Variation in the streamwise direction is scaled at O(1). As expected, and indeed found, the solver is virtually independent upon the number of streamwise, I_{max} steps. The gentle streamwise change is shown in the Figure 5.5:

Similarly, it is found that the total solution is virtually independent of the number of terms of the series used to evaluate the numerical portion of the total solution for G, i.e. N_{max}. As shown in the previous figure, the relatively small size of the primary stream denotes a small value for h_s, hence reducing the required value for n.

$$n = \frac{1}{2}\left(1 + h_s + (2a^*)^{\frac{1}{2}} x \left\{ -\ln\left[\frac{2(2a^*)^{\frac{1}{2}} x \frac{\partial \phi_{an}}{\partial y}}{(\phi_{10} - \phi_{20})} \right] \right\}^{\frac{1}{2}} \right) \tag{5.4}$$

In fact, it is expected the numerical contribution for this case to be negligible.

We do not desire to leave the reader with impression, that the numerical solver is unimportant. If one considers an alternative supersonic constant area shroud test problem and print out the values for $(G_{an}-G_{num})/G_{an}$, it is possible to see that, indeed the numerical contribution to the solution is non-negligible. See Figure 5.6. Additionally, the local streamwise changes in the number of terms used in the numerical solution are apparent, i.e. x=3. Further, as expected, the numerical contribution near the shear layer is small and increases upon approach to the boundaries (especially the y=1 boundary).

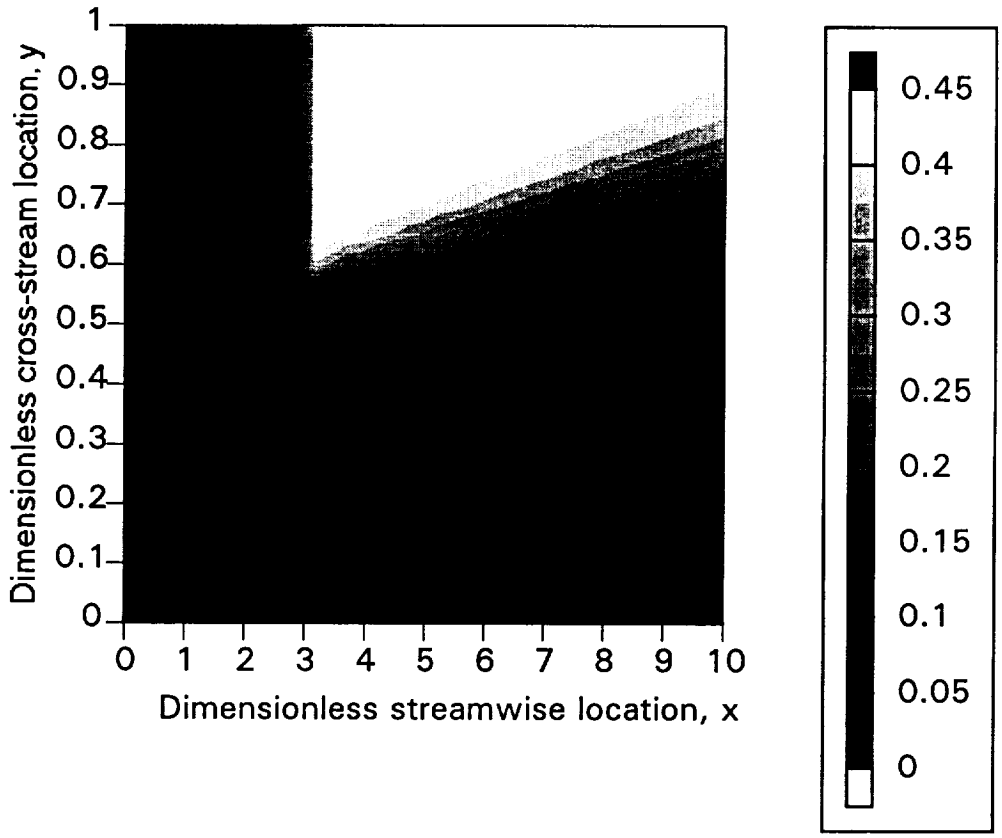

FIGURE 5.6 Contour plot of $(G_{an}-G_{num})/G_{an}$ for a constant area supersonic ejector indicating non-trivial numerical contribution far from centerline; y=0.

Performing the same types of grid independence tests for this problem, Figure 5.7:

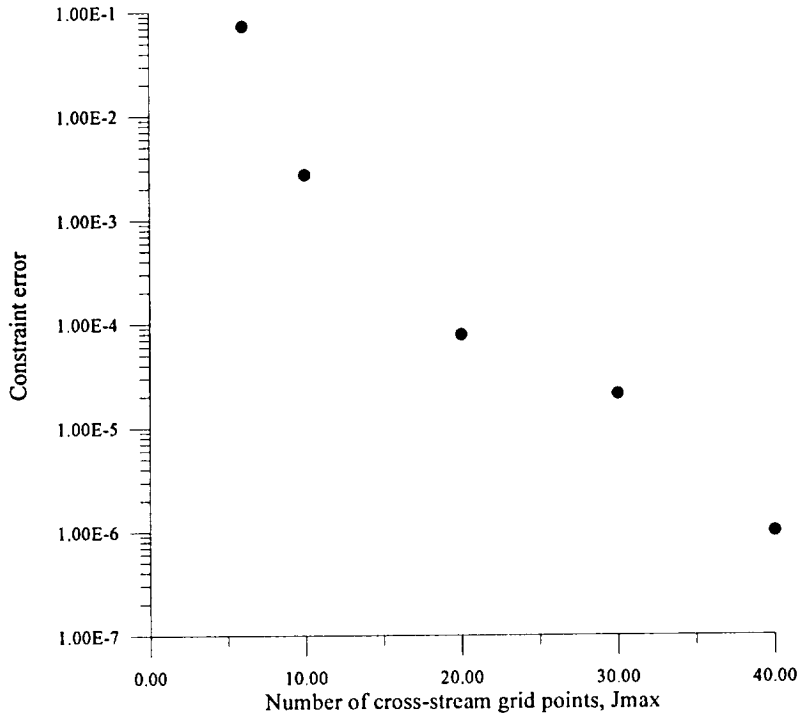

FIGURE 5.7 Relative error in satisfaction of the integral constraint versus number of cross stream grid points evaluated at the ejector exit plane for a supersonic ejector.

The constraint error for the supersonic problem is also decaying at a rapid rate. Regression and Figure 5.8 indicate that the exponent for this problem is approximately, -5.5.

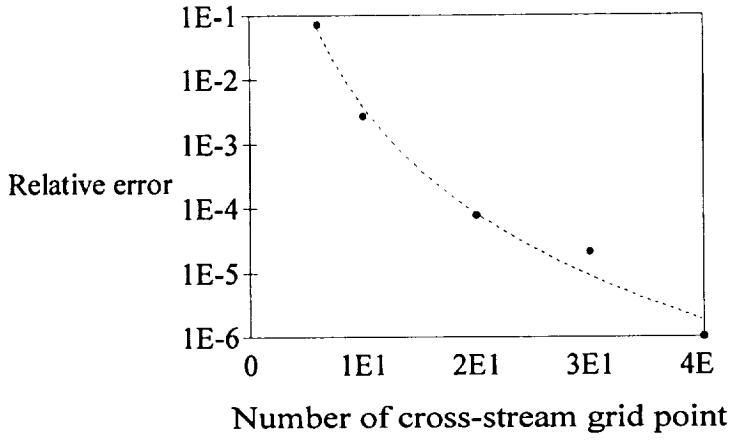

FIGURE 5.8 A regression fit of relative error versus the number of cross-stream grid points at the exit plane which demonstrates 4th order accuracy for a supersonic ejector.

Value indicates, that the numerical solver and the numerical integration algorithm are indeed yield fourth order accuracy (or better!).

This completes our discussion of grid independence and conservative integral constraints. It is reasonable to conclude that the combined numerical/analytical solution is providing a consistently high accuracy solution. Of course, this conclusion must be tempered, by the reality that though the equations are being solved accurately and consistently, the value of the solution is only as good as it compares to physical solutions. This demands a comparison with experimental results (which may contain measurement and reduction error) but have the greatest chance of mimicking the physical prototype, in that they are measurements of physical processes and quantities. Comparison with experiment is discussed in the next section.

5.1.2 Summary of comparisons

Here a family of test cases of increasing complexity is presented. The latter two test cases are from current industry/NASA sources. Comparison to this data is critical since it represents the forefront of aerodynamic ejector technology, which is the family of problems that DREA has been designed to model. Hence use of this data indicates that DREA can make a significant contribution to actual modeling problems.

The list of ejectors modeled is presented in Table 5.2.

Experiment	Primary Conditions	Secondary	Shroud Geometry	Mixer/ splitter plate	comments
Gilbert and Hill (1973)	M_1=1.0 P_{01}=4551.8 psf T_{01}=827.2 R	M_2=self induced P_{02}=2103.8 psf T_{02}=533.0 R	variable	simple, 2-d slot mixer	fully subsonic ejector, streamwise profiles, pumping
Goebel and Dutton (1991)	M_1=2.35 P_{01}=10,166.32 psf T_{01}=648.0 R	M_2=0.3 (fixed) P_{02}=800.31 psf T_{02}=522.0 R	fixed	simple, 2-d slot mixer	shear layer mixing, Cross-stream profiles
Fernando and Menon (1993)	M_1=2.5 P_{01}=12,322.4 psf T_{01}=530 R	M_2=1.0 (fixed) P_{02}=1274 psf T_{02}=530.0 R	fixed (locally)	Re_{vort}=0.087 h_0/λ=0.428 $h_0/h(0)$=0.0061	shear layer mixing, secondary stream controlled, vortical mixer
Arney and Lidstone	M_1/M_2=2.86 P_{01}/P_{02}=3.36 T_{01}/T_{02}=1.0-3.0	M_2=(fixed)	fixed	simple, 2-d slot mixer	shear layer mixing, secondary stream controlled, CFG and entrainment
Thayer et al.	M_1/M_2=self induced P_{01}/P_{02}=3.5 T_{01}/T_{02}=2.2	M_2=self induced	fixed and variable	Re_{vort}=2.0 $h_0/h(0)$=1.0	shear layer mixing, CFG and entrainment

TABLE 5.2 Summary of comparisons and results.

5.1.3 Gilbert and Hill (1973)

This is a two-dimensional, (planar splitter plate), subsonic (choked primary), variable area shroud ejector. Results are provided for pumping in Table 5.3 and streamwise mixing (including pressure, velocity and temperature fields).

Entrainment	experimental measurement	DREA computation	relative error
w_2/w_1	3.76	3.69	1.86%

TABLE 5.3 Comparison of DREA simulation entrainment prediction with Gilbert and Hill (1973).

The comment may be made that the entrainment prediction is very good. This type of accuracy is probably fortunate, rather, than something to be relied upon. Additionally, since the ejector is completely subsonic, it should be expected that the entrainment will be insensitive to the length of the shroud. Of course, this is an approximation.

To gain a feeling for the flow field mixing, consider the normalized velocity, static pressure and static temperature. They are presented in Figures 5.9, 5.10 and 5.11, respectively:

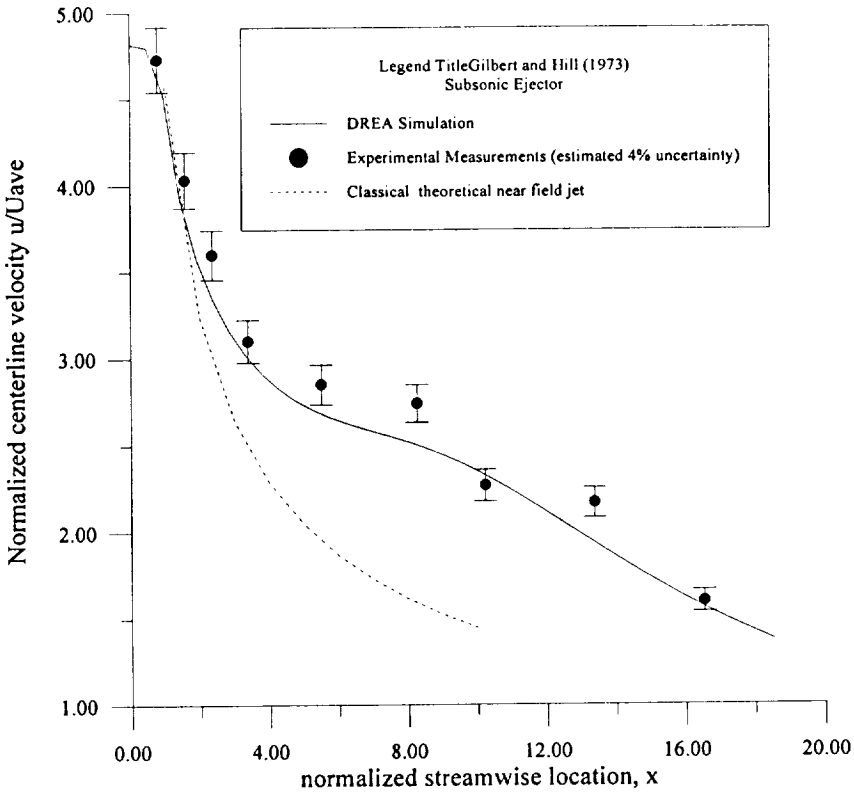

FIGURE 5.9 A comparison between the DREA simulation and experimental data of Gilbert and Hill (1973) showing centerline velocity versus streamwise location with uncertainties estimated from the literature.

We note that the simulation provides a reasonable comparison to the experimental data over the entire range. Some deviation is observed in the mid region of the flow, where variable area shroud effects are especially important (and not precisely modeled). Fortunately, the Gilbert and Hill (1973) report, relative to other data sets, provides information on the experimental error and, more importantly, information on the associated uncertainty. Gilbert and Hill estimate their uncertainty to be on the order of 4%. This uncertainty estimate is the experimental workers best estimate of error propagation, as well as, an estimate of the degree of scatter from repeatability tests. Four- percent error bars are introduced into Figure 5.9.

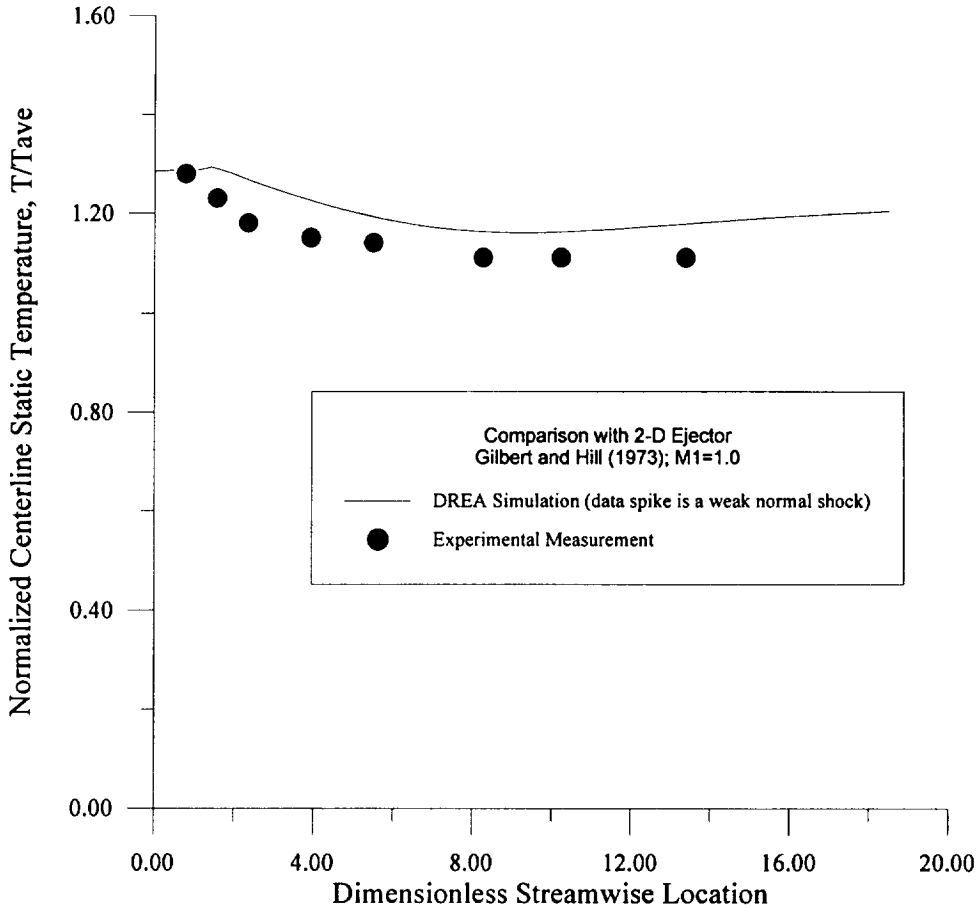

FIGURE 5.10 A comparison between the DREA simulation and experimental data of Gilbert and Hill (1973) showing the centerline static temperature versus streamwise location.

Comparison with the static temperature, shown in Figure 5.10 is adequate. Though the plot tends to "magnify" the error, the relative error is no more than 8%.

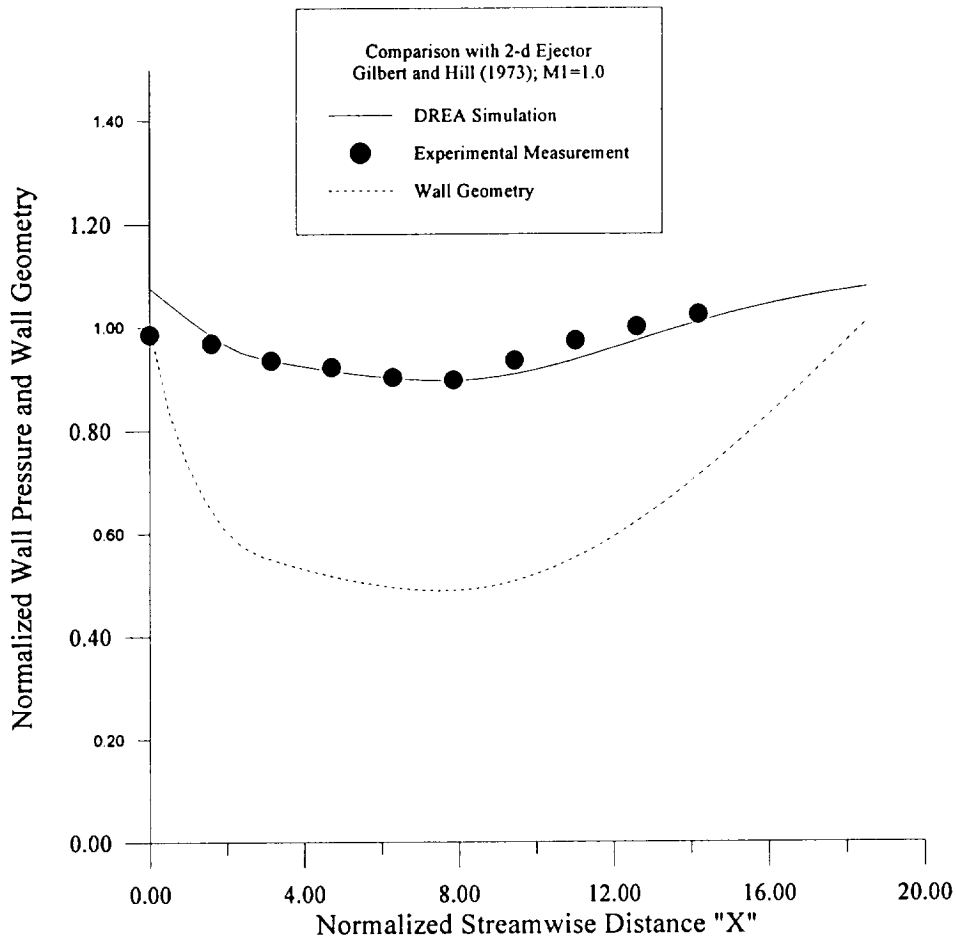

FIGURE 5.11 A comparison between the DREA simulation and experimental data of Gilbert and Hill (1973) showing wall static pressure versus streamwise location.

Wall pressure values are well modeled as shown in Figure 5.11. Here we have introduced the low Mach number wall correction described in Section 2. Next a supersonic/subsonic mixing layer problem is considered.

5.1.4 Goebel and Dutton (1991)

This is a supersonic subsonic mixing problem. The primary Mach number, M_1=2.5 and the secondary is M_2=0.3. The secondary static conditions are controlled so as to force matching (or closely approximate it) of the static pressures at the interface. As such, no independent entrainment information is available.

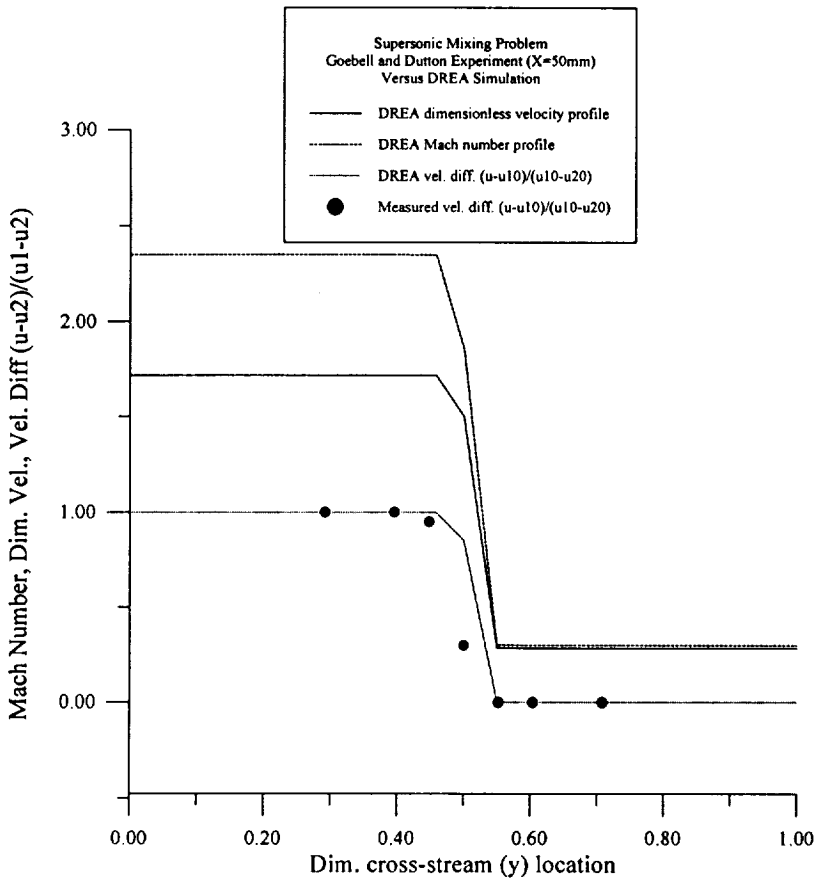

FIGURE 5.12 Comparison between DREA simulation and experimental data of Goebel and Dutton (1991); dimensionless velocity difference profile, $(u-u_2)/(u_1-u_2)$; x=50 mm.

It is possible, though, to assess the degree of mixing in the flow. Here, the interest is the width of the mixing zone. Comparisons are provided for two streamwise locations x=50 mm and 100 mm, Figures 5.12 and 5.13 respectively, measured from the splitter plate.

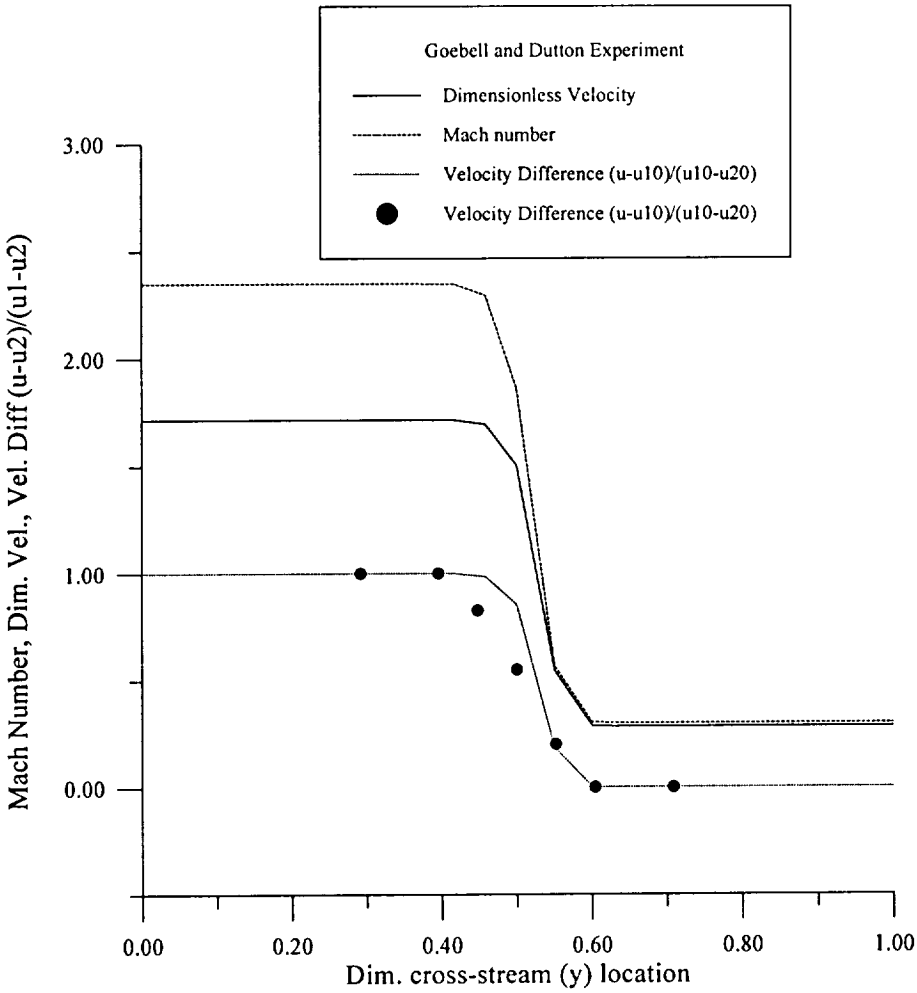

FIGURE 5.13 Comparison between DREA simulation and experimental data of Goebel and Dutton (1991); dimensionless velocity difference profile, $(u-u_2)/(u_1-u_2)$; x=100 mm.

As can be seen, the mixing width (slope of the mixing layer) is predicted very well. This is encouraging, indicating that, at least locally, the turbulence model is providing a correct estimate of the mixing rate. Unfortunately the location of the mixing layer is not as good. Several explanations for this minor disagreement are possible. One possibility is that there are wall boundary layer blockage effects, distorting the streamlines. More likely, there are small pressure imbalances (even locally) which result in expansion or contraction of the dividing slipline.

5.1.5 Fernado and Menon (1993)

The next problem, considered is a supersonic (Mach 2.5 and, choked flow (Mach 1.0) mixing problem studied by Fernando and Menon (1993). This study involves a 2-d mixing layer shown schematically in Figure 5.14.

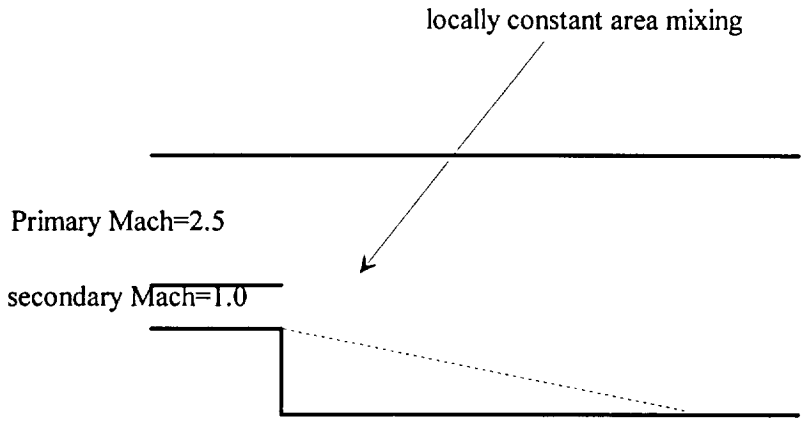

FIGURE 5.14 A diagram of the basic experimental apparatus for Fernado and Menon (1993).

Due to the large change in shroud geometry, this flow is modeled as a straight wall (and our comparison is confined to early in the flow field). Figure 5.15 shows a 2-d slot ejector, which is essentially a reference case. Comparison with experiment is adequate. Again, the physical location of the shear layer is not exactly predicted. Here, wave expansion/compression effects around the step are unavoidable, potentially modifying the interface slipline. Results are presented in Figure 5.15.

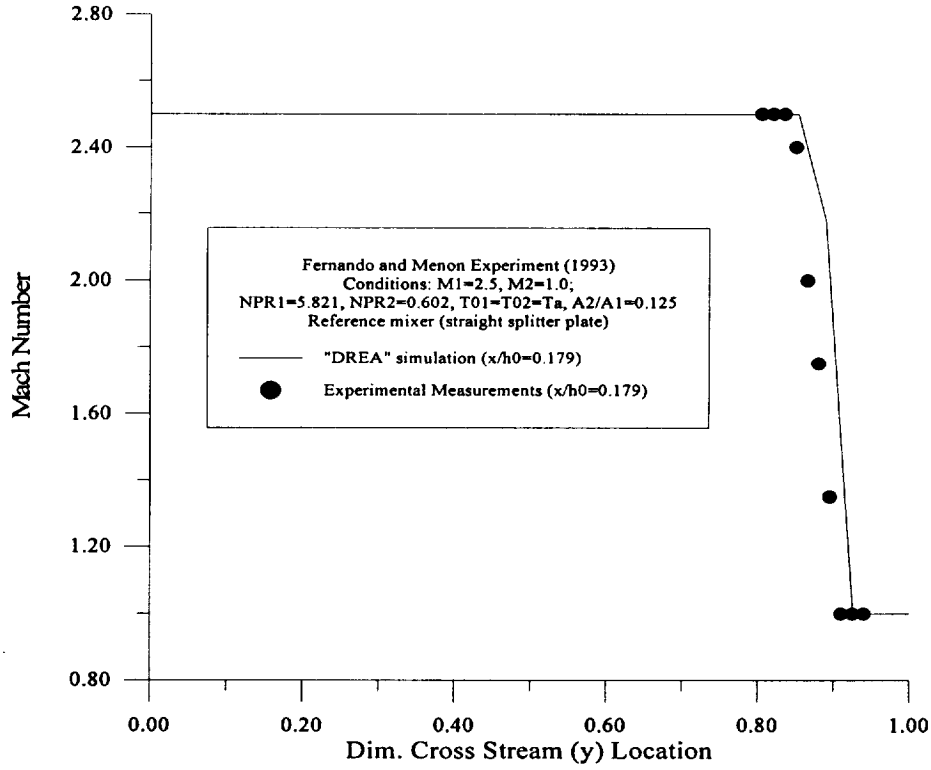

FIGURE 5.15 A comparison between the DREA simulation and experimental data of Fernando and Menon (1993) showing the Mach number profile for a slot mixer.

The second case considered, is a vortically mixed convoluted, splitter plate. The three vortical parameters for this case are presented in Table 5.4.

Vortical Reynolds Number	Lobe total height/lobe wavelength	Lobe total height
Re_{vort}=0.087	h_0/λ=0.428	$h_0/h(0)$=0.0061

TABLE 5.4 Vortical parameters for Fernando and Menon (1993).

Since the lobe penetration (height) is relatively small, the effect on overall mixing is slight. Locally, however the flow is locally accelerated near the chute causing the experimental jump in Mach number.

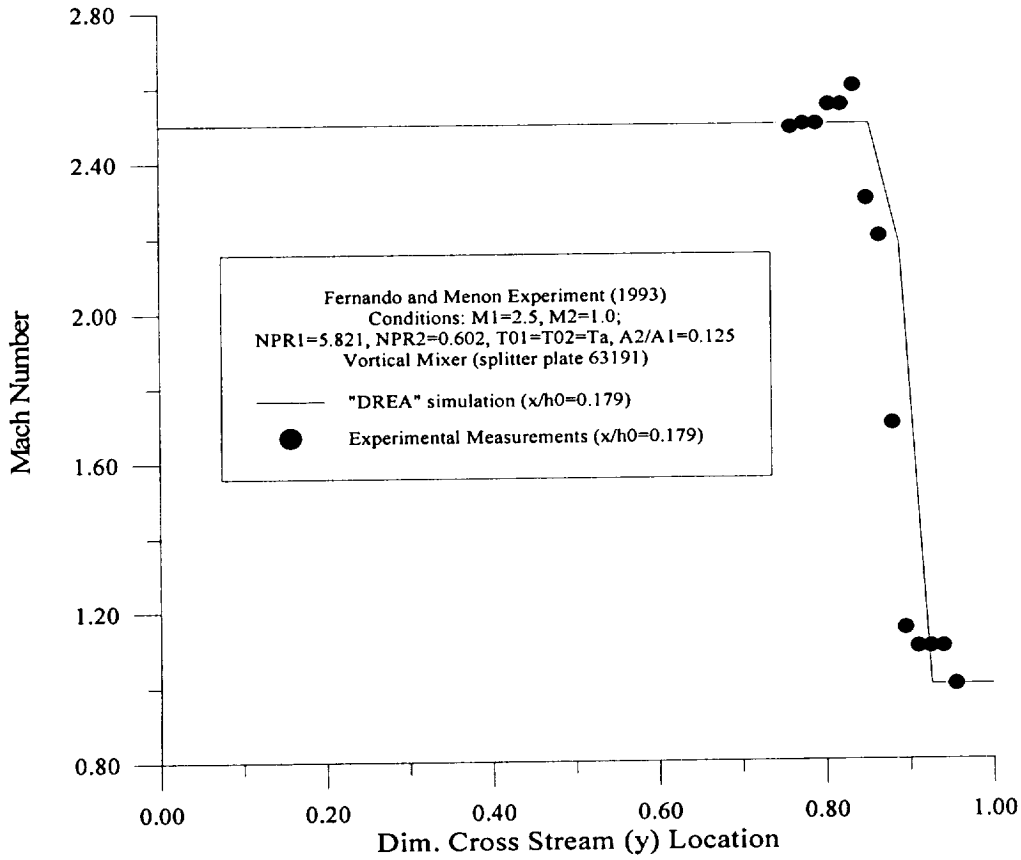

FIGURE 5.16 A comparison between the DREA simulation and experimental data of Fernando and Menon (1993) showing the Mach number profile for a vortical mixer.

From figure 5.16, it is clear that the computational model, though, cannot predict this local acceleration as the flow comes off the chutes (recall, that our model is averaged in the z-direction). Alternatively stated, the computational model cannot detect local primary or secondary chute disturbances. The model does, however,

include the enhanced mixing effect upon the average stream conditions. Considering the overall Mach number, though, we see that the mixing zone width is well predicted.

5.1.6 Arney and Lidstone

The next family of predicted problems involves advanced nozzles tested at Boeing. These are combined supersonic primary and subsonic secondary stream mixing flows, M_1/M_2=2.86. A large family of tests has been considered here. Concentration is placed upon several of them. The Boeing nozzle tests are a simple, slot ejector problem. The intention of these tests though is provide local information, since in close proximity to a lobe, the flow acts like a 2-d shear layer.

Though it is not totally clear from the report, it seems apparent that secondary quantities have been controlled, hence secondary entrainment is not an independent code predicted quantity. These cases, though, do provide an excellent test of mixing within the duct. Experimental data was taken using LDV Laser-Doppler velocimetry. The conditions simulated in this report are listed in Table 5.5.

Figure	Total Temperature ratio; T_{02}/T_{01}	Total Pressure ratio; p_{02}/p_{01}	Streamwise Location, x/h(0)
5.17	1.0	3.5	1.05
5.18	1.0	3.5	4.2
5.19	0.49	3.5	1.05
5.20	0.49	3.5	4.2
5.21	0.332	3.18	4.2

TABLE 5.5 Parameter summary Arney and Lidstone.

Additionally, limited experimental error estimates have been provided, especially for the LDV system. No data uncertainty estimates have been provided at all.

The first set of comparisons Figures 5.17 and 5.18 are for the conditions with NPR (nozzle pressure ratio, i.e. p_{01}/p_{∞}) of 3.5. Total temperatures are matched for this case.

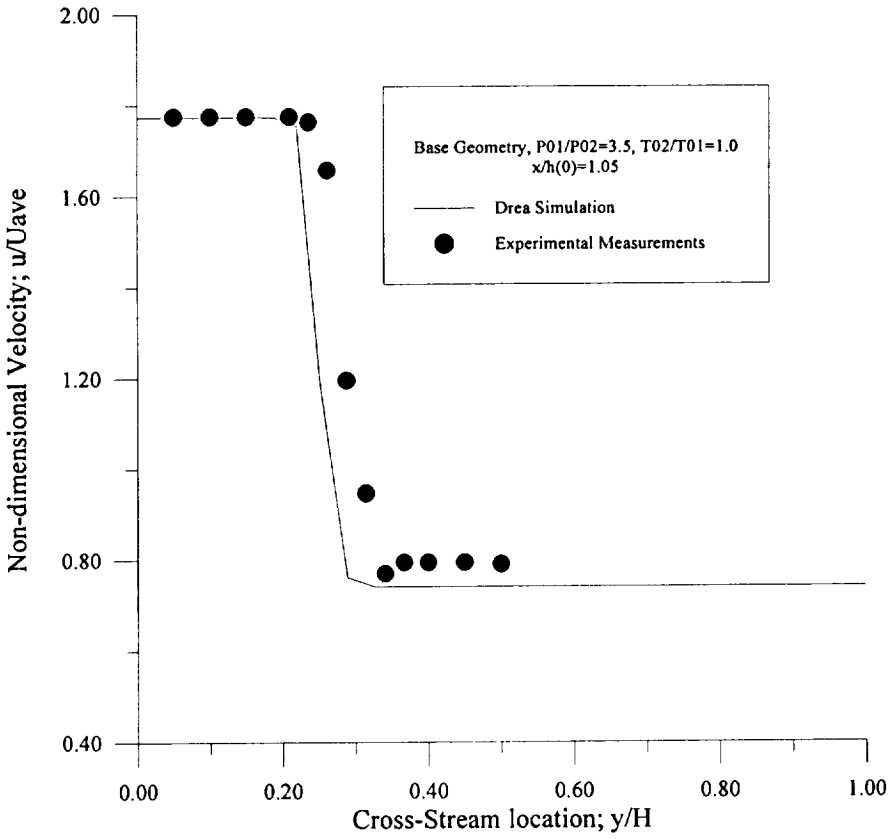

FIGURE 5.17 A comparison between the DREA simulation and experimental data of Arney and Lidstone using a dimensionless velocity profile for a slot mixer, with x/h(0)=1.05.

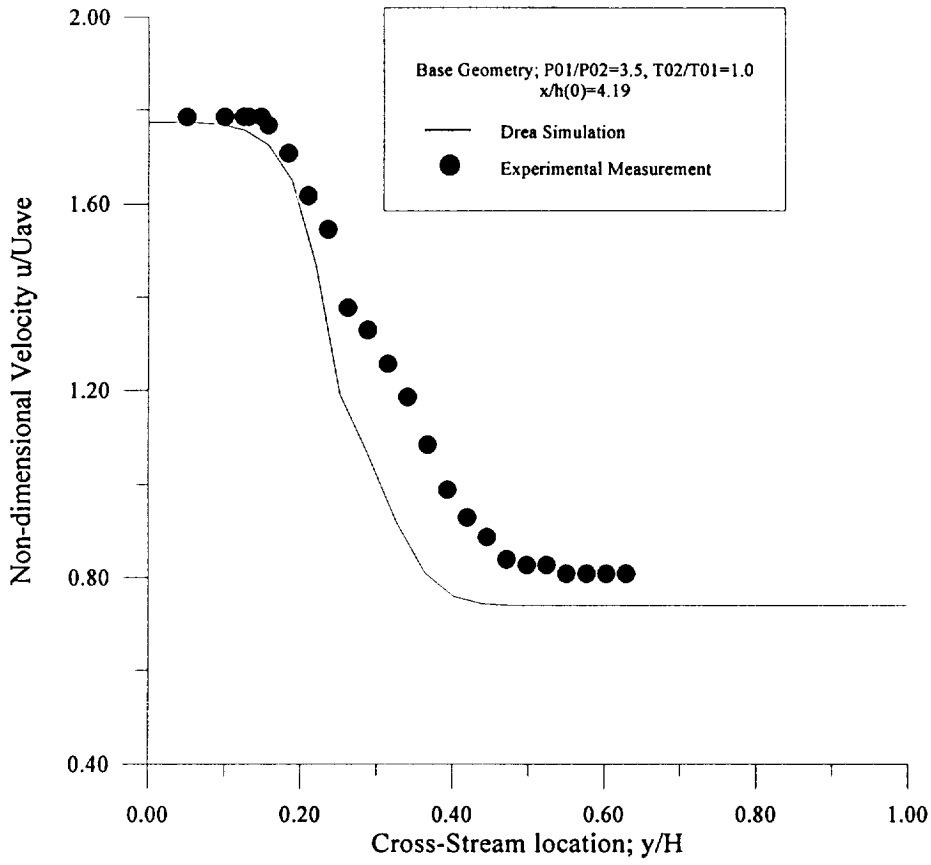

FIGURE 5.18 A comparison between the DREA simulation and experimental data of Arney and Lidstone using a dimensionless velocity profile, a slot mixer, x/h(0)=4.2 and matched total temperatures.

Alternatively, a hot flow set of measurements (implying dissimilar total temperatures), Figures 5.19 and 5.20, is considered:

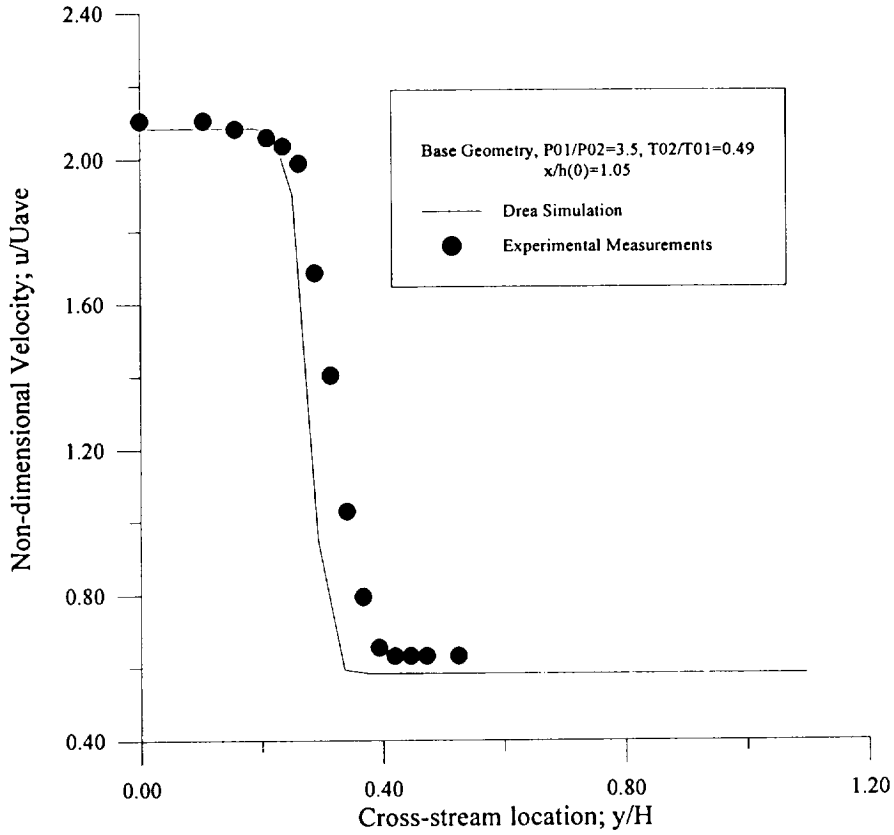

FIGURE 5.19 Comparison between DREA simulation and experimental data of Arney and Lidstone; dimensionless velocity profile, slot mixer, x/h(0)=1.05. Hot flow case; T_{02}/T_{01}=0.4890.

and at a location farther downstream:

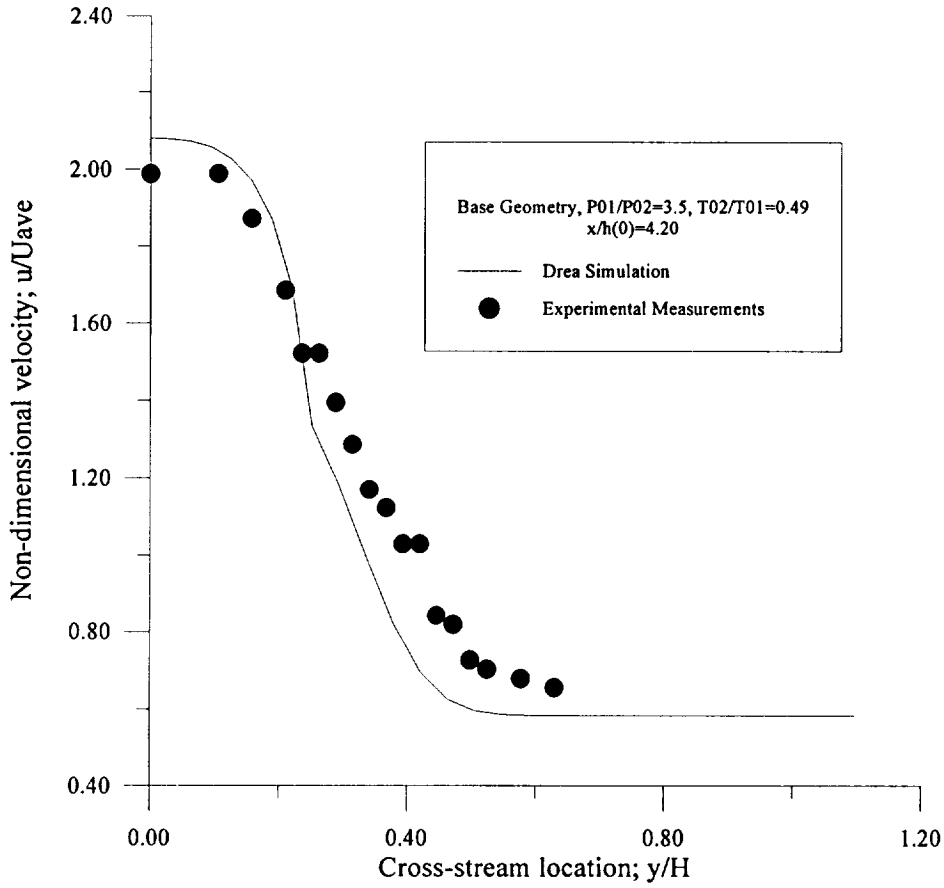

FIGURE 5.20 A comparison between the DREA simulation and experimental data of Arney and Lidstone using a dimensionless velocity profile, slot mixer, x/h(0)=4.2 and T_{02}/T_{01}=0.4890.

Finally a further set of hot flow measurements, i.e. strongly dissimilar total temperatures, are shown in Figure 5.21:

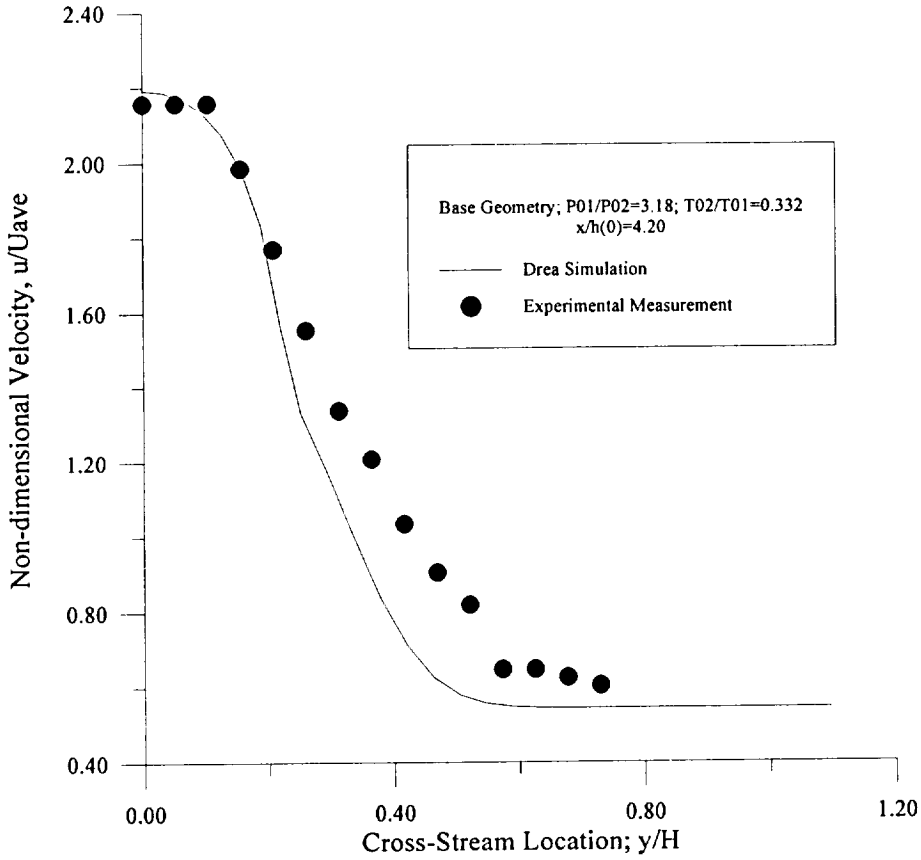

FIGURE 5.21 A comparison between the DREA simulation and experimental data of Arney and Lidstone using a dimensionless velocity profile, slot mixer, x/h(0)=4.2 and T_{02}/T_{01}=0.3317.

Equally important are thrust considerations. In the following figure, Figure 5.22, CFG (Gross thrust coefficient) and pumping (entrainment) are provided.

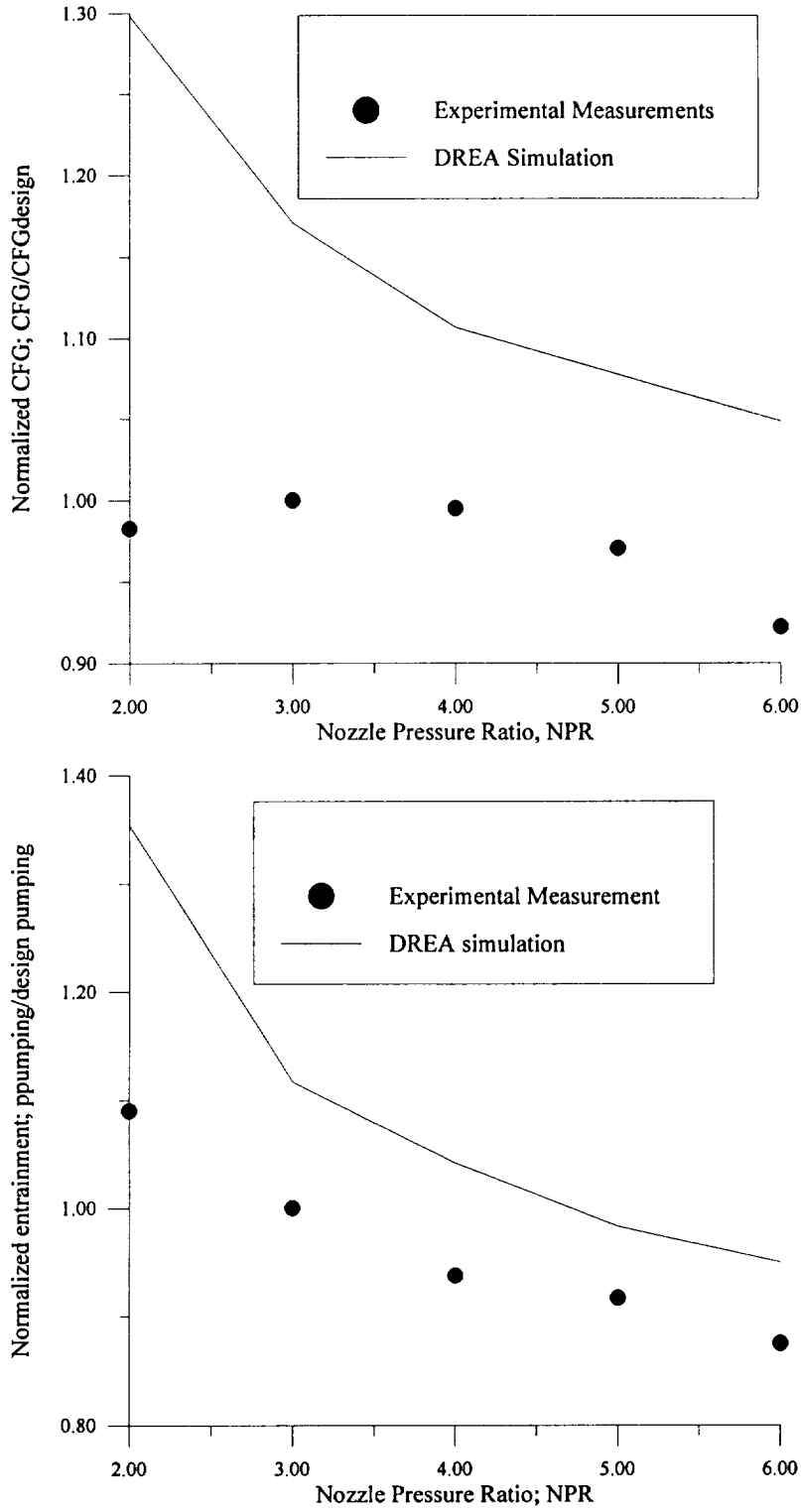

FIGURE 5.22 A comparison between the DREA simulation and experimental data of Arney and Lidstone showing entrainment and gross thrust coefficient for a slot mixer. This is a hot flow case.

While it is clear that the trend is correctly predicted, the values are in moderate to large relative error. Of special importance (this is related to the flight regime of interest) is the mid location of these graphs (i.e. NPR 2-4), where one may note relative errors on the order of 11-23%. The normalization values used are the CFG and entrainment values evaluated at an NPR of 3.0, respectively.

The source of this error is somewhat hard to estimate. Since the velocity field has been matched adequately as presented in Figures 5.17-5.21, only the density computation or (and we believe this to be most likely error source) the inlet cross-sectional areas are incorrect. Recall that, since the secondary stream was controlled by upstream valves, the control volume pumping routine has not been employed, and is therefore not the cause of this discrepancy. That some form of inconsistency may be contained within the data is also supported by the CFD simulations performed by R. K Henke (1994) who showed good velocity match, but an unrealistic expansion\compression interface structure (the static between stream is matched, hence the "shock diamond" system is erroneous). Henke notes the problem, but offers no explanation. Our computations indicate that the static pressure is indeed matched. The possibility that boundary layer blockage is biasing the computations must also be considered.

5.1.7 Thayer et al.

The final set of cases are vortical supersonic/subsonic (subsonic at exit) cases. Figure 23 compares the CFG and entrainment computed by DREA with that from the test data.

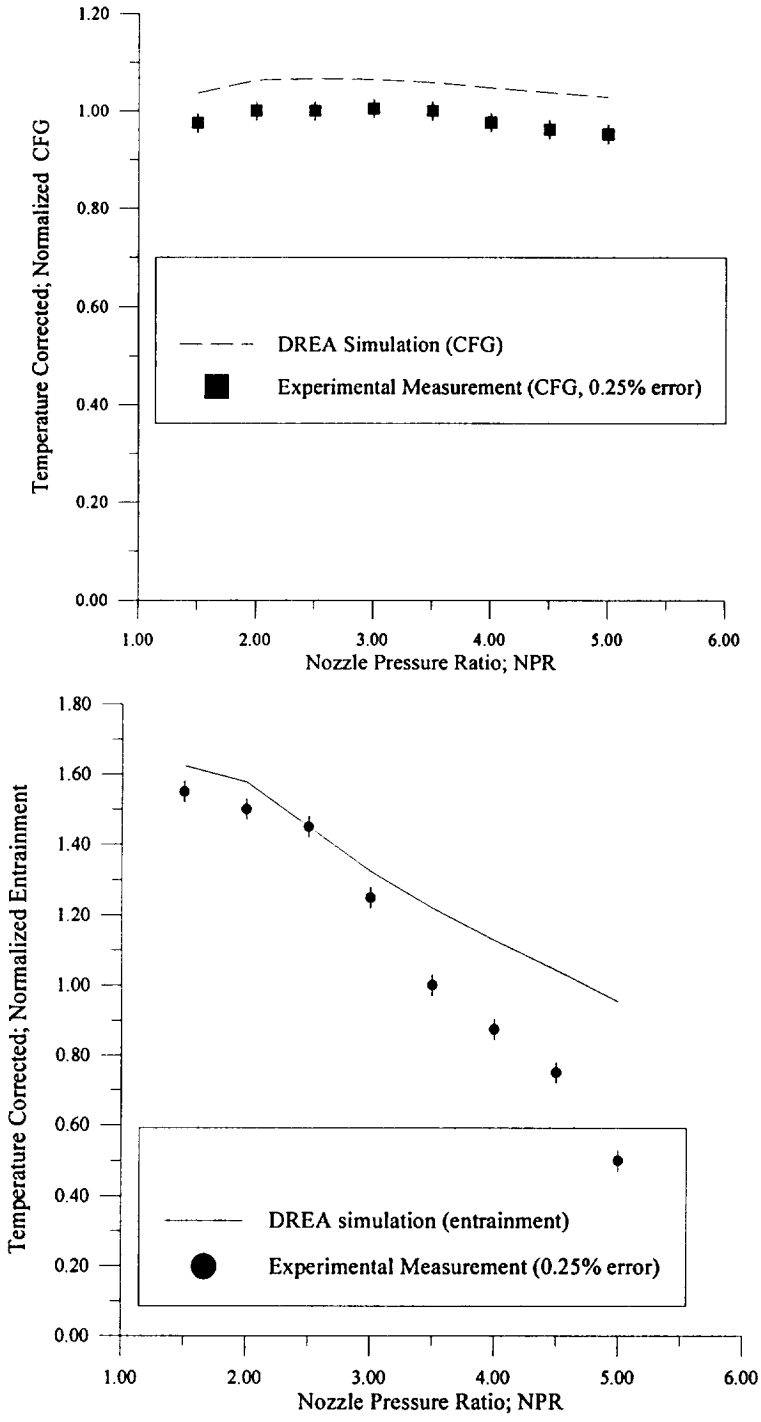

FIGURE 5.23 A comparison between the DREA simulation and experimental data of Thayer et al. with estimated experimental error for a vortical mixer.

As can be seen from Figure 5.23, the error here is relatively small for the CFG, 10-12%, but ranges from negligible to 100% for entrainment. The temperature corrections consist of multiplying CFG and

entrainment by $(T_{02}/T_{01})^{1/2}$, respectively. The normalization values are chosen at an NPR of 3.5. Of special interest is the middle range which again shows tolerable error. The error bars represent a 0.25% measurement error. No uncertainty estimates are available.

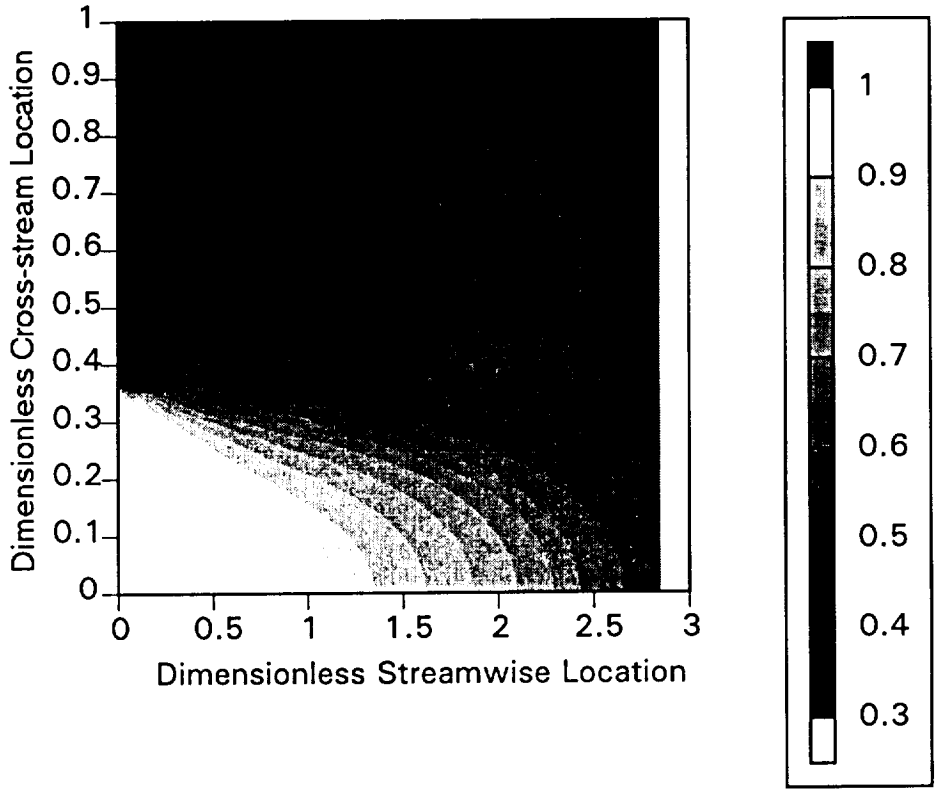

FIGURE 5.24 Normalized Mach number field for vortical mixer, chute acceleration neglected.

It should be noted that flow field geometry (in particular ejector width) was not supplied and had to be estimated, thus introducing potentially large entrainment and CFG error. The normalized Mach number field, $M(x,y)/M_1$, is presented for this case in Figure 5.24.

These tests are for a vortical mixer ejector nozzle with the mixer parameters listed in Table 5.6.

Vortical Reynolds Number	Lobe total height
Re_{vort}=2.0	$h_0/h(0)$=1.0

TABLE 5.6 The vortical parameters for the Thayer et al. experiment.

This is clearly a stronger mixer than described previously. Recall that the DREA simulation cannot predict local Mach number acceleration of the chutes. As such internal static quantities are poorly predicted. To understand this limitation more completely, consider the dimensionless mixing duct static pressure for this problem, with the modification of 16% higher inlet Mach number, shown in Figure 5.24.

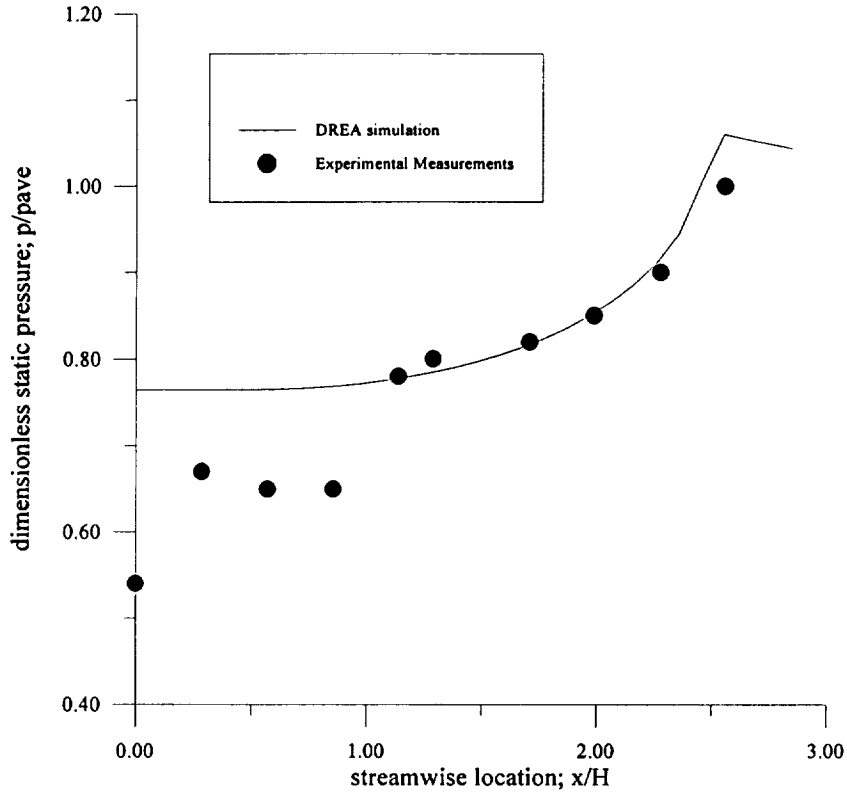

FIGURE 5.25 A comparison between the DREA simulation and experimental data of Thayer et al. using a dimensionless static pressure $p(x)/p_\infty$ for a vortical mixer.

Figure 5.25 indicates that the local static pressure near the inlet is not correctly predicted. A higher inlet Mach number would permit better pressure matching, but at the expense of even worse prediction of the integral quantities. Notice also, the weak shock near the exit of the ejector and the diffusion of the high pressure flow from this point. This is illustrated by the dimensionless contour plot (here, $p(x,y)/p_\infty$) in Figure 5.26:

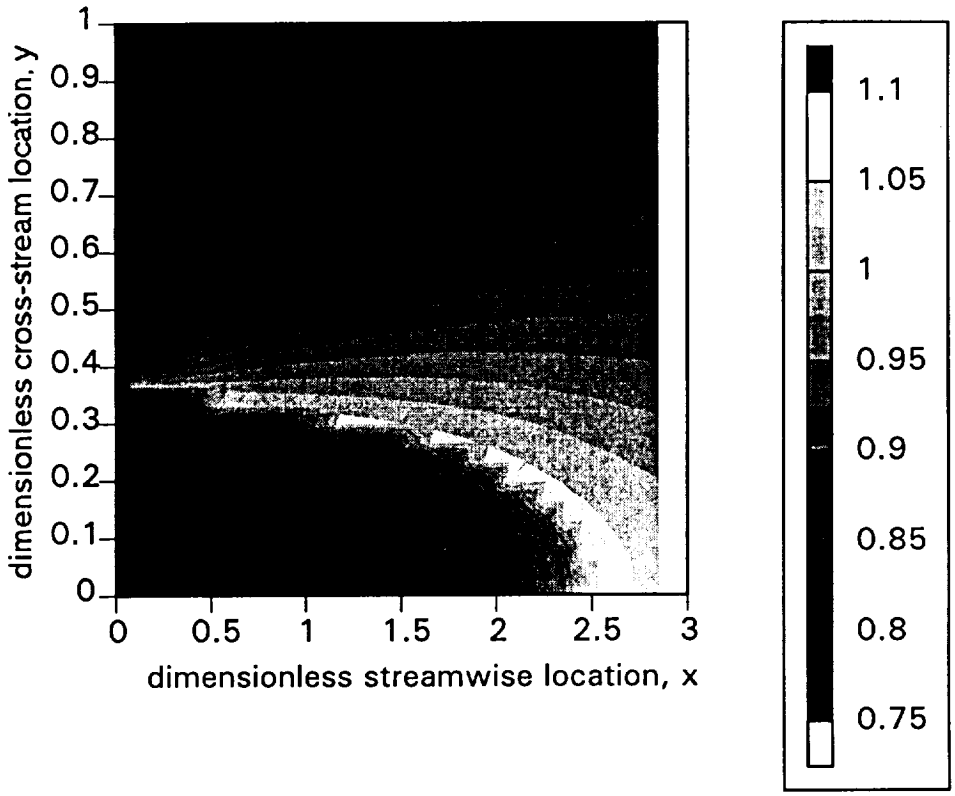

FIGURE 5.26 Contour plot of $p(x,y)/p_{\infty}$, vortical mixer.

Notice the high primary stream terminating in a long shock train. As expected, the static pressure reaches a maximum at the sonic point (location of the weak shock system. This correspondence is shown in Figure 5.27 by the normalized Mach number, $M(x,y)/M_{10}$, for this case:

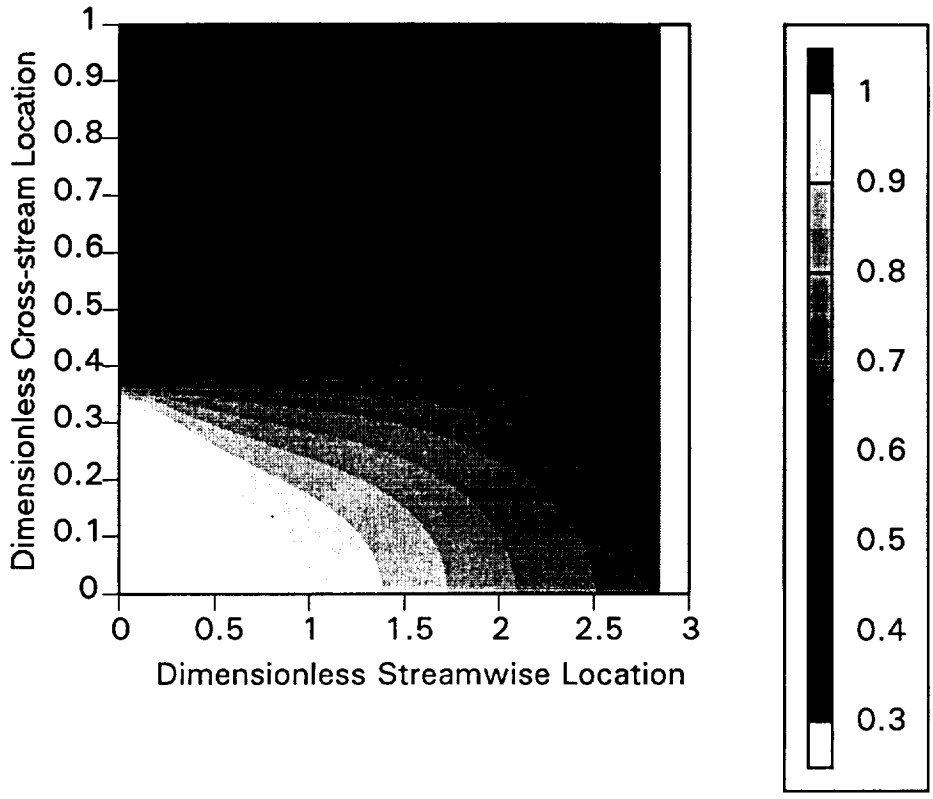

FIGURE 5.27 Contour plot of normalized Mach number, $M(x,y)/M_{10}$, vortical mixer.

Recalling that the inlet flow characteristics have been modified, i.e. local increase in average Mach number, it should be expected that a poor match to the integral quantities, entrainment and CFG, would exist. This is indeed the case as shown in Figure 5.28:

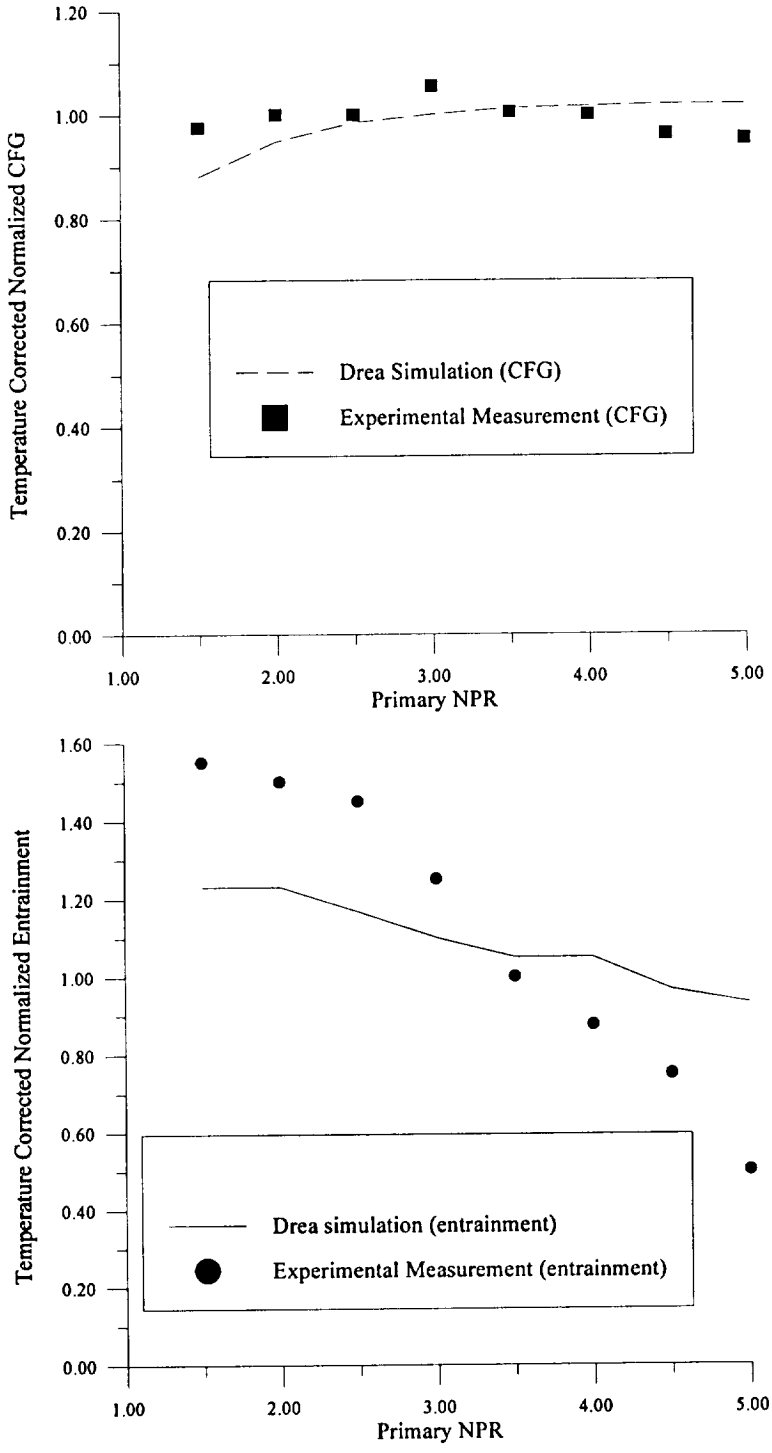

FIGURE 5.28 A comparison between the DREA simulation and experimental data of Thayer et al. showing entrainment and CFG, using a vortical mixer and modified initial conditions to account for mixer lobe acceleration.

Once again, it is apparent that some error has been introduced. Clearly, the entrainment is suppressed for the higher Mach number case. The failure of the code to predict the local acceleration due to the lobes of the mixer has caused most of this discrepancy. Methods to extend our model to begin to account for these effects are discussed in Section 5.2.

5.1.8 NASA Lewis design study, 1996

As a support for design trade studies and as a demonstration of another solution of the code, preliminary results from a NASA "in house" parametric study have also been included. This study has been chosen, in spite of the fact that no experimental data is available, since it illustrates an ejector running in an aerodynamic or Fabri choked mode. Presented in Figure 5.29 is the normalized flow field Mach number:

Figure 5.29 shows a supersonic stream initially mixing with a subsonic stream. At x=1.6 a rapid acceleration of the secondary stream is occurs. This is the estimated (using the interface streamline model) location of the aerodynamic or Fabri choke. It should be noted that the rapid acceleration is an artifact of our analysis and should indeed be more gentle. This is a clear indication of the limitations caused by being unable to model the wave phenomenon (expansion/compression system) within this flow. The blending function approach discussed in Section 2 was found to produce unrealistic results.

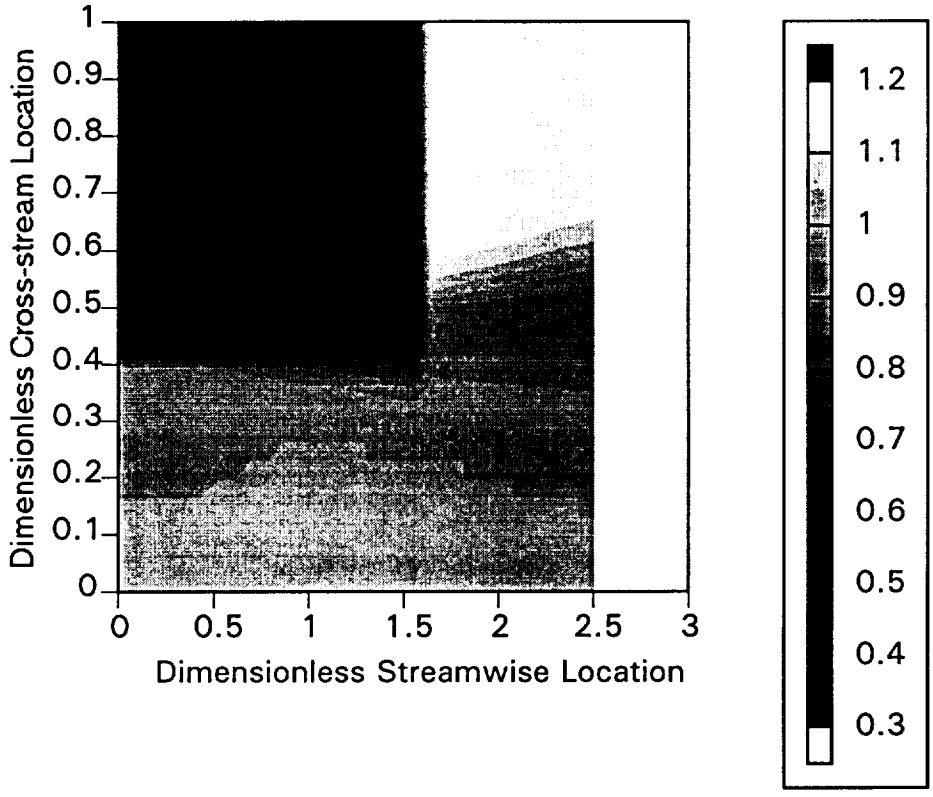

FIGURE 5.29 Contour plot of normalized Mach number, $M(x,y)/M_1$, for Fabri choked flow, NASA Lewis design study.

5.1.9. Preliminary computational time studies

The NASA design study is also useful, in that it is potentially the most complex type of flow problem we are likely to run. As such some crude computational time studies have been performed on a Pentium 90 PC platform using Microsoft FORTRAN V. 1.0 (all compiler optimization options are set for default). These are user time studies for code, i.e. time experienced by the user from initial submission of the job to completion and are probably I.O. limited rather than CPU limited. Results are presented in Table 5.7:

Streamwise grid I_{max}	Cross-stream grid J_{max}	Time (seconds)
0	0	3.15
20	10	4.66
20	20	5.12
20	30	6.18
30	10	5.13
30	20	6.5
30	30	10.1
100	30	20.0

TABLE 5.7 Elementary computational time studies.

We note that the first case represents a run computing integral quantities, such as entrainment and CFG only. To our satisfaction, we note that the results of this computation compare favorably to the time required by Fung (1995) of about 4 seconds on an IBM RS6000 workstation, to obtain their "momentum mixedness" parameter and integral quantities. At the cost of on the order 0.5 to 1.5 seconds more, our analysis provides flow field information at 200-400 grid points within the shroud using a less powerful (and vastly more accessible) computational platform. Indeed, though comparison of computational platforms is difficult (for example integer performance versus floating point performance) it is reasonable to expect that a IBM RS6000 560 platform should be on the order of 3-4 times as fast for floating point computations. With this in mind, it is apparent that the DREA code is providing vastly more information at essentially half the cost!

For comparison purposes it would be useful to have an empirical formula relating grid points to computational time. Since I_{max} is not a strong variable in this determination it is held constant, i.e. I_{max} =20 and we compare J_{max} to computational time as shown in Figure 5.30:

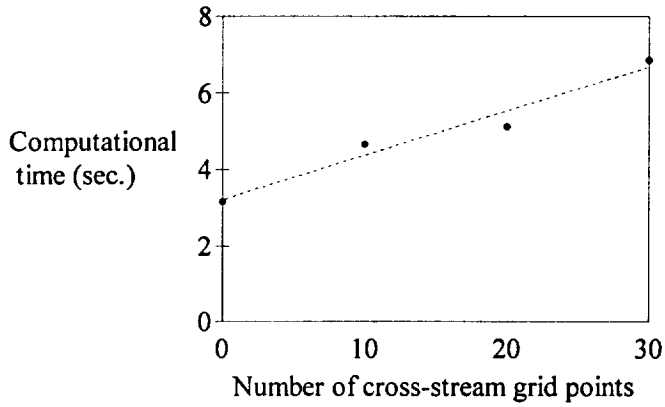

FIGURE 5.30 A regression fit of the computational time on PC Pentium 90 platform versus the number of cross-stream grid points.

Clearly, the cost of larger numbers of computational points is found to reasonable and increases in a linear manner. Of course, this empirical relationship could have well been fitted by a power law expression: $y=3.31x^{1.02}$, but again it is apparent that this is a virtually linear relationship. Additionally we can see that for no more twice the cost of a control volume solver, which provides no length scale or internal mixing information, we can use this model to obtain approximately 600 points of information within the mixing duct!

At this point our discussion of the validation cases is concluded. These six cases and the parametric case have helped us ascertain that the code seems to provide reasonably accurate mixing or flowfield, entrainment and thrust information. We have also observed the limitations inherent to the model. Both of these topics are developed in the next section.

5.2 Conclusions and recommendations

The mathematics, numerics, supporting experimental research and comparisons of the DREA simulation code have been presented. It is now important to draw conclusions for this research, as well as rigorously define extensions and areas of further work to improve or supersede this work.

5.2.1 Conclusions

In this section the success/or lack of success achieved by this development project is discussed. There are two major components to this research.

1. *General goal*: To develop a new and useful family of approximate fluid dynamic equations which provide alternatives to classical hierarchies. It was also our intention to directly couple analytical with numerical solution methods to obtain an efficient alternative to other more standard formulations.
2. *Applied Goal*: To use this new methodology to develop a system of analytical and numerical ejector/mixer nozzle models which require minimal empirical input. It is the goal of this research to provide more information than a control volume model; at a computational cost which is competitive with control volume methods. The DREA model is of direct use to the High Speed Civil Transport Program and is in the process of being adopted by both NASA and industry. Though most testing was done using

ejector/mixing data from the literature, new data was obtained using a hydraulic/gas flow analog model. These measurements provided information about the inviscid mixing interface structure.

5.2.1.1 General goal

As described in Section 1, despite the rapid advances in both scalar and parallel computational tools, the large number and breadth of variables involved in both design and inverse problems make the use of sophisticated and even relatively simple (parabolized or boundary layer) fluid flow models impractical. With this restriction, one may concluded that an important family of methods for mathematical/computational development is reduced or approximate models. This model was related to other approximation methods as shown in Table 5.8 repeated here for convenience:

Perturbation Method/Approximation	Comments:
Integral/Control volume (.i.e. 1-d or quasi-1-d)	Satisfy integral forms of conservation equations. Cannot predict local values.
Current DREA model O(1) equation system	Parabolic in terms of conservative flux quantities. Primitive quantities: u, v, p, ρ, M, locally predicted. PNS subsonic pressure approximation
Boundary layer	Parabolic in terms of u, v for all flows; p(x), thin layer, p(x) must be specified by an auxiliary relationship
Viscous-shock layer	Parabolic for supersonic flow; u, v, p(x) specified by auxiliary relationship, p(x,y) specified by inviscid y-momentum; PNS subsonic pressure approximation.
Parabolized Navier-Stokes	Parabolic (in space) for supersonic flow, elliptic subsonic regions; u, v, p(x), p(x,y) Viscous y-momentum. PNS subsonic pressure approximation
Full Navier-Stokes Analysis	Parabolic-hyperbolic, fully viscous equations. Always solved using unsteady or iterative method.

TABLE 5.8 Classical and current approximation methods in fluid dynamics.

To overcome this limitation, a successful combination of perturbation/numerical modeling methodologies, which provide a rigorously derived hierarchy of solutions, has been developed. Additionally, the solution to these models utilized analytical solutions to resolve singular behavior as required. Hence, classical methods are to be combined with efficient numerical methods to yield an efficient and original class of fluid flow models.

By way of conclusion, it is the author's opinion, that classical, asymptotic and reduced modeling methods are to be preferred over gross application of computational tools. Having said this, though, it is important to recall that perturbation methods and their intimate connection with classical methods have significant limitations, principally that they are difficult, if not impossible, to apply for problems where some form of linearization is unavailable, or where the nonlinearity is intimately connected to the problem. Progress in

handling highly nonlinear problems is discussed by Malmuth (1993) in a paper appropriately titled: "Some Applications of Combined Asymptotic and Numerics in Fluid Mechanics and Aerodynamics". An interesting set of asymptotic analyses is provided in Ockenden and Ockenden (1995).

5.2.1.2 Applied goal

In particular, the main objective of this research was to develop a system of analytical and numerical ejector/mixer nozzle models that require minimal empirical input. A code, DREA Differential Reduced Ejector/mixer Analysis has been written with the ability to run sufficiently fast such that it may be used either as a subroutine or called by an design optimization routine. We believe that this experimental validation of these models is provided by comparison to results obtained from the literature, industry data, as well as, dedicated experiment performed at Texas A&M. The error associated with the comparison of these models to the DREA simulation is summarized in Table 5.9.

Experiment	Mixer/ splitter plate	relative error/comments
Gilbert and Hill (1973)	simple, 2-d slot mixer	entrainment error 1.86% flow field prediction good, max. err. 8%
Goebel and Dutton (1991)	simple, 2-d slot mixer	Flow field profile results: spreading layer width good, location, moderate
Fernando and Menon (1993)	Re_{vort}=0.087 h_0/λ=0.428 $h_0/h(0)$=0.0061	Flow field profile results: spreading layer width good, location, moderate. Failure to predict local acceleration at chutes.
Arney and Lidstone	simple, 2-d slot mixer	Flow field profile results: spreading layer width good-moderate, location, good-moderate. CFG, 11%, entrainment 23% "design" NPR
Thayer et al.	Re_{vort}=2.0 $h_0/h(0)$=1.0	CFG, 10% full range; entrainment 20-25% at "design" NPR. Failure to predict local acceleration at chutes. Reasonable comparison with "local" acceleration modification

TABLE 5.9 Summary of results of comparison with test cases.

It is possible to conclude that although the DREA simulation has limitations (especially in predicting entrainment for short shroud ejectors and prediction of local acceleration effects due to vortical mixing), it clearly provides a useable engineering predictive tool. Additionally, the DREA code uses a very limited number of empirical constants. In fact depending upon how one counts an empirical constant, there are really only two truly empirical constants, i.e. the effective viscosity and the local vortex strength used in the vortical

mixing analysis. On the other hand, the author must admit that at least some of the analyses developed here are so approximate that they are little better than order of magnitude or scaling arguments. Nevertheless, they do not require additional empirical input. Given this limited dependence upon experimental input, it is anticipated that the solutions will be valid (at least to the level of accuracy described here) for a wide range of problems. This discussion brings us back to the comparison of the DREA code with other models. Recall that the other models of at least computational speed approximately equivalent with the DREA analysis were, a code developed at MIT, Fung (1995), as well a code developed at Boeing by Clark (1995). The comparison table used in section 1, here Table 5.10 is presented:

Criterion	DREA (Texas A&M)	Fung (MIT)	Clark (CFA)
Vortical Mixing	yes; analytically based turbulence model	yes, piecewise model and scaling functions	no, multiple lobe only
governing equations	simplified 2-d, conservative	scaling law	1-d
primitive variable profiles	yes	no	two stream model
empiricism	limited	moderate ("scaling" constants)	limited (unknown)
compressible	expressly developed for compressible flow	1-d and extensions	1-d and extensions
internal shock /choke structure	yes; Fabri-choke and back pressure limited	no, pumping only	current version no
computational speed (suitable for preliminary design/optimization)	fast (user may choose control volume and/or mixing)	fast	fast
experimental validation	yes, literature, proprietary data and experiments	yes, literature and experiments	yes, experiments
publications	journal articles, conference papers, dissertation and reports	thesis, conference papers	conference papers (main code proprietary)
status availability	preliminary summer 1996, fully tested and documented 05-97	complete	complete

TABLE 5.10 Comparison of mixer/ejector models suitable for preliminary design/optimization.

One may reasonably conclude, that the DREA code does indeed provide a significant improvement over the other current models all of which have been developed to fill need for a fast, yet sufficiently powerful computational model.

Finally, then an analysis code, DREA, i.e. one for which geometry and operating conditions have been specified has been developed. Performance characteristics (thrust, noise, degree of mixing, and pumping) are predicted in an efficient manner by this code to an adequate level of accuracy. Ultimately, this type of tool may be used to generate off line performance information in the form of "ejector" maps, which are tabular lists of performance characteristics. It is also sufficiently computationally efficient to be run in a "real time" fashion or serve as the basis for an inverse design type of tool.

5.2.2 Recommendations for further work

In this section modification to the current work are discussed. As with the conclusion, we split our recommendations into two types:

1. Near term modifications to the DREA, O(1) system of equations. These types of modifications are intended to leave the basic solver and governing system intact, while improving the comparison with experimental data or extending the range of validity of the current tool.
2. Long term, major modifications to DREA code. These include modifying either/or the basic solution method or the fundamental formulation.

Of course, these two areas of recommended further work are not mutually exclusive. For example if one were to upgrade the mixing equations to model wave effects, it would make little sense not to simultaneous upgrade the entrainment model, which ultimately provides the initial conditions to the marching equations.

5.2.2.1. Recommendations for near term further work

In this section, a brief discussion of potential moderate extensions to the current research is presented. These include:

- Improvement of ideal and non-ideal entrainment computations for both back pressure dominated and back pressure independent (aerodynamically choked) flows. Though it is unquestionably possible to incrementally improve and upgrade our simple ordinary differential equation models, which estimate losses in entrainment, or even invoke an iterative matching procedure using our full equation, the fact remains that modeling flows with large regions of subsonic flow will be difficult using single pass space marching, i.e. "PNS like" methods. Examples of flows like this are presented in Figure 5.31.
- These flows are fundamentally elliptic, demanding an iterative or relaxation solution technique. This area remains a challenge for CFD development work. A potential opportunity may exist for our combined analytical/numerical methodology, where by, regions of the flow field, such as the elliptic portions may be modeled using analytical tools, while well posed supersonic regions may be modeled (in their full non-linearity) using numerical methods.

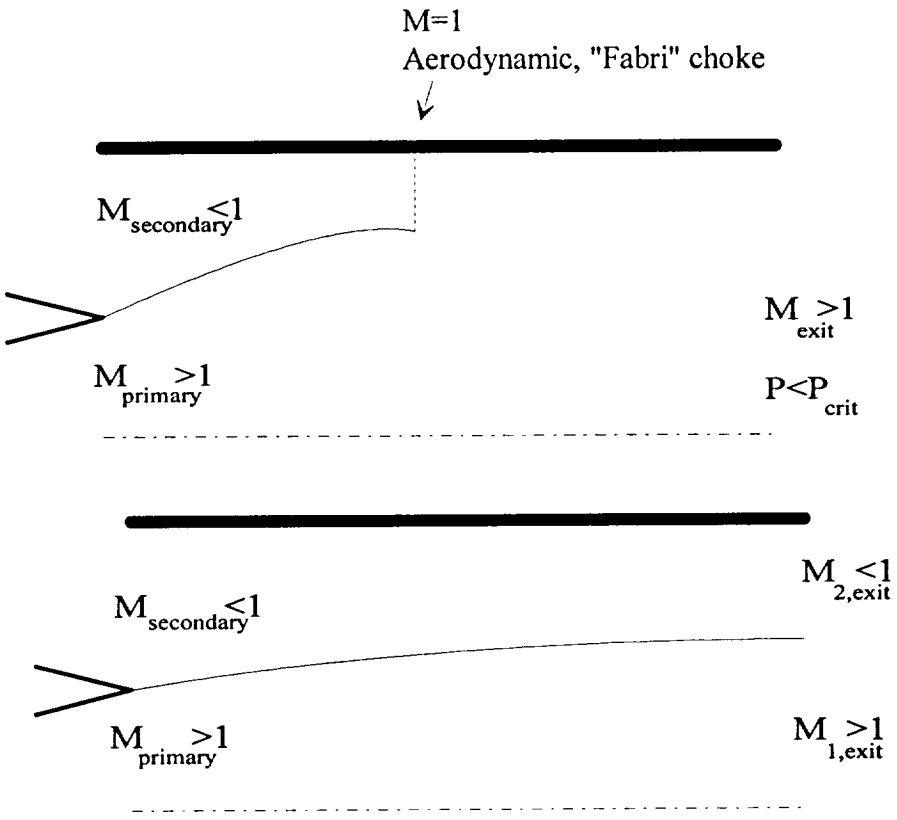

FIGURE 5.31 A schematic of flow fields with substantial subsonic flow regions.

- Developing a simplified "map" of basic ejector characteristics. This is a difficult process, in that there still does exist a completely adequate physical criterion for predicting the ejector operation mode (i.e. subsonic exit or supersonic flow at the exit). Analytical and control volume methods give us perhaps the best chance of developing a rational basis to understand the scope and limits of ejector operation.
- Develop a methodology to model truly three-dimensional vortical effects with local acceleration effects. If one can accept a moderate development effort, these effects may be modeled using a new family of approximations. Consider the three dimensional mixing model:

$$\frac{\partial \phi}{\partial x} = \left(\frac{\nu_{eff}}{U}\right)_{xy} \frac{\partial^2 \phi}{\partial y^2} + \left(\frac{\nu_{eff}}{U}\right)_{xz} \frac{\partial^2 \phi}{\partial z^2} \tag{5.5}$$

The initial conditions associated with this type of flow are shown in Figure 5.32.

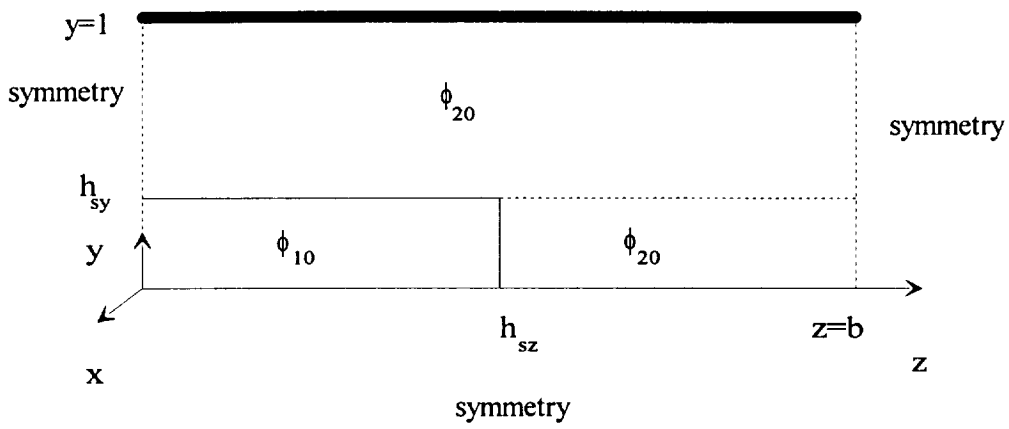

FIGURE 5.32 Geometry definitions for a single lobe, 3-d model.

Unfortunately, there is no simple decomposition method that will permit us to model this three-dimensional flow in a completely satisfactory manner. To solve a relationship, like the one found above, it is necessary to develop a three dimensional solution, i.e. $\phi=\phi(x,y,z)$.

Though a solution is not developed in significant detail (since it outside the scope of the current research), a purely analytical solution based upon 2-d Fourier transforms (alternatively Green's function expansions) is presented. The governing equation solved (note the local "y" and "z" linearizations):

$$\frac{\partial \phi}{\partial x} = a^{*}_{xy} x \frac{\partial^2 \phi}{\partial y^2} + a^{*}_{xz} x \frac{\partial^2 \phi}{\partial z^2} \tag{5.6}$$

with the boundary conditions described in Figure 5.32. The solution is:

$$\phi(x,y,z) = \frac{(\phi_{10}-\phi_{20})}{4} \sum_{-\infty}^{\infty}\sum_{-\infty}^{\infty} \left[erf\left(\frac{y+h_{sy}-2n}{\left(2a^{*}_{xy}\right)^{1/2}x}\right) - erf\left(\frac{y-h_{sy}-2n}{\left(2a^{*}_{xy}\right)^{1/2}x}\right)\right] * \left[erf\left(\frac{z+h_{sz}-2m}{\left(2a^{*}_{xz}\right)^{1/2}x}\right) - erf\left(\frac{z-h_{sz}-2m}{\left(2a^{*}_{xz}\right)^{1/2}x}\right)\right] + \phi_{20} \tag{5.7}$$

Equation (5.7) is a double infinite series in terms of Green's functions. Like it's 1-d counterpart, it seems reasonable to expect, that this solution would be very efficient, i.e. requiring a minimum number of terms, close to the initial condition. Extension of the numerical solution to 2-d is significantly more difficult. Here it would also be necessary to develop some form of a higher order solution method appropriate for parabolic equations, for example a fourth order, compact ADI scheme, see Hirsch (1975).

- Continuation of testing of the current DREA model exploring the possibility of a static pressure correction equation. This would employ a decomposition of the form:

$$p = \omega p + (1-\omega)\tilde{p} \tag{5.8}$$

where the term ω is the Vigneron (Vigneron et al. (1978)), (See also Appendix E)) parameter developed earlier and used to provide a well posed spatial marching method for subsonic regions. Its value is:

$$\omega = \frac{\gamma M^2}{1+(\gamma-1)M^2} \tag{5.9}$$

for M<1 and 1 for M>1. Using this parameter, the pressure is split into two portions: (1) a locally computed value and (2) a boundary layer portion (a function of x only). Of course, this decomposition requires a knowledge of the Mach number distribution, M(x,y), which is not explicitly known. As such it is not a completely satisfactory solution.

- Consider the introduction of inverse design methodologies. Clearly the reason to develop any a design code is to have a tool of sufficient efficiency such that trade studies are possible. Automating these studies using optimization methods (see Luenberger (1984) for classical gradient based methods, and Goldberg (1989) for genetic based methods or simulated annealing (Press et al. (1992)) is course, desirable. The computational cost of identifying global minima can be truly amazing. Upon considering the cost of performing a direct search in say N variable (of course this is highly inefficient, but it can and will delineate a local minima) using a 100 node mesh, one is now faced with performing at least 100^N marching computations. For N=3 and assuming 6 seconds/ run it would be expected to require a PC for on the order of 70 days! Of course, we would probably not use such a conservative algorithm, but optimization is a dangerous (and expensive) game. Additionally, only running the code for a control volume case would reduce the cost by half.

  This discouraging assessment of optimization costs is offset when one considers the use faster scalar machines or indeed parallel machines (See Geist et al. (1996)). A message passing variant of this code and an optimization algorithm (for example a genetic method) could make robust optimization extremely competitive. Of course, this places a tremendous impetuous upon us to develop the most realistic, accurate and reliable basic model possible.

5.2.2.2. Recommendations for long term further work

In the realm of long term recommendations, the possibility of considering new fundamental governing equations and modeling effect heretofore unattainable using more limited equations is considered. Clearly, the most pressing modeling concerns for the governing equations system is:

1. Directly coupling wave effects
2. Dealing with the static pressure term in as a complete manner as possible.
3. Modeling three dimensional effects.

We address these limitations next.

Section 1 developed equations that were even less complex than the boundary layer family. Unfortunately, it was shown that, though the mixing was well modeled, the wave phenomena, such as, expansion compression/shock systems and normal shocks could not be directly modeled at all. To deal with these

features, a double valued transformation was used, which contained two possible solutions. This worked well in the streamwise direction, but lead to significant problems in the cross-stream. To deal with this situation, the modified inversion transformation was introduced and used in transonic mixing regions (recall this required neglecting a portion of the static pressure field). Additionally information describing the location of the choke was also needed. These limitations clearly indicate, in spite of the fact that the equations used were very simple and linear, cannot serve as a completely satisfactory model.

With this in mind, it is of interest to consider a set of equations that explicitly model two-dimensional wave phenomena and mixing simultaneously. This set is rather easily written:

x-momentum:

$$\frac{\partial}{\partial x}(\rho u^2)+\frac{\partial}{\partial y}(\rho v^2)+\frac{\partial p}{\partial x}=-\frac{\partial}{\partial y}(\rho u'v')\equiv\frac{\partial}{\partial y}(\mu_{eff}\frac{\partial u}{\partial y}) \tag{5.10}$$

y-momentum:

$$\frac{\partial}{\partial x}(\rho uv)+\frac{\partial}{\partial y}(\rho v^2)+\frac{\partial p}{\partial y}=0 \tag{5.11}$$

energy:

$$\frac{\partial}{\partial x}(\rho uH)+\frac{\partial}{\partial y}(\rho vH)=-\frac{\partial}{\partial y}(\rho v'H')\equiv\frac{\partial}{\partial y}(\frac{\mu_{eff}}{\mathrm{Pr}_{turb}}\frac{\partial H}{\partial y}) \tag{5.12}$$

and continuity:

$$\frac{\partial}{\partial x}(\rho u)+\frac{\partial}{\partial y}(\rho v)=0 \tag{5.13}$$

Note that as before, that the Prandtl number has been assumed to be close to unity, hence dissipation terms in the energy equation, may be neglected

Given suitable turbulence modeling for the right hand sides (mixing terms), it is claimed that this set will support both viscous mixing (parabolic) and hyperbolic wave expansion. This claim is verified by the fact, that given isentropic flow (irrotational), and neglecting the viscous and heat transfer terms, that we derive the classical (non-linear) potential equation:

$$\left[1-\Phi_x^2\right]\Phi_{xx}+\left[1-\Phi_y^2\right]\Phi_{xx}-\frac{x\quad y}{a^2}=0 \tag{5.14}$$

where Φ, is the velocity potential and a= speed of sound. The speed of sound is related to the energy equation, by noting that H_0=constant satisfies energy equation and using state. Unfortunately this equation set equations

(5.10)-(5.13), which are essentially a set of "viscous shock layer equations" are computationally difficult to deal with.

The question arises: under what circumstances would the perturbation expansion system developed in Section 1 first exhibit explicit wave phenomenon? To ascertain this one must consider the absolute minimum governing equation system required to derive a linear wave equation. This minimum system is written:

x-momentum:

$$\rho u \frac{\partial u}{\partial x} + \frac{\partial p}{\partial x} = 0 \tag{5.15}$$

y-momentum:

$$\frac{\partial p}{\partial y} = 0 \tag{5.16}$$

continuity:

$$\frac{\partial(\rho u)}{\partial x} + \frac{\partial(\rho v)}{\partial y} = 0 \tag{5.17}$$

energy:

$$\frac{\partial(\rho u H)}{\partial x} + \frac{\partial(\rho v H)}{\partial y} = 0 \tag{5.18}$$

a form of the state equation:

$$dp = -a^2 d\rho \tag{5.19}$$

and finally, the irrotational condition:

$$\frac{\partial v}{\partial x} = \frac{\partial u}{\partial y} \tag{5.20}$$

Clearly, it is apparent that given the absence of mixing terms, that the governing equation set is complete even when considering only the O(1) mixing problem, except for the final irrotational condition. It is this condition which, according to our expansion suppresses wave phenomenon. Considering this last equation, we note that even with "y" scaling at O(1), that the first term in our expansion for v, i.e. v_0 is assumed to be $O(\varepsilon)$. Therefore, wave compression/expansion features will be suppressed till $O(\varepsilon)$. To emphasize this, we write the $O(\varepsilon)$ wave equation system:

$$\left[M^2 - 1\right]\frac{\partial u_2}{\partial x} - \frac{\partial v_0}{\partial y} = other\ terms \tag{5.21}$$

and

$$\frac{\partial v_0}{\partial x} = \frac{\partial u_2}{\partial y} + other\ terms \tag{5.22}$$

where the "other terms" signify other expansion terms which do not contribute to the structure of the linearized wave portion of the equation.

Hence, it is apparent that wave phenomenon have been suppressed to higher order using the perturbation expansion developed here. The order of magnitude limitation (and the one common to all boundary layer analysis or parallel flow analysis) is associated the cross-stream velocity, v, to be O(ε). This prompted the supplemental analyses, i.e. the inviscid choke location described in Section 2, and the discussion of more complete (for example the viscous shock layer equations) developed previously.

Finally it is necessary to consider 3-d effects. If we are willing to accept a family of governing equations of considerably greater complexity, such as the VSL equations, modeling of three-dimensional effects becomes relatively straight forward. Our governing equations take the form:

x-momentum:

$$\frac{\partial}{\partial x}(\rho u^2) + \frac{\partial}{\partial y}(\rho uv) + \frac{\partial}{\partial z}(\rho uw) + \frac{\partial p}{\partial x} = \frac{\partial}{\partial y}(\mu_{eff}\frac{\partial u}{\partial y}) + \frac{\partial}{\partial z}(\mu_{eff}\frac{\partial u}{\partial z}) \tag{5.23}$$

y-momentum:

$$\frac{\partial}{\partial x}(\rho uv) + \frac{\partial}{\partial y}(\rho v^2) + \frac{\partial}{\partial z}(\rho vw) + \frac{\partial p}{\partial y} = 0 \tag{5.24}$$

z-momentum:

$$\frac{\partial}{\partial x}(\rho uw) + \frac{\partial}{\partial y}(\rho vw) + \frac{\partial}{\partial z}(\rho w^2) + \frac{\partial p}{\partial z} = \frac{\partial}{\partial y}(\mu_{eff}\frac{\partial w}{\partial y}) + \frac{\partial}{\partial z}(\mu_{eff}\frac{\partial w}{\partial z}) \tag{5.25}$$

energy:

$$\frac{\partial}{\partial x}(\rho uH) + \frac{\partial}{\partial y}(\rho vH) + \frac{\partial}{\partial z}(\rho wH) = \frac{\partial}{\partial y}(\frac{\mu_{eff}}{\mathrm{Pr}_{turb}}\frac{\partial H}{\partial y}) + \frac{\partial}{\partial z}(\frac{\mu_{eff}}{\mathrm{Pr}_{turb}}\frac{\partial H}{\partial z}) \tag{5.26}$$

and continuity:

$$\frac{\partial}{\partial x}(\rho u) + \frac{\partial}{\partial y}(\rho v) + \frac{\partial}{\partial z}(\rho w) = 0 \tag{5.27}$$

Once again, the Prandtl number has been assumed to be close to unity, hence dissipation terms in the energy equation are neglected.

The expansions are more complex, since the unknown "z" direction mass flux: ρw, has been added to the solution set and the resulting equation system will need to be factorized as described in Anderson et al. (1984). It is important to point out that in development work it is necessary to be cautious not to "reinvent the wheel" since the equations that we have now described are indeed essentially PNS equations. With this complex set of equations, we have come almost full circle. As such the development of modeling methodologies described here is concluded.

(This page intentional left blank.)

REFERENCES

ABDOL-HAMID, K. S. UENISHI, K. KEITH B. D. & CARSON, J. R. 1993 Commercial turbofan engine exhaust nozzle flow analyses. *Journal of Propulsion and Power.* **9**, 3, 431-436.

ABE, T. FUNABIKI, K. ARIGA, H. & HIRAOKA K. 1992 Effect of streamwise pressure gradient on the supersonic shear layer. *AIAA Journal.* **30**, 10, 2564-2566.

ABRAMOVICH, G. N. 1963 *The Theory of Turbulent Jets.* MIT Press, Cambridge, Massachusetts.

ABRAMOWITZ, M. & STEGUN, I. A. 1964 *Handbook of Mathematical Functions.* National Bureau of Standards or Dover, New York.

ADDY, A. L. DUTTON, J. C. & MIKKELSEN, C. D. 1981 Supersonic ejector-diffuser theory and experiments. Report UILU-ENG-82-4001, Department of Mechanical and Industrial Engineering, University of Illinois at Urbana-Champaign, Urbana, Illinois.

ALPERIN, M. & WU, J. J. 1983a Thrust augmenting ejectors, part I. *AIAA Journal.* **21**, 10, 1428-1436.

ALPERIN, M. & WU, J. J. 1983b Thrust Augmenting Ejectors, Part II. *AIAA Journal.* **21**, 12, 1698-1706.

ANDERSON, D. A. TANNEHILL, J. C. & PLETCHER, R. H. 1984 *Computational Fluid Mechanics and Heat Transfer.* Hemisphere, New York.

ANDERSON, J. D. 1985 *Modern Compressible Flow, 2nd ed.* McGraw-Hill, New York.

ANDERSON, J. D. 1989 *Hypersonic and High Temperature Gas Dynamics.* McGraw-Hill, New York.

ANDREWS, M. J. 1993 The large-scale fragmentation of the intact liquid core of a spray jet. *Atomization and Sprays.* **3**, 29-54.

ARNEY, L. D. & LIDSTONE, G.L. Boeing nozzle test data.

ARPACI, V.S. & LARSEN, P. S. 1984 *Convective Heat Transfer.* Prentice-Hall, Englewood Cliffs, New Jersey.

BARBER, T. J. PATERSON, R. W. & SKEBE, S. A. 1988 Turbofan forced mixer lobe flow modeling. I-experimental and analytical assessment. *NASA Contractor Report* 4147.

BARBER, T. J. & ANDERSON, O. L. 1991 An analytical study of a supersonic mixer ejector exhaust system. *AIAA Paper* 91-0126.

BEAM, R. M. & WARMING, R. F. 1976 An implicit finite-difference algorithm for hyperbolic systems in conservation law form. *Journal of Computational Physics.* **22**, 87-110.

BEAM, R. M. & WARMING, R. F. 1978 An implicit factored scheme for compressible Navier-Stokes equations. *AIAA Journal* **16**, 393-401.

BEAR, J. 1972 *Dynamics of Fluids in Porous Media.* Dover, New York.

BEVILAQUA, P. M. 1978 Lifting surface theory for thrust-augmenting ejectors. *AIAA Journal.* **16**, 5, 475-481.

BLUMEN, W. 1970 Shear layer instability of an inviscid compressible fluid. *Journal of Fluid Mechanics.* **40**, 769-781.

BLUMEN, W. DRAZIN, P. G. & BILLINGS, D. F. 1975 Shear layer instability of an inviscid compressible fluid. part 2. *Journal of Fluid Mechanics.* **71**, 305-316.

BOGDANOFF, D. W. 1983 Compressibility effects in turbulent shear layers. *AIAA Journal.* **21**, 926-927.

BOOHER, M. E. KWON, O. BARTA, A. B. VITTAL, B. R. & KRISHNAN, M. R. 1993 Development of an advanced exhaust mixer for a high bypass ratio turbofan engine. *AIAA Paper* 93-2435.

BOYCE, W. E. & DIPRIMA, R. C. 1965 *Elementary Differential Equations and Boundary Value Problems.* Wiley, New York.

BRADEN, R. P. NAGARAJA, K. S. & VON OHAIN, H. J. P. 1982 Proceedings: ejector workshop for aerospace applications. Air Force Wright Aeronautical Laboratories, Flight Dynamics Laboratory (AFWAL/FIM), Report AFWAL-TR-82-3059.

BROWN, G. L. & ROSHKO, A. 1974 On density effects and large scale structures in turbulent mixing layers. *Journal of Fluid Mechanics.* **64**, 775-781.

BURDEN, R. L. & FAIRES, J. D. 1993 *Numerical Analysis.* PWS-Kent Publishing Co. Boston.

CHAMPAGNE, G. A. 1991 Jet noise reduction concepts for the supersonic Transport. *AIAA Paper* 91-332.

CHANDRASEKHARA, M. S. KROTHAPALLI, A. & BAGANOFF D. 1991 Performance characteristics of an underexpanded multiple jet ejector. *Journal of Propulsion.* 7, 3, 462-464.

CHINZEI, N. MASUYA, G. KOMURO, T. MURAKAMI , A. & KUDOU, K. 1986 Spreading of two-stream supersonic turbulent mixing layers. *Physics of Fluids*, **29**, 5, 1345-1347.

CHOW, W. L. & ADDY, A. L. 1964 Interaction between primary and secondary streams of supersonic ejector systems and their performance characteristics. *AIAA Journal.* **2**, 4, 686-695.

CHOW, W. L. & YEH, P.S. 1965 Characteristics of supersonic ejector systems with non-constant area shroud. *AIAA Journal.* **3**, 526-527.

CHURCHILL, R. V. & BROWN, J. W. 1978 *Fourier Series and Boundary Value Problems. 3rd Ed.* Mc-Graw Hill. New York.

CLARK, L T. 1995 Applications of compound flow analysis to supersonic ejector-mixer performance prediction. *AIAA Paper* 95-0645.

COLE, J. D. & COOK, L. P. 1986 *Transonic Aerodynamics.* North-Holland, Amsterdam.

COLLATZ, L. 1966 *The Numerical Treatment of Differential Equations.* Springer-Verlag, Berlin.

CURLE, N. 1961 The generation of sound by aerodynamic means. *Journal of the Royal Aeronautical Society.* **65**, 724-728.

DEBONIS, J. R. 1992 Full Navier-Stokes analysis of a two-dimensional mixer/ejector nozzle for noise suppression. *AIAA Paper* 92-3570.

DE CHANT, L. J. 1993 Simplified inverse ejector design tool. *NASA Contractor Report,* 194438.

DE CHANT, L. J. 1994 An analysis code for the rapid engineering estimation of momentum and energy losses (REMEL). *NASA Contractor Report,* 191178.

DE CHANT, L. J. SEIDEL, J. A. & ANDREWS, M. J. 1996 Interface wavelength between supersonic jets and subsonic flowfields. *AIAA Journal*, **34**, 9, 1946-1948.

DE CHANT, L. J. & CATON, J. A. 1996 Measurement of confined supersonic, 2-d, jet lengths using the hydraulic analogy. *Experiments in Fluids*. in review.

DE CHANT, L. J. CATON, J. A. & ANDREWS, M. J. 1997 Interface wavelengths in mixer/ejector nozzles. *AIAA Journal*, in review.

DRAZIN, P. G. & REID, W. H. 1981 *Hydrodynamic Stability*. Cambridge University Press, London.

DUTTON J. C. & CARROLL, B. F. 1986 Optimal supersonic ejector designs. *Transactions of the ASME, Journal of Fluids Engineering*. **108**, 414-420.

DUTTON, J.C. & CARROLL, B. F. 1988 Limitation of ejector performance due to exit choking. *Transactions of the ASME, Journal of Fluids Engineering*. **110**, 91-93.

ELLIOTT, J. K. 1990 A computational investigation of the fluid dynamics of a three-dimensional, compressible mixing layer with strong streamwise vorticity. Ms Thesis, Department of Aeronautics and Astronautics, MIT.

ELLIOTT, J. K. MANNING, T. A. QUI, Y. J. GREITZER, E. M. TAN, C. S. & TILLMAN, T. G. 1992 Computational and experimental studies of flow in multi-lobed forced mixer. *AIAA* paper 92-3568.

EWING, R. E. (ed.) 1983 *The Mathematics of Reservoir Simulation*. SIAM, Philadelphia.

FABRI, J. & SIESTRUNCK, R. 1958 Supersonic air ejectors. *Advances in Applied Mechanics*. Vol V. Academic Press, New York. 1-34.

FELLING, M. 1992 Hydraulic analogy simulation of internal supersonic jet discharging into a sudden enlargement. Ms Thesis, Department of Mechanical Engineering, Texas A&M University.

FERNANDO, E. M & MENON, S. 1993 Mixing enhancement in compressible mixing layers: an experimental study. *AIAA Journal*. **31**, 2, 278-285.

FERZIGER, J. H. 1981 *Numerical Methods for Engineering Application*. Wiley, New York.

FLETCHER, C. A. J. 1984 *Computational Galerkin Methods*. Springer-Verlag, New York.

FUNG, A. K. S. 1995 Modeling of mixer-ejector flows. Ms Thesis, Department of Aeronautics and Astronautics, MIT.

GERALD, C. F. 1980 *Applied Numerical Analysis*. Addison-Wesley, New York.

GEIST, A. BEGUILIN, A. DONGARRA, J. JIANG, W. MANCHECK, R. & SUNDERMAN, V. 1996 *PVM Parallel Virtual Machine, A users Guide and Tutorial for Networked Parallel Computing*. MIT press. Cambridge, Massachusetts.

GILBERT, G. B. & HILL, P. G. 1973. Analysis and testing of two-dimensional slot nozzle ejectors with variable area mixing sections. *NASA Contractor Report* CR-2251.

GILKEY, S. C. & HINES, R. W. 1991 A joint propulsion perspective of the next generation supersonic transport. *AIAA Paper*, 91-3330.

GINOUX, J. J. (ed.) 1972 Supersonic ejectors. AGARDograph 163, AGARD-AG-163.

GOEBEL S. G. & DUTTON, J. C. 1991 Experimental study of compressible turbulent mixing layers. *AIAA Journal.* **29**, 4, 538-546.

GOLDBERG, D. E. 1989 *Genetic Algorithms in Search, Optimization and Machine Learning.* Addison-Wesley, Reading, Massachusetts.

GROPENGIESSER, H. 1970 Study of stability of boundary layers in compressible fluids. NASA TT-F-12. (reprints of this report may be obtained from: NASA STI Program, NASA Access Help Desk, NASA Center for Aerospace Information, 800 Elkridge Landing Rd., Linthicum Heights, MD, 21090-2934, e-mail: help@sti.nasa.gov.)

HARRIS, J. E. MARVIN, ERLENBACHER, J. G. & LIOU, M. 1990 Turbulence modeling for hypersonic flows. *NASA Technical Memorandum* 1114.

HABERMAN, R. 1983 *Elementary Applied Partial Differential Equations.* Prentice-Hall, Englewood Cliffs, New Jersey.

HEDGES, K. R. & HILL, P. G. 1974a Compressible flow ejectors, part I development of a finite-difference flow model. *Transactions of the ASME, Journal of Fluids Engineering.* 272-281.

HEDGES, K. R. & HILL, P. G. 1974b Compressible flow ejectors, part II, flow field measurements and analysis. *Transactions of the ASME, Journal of* Fluids *Engineering* 282-288.

HENKE, R. K. Navier-Stokes analysis of Boeing nozzle test data.

HINZE, J. O. 1959 *Turbulence.* Mc-Graw Hill, New York.

HIRSCH, C. 1975 Higher order accurate difference solutions of fluid mechanics problems by a compact difference scheme. *Journal of Computational Physics.* **19**, 90-109

HIRSCH, C. 1988 *Numerical Computation of Internal and External Flows: Volume 1 and 2.* Wiley, New York.

HORNBECK, R. W. 1973 Numerical marching techniques for fluid flows with heat transfer. *NASA Special Publication,* SP-297.

JOHNSON, L. W. & RIESS, R. D. 1982 *Numerical Analysis.* Addison-Wesley. Reading, Massachusetts.

KAMARCHETI, K. 1966 *Principles of Ideal-Fluid Aerodynamics.* Krieger, Malabar, Florida.

VON KARMAN, T. & TSIEN, H. S. 1938 Boundary layers in compressible flow. *Journal of the Aeronautical Sciences.* 227-232.

KEENAN, J. H. NEUMAN, E. P. & LUSTWERK, F. 1950 An investigation of ejector design by analysis and experiment. *Journal of Applied Mechanics.* **17**, 3, 299-309.

KEITH, B. D. UENISI, K. & DIETRICH, D. A. 1993 CFD-based three-dimensional turbofan exhaust nozzle analysis system. *Journal of Propulsion and Power.* **9**, 6, 840-846.

KEVORKIAN, J. & COLE, J. D. 1981 *Perturbation Methods in Applied Mathematics.*Springer-Verlag, New York.

KLEMP, J. B. & ACRIVOS, A. 1972 A note on the laminar mixing of two uniform parallel semi-infinite streams, part I. *Journal of Fluid Mechanics.* **55**. 25-30.

KLINE, S. J. & MCCLINTOCK, F. A. 1953 Describing uncertainties in single-sample experiments. *Mechanical Engineering*. **75**, 3-8.

KOUTOMOS, P. & McGUIRK, J. J. 1989 Isothermal velocity and turbulence measurements downstream of a model multilobed turbofan mixer. *Experiments in Fluids*. **8**, 183-191.

KREISS, H. & OLIGER, J. 1973 Methods for approximate solution of time dependent problems. GARP publication series 10, World Meteorological Organization.

LAWTON, S. H. 1989 A study of exhaust plume interactions with external flow by the hydraulic analog. Ms Thesis, Department of Mechanical Engineering, Texas A&M University.

LIEPMANN, H. W. & ROSHKO A. 1957 *Elements of Gasdynamics*. Wiley, New York. 218-251.

LIGHTHILL, M. J. 1952 On sound generated aerodynamically. *Proceedings of the Royal Society A.* **211**, 564-587.

LIGHTHILL, M. J. 1953 On boundary layers and upstream influence, part II. supersonic flows without separation. *Journal of Fluid Mechanics*. **217**. 478-507.

LIGHTHILL, M. J. 1954 On sound generated aerodynamically II. turbulence as a source of sound. *Proceedings of the Royal Society A.* **222**, 1-32.

LIGHTHILL, M. J. 1958 On displacement thickness. *Journal of Fluid Mechanics.* **4**. 383-392.

LIGHTHILL, M. J. 1961 Sound generated aerodynamically, the Bakerian lecture. *Proceedings of the Royal Society A*. **267**, 147-182.

LIGHTHILL, M. J. 1963 Jet noise. *AIAA Journal*. **1**, 7, 1507-1517.

LIOU, W. W. & MORRIS, P. J. 1992 Weakly nonlinear models for turbulent mixing in a plane layer. *Physics of Fluids A*, **4**, 12, 2798-2808.

LOCK, R. C. 1950 The velocity distribution in the laminar boundary layer between parallel streams, part I. *Quarterly Journal of Mechanics and Applied Mathematics.* **4**, 44-63.

LOGAN, J. D. 1978 *Applied Mathematics*. Wiley, New York.

LOH, W. H. T. 1959 Hydraulic analogy for two-dimensional and one-dimensional flows. *Journal of the Aeronautical Sciences*. 389-391.

LOH, W. H. T. (ed.) 1969 Theory of the hydraulic analogy for steady and unsteady gas dynamics. *Modern Developments in Gas Dynamics*. Plenum, New York, 1-61.

LORD, W. K. JONES, C. W. STERN, A. M. HEAD, A. & KREJSA, E. A. 1990 Mixer ejector nozzle for jet noise suppression. *AIAA Paper* 90-1909.

LOVE, E. S. GRIGSBY, C. E. LEE, L P. & WOODLING, M. J. 1959 Experimental and theoretical studies of axisymmetric free jets. *NASA Technical Report* R-6.

LU, G. & LELE, S. 1994 On the density ratio effect on the growth rate of a compressible mixing layer. *Physics of Fluids A.* **6**, 2, 1073-1075.

LUENBERG, D. G. 1984 *Linear and Nonlinear Programming*. Addison-Wesley, Reading Massachusetts.

MALECKI, R. & LORD, W. 1990 Navier-Stokes analysis of a lobed mixer and nozzle. *AIAA Paper*. 90-0453.

MALMOUTH, N. D. 1993 Some applications of combined asymptotic and numerics in fluid mechanics and aerodynamics. in *Transonic Aerodynamics*. L. P. Cook (ed.)SIAM, Philadelphia. 65-88.

MANNING, T. A. 1991 Experimental studies of mixing flows with streamwise vorticity.Ms Thesis, Department of Aeronautics and Astronautics, MIT.

MARBLE, F. E. 1985 Growth of a diffusion flame in the field of a vortex. *Recent Advances in the Aerospace Sciences.* C. Casci (ed.) Plenum Publishing. 395-413.

MARSDEN, J. E & TROMBA, A. J. 1976 *Vector Calculus*. W. H. Freeman, New York.

MCCORMICK, D. C. 1992 Vortical and turbulent structure of planar and lobed mixer free-shear layers. PhD Thesis, Department of Mechanical Engineering, University of Connecticut.

MILES, J. W. 1958 On the disturbed motion of a plane vortex sheet. *Journal of Fluid Mechanics*, **4**, 538-552.

MORRIS, P. J., GIRIDHARAN, M. G. & LILLEY, G. M. 1990 On the turbulent mixing of compressible free shear layers. *Proceedings of the Royal Society of London A*. **431**, 219-243.

MORRISON, G. L. 1996 Personal communication. Department of Mechanical Engineering, Texas A&M University.

NAYFEH, A. 1973 *Perturbation Methods*. Wiley, New York.

OCKENDON, H. & OCKENDON, J. R. 1995 *Viscous Flow*. Cambridge University Press. London.

O'SULLIVAN, M. N. 1993 A computational study of the effects of viscosity on lobed mixer flow fields. Ms Thesis, Department of Aeronautics and Astronautics, MIT.

PACK, D. C. 1950 A note on Prandtl's formula for the wavelength of a supersonic gas jet. *Quarterly Journal of Mechanics and Applied Mathematics*. **3**, 2. 173-181.

PAI, S. I. 1952 On two-dimensional supersonic flow of a jet in a uniform stream.. *Journal of the Aeronautical Sciences*. **19**, 1, 61-65.

PAI, S. I. 1954 *Fluid Dynamics of Jets*. Van Nostrand, New York.

PAI, S. I. 1959 On the stability of a vortex sheet in an inviscid compressible fluid. *Journal of the Aeronautical Sciences.* **21**, 325.

PAL, A. K. & BOSE, B. 1993 A new optical study of supersonic flow past wedge profiles by hydraulic analogy. *Experiments in Fluids*. **14**, 3, 210-213.

PAPAMOSCHOU, D. & ROSHKO, A. 1988 The compressible turbulent shear layer: an experimental study. *Journal of Fluid Mechanics*. **197**, 453-477.

PAPAMOSCHOU, D. 1993 Model for entropy production and pressure variation in confined turbulent mixing. *AIAA Journal*. **31**, 1643-1650.

PEYRET, R. & TAYLOR, T. D. 1984 *Computational Methods for Fluid Flow*. Springer-Verlag, New York.

PORTER, J. L. & SQUYERS, R. A. 1978 A summary/overview of ejector augmentation. ATC Report R-91100/9CR-47A, Vol. II. Vought Corporation Advanced Technology Center, Dallas, Texas.

POVINELLI, L. A., ANDERSON, B. H. and GERSTENMAIER W. 1980 Computation of three-dimensional flow in turbofan mixers and comparison with experimental data. *AIAA Paper* 80-0227.

PATERSON, R. W. 1984 Turbofan mixer nozzle flow field- a benchmark experimental study. *Journal of Engines Gas Turbines and Power.* **106**, 692-698.

PRANTL, L., 1904. Ueber die stationaeren wellen in einem gasstrahle. *Physik Z.* **5**, 599-601.

PRESS, W. H., TEUKOLSKY, S. A., VETTERLING, W. T. & FLANNERY, B. P. 1992 *Numerical Recipes in FORTRAN, the Art of Scientific Computation.* Cambridge University Press, New York.

PRESZ, W. M. GOUSY, R. G. & MORIN, B. L. 1986 Forced mixer lobes in ejector designs. *AIAA Paper* 86-1614.

PRESZ, W. M. MORIN, B. L. BLINN, R. F. & GOUSY, R. G. 1987a Mixer-ejector performance study. United Technologies Research Center Report. UTRC87-26.

PRESZ, W. M. BLINN, R. F. & MORIN, B. L. 1987b Short efficient ejector systems. *AIAA Paper* 87-1837.

PRESZ, W. M. 1990 Mixer-ejector noise suppressers. *AIAA Paper* 90-1909.

PRIESWERK, E. 1940 Application of the methods of gas dynamics to water flows with free surface, part I: flows with no energy dissipation. part II: flows with momentum discontinuities (hydraulic jumps). *NACA Technical Memorandum.* 934 and 935.

QUI, Y. J. 1992 A study of streamwise vortex enhanced mixing in lobed mixer devices. PhD Thesis, Department of Aeronautics and Astronautics, MIT.

QUINN, B. 1973 Compact ejector thrust augmentation. *Journal of Aircraft*, **10**, 8., 481-486.

RAJARATNAM, N. 1976 *Turbulent Jets.* Elsevier, Amsterdam.

ROACHE, P. J. 1972 *Computational Fluid Dynamics.* Hermosa Publishers. Albuquerque, New Mexico.

RODI, W. 1993 *Turbulence Models and Their Application in Hydraulics*, IAHR Monograph, A. A. Balkema, Rotterdam.

RUBIN, S. G. & KHOSLA, P. K. 1977 Polynomial interpolation method for viscous flow calculations. *Journal of Computational Physics*, **24**, 217-246.

SCHETZ, J. A. & JANNONE, J. 1965 A study of linearized approximations to the boundary-layer equations. *Journal of Applied Mechanics.* 757-764.

SCHLICHTING, H. 1979 *Boundary Layer Theory, 7th ed.* McGraw-Hill, New York.

SHAPIRO, A. H. 1953 *The Dynamics and Thermodynamics of Compressible Fluid Flow Volume I.* Ronald Press Co., New York.

SHAPIRO, A. H. 1954 *Free Surface Water Table.* Vol. IX, Princeton Series in High Speed Aerodynamics and Jet Propulsion, Princeton, New Jersey.

SKEBE, S. A. MCCORMICK, D. C. & Presz, W. M. 1988a Parameter effects on mixer-ejector pumping performance. *AIAA Paper* 88-0188.

SKEBE, S. A. PATERSON, R. W. & BARBER, T. J. 1988b Experimental investigation of three-dimensional forced mixer lobe flow fields. *AIAA Paper* 88-3785.

TAM, C. K. W. & CHEN, K. C. 1979. A statistical model of turbulence in two-dimensional mixing layers. *Journal of Fluid Mechanics.* **92**, 303-326.

TENNEKES, H. & LUMLEY, J. L. 1972 *A First Course in Turbulence.* MIT Press, Cambridge, Massachusetts.

TEW, D. E. 1992. A computational study of mixing downstream of a lobed mixer with a velocity difference between the co-flowing streams. Ms Thesis, Department of Aeronautics and Astronautics, MIT.

THAYER, E. B. GAMBLE, E. J. GUTHRIE, A. R. KEHRET, D. F. BARBER, T. J. HENDRICKS, G. J. NAGARAJA, K. S. & MINARDI, J. E. NASA Lewis Research Center nozzle test data.

TILLMAN, T. G., PATERSON, R. W. & PRESZ, W. M. 1992 Supersonic nozzle mixer ejector. *Journal of Propulsion and Power*, **8**, 2, 513-519

TING, L. 1959 On the mixing of two parallel streams. *Journal of Mathematics and Physics.* **38**. 153-165

TOWNSEND, A. A. 1976. *The Structure of Turbulent Shear Flow.* Cambridge University Press, London.

VAN DYKE, M. 1975 *Perturbation Methods in Fluid Mechanics.* Parabolic Press, Stanford, California.

VIGNERON, Y. C. RAKICH, J. V. & TANNEHILL, J. C. 1978 Calculation of supersonic viscous flow over delta wings with sharp subsonic leading edges. *AIAA Paper* 78-1137.

WEINBERGER, H. F. 1965 *A First Course in Partial Differential Equations.* Wiley, New York.

WERLE, M. J. & PATERSON, R. W. 1987 Flow structure in a periodic axial vortex array. *AIAA Paper* 87-0610.

WHITE, F. M. 1974. *Viscous Fluid Flow, 1st ed.*. McGraw-Hill, New York.

WHITE, F. M. 1986. *Fluid Mechanics.* McGraw-Hill, New York.

WHITE, F. M. 1991. *Viscous Fluid Flow, 2nd ed.* McGraw-Hill. New York.

WILLIAMS, F. A. 1988. *Combustion Theory.* Addison-Wesley. New York.

YANG, T. NTONE, F. JIANG, T. & PITTS, D. R. 1985 An investigation of high-performance, short thrust augmenting ejectors. *Transactions of the ASME, Journal of Fluids Engineering.* **107**, 23-30.

YOUNGS, D. L. 1984 Numerical simulation of turbulent mixing by Rayleigh-Taylor instability. *Physica*, **12D**. 32-44.

APPENDIX A

FORMAL HIGHER ORDER EXPANSION, $O(\varepsilon^{1/2})$, EQUATION SYSTEMS

As discussed in Chapter I, one of the main strengths of the overall modeling methodology is development of a formal perturbation hierarchy. This type of expansion method permitted the "apriori" estimation of the error associated with a particular approximation, as well as, the formulation of corrections to the lower order approximations. In this appendix, formal development of both the first order, i.e. O(1), and second order, $O(\varepsilon^{1/2})$ expansions are derived. Since the first order expansion has been developed in the text, concentration is placed upon the mathematical character of the second order expansion.

Our work in this section will be to develop a system of partial differential equations describing viscous mixing. As such, we begin by considering compressible, two-dimensional Reynolds equations. The Prandtl number has been assumed to be close to unity, hence dissipation terms in the energy equation, may be neglected. As before, the conservation equations are written:

x-momentum:

$$\frac{\partial}{\partial x}(\rho u^2)+\frac{\partial}{\partial y}(\rho v^2)+\frac{\partial p}{\partial x}=-\frac{\partial}{\partial y}(\rho u'v')-\frac{\partial}{\partial x}(\rho u'u') \tag{A.1}$$

y-momentum:

$$\frac{\partial}{\partial x}(\rho uv)+\frac{\partial}{\partial y}(\rho v^2)+\frac{\partial p}{\partial y}=-\frac{\partial}{\partial x}(\rho u'v')-\frac{\partial}{\partial y}(\rho v'v') \tag{A.2}$$

energy:

$$\frac{\partial}{\partial x}(\rho uH)+\frac{\partial}{\partial y}(\rho vH)=-\frac{\partial}{\partial y}(\rho v'H')-\frac{\partial}{\partial x}(\rho u'H') \tag{A.3}$$

and continuity:

$$\frac{\partial}{\partial x}(\rho u)+\frac{\partial}{\partial y}(\rho v)=0 \tag{A.4}$$

To proceed with the analysis, it is first recognized that when non-dimensionalized, there are a number of "small terms" inherent to the governing equations. The small terms come from both the magnitude of the dependent and independent variables. For many problems, the flux difference between streams is relatively small, as is the mixing layer thickness compared to the streamwise distance. Formally stated this yields a set of characteristically small parameters:

$$\varepsilon = \frac{(U_{10} - U_{20})}{(U_{10} + U_{20})} \approx \varepsilon_G = \frac{(G_{10} - G_{20})}{(G_{10} + G_{20})} \approx \frac{\delta_{mix}}{L} \tag{A.5}$$

where δ_{mix} refers to the mixing layer thickness. As indicated in Chapter I, it should be noted that $\varepsilon \approx \varepsilon_G$ may not be small for all problems of interest. It will be shown, though, that this choice of expansion parameters provides reasonable results despite the fact they are formally not good approximations. Since it is important to have differential equations that can resolve the mixing layer itself, it is necessary to rescale (stretch) the cross-stream or "y" coordinate:

$$x \approx O(1) \quad y \equiv \varepsilon^{\frac{1}{2}} y^* \qquad \frac{\partial}{\partial y} \equiv \frac{1}{\varepsilon^{\frac{1}{2}}} \frac{\partial}{\partial y^*} \tag{A.6}$$

As before, the streamwise variables are simply expanded:

$$\rho f^* = \rho f_0^* + \rho f_1^* \varepsilon^{\frac{1}{2}} + \rho f_2^* \varepsilon + \ldots \qquad f^* \equiv u^*, \; H^*$$

$$g = g_0^* + g_1^* \varepsilon^{\frac{1}{2}} + g_2^* \varepsilon + \ldots \qquad g^* \equiv p^*, \; u^*, \; H^* \tag{A.7}$$

Recall that the expansion of the cross-steam flux and velocity took more care. It is expected that for the basically parallel flows of interest, that the cross stream velocity, v, is very small, O(ε). The cross stream mass flux, ρv, is also small, but in order to conserve mass this flux must be an order of magnitude larger, i.e. $O(\varepsilon^{1/2})$. With these estimates, the cross-stream mass flux and velocity are written:

$$\rho v^* = \rho v_0^* \varepsilon^{\frac{1}{2}} + \rho v_1^* \varepsilon + \ldots$$

$$v^* = v^*{}_0 \varepsilon + v_1^* \varepsilon^{\frac{3}{2}} + v_2^* \varepsilon^2 + \ldots \tag{A.8}$$

Proceeding with the scaled problem, the magnitude of the Reynolds stress terms (note we have suppressed the * denoting non-dimensionalization of the dependent variables to simplify the notation) are estimated. Following the development given in chapter I we give to $O(\varepsilon^{1/2})$ the conservation relationships:

$$\rho u' v' = -\left(\frac{\nu_{eff}}{U}\right)_G^* \frac{\varepsilon_G}{\varepsilon^{\frac{1}{2}}} \frac{\partial}{\partial y^*} \left[(\rho u_0 + (\rho u_1 u_0 + \rho u_0 u_1) \varepsilon^{\frac{1}{2}} + \ldots \right] +$$

$$-u_1 \left(\frac{\nu_{eff}}{U}\right)_G^* \frac{\varepsilon_G}{\varepsilon^{\frac{1}{2}}} \frac{\partial}{\partial y^*} (\rho u_0{}^2) \varepsilon^{\frac{1}{2}} + \ldots \tag{A.9}$$

Notice the last term which resulted from our linearization of ρG'u'/u. This non-linear term will provide the fundamental coupling between the O(1) system and the $O(\varepsilon^{1/2})$ system.

Since the interest in this appendix is in higher order expansions, it is necessary to estimate the size of the other Reynolds stress terms. Consider the other Reynolds stress term ρv'v' (which is the transport of turbulent cross-stream momentum flux by cross-stream turbulent velocity):

$$\rho v'v' \approx -\left(\frac{\nu_{eff}}{U}\right)^{*}_{G} \frac{\varepsilon_G}{\varepsilon^{\frac{1}{2}}} \frac{\partial}{\partial y^{*}}(\rho uv) = -\left(\frac{\nu_{eff}}{U}\right)^{*}_{G} \frac{\varepsilon_G}{\varepsilon^{\frac{1}{2}}} \frac{\partial}{\partial y^{*}}\left[u_0 \rho v_0 \varepsilon^{\frac{1}{2}} + \ldots\right] \tag{A.10}$$

The term, ρu'u' (which is the transport of turbulent streamwise momentum flux by streamwise turbulent velocities) is estimated to be:

$$\rho u'u' \approx -\left(\frac{\nu_{eff}}{U}\right)^{*}_{G} \varepsilon_G \frac{\partial}{\partial x}(\rho uv) = -\left(\frac{\nu_{eff}}{U}\right)^{*}_{G} \varepsilon_G \frac{\partial}{\partial x}\left[\rho u_0 v_0 \varepsilon + \ldots\right] \tag{A.11}$$

which is $O(\varepsilon^2)$ and, as expected, is much smaller, than either ρu'v' or ρv'v'.

Using equation (A.9) and invoking the additional well founded approximation that the turbulent Prandtl number Pr_t=O(1), the Reynolds transport of total enthalpy is written:

$$\rho H'v' = -\frac{1}{\mathrm{Pr}_t}\left(\frac{\nu_{eff}}{U}\right)^{*}_{G} \frac{\varepsilon_G}{\varepsilon^{\frac{1}{2}}} \frac{\partial}{\partial y^{*}}\left[\rho u_0 H_0 + (\rho u_1 H_0 + \rho u_0 H_1)\varepsilon^{\frac{1}{2}}\right] + \tag{A.12}$$

$$- - \frac{u_1}{\mathrm{Pr}_t}\left(\frac{\nu_{eff}}{U}\right)^{*}_{G} \frac{\varepsilon_G}{\varepsilon^{\frac{1}{2}}} \frac{\partial}{\partial y^{*}}\left[\rho u_0 H_0\right] +$$

Substituting the expansions and collect terms yields, the two lowest order systems. As before, the O(1) system may be written:

x-momentum:

$$\frac{\partial}{\partial x}(\rho u_0^2 + p_0) = \frac{\partial}{\partial y^{*}}\left[\left(\frac{\nu_{eff}}{U}\right)^{*}_{G} \frac{\varepsilon_G}{\varepsilon} \frac{\partial}{\partial y^{*}}(\rho u_0^2)\right] \tag{A.13}$$

y-momentum:

$$\frac{\partial p_0}{\partial y^*} = 0 \tag{A.14}$$

energy:

$$\frac{\partial}{\partial x}(\rho u_o H_0) = \frac{\partial}{\partial y^*}[\frac{1}{Pr_t}\left(\frac{\nu_{eff}}{U}\right)^*_G \frac{\varepsilon_G}{\varepsilon}\frac{\partial}{\partial y^*}(\rho u_o H_0)] \tag{A.15}$$

and mass conservation:

$$\frac{\partial}{\partial x}(\rho u_0) + \frac{\partial}{\partial y^*}(\rho v_0) = 0 \tag{A.16}$$

This is the O(1) system, that is solved. Again, as it is written, it is not possible proceed, since the last term in the preceding equations is not closed. To solve this system it is necessary to approximate the cross-stream mass flux term:

$$\rho v_0\ \varepsilon^{\frac{1}{2}} \approx -\frac{1}{Sc_t}\left(\frac{\nu_{eff}}{U}\right)^*_G \frac{\varepsilon_G}{\varepsilon^{\frac{1}{2}}}\frac{\partial}{\partial y^*}(\rho u_0) \tag{A.17}$$

where Sc_t is the turbulent Schmidt number, a O(1) term. Equation (A.17) is essentially a linearization of our Reynolds stress closure.

One more convenient modification can be made. Since the cross-stream pressure gradient $\partial p/\partial y \approx O(\varepsilon)^{1/2}$, it is permissible to add this term to the right hand side of the streamwise momentum equation thus yielding:

$$\frac{\partial}{\partial x}(\rho u_0^2 + p_0) = \frac{\partial}{\partial y^*}[\left(\frac{\nu_{eff}}{U}\right)^*_G \frac{\varepsilon_G}{\varepsilon}\frac{\partial}{\partial y^*}(\rho u_0^2 + p_0)] \tag{A.18}$$

This completes the formal perturbation development of the system O(1) of equations used in this project.

Now, the $O(\varepsilon^{1/2})$ system is also presented in this appendix. The conservation equations take the form:

x-momentum:

$$\frac{\partial}{\partial x}(\rho u_0 u_1 + \rho u_1 u_0) + \frac{\partial}{\partial y}(\rho u_0 v_0) + \frac{\partial p_1}{\partial x} =$$

$$\frac{\partial}{\partial y^*}\left[\left(\frac{\nu_{eff}}{U}\right)^* \frac{\varepsilon_G}{\varepsilon}\frac{\partial}{\partial y^*}(\rho u_0 u_1 + \rho u_1 u_0)\right] - \frac{\partial}{\partial y^*}\left[u_1\left(\frac{\nu_{eff}}{U}\right)^*_G \frac{\varepsilon_G}{\varepsilon}\frac{\partial}{\partial y^*}(\rho u_0^2)\right] \tag{A.19}$$

y-momentum:

$$\frac{\partial p_1}{\partial y} = \frac{\partial}{\partial y^*}\left[\left(\frac{\nu_{eff}}{U}\right)^*_G \frac{\varepsilon_G}{\varepsilon}\frac{\partial}{\partial y^*}(\rho v_0 u_0)\right] \tag{A.20}$$

energy:

$$\frac{\partial}{\partial x}(\rho u_0 H_1 + \rho u_1 H_0) + \frac{\partial}{\partial y^*}(\rho v_0 H_0) =$$

$$-\frac{\partial}{\partial y^*}\left[u_1 \frac{1}{Pr_t}\left(\frac{\nu_{eff}}{U}\right)^*_G \frac{\varepsilon_G}{\varepsilon}\frac{\partial}{\partial y^*}(\rho u_o H_0) + \right. \tag{A.21}$$

$$\left.\frac{\partial}{\partial y^*}\left[\frac{1}{Pr_t}\left(\frac{\nu_{eff}}{U}\right)^*_G \frac{\varepsilon_G}{\varepsilon}\frac{\partial}{\partial y^*}(\rho u_0 H_1 + \rho u_1 H_0)\right.\right.$$

and continuity:

$$\frac{\partial}{\partial x}(\rho u_1) + \frac{\partial}{\partial y^*}(\rho v_0) = 0 \tag{A.22}$$

A state equation, which is assumed to be a thermally perfect ideal gas, is included. Combining the ideal gas state equation with the definition of total enthalpy and retaining second order terms yields:

$$p_1 = \frac{\gamma - 1}{\gamma}\left[\rho H_1 + \left(\rho u_0 u_1 + \rho u_1 u_0\right)\right] \tag{A.23}$$

Equations (A.19)-(A.23) provide the governing set of equations to $O(\varepsilon^{1/2})$ which are listed in Table A.1.

Equation	Unknown
momentum, equation (A.19)	u_1
energy; equation (A.21)	H_1 or T_1
mass; equation (A.22)	p_1
y-momentum equation (A.20)	ρv_1
state; equation (A.23)	ρ_1
Total=5	Total=5

TABLE A.1 Equation versus unknown count for $O(\varepsilon^{1/2})$, system.

Comparison is now made between the $O(\varepsilon^{1/2})$ system with the O(1) set and other classical fluid flow approximations. The $O(\varepsilon^{1/2})$ family of equations is essentially linearized boundary layer or, alternatively stated, the $O(\varepsilon^{1/2})$ system are essentially linearized second order boundary layer equations (Van Dyke (1975)). The most striking addition to the $O(\varepsilon^{1/2})$, is that now, the y-momentum equation, equation (A.20) has become non-trivial. As such, p_1 or ρv_1 does not require the addition of the mixing mass flux closure relationship. Similar to classical boundary layer approximations, though, the cross-stream pressure gradient is explicit. In our system p_1 is computed using explicit information from the O(1) solution, through equation (A.20). This bears close analogy with classical second order boundary layer equations where the pressure gradient is coupled to the streamline displacement using the inviscid solution of Lighthill (1958). Displacement thickness and the pressure gradient may be directly computed in our $O(\varepsilon^{1/2})$ problem by invoking local continuity and local cross-stream momentum conservation. As before, other quantities, such as Mach number and total pressure, are supplemented by their own specific definitions.

This completes the formal perturbation development of the systems of equations used in this project. Recall that the goal was to obtain governing equations that were simpler than classical boundary layer, but more powerful than quasi-1-d equations. This goal has certainly been achieved by the O(1) system. Additionally, the higher order $O(\varepsilon^{1/2})$ system has been shown to retain many of the characteristic of classical, second order boundary layer methods. This close connection is to be expected, since the higher order equations should be consistent with the classical perturbation hierarchy, Table 1.3; a portion of which is repeated below as Table A.2.

Perturbation Method/Approximation	Comments:
Integral/Control volume (.i.e. 1-d or quasi-1-d)	Satisfy integral forms of conservation equations. Cannot predict local values.
Current DREA Model O(1) equation system	Parabolic in terms of conservative flux quantities. primitive quantities: u, v, p, ρ, M, locally predicted. PNS subsonic pressure approximation
Boundary layer	Parabolic for all flows; u, v, p(x), thin layer, p(x) specified by auxiliary relationship

TABLE A.2 Classical perturbation approximations and current DREA model.

This concludes our discussion of the higher order perturbation system. It is worth noting however, that both the previous systems are essentially parabolic in nature. As discussed in Chapter V, the wave effects (i.e. expansion-compression) structures inherent to our problem are not be modeled by either the O(1) nor the $O(\varepsilon^{1/2})$ equation sets. To do this requires using our expansions, retaining terms through $O(\varepsilon^{3/2})$. The considerable delay in the appearance of wave effects indicates, that to model wave phenomena, that it may be necessary to start with an entirely different perturbation expansion scaling.

APPENDIX B

CRITICAL BACK PRESSURE COMPUTATION AND SUBSONIC FLOW LIMITING CONDITIONS

The text developed in some detail two fundamental modes of ejector flow, namely, back pressure constrained and back pressure unconstrained flows. These two flow regimes have significantly different modeling methods associated with them. Although the distinction that two flow problems exist is clear, at no point did we discuss how one chooses, a priori, which is the appropriate model. In this section an approximate model to identify the appropriate flow regime is discussed. In addition to the supersonic/subsonic regime transition there are a series of constraints imposed upon the subsonic operation of an ejector. Attempting to operate outside of these constraints will cause DREA to fail due to physical reasons. As such, it is of considerable interest to provide an analysis to delineate these operational regions. Though it is beyond the scope of this project to develop operational maps using the full suite of constraints, as an example, one of the "back flow" constraint problem is modeled. Results of the back flow problem are compared with DREA to show that the convergence failure of DREA is indeed associated with one of the physical constraints, rather than some numerical difficulty.

B.1 Critical back pressure computation

The choice of the proper condition is dependent, as one would expect, upon the back pressure or exit pressure level that the ejector senses. Here, a value for the exit pressure which separates the back pressure dependent regime from the back pressure independent regime is developed. This value is defined as the critical back pressure or p_{crit}. The computation of this value follows. Referring to figure B.1, we consider the combined model.

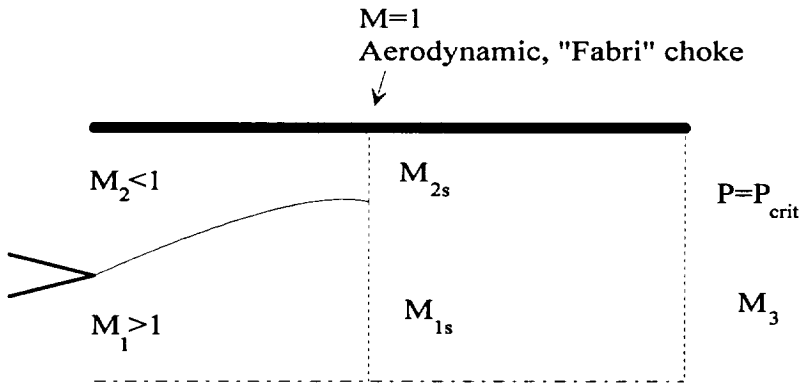

FIGURE B.1 Control volume definitions for the critical back pressure computation.

The first portion of the model involves the Fabri limited flow. The solution for this problem (which is described in Section 2.2.4 are the conditions associated with supersonic flow and choking in the secondary stream. Hence, if the exit conditions associated with this flow are known, then so would be the critical back pressure level.

Given a value for the critical back pressure, the two possible flow regimes are defined: if the back pressure level is below p_{crit}, then the Fabri-choke is the correct solution. Alternatively, if the back pressure level is

greater than p_{crit} then the flow is not properly modeled using Fabri theory and should be modeled using the back pressure dependent model. These criteria are summarized in table B.1

$(\frac{p_e}{p_{01}}) \leq (\frac{p_{crit}}{p_{01}})$	Back pressure independent flow Section 2.2.4
$(\frac{p_e}{p_{01}}) \geq (\frac{p_{crit}}{p_{01}})$	Back pressure dependent flow Section 2.2.3

TABLE B.1 Critical back pressure formulations.

From Table, B.1 it is clear that the key parameter governing the ejector flow mode is the value of p_{crit}/p_{01}. It is possible to compute p_{crit}/p_{01} by reformulating a set of 1-d conservation relationships. These are repeated for convenience:

$$\dot{m}_{1s} + \dot{m}_{2s} = \dot{m}_3 \tag{B.1}$$

$$\dot{m}_{1s} u_{1s} + p_{1s} A_{1s} + \dot{m}_{2s} u_{2s} + p_{2s} A_{2s} = \dot{m}_3 u_3 + p_3 A_3 \tag{B.2}$$

$$\dot{m}_{1s} T_{01s} + \dot{m}_{2s} T_{02s} = \dot{m}_3 T_{03} \tag{B.3}$$

and the exit pressure definition:

$$p_3 = p_c = p_\infty \tag{B.4}$$

Combining equations (B.1)-(B.4), it is possible to obtain a relationship in terms of M_{1s}, M_{2s}, and the critical pressure ratio p_{crit}/p_{01}. Provided below are the details of this procedure. Starting by rewriting the secondary or primary stream inlet terms as functions of M_{2s} or M_{1s} yields:

$$\dot{m} = \rho u A = \frac{\gamma M P_0 A}{a_0}\left[1 + \frac{\gamma - 1}{2} M^2\right]^{\frac{\gamma+1}{2(1-\gamma)}} \tag{B.5}$$

$$\dot{m}T = \frac{\gamma M P_0 A_2 T}{a_0}\left[1 + \frac{\gamma - 1}{2} M^2\right]^{\frac{\gamma+1}{2(1-\gamma)}} \tag{B.6}$$

$$\dot{m}u + pA = P_0 A\left[1 + \frac{\gamma - 1}{2} M^2\right]^{\frac{\gamma}{(1-\gamma)}}\left[1 + \gamma M^2\right] \tag{B.7}$$

To proceed, it is necessary to rewrite the exit conditions in terms of the upstream quantities and the exit pressure p_{crit}. Mass and energy can be easily rewritten in terms of upstream quantities, while, momentum is more difficult due to the velocity term (a non-conservative variable). To eliminate the exit velocity, it is possible to use energy and state:

$$\dot{m}_{1s} H_{01s} + \dot{m}_{2s} H_{02s} \equiv E = W\left[\frac{\gamma}{\gamma - 1}\frac{p_{crit} A_3 u_3}{W} + \frac{1}{2} u_3^2\right] \tag{B.8}$$

where $W=m_1+m_2$. This is a second-degree equation for u_3. Solving it yields:

$$u_3 = \left[\left(\frac{\gamma}{\gamma - 1}\frac{p_{crit} A_3}{W}\right)^2 + \frac{2E}{W}\right]^{\frac{1}{2}} - \frac{\gamma}{\gamma - 1}\frac{p_{crit} A_3}{W} \tag{B.9}$$

Recall that E and W are known in terms of the upstream variables. Rewriting momentum:

$$m_{1s} u_{1s} + p_{1s} A_{1s} + m_{2s} u_{2s} + p_{2s} A_{2s} = m_3 u_3 + p_{crit} A_3 \tag{B.10}$$

where (using energy) mu_3 is written:

$$\dot{m}u_3 = \left[\left(\frac{\gamma}{\gamma - 1} p_{crit} A_3\right)^2 + \frac{2\gamma R}{\gamma - 1}\left(\dot{m}_{1s} T_{01s} + \dot{m}_{2s} T_{02s}\right)\left(\dot{m}_{1s} + \dot{m}_{2s}\right)\right]^{\frac{1}{2}} + \\ - \frac{\gamma}{\gamma - 1} p_{crit} A_3 \tag{B.11}$$

Now, normalizing equation (B.11) by $P_{01}A_1$, and substituting our expressions for the upstream quantities in terms of M_{2s} or M_{1s} yields (with considerable manipulation) the non-linear, algebraic equation:

$$(1+\frac{\gamma-1}{2}M_{1s})^{\frac{\gamma}{1-\gamma}}(1+\gamma M_{1s}^2)+(\frac{p_{02}}{p_{01}})(\frac{A_2}{A_1})(1+\frac{\gamma-1}{2}M_{2s})^{\frac{\gamma}{1-\gamma}}(1+\gamma M_{2s}^2)-$$

$$+[\frac{\gamma}{\gamma-1}(\frac{p_e}{p_{01}})^2+\frac{2\gamma^2}{\gamma-1}[M_{1s}^2(1+\frac{\gamma-1}{2}M_{1s}^2)^{\frac{\gamma+1}{1-\gamma}}+$$

$$+M_{1s}M_{2s}(\frac{p_{01}}{p_{02}})(\frac{A_2}{A_1})(\frac{T_{01}}{T_{02}})^{\frac{1}{2}}(1+\frac{T_{01}}{T_{02}})(1+\frac{\gamma-1}{2}M_{1s}^2)^{\frac{\gamma+1}{2(1-\gamma)}}(1+\frac{\gamma-1}{2}M_{2s}^2)^{\frac{\gamma+1}{2(1-\gamma)}}+ \quad \text{(B.12)}$$

$$+M_{2s}^2(\frac{p_{02}}{p_{01}})^2(\frac{A_2}{A_1})^2(1+\frac{\gamma-1}{2}M_{2s})^{\frac{\gamma+1}{1-\gamma}}]^{\frac{1}{2}}]+\frac{1}{\gamma-1}(\frac{p_e}{p_{01}})(\frac{A_3}{A_1})=0$$

This rather cumbersome expression, equation (B.12) relates the critical pressure ratio p_{crit}/p_{01} to the aerodynamic choke quantities, A_{1s}, M_{1s}, A_{2s} and M_{2s}. Solution of these relationships is relatively straight forward, in that, p_{crit}/p_{01} is decoupled from the Fabri analyses, permitting solution of the Fabri problem and inversion (using a single variable, nonlinear equation solver) to compute the critical pressure ratio.

B.2 Subsonic limiting flows

In this section the limiting flow field conditions for subsonic mixing are discussed. The meaning of a "limiting" subsonic flow in this application describes flow fields for which the intended ejector operation; i.e. primary stream flow inducing secondary entrainment, thereby, satisfying the downstream pressure constraint fails. It is possible to identify three possible limiting subsonic limiting flow situations:

1. Incipient reverse flow into the secondary inlet.
2. Choked flow in the secondary inlet.
3. Choked flow in the exit mixing stream.

These three cases are illustrated in Figure B.2:

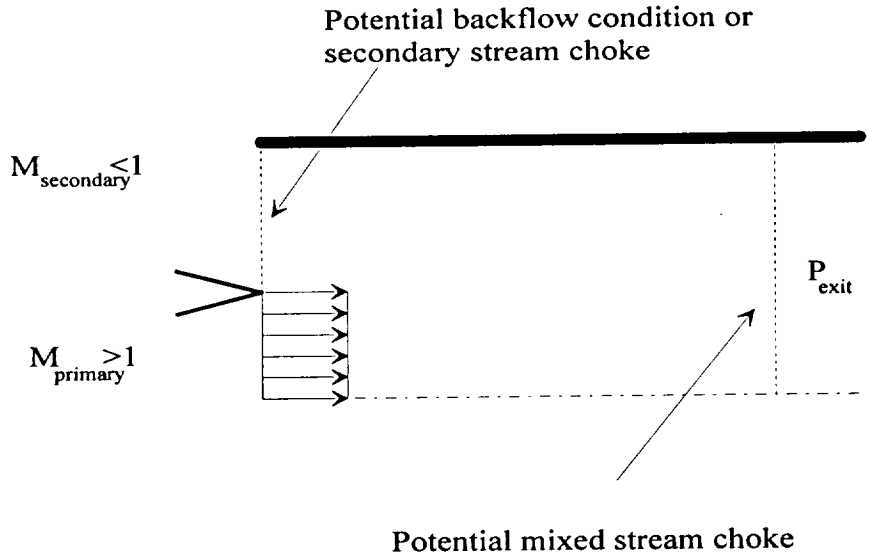

FIGURE B.2 A diagram showing possible limiting subsonic flow fields.

Our task is to determine upper and lower bounds on $(P_{02}/P_{01})(A_2/A_1)$, such that there is sufficient secondary pressure to prevent back flow, without inducing secondary inlet choking or exit stream choking. Hence a $(P_{02}/P_{01})(A_2/A_1)_{crit}$ used to delimit various flow regimes is to be developed.

Analysis of the critical condition problems may be performed by considering the system:

$$\dot{m}_1 + \dot{m}_2 = \dot{m}_3 \tag{B.13}$$

$$\dot{m}_1 u_1 + p_1 A_s + \dot{m}_2 u_2 + p_2 A_2 = \dot{m}_3 u_3 + p_3 A_3 \tag{B.14}$$

$$\dot{m}_1 T_{01} + \dot{m}_2 T_{02} = \dot{m}_3 T_{03} \tag{B.15}$$

and the exit pressure definition:

$$p_3 = p_\infty \tag{B.16}$$

Equation (B.13-B.16) can be placed into a more useful form for characterizing the critical flow conditions by rewriting them:

$$G \equiv \frac{\left[\left(1+\gamma M_1^2\right)+\left(\frac{\dot{m}_2}{\dot{m}_1}\right)\left(\frac{u_2}{u_1}\right)\left\{\left(\frac{M_1}{M_2}\right)^2+1\right\}\right]^2}{\left[M_1^2\left(1+\frac{\gamma-1}{2}M_1^2\right)+\left(\frac{M_1}{M_2}\right)^2\left(\frac{\dot{m}_2}{\dot{m}_1}\right)\left(\frac{u_2}{u_1}\right)^2\left(1+\frac{\gamma-1}{2}M_2^2\right)\right]\left[1+\left(\frac{\dot{m}_2}{\dot{m}_1}\right)\right]} \tag{B.17}$$

$$\left[(1-\frac{G}{2})\gamma^2+\frac{G\gamma}{2}\right]M_3^4+\left[(2-G)\gamma\right]M_3^2+1=0 \tag{B.18}$$

$$\left(\frac{M_1}{M_3}\right)\left(\frac{P_{01}}{P_\infty}\right)\left(\frac{A_1}{A_3}\right)\frac{\left[1+\left(\frac{\dot{m}_2}{\dot{m}_1}\right)\left(\frac{T_{02}}{T_{01}}\right)^{\frac{1}{2}}\right]^{\frac{1}{2}}\left[1+\left(\frac{\dot{m}_2}{\dot{m}_1}\right)\right]^{\frac{1}{2}}}{M_3\left(1+\frac{\gamma-1}{2}M_3^2\right)\left(1+\frac{\gamma-1}{2}M_1^2\right)^{\frac{\gamma+1}{2(\gamma-1)}}}-1=0 \tag{B.19}$$

Completing this set of equations are the definitions:

$$\frac{\dot{m}_2}{\dot{m}_1}=\left(\frac{M_2}{M_1}\right)\left(\frac{P_{02}}{P_{01}}\right)\left(\frac{A_1}{A_3}\right)\left(\frac{T_{02}}{T_{01}}\right)^{\frac{1}{2}}\left[\frac{1+\frac{\gamma-1}{2}M_1^2}{1+\frac{\gamma-1}{2}M_2^2}\right]^{\frac{\gamma+1}{2(\gamma-1)}} \tag{B.20}$$

$$\frac{u_2}{u_1}=\left(\frac{M_2}{M_1}\right)\left(\frac{T_{02}}{T_{01}}\right)^{\frac{1}{2}}\left[\frac{1+\frac{\gamma-1}{2}M_1^2}{1+\frac{\gamma-1}{2}M_2^2}\right]^{\frac{1}{2}} \tag{B.21}$$

Equations (B.17-B.21) provide the governing equations for the mixing problem in terms of the quantities of interest. As such, we may now pose the three limiting flow problems, listed in Table B.2.

Flow Limit	Unknowns
$M_2=0$	M_3, $(P_{02}/P_{01})(A_2/A_1)_{crit}$, G
$M_2=1$	M_3, $(P_{02}/P_{01})(A_2/A_1)_{crit}$, G
$M_3=1$	M_2, $(P_{02}/P_{01})(A_2/A_1)_{crit}$, G

TABLE B.2 Limiting flow problems.

where the parameter of greatest interest is, again, $(P_{02}/P_{01})(A_2/A_1)_{crit}$. The above problems may be solved using any one of the nonlinear system solvers developed previous.

An example of one of these limiting flows is an ejector which has a sufficiently high back pressure (one of several parameters which might cause this) such that the flow does not exit from the mixing duct exit, but reverses in the mixing duct and dumps out the secondary inlet (the first case in Table B.2). This flow field is illustrated in Figure B.3:

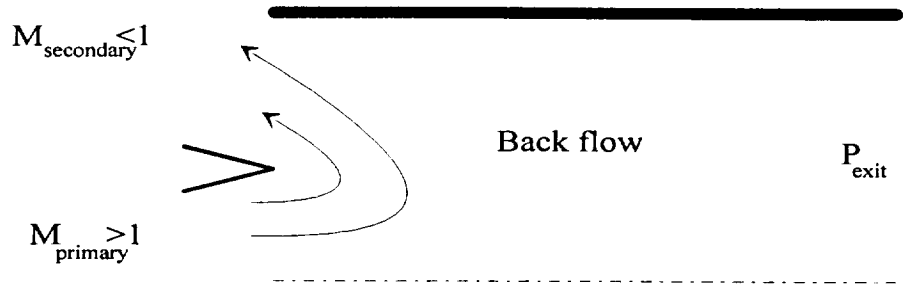

FIGURE B.3 A limiting flow problem, i.e. potential incipient back flow.

This type of operation is clearly unacceptable, both physically and mathematically. Our task is to identify conditions where this flow is imminent and to show that this is where the DREA simulation code becomes unusable.

The condition for incipient reversed flow into the secondary inlet is relatively simple; namely the secondary velocity and mass flow rate are zero, i.e. $u_2=m_2=0$. Hence, the governing equations reduce to relatively simple forms. The unknown in this system is ultimately $(P_{02}/P_{01})(A_2/A_1)_{crit}$. This parameter is important because if the ejector operating conditions have $(P_{02}/P_{01})(A_2/A_1)>(P_{02}/P_{01})(A_2/A_1)_{crit}$, then back flow will be prevented. Conversely for $(P_{02}/P_{01})(A_2/A_1)<(P_{02}/P_{01})(A_2/A_1)_{crit}$, reverse flow will occur and the DREA solution method is ill-posed:

$$G \equiv \frac{P^2{}_{mom}}{REW} = \frac{\left[\left(1+\frac{\gamma-1}{2}M_1^2\right)^{\frac{\gamma}{1-\gamma}}\left(1+\gamma M_1^2\right)+\left(\frac{P_{02}}{P_{01}}\right)\left(\frac{A_2}{A_1}\right)\right]^2}{\gamma M_1^2\left(1+\frac{\gamma-1}{2}M_1^2\right)^{\frac{\gamma}{1-\gamma}}} \tag{B.22}$$

$$\left[(1-\frac{G}{2})\gamma^2+\frac{G\gamma}{2}\right]M_3^4+\left[(2-G)\gamma\right]M_3^2+1=0 \tag{B.23}$$

$$\left(\frac{M_1}{M_3}\right)\left(\frac{P_{01}}{P_\infty}\right)\left(\frac{A_1}{A_3}\right)\frac{\left(1+\frac{\gamma-1}{2}M_1^2\right)^{\frac{\gamma}{2(1-\gamma)}}}{\left(1+\frac{\gamma-1}{2}M_1^2\right)^{\frac{1}{2}}}-1=0 \tag{B.24}$$

Equations (B.22-B.24) may be solved to yield the critical value; i.e. $(P_{02}/P_{01})(A_2/A_1)_{crit}$. As an example of the use of this method; consider a subsonic constant area mixing problem. The application of DREA for a primary NPR value of approximately 2.09 ends in convergence failure. The DREA total pressure area ratio,

$(P_{02}/P_{01})(A_2/A_1)$=8.76. It is suspected that this convergence failure is due to incipient back flow into the secondary inlet. Is this true? Solving equations (B.22-B.24) at various primary NPR's and comparing with the DREA simulation yields Figure B.4.

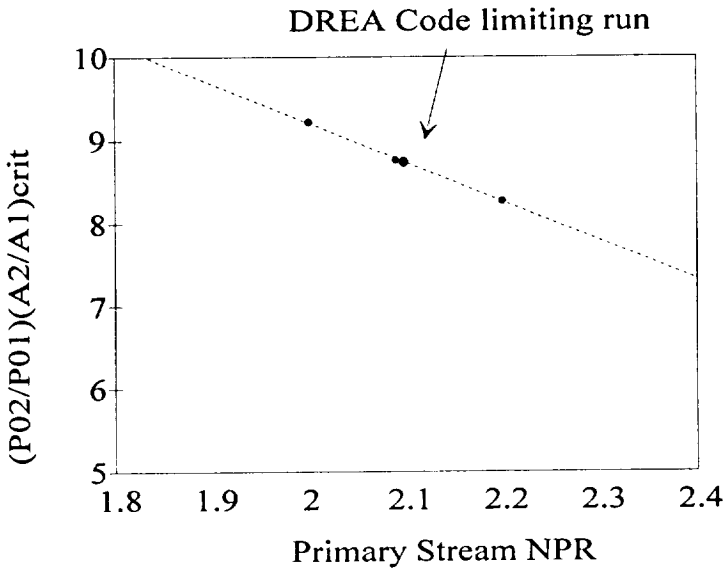

FIGURE B.4 Comparison of a limiting flow solution with a non-convergent DREA simulation.

From Figure B.4, it is apparent, that the convergence failure in the DREA simulation is indeed caused by incipient back flow into the secondary stream.

Unfortunately, due to the relative complexity of the necessary compressible formulation, it is difficult to get a sense of the influence of the parameters. As an aid to understanding, it is useful to consider an incompressible solution to the critical pressure ratio problem (this is effectively the secondary pressure needed to prevent reversed flow):

$$\left(\frac{p_2}{p_1}\right)\left(\frac{A_2}{A_1}\right) = \frac{p_\infty}{p_1}\frac{A_3}{A_1} + \frac{\rho u_1^2}{p_1}\left(\frac{A_1}{A_3} - 1\right) \tag{B.25}$$

From equation (B.20) the following trends may be identified:

1. Large back pressure; i.e. small NPR causes an increased likelihood of back flow.
2. Large exit stream area causes an increased likelihood of back flow.
3. Large primary mass flow (i.e. large u_1) causes an increased likelihood of back flow.

Though these conditions are much more easily ascertained using this incompressible analysis; it is believe that the trends identified using equation (B.25) will remain consistent even for the compressible problem.

This completes our discussion of limiting subsonic flow cases as well as subsonic/supersonic transition flows. Ultimately an operational map of limiting criteria is to be designed but is beyond the scope of this

study. As a demonstration of the ultimate importance of estimating operational characteristics, consider a LERD restricted, subsonic ejector nozzle which is presented in Figure B.5:

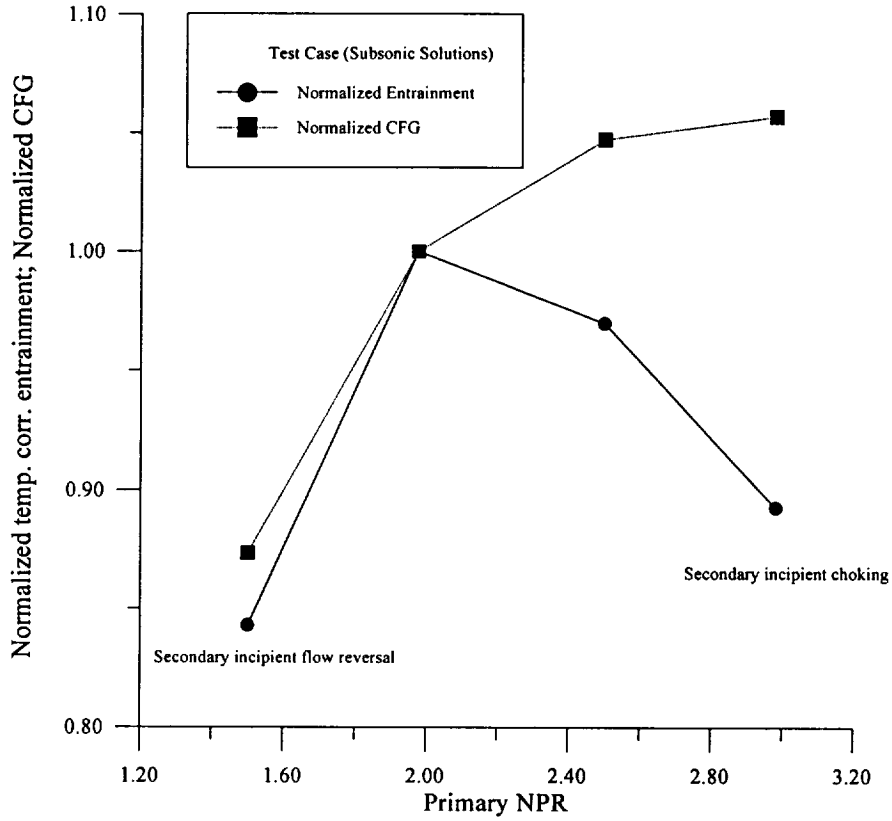

FIGURE B.5 Example of subsonic flow field limitations.

The upper and lower bound upon primary stream pressures are immediately obvious from Figure B.5. As a first step to obtaining the types of maps, it may be noted that the governing equations provided in Appendix D provide the preliminary basis for these operational maps.

APPENDIX C

INVISCID SUPERSONIC/SUBSONIC INTERFACE ANALYSIS

As discussed in Section 2, estimates of the boundaries of subsonic and supersonic flow are required to model the classical supersonic ejector problem. These transitions between flow regimes are directly related to expansion-compression effects in the ejector flow field. A simplified analysis is developed here to provide estimates of these regions.

C.1 Problem description

The problem under consideration is a two-dimensional, unconfined, supersonic primary stream with a subsonic secondary stream shear layer as shown in Figure C.1.

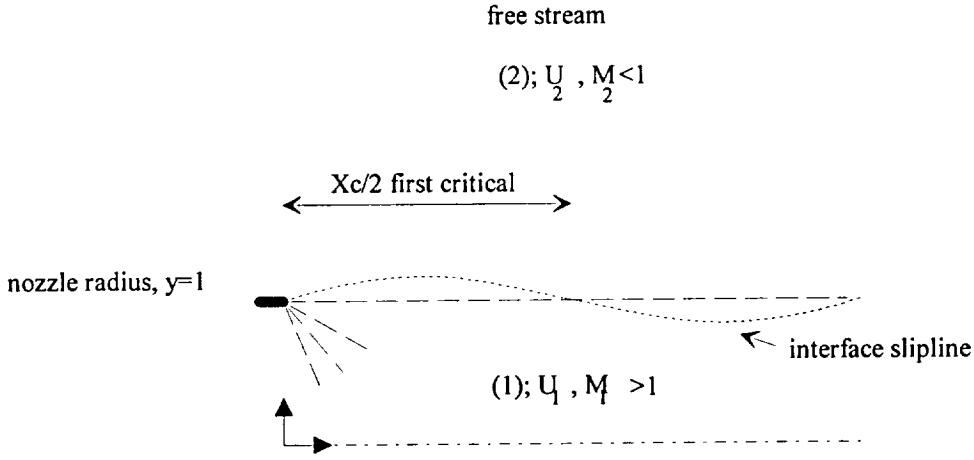

FIGURE C.1 Diagram of the unconfined supersonic-subsonic interface (slipline) problem.

The following assumptions are made:

(1) The flow quantities may be decoupled into a base quantity plus a perturbation value. Non-linear terms are neglected.
(2) The fluids are ideal gases.
(3) The flow is inviscid and irrotational except at the interface, where h=r=1.

According to Pai (1954) this is an acceptable approximation for large Reynolds number flows at locations where turbulent mixing is still relatively unimportant. Further, the vortex sheet approximation is a fundamental assumption of the Fabri choke analysis (Fabri and Seistrunck (1958) and Addy et al. (1981)).

The flow is modeled as irrotational, so a small disturbance velocity potential, ϕ', is used:

$$u_i = U_i + u_i = U_i + \frac{\partial \phi'_i}{\partial x} \tag{C.1}$$

where the subscript "i" describes the stream, primary (1) or secondary (2). For later reference, the governing, small disturbance, potential equations, (Anderson (1985)) for the primary (supersonic) stream are:

$$\beta_1^2 \frac{\partial^2 \phi_1'}{\partial x^2} - \frac{\partial^2 \phi_1'}{\partial y^2} = 0 \quad ; \beta_1^2 = M_1^2 - 1 \tag{C.2}$$

and, for the secondary (subsonic) stream:

$$\beta_2^2 \frac{\partial^2 \phi_2'}{\partial x^2} + \frac{\partial^2 \phi_2'}{\partial y^2} = 0 \quad ; \beta_2^2 = 1 - M_2^2 \tag{C.3}$$

This completes our description of the governing equations. In the next section a brief review of the classical results giving several important relationships for later reference is presented. These results are limited in applicability to small stream pressure differences. Afterwards a description of the formulation of a strained coordinate modification to the slipline model, applicable for a larger range of static pressure ratios, is provided.

C.2 Review of classical results

This section discusses the strength and weaknesses of two classical, approximate methods which include an inlet perturbation model and a slipline perturbation model with its associated base flow model.

C.2.1 Inlet perturbation model

This section describes an inlet perturbation model for confined flows which linearizes the flow about the inlet stream quantities. The analysis is closely related to normal mode methods and, as such, contains no initial condition information. Additionally, static pressure imbalances must be very small. From Pai (1952) the 2-d jet eigenvalue relationship for the wave number k is:

$$\tan(k\beta_1) = \left(\frac{M_1}{M_2}\right)^2 \left(\frac{\beta_2}{\beta_1}\right) \tag{C.4}$$

Equation (C.4) is used to compute the critical wave number k_c and hence the wavelength λ_c. This critical wavelength, λ_c is the location of the first minimum value of the interface and is more usually expressed as a critical location $x_c=\lambda_c=2\pi/k_c$. The fundamental period, T_c, is found using an area weighted velocity:

$$T_c = \frac{\lambda_c}{U_w} \qquad U_{ave} \equiv U_1 + U_2(H-1) \tag{C.5}$$

where H denote the upper wall. These relationships are for two-dimensional geometries. Using axi-symmetric versions of equations (C.2)-(C.3) (Liepmann and Roshko (1957)) the eigenvalue relationship for axi-symmetric flows as found by Pai (1954) may be written:

$$\frac{J_1(\beta_1 k)}{J_0(\beta_1 k)} \frac{K_0(\beta_2 k)}{K_1(\beta_2 k)} = \left(\frac{M_1}{M_2}\right)^2 \left(\frac{\beta_2}{\beta_1}\right) \tag{C.6}$$

in terms of Bessel functions and modified Bessel functions (see Abramowitz and Stegun (1964)). Furthermore, a secondary stream that is stationary or incompressible yields:

$$\frac{x_c}{2} = 2\beta_1 = 2(M_1^2 - 1)^{\frac{1}{2}} \tag{C.7}$$

which is Prandtl's (1904) result for a two-dimensional jet effluxing into a stagnant environment. The analogous relationships for axi-symmetric flows, Equation (C.7), for M_2=0 are:

$$J_0(\beta_1 k) = 0 \qquad x_c = 1.307(M_1^2 - 1)^{\frac{1}{2}} \tag{C.8}$$

which also agrees with Prandtl's result as quoted in Pai (1954).

C.2.2 Slipline perturbation model

The inlet perturbation model above is useful for small pressure disturbances but comparison with available experimental information is poor (Love et al. (1959)). Pack (1950), developed an alternative linear analysis for free jets involving a perturbation about the slipline itself. Here, for later reference, Packs model is outlined. Since Pack's model is intimately related to the strained coordinate model it is appropriate to give some details of the analysis instead of merely quoting it. Referring to Figure C.1, the analysis perturbs the flow about the streamline or slipline locations. Equations (C.1)- (C.3) remain the same, except, that a location subscript, "s" is used to indicate that the perturbation has been made about the slipline values. Using a perturbation expansion yields:

$$\frac{u}{U_{1s}} = 1 + \frac{\partial \phi}{\partial x}\varepsilon + \ldots \qquad \varepsilon \equiv (1 - \frac{U_1}{U_{1s}}) \tag{C.9}$$

The slipline perturbation method describes the flow better than the inlet perturbation because it represents the Prandtl-Meyer expansion in the primary stream, whereas, the inlet perturbation method merely approximates it. However the price is the solution of a nonlinear system of equations, the O(1) system, although for the free jet case, these relationships are relatively simple and may be solved explicitly. Perturbation methods that retain as much nonlinearity in their lowest order expansion as practical are more physically complete and hence powerful relative to their less complex counterparts.

C.2.3 Base flow slipline analysis

The base or lowest order flow is a set of isentropic expansions (or weak compressions) in the primary and secondary flows. Since the flows being considered are typically under expanded, it is reasonable to expect expansions of the primary flow and compression of the secondary flow. Modeling of a slightly overexpanded primary flow is also possible because for small pressure differences, the increase in entropy for the compression (oblique shock) is negligible.

Applying the static pressure matching condition and total pressure definition (Anderson (1985)) at the slipline interface yields:

$$M_{1s}^2 = \frac{2}{\gamma - 1}\left[\left(\frac{P_{02}}{P_{01}}\right)^{\frac{1-\gamma}{\gamma}}\left(1 + \frac{\gamma - 1}{2} M_2^2\right) - 1\right] \tag{C.10}$$

For the degenerate case of a supersonic jet effluxing into a stagnant atmosphere, which was also reported by Pack, equation (C.10) reduces to:

$$M_{1s}^2 = \frac{2}{\gamma - 1}\left[\left(1 + \frac{\gamma - 1}{2} M_1^2\right)\left(\frac{p_1}{p_2}\right)^{\frac{\gamma-1}{\gamma}} - 1\right] \tag{C.11}$$

C.3 First order slipline analysis

With the lowest order slipline quantities available from equations (C.10) and (C.11) the governing equations for the higher order, O(ε), portion of the analysis may now be derived. The equation governing the primary stream perturbation flow is similar to equation (C.2), except for the subscript "s", and for an axi-symmetric flow:

$$\beta_{1s}^2 \frac{\partial^2 \phi_1}{\partial x^2} = \frac{\partial^2 \phi_1}{\partial r^2} + \frac{1}{r}\frac{\partial \phi_1}{\partial r} \tag{C.12}$$

The appropriate boundary conditions for the flow are:

- at the centerline:

$$\phi_1(x, 0) = \textit{finite value} \tag{C.13}$$

- at the slipline defined by ξ(x):

$$\frac{\partial \phi_1(x, 1 + \xi)}{\partial x} = 0 = \frac{\partial \phi_1(x, 1)}{\partial x} + \frac{\partial^2 \phi_1(x, 1)}{\partial x \partial r}\xi + \ldots \approx \frac{\partial \phi_1(x, 1)}{\partial x} \tag{C.14}$$

Equation (C.14) introduces a transfer of boundary condition approximation often used in slender body theory, (Van Dyke (1975) and Nayfeh (1973)), and if the displacement, ξ, is small, the approximation is reasonable. It is this boundary condition that causes limitations as the stream pressure ratio increases. To complete the set of equations, the initial conditions are:

$$\phi_1(0, r) = 0 \qquad \frac{\partial \phi_1(0, r)}{\partial x} = -1 \tag{C.15}$$

Since our goal is to find the slipline geometry $\xi(x)$, the use of the kinematic condition (Drazin and Reid (1981)) is appropriate:

$$\frac{\partial \phi_1(x,1)}{\partial r} = \frac{d\xi}{dx} \quad , \quad \xi(0) = 0 \tag{C.16}$$

Equations (C.12)-(C.16) describe the primary stream flow field and the slipline location. This contrasts with the inlet perturbation method in which governing equations were required for both streams. The difference lies in that for the slipline perturbation method information about the secondary stream is contained in the first order solution and is passed to the higher order analysis through the coefficient β_{1s} in equation (C.14), whereas, the inlet perturbation method requires explicit information about the secondary stream in the higher order $O(\varepsilon)$, equation system. In addition, initial condition information is built into the slipline perturbation method unlike the "normal mode" method of the inlet perturbation model.

Equations (C.12)-(C.16) have been solved using eigenfunction methods (Pack (1950)) to yield the potential and the displacements. Since the goal is to later obtain improvements to Pack's solution for unconfined flows it is necessary describe the velocity potential and displacement potentials:

$$\phi(x,r) = -2\beta_{1s}\sum_{n=1}^{\infty}\frac{1}{\lambda_n^2 J_1(\lambda_n)} J_0(\lambda_n r)\sin(\lambda_n \frac{x}{\beta_{1s}}) \tag{C.17}$$

and the displacement is:

$$\xi(x) = 4\beta_{1s}^2\sum_{n=1}^{\infty}\frac{1}{\lambda_n^2}\sin^2(\frac{\lambda_n x}{2\beta_{1s}}) \quad ; \quad J(\lambda_n) = 0 \tag{C.18}$$

From Pack (1950), the critical location (first minimum) is at:

$$\frac{x_c}{2} = 1.22\beta_{1s} \tag{C.19}$$

for axi-symmetric flows. The analogous relationship for two-dimensional flows is:

$$\frac{x_c}{2} = 2\beta_{1s} \tag{C.20}$$

Equations (C.19) and (C.20) contain the pressure ratio as β_{1s}, consequently it is expected that they are a improvement over the inlet perturbation solutions. The next section shows, that in spite of the improvements due to the slipline method, equations (C.19) and (C.20) are still limited to relatively small pressure ratios between streams. Additionally, equation (C.17) admits the trivial solution of: $\phi_1(x,r)=\xi(x)=0$ for $\varepsilon=0$ which is not experimentally or analytically valid as shown by Love et al. (1959). Love, et al. indicate that there is a particular solution valid for both two-dimensional and axi-symmetric flows for $p_2/p_1=1$ which states $x_c/2=\beta_{1s}$. This particular solution should be recovered by equations (C.20) and (C.19) but is not.

C.4 Strained coordinate model

To overcome the limitations of Pack's streamline perturbation analysis, namely, small pressure ratio restrictions and singularity for $\varepsilon=0$, a strained coordinate slipline perturbation method has been formulated. The origin and full description of the strained coordinate method may be found in Van Dyke (1975), Nayfeh (1973) and Kevorkian and Cole (1981). A related approach is the Rayleigh-Schrodinger method described by Nayfeh (1973). Motivation for the use of the strained coordinates comes from the recognition, that Pack's analysis fails for large pressure ratios between streams that are associated with large displacement of the interface. This causes the boundary condition transfer analysis in equation (14) to become a weak approximation. Defining new coordinates that better approximate the location of the slipline velocity boundary condition might be expected to give a better solution. This idea is central to Lighthill's method of strained coordinates described by Van Dyke (1975).

The strained coordinate method starts by considering the solution of ordinary differential equations resulting from a separation of variable solution of equation (C.12) with $\phi(x,r)=f(x)g(r)$. Without the transfer of boundary conditions approximation of equation (C.14) the streamwise varying differential equation for f(x), is obtained as:

$$\frac{d^2 f}{d x^2} + [\frac{\lambda_n}{\beta_{1s}}]^2 \frac{1}{(1+\xi(x))^2} f = 0 \quad ; \quad J_0(\lambda_n) = 0 \tag{C.21}$$

Following the slipline perturbation solution method the slipline displacement, $\xi(x)$ of equation (C.18), is approximated as:

$$\xi(x) \approx \xi_m \sin^2(\frac{\lambda_n x}{2\beta_{1s}}) \qquad \xi_m \equiv \beta_{1s}^2 \varepsilon \equiv \beta_{1s}^2 \left[1 - \frac{U_1}{U_{1s}}\right] \tag{C.22}$$

Since Pack's solution is known to be singular for zero displacement, $\xi \sim \varepsilon = 0$, a stretching transformation on the displacement:

$$\tilde{\xi}(x) = \frac{\xi(x)}{\xi_m^{\frac{1}{2}}} = \xi_m^{\frac{1}{2}} \sin^2(\frac{\lambda_n x}{2\beta_{1s}}) \tag{C.23}$$

is needed, where the displacement magnitude ξ_m as the appropriate perturbation parameter is selected. Although appropriate for $\xi_m \ll 1$, this transformation amplifies the problem of convergence of the series, see equation (C.9), for large displacement magnitudes. This problem of convergence, though, is precisely the type of situation where the method of strained coordinates is useful. Introducing new (strained) coordinates:

$$x = s + x_2(s)\xi_m^{\frac{1}{2}} + .. \tag{C.24}$$

where "s" is our new coordinate and $x_2(s)$ is to be determined. Similarly the basic solution is perturbed as:

$$f = f_0 + \xi_m^{\frac{1}{2}} f_1 + ... \tag{C.25}$$

Equation (C.24) is used to transform derivatives such as:

$$\frac{d}{dx} = (1 - x_2' \xi_m^{\frac{1}{2}}) \frac{d}{ds} + \ldots \tag{C.26}$$

and

$$\frac{d^2}{dx^2} = (1 - 2x_2' \xi_m^{\frac{1}{2}}) \frac{d^2}{ds^2} - x_2'' \xi_m^{\frac{1}{2}} \frac{d}{ds} + \ldots \tag{C.27}$$

The expansions defined by equations (C.24) and (C.25), and the transformed derivatives are substituted into equation (C.21) to give to O(1):

$$\frac{d^2 f_0}{ds^2} + [\frac{\lambda_n}{\beta_{ls}}]^2 f_0 = 0 \tag{C.28}$$

Solution of equation (C.28) yields the previously derived harmonic solution, which forms the basis of equation (C.17). To $O(\xi_m^{1/2})$, equation (C.28) yields:

$$\frac{d^2 f_1}{ds^2} + [\frac{\lambda_n}{\beta_{ls}}]^2 f_1 = x_2'' \frac{df_0}{ds} + 2x_2' \frac{d^2 f_0}{ds^2} + 2\sin^2(\frac{\lambda_n s}{2\beta_{ls}})[\frac{\lambda_n}{\beta_{ls}}]^2 f_0 \tag{C.29}$$

To prevent the existence of solutions, which grow unphysically large, $x_2(s)$, is chosen so that it approximately eliminates the right hand side of equation (C.29). This can be considered as eliminating a forcing term in a harmonic system. One possible choice to remove the right hand side is to require:

$$x_2' = \sin^2(\frac{\lambda_n s}{2\beta_{ls}}) \quad so\ that \quad x_2(s) = \frac{1}{2}s - \frac{1}{2}\frac{\beta_{ls}}{\lambda_n}\sin(\frac{\lambda_n s}{2\beta_{ls}}) \tag{C.30}$$

For large λ_n the last term in equation (C.30) may be neglected, giving $x_2(s)=s/2$, then $x''_2 = 0$ and from equation (C.24), and the strained coordinate "s" is given by:

$$s = \frac{x}{1 + \frac{1}{2}\xi_m^{\frac{1}{2}}} \tag{C.31}$$

The O(1) solution of equation (C.21) is the same as the unstrained problem (except x=s), so that following Lighthill's method (as described by Van Dyke (1975)), equation (C.31) may be introduced into the solutions for the unstrained solutions: equations (C.17) and (C.18). Further, since equation (C.31) involves straining by a

constant, the minimization of equation (C.18) remains valid to within a constant, hence equations (C.19) and (C.20) may be written:

•axi-symmetric:

$$\frac{x_c}{2} = 1.22\beta_{eff} \equiv 1.22(1+\frac{1}{2}\xi_m^{\frac{1}{2}})\beta_{1s} \tag{C.32}$$

•two-dimensional:

$$\frac{x_c}{2} = 2\beta_{eff} \equiv 2(1+\frac{1}{2}\xi_m^{\frac{1}{2}})\beta_{1s} \tag{C.33}$$

Equations (C.32) and (C.33) represent the strained coordinate modifications of Pack's slipline analysis. Since the problem is valid for small pressure ratios due to the stretching transformation of equation (C.32), it is permissible to modify the strained coordinate solutions using the particular solution referenced by Love et al. (1959), valid for pressure ratios precisely equal to one. Thus:

•axi-symmetric:

$$\frac{x_c}{2} = 1.22\beta_{eff} - .22\beta_{1s} \equiv 1.22(1+\frac{1}{2}\xi_m^{\frac{1}{2}})\beta_{1s} - .22\beta_{1s} \tag{C.34}$$

•two-dimensional:

$$\frac{x_c}{2} = 2\beta_{eff} - \beta_{1s} \equiv 2(1+\frac{1}{2}\xi_m^{\frac{1}{2}})\beta_{1s} - \beta_{1s} \tag{C.35}$$

where $\beta_{1s}=(M_{1s}^2-1)^{1/2}$ and $\xi=\beta_{1s}^2[1-U_1/U_{1s}]$. Equations (C.34) and (C.35) are the final modified solutions for the critical slipline location. These relationships comprise our solution for the location of the first minimum of the slipline.

C.5 Results and comparison of models

In this section, we compare the different models using a degenerate free jet case. The critical location and period of the interface, x_c and T_c, are the parameters of primary interest in this analysis and are obtained from the model solutions listed in Table C.1.

Model Type	Axi-symmetric	Two-dimensional
Inlet Perturbation (IP)	equation (C.8)	equation (C.7)
Slipline Perturbation (SP)	equation (C.19)	equation (C.20)
Strained Coordinate (SC)	equation (C.34)	equation (C.35)

TABLE C.1 A summary of inviscid slipline solution types.

C.5.1 Inlet perturbation model

Results for an axi-symmetric free jet, equation (C.8), are not presented since the model is limited to matched static pressure flows. Although equation (C.8) does provide an adequate comparison for sonic primary jet problems, it becomes poor as the Mach number increases. This poor comparison is attributed to both the pressure ratio between streams playing no role in the analysis and the linearization of the primary stream expansion. These limitations are removed using the slipline perturbation method.

C.5.2 Slipline perturbation

Comparison of axi-symmetric free jet results from the slipline perturbation solutions (SP) of Pack (1950) with the data of Love et al. (1959), are shown in Figure C.2 for several Mach numbers. Figure C.2 shows a good comparison with the data of Love et al. for small pressure ratios and low primary Mach numbers. In general, the axi-symmetric solutions for a free jet show considerable improvement over the inlet perturbation solutions. The improvement is attributed to the slipline perturbation containing the pressure ratio as an explicit parameter. However, the solution yields poor results for large pressure ratios and the error is also large for equal pressure ratios. These results prompted the development of the strained coordinate streamline perturbation model.

C.5.3 Strained coordinates

The strained coordinate modification of Pack's solution (SC) is compared with the axi-symmetric, free-jet experiment of Love et al. (1950), for several primary Mach numbers, in Figure C.2. Love et al. provides a semi-empirical curve fit relationship for the critical location that takes the form:

$$\frac{x_c}{2} = 1.55[M_1^2(\frac{p_1}{p_2}) - 1]^{\frac{1}{2}} - 0.55\beta_1 \qquad \frac{p_1}{p_2} \leq 2$$

$$\frac{x_c}{2} = 1.52(\frac{p_1}{p_2})^{0.437} + 1.55([2M_1^2 - 1]^{\frac{1}{2}} - 1) - 0.55\beta_1 + 0.5[\frac{1}{1.55}[(\frac{p_1}{p_2} - 2)\beta_1]^{\frac{1}{2}} - 1] \quad \text{(C.36)}$$

$$\frac{p_1}{p_2} \geq 2$$

Equation (C.36) provides a good fit to the data over the range compared here. It should also be noted, that although equation (C.36) provides a useful empirical relationship it may be difficult to directly extend the solution to other flow problems, for example confined flows, since it does not have a completely rational basis.

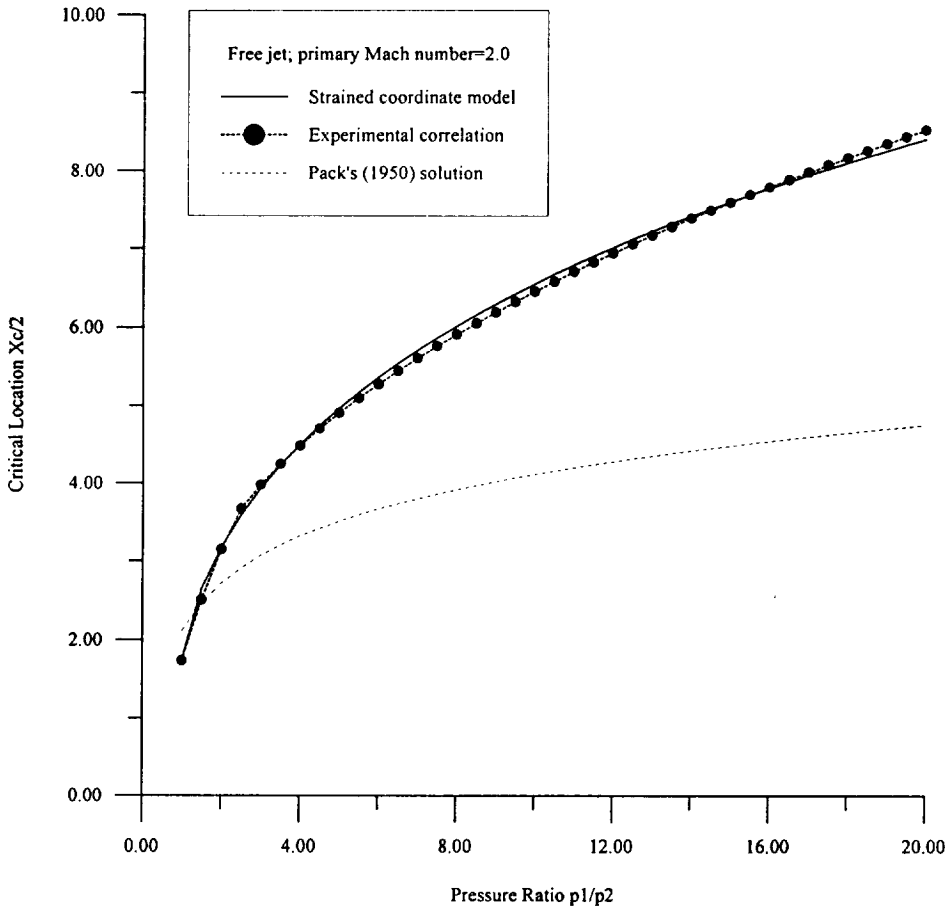

FIGURE C.2 A comparison of the strained coordinate solution with Pack's (1950) solution and the experimental correlation of Love et al. (1950).

Figure C.2 shows that the comparison between the strained coordinate model and the experimental data is excellent. Inspection of the figures shows that the strained coordinate theory provides a considerable improvement over the simple slipline perturbation (SP) method for all primary Mach numbers and for a large range of pressure ratios. However, the agreement is poorer for sonic primary Mach numbers, but this is to be expected because the strained coordinate analysis was developed to handle large, O(1), slipline perturbations. Since the slipline amplitude scales according to:

$$\xi_m \equiv \beta_{1s}\,\varepsilon = [M_{1s}^2 - 1]^{\frac{1}{2}}\,\varepsilon \tag{C.37}$$

The amplitude is expected to be relatively small for Mach numbers close to one and hence the strained coordinate modification is not formally appropriate. In spite of these formal limitations the strained coordinate model has shown good comparison (maximum of 10% relative error) for Mach numbers ranging from approximately sonic, Mach 1.2, to Mach 4.0. A maximum relative and root mean squared errors may be defined:

$$err_{rms} \equiv \left[\frac{\sum_{1}^{n} [(\frac{x_c}{2})_{exper.} - (\frac{x_c}{2})_{anal.}]^2}{\sum_{1}^{n} (\frac{x_c}{2})^2_{exper.}} \right]^{\frac{1}{2}} x100\% \tag{C.38}$$

Applying this definition to the SC method and the experimental correlation of Love, equation (C.36), yields the results presented in Table C.2 for a pressure ratio range of p_1/p_2=1.0-20.0.

Primary Mach number	RMS error equation (C.38)	Maximum relative error
1.2	6.34 %	9.48 %
2.0	1.15 %	5.44 %
3.0	4.12 %	5.19 %
4.0	9.03 %	10.10 %

TABLE C.2 RMS error and maximum relative error between strained coordinate model and measurements of Love et al. (1959).

Finally, it must be noted that for precisely sonic flow with pressure matching, p_2/p_1=1, the error is zero, but increases for larger pressure ratios as discussed previously. Therefore, the strained coordinate solution provides a greatly improved prediction of free jet critical locations over a full range of Mach numbers and pressure ratios. This concludes our discussion of the supersonic/subsonic interface problem. The use of these relationships in the main ejector code is described in Section 2.

APPENDIX D

ANALYTICAL SOLUTION OF MIXING DIFFERENTIAL EQUATIONS USING COSINE TRANSFORM AND METHOD OF IMAGES

As developed in Section 2.4, the governing equations may be written for the conservation quantities in terms of the general linear parabolic equation (the canonical form):

$$\frac{\partial \phi}{\partial x} = a(x)\frac{\partial^2 \phi}{\partial y^2} \tag{D.1}$$

with the boundary conditions:

$$\frac{\partial \phi(x,0)}{\partial y} = \frac{\partial \phi(x,1)}{\partial y} = 0 \tag{D.2}$$

with the initial condition:

$$\phi(0,y) = \begin{pmatrix} \phi_{10} & 0 \le y \le h_s \\ \phi_{20} & h_s < y \le 1 \end{pmatrix} \tag{D.3}$$

and ϕ is defined by:

$$\phi(x,y) \equiv \begin{pmatrix} \rho u^2 + p \\ \rho u H \\ \rho u \end{pmatrix} \tag{D.4}$$

Recall, that the turbulence model admitted the local result, that the function a(x) may be approximated by the linear function $a(x)=a^* x$. The choice of the locally linear functional form is justified by the development of the near field turbulence model, which did indeed show a locally linear function, equation (2.89), e.g.:

$$kx\varepsilon_G = \frac{1}{2}\frac{x}{\left(\eta^*_\infty\right)^2}\left(\frac{\delta}{x}\right)^2 \tag{D.5}$$

With this local approximation, it is possible to write equation (D.1) in the form:

$$\frac{\partial \phi}{\partial x} = a^* x\frac{\partial^2 \phi}{\partial y^2} \tag{D.6}$$

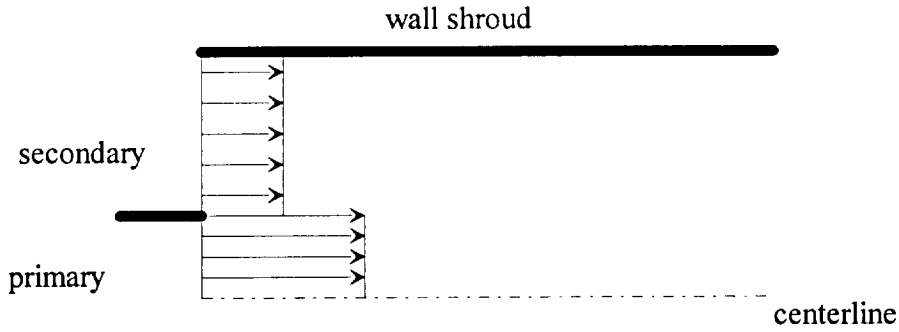

FIGURE D.1 Discontinuous initial conditions for the mixing problem.

As indicated previously and repeated here in Figure D.1, the discontinuous nature of the initial condition (which is not even a continuous, C^0, function (Marsden and Tromba (1976)), causes considerable difficulties both for numerical and analytical solutions. What is required is an analysis capable of dealing with extremely rapidly changing functions or more properly distribution. Fortunately, a solution method from classical analysis is available which is based upon distribution theory rather than requiring continuous functions. This is the method of Green's function expansions (Haberman (1983) or Weinberger (1965)). It is actually more useful to derive the solution using a cosine transform and the method of images, (Haberman (1983) or Weinberger (1965)). The ultimately desired result is:

$$\phi_{an} = \frac{1}{2}(\phi_{10} - \phi_{20}) \sum_{-\infty}^{\infty} \left[erf\left(\frac{y + h_s - 2n}{(2a^*)^{\frac{1}{2}} x} \right) - erf\left(\frac{y - h_s - 2n}{(2a^*)^{\frac{1}{2}} x} \right) \right] + \phi_{20} \tag{D.7}$$

The strategy used to obtain this result is:

- Derive a semi-infinite solution for our problem using cosine transforms (a special, semi-infinite, even function case of Fourier transforms).
- Specialize this semi-infinite result for our finite problem using the method of images.

Starting, by considering a more canonical form of the governing equation (D.6), it is necessary to introduce the new variable, $t=1/2x^2$. To solve the semi-infinite problem then, it is necessary to consider (notice, also, the introduction of the dependent variable "u" which is used to signify the generality of the canonical form):

$$\frac{\partial u}{\partial t} = a^* \frac{\partial^2 u}{\partial y^2} \tag{D.8}$$

with the boundary conditions:

$$\frac{\partial u(t,0)}{\partial y} = 0 \quad \phi(t, y \to \infty) = 0 \tag{D.9}$$

Initial conditions are generalized to:

$$u(0, y) = \begin{pmatrix} 1 \; 0 \le y \le h_s \\ 0 \;\; h_s < y \le 1 \end{pmatrix} \tag{D.10}$$

which is shown diagramtically in Figure D.2:

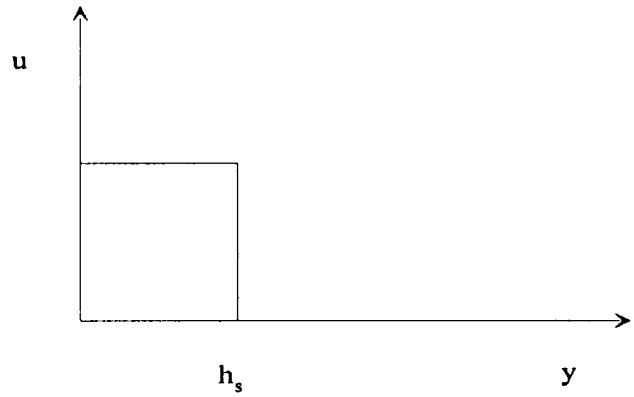

FIGURE D.2 Diagram of the canonical, step function initial conditions.

Formally transforming equation (D.8) and solving the resulting ordinary differential equation yields:

$$U(\omega, t) = C(\omega) e^{-\omega^2 a^* t} \tag{D.11}$$

Then summing (integrating) over all wave numbers, one obtains:

$$u(y, t) = \int_0^\infty C(\omega) \cos(\omega y) e^{-\omega^2 a^* t} \, d\omega \tag{D.12}$$

where the unknown function C(ω) is compute using the cosine transform pair for t=0:

$$C(\omega) = \frac{2}{\pi} \int_0^\infty u(0, t) \cos(\omega y) dy \tag{D.13}$$

Applying our initial condition and computing the elementary integral yields the formal solution:

$$u(y, t) = \frac{2}{\pi} \int_0^\infty \frac{1}{\omega} \sin(\omega h_s) \cos(\omega y) e^{-\omega^2 a^* t} \, d\omega \tag{D.14}$$

Unfortunately, this formal solution is in terms of an infinite integral, which makes its practical evaluation tedious.

An alternative method to this situation is to return to equation (D.11) and apply a cosine transform convolution theorem (Haberman (1983)):

$$C^{-1}\{F(\omega)G(\omega)\} = \frac{1}{\pi}\int_0^{\infty} g(\bar{y})\left[f(y-\bar{y}) + f(y+\bar{y})\right]d\bar{y} \tag{D.15}$$

where for our problem F(ω) is the exponential term in equation (D.11) and G(ω) is the step function initial condition. Fortunately, the inversion of the exponential term is tabulated:

$$C^{-1}\left\{2\frac{1}{\sqrt{4\pi\alpha}}e^{-\omega^2/4\alpha}\right\} = e^{-\alpha t^2} \tag{D.16}$$

and the step function merely carries through to yield:

$$u(y,t) = C^{-1}\{U(\omega,t)\} = \frac{1}{\sqrt{4\pi a^* t}}\left[\int_0^{h_s}\exp\left(-\frac{(y-\bar{y})}{4a^* t}\right) + \exp\left(-\frac{(y+\bar{y})}{4a^* t}\right)d\bar{y}\right] \tag{D.17}$$

The step function has been used to evaluate the infinite integral. From this point, the integrals in equation (D.17) are evaluated using straightforward substitution, which yields the expected error function (Abramowitz and Stegun (1964)) form:

$$u(y,t) = \frac{1}{2}\left[erf\left(\frac{(y+h_s)}{(4a^* t)^{\frac{1}{2}}}\right) - erf\left(\frac{(y-h_s)}{(4a^* t)^{\frac{1}{2}}}\right)\right] \tag{D.18}$$

Equation (D.18) has been derived to satisfy the unit step function initial condition. By elementary substitution one may modify this condition to apply for the physical initial condition required by equation (D.3):

$$u_{semi-inf}(y,t) = \frac{1}{2}(\phi_{10} - \phi_{20})\left[\mathrm{erf}\left(\frac{(y+h_s)}{(4a^* t)^{\frac{1}{2}}}\right) - \mathrm{erf}\left(\frac{(y-h_s)}{(4a^* t)^{\frac{1}{2}}}\right)\right] + \phi_{20} \tag{D.19}$$

Equation (D.19) satisfies all the conditions (initial, governing equation and zero boundary condition), but will fail to respect the wall Nuemann condition, $\partial u/\partial y(y=1)=0$. To satisfy this condition, it is necessary to invoke the method of images. Literally, it is necessary to place a family of image sources such that the new condition is respected. Equation (D.19) may be thought of as two sources of equal strength placed on either side of the y axis origin. It is possible to extend this idea (basically a symmetry operation, which uses linear superposition) to satisfy the entire finite condition. Following figure D.3:

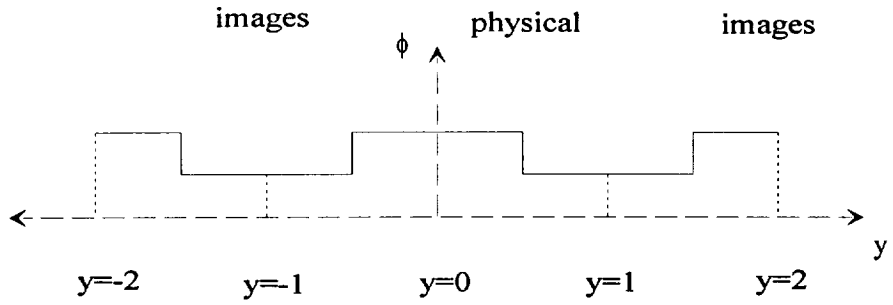

FIGURE D.3 Image "sources" used to satisfy the y=1, Nuemann condition.

and changing variables, $t=1/2x^2$, yields:

$$\phi_{an} = \frac{1}{2}(\phi_{10} - \phi_{20}) \sum_{-\infty}^{\infty} \left[erf\left(\frac{y + h_s - 2n}{(2a^*)^{\frac{1}{2}} x} \right) - erf\left(\frac{y - h_s - 2n}{(2a^*)^{\frac{1}{2}} x} \right) \right] + \phi_{20} \tag{D.20}$$

Which is the expected solution, equation (D.7).

Now, since the project uses this solution in a combined analytical/numerical solution scheme, it is useful to include the associated partial derivatives:

$$\frac{\partial \phi_{an}}{\partial y} = \frac{\frac{1}{2}(\phi_{10} - \phi_{20})}{(2a^*)^{\frac{1}{2}} x} \sum_{-\infty}^{\infty} \left[exp\left[-\left(\frac{y + h_s - 2n}{(2a^*)^{\frac{1}{2}} x} \right)^2 \right] - exp\left[-\left(\frac{y - h_s - 2n}{(2a^*)^{\frac{1}{2}} x} \right)^2 \right] \right] \tag{D.21}$$

and

$$\frac{\partial^2 \phi_{an}}{\partial y^2} = \frac{\frac{1}{2}(\phi_{10} - \phi_{20})}{a^* x^2} \sum_{-\infty}^{\infty} \left[\begin{array}{l} -\left(\frac{y + h_s - 2n}{(2a^*)^{\frac{1}{2}} x} \right) exp\left[-\left(\frac{y + h_s - 2n}{(2a^*)^{\frac{1}{2}} x} \right)^2 \right] + \\ \\ +\left(\frac{y - h_s - 2n}{(2a^*)^{\frac{1}{2}} x} \right) exp\left[-\left(\frac{y - h_s - 2n}{(2a^*)^{\frac{1}{2}} x} \right)^2 \right] \end{array} \right] \tag{D.22}$$

Either by direct computation or referring to the governing equation, equation (D.6) it is clear that:

$$\frac{\partial \phi_{an}}{\partial x} = \frac{\frac{1}{2}(\phi_{10} - \phi_{20})}{x} \sum_{-\infty}^{\infty} \left[\begin{array}{l} -\left(\frac{y + h_s - 2n}{(2a^*)^{\frac{1}{2}} x} \right) exp\left[-\left(\frac{y + h_s - 2n}{(2a^*)^{\frac{1}{2}} x} \right)^2 \right] + \\ \\ +\left(\frac{y - h_s - 2n}{(2a^*)^{\frac{1}{2}} x} \right) exp\left[-\left(\frac{y - h_s - 2n}{(2a^*)^{\frac{1}{2}} x} \right)^2 \right] \end{array} \right] \tag{D.23}$$

Which verifies that this solution does indeed satisfy the governing equation. This concludes the discussion of the method used to compute the analytical portion of our equation system.

APPENDIX E

AN APPROXIMATE DERIVATION OF THE "VIGNERON" PARAMETER, ω

In this appendix a value for the Vigneron parameter, ω, (Vigneron et al. (1978)) is derived by analyzing an approximate family of equations. Though approximate, this development provides a direct connection to the governing equations used in this project. More compete derivations are possible (see Anderson et al. (1984)), but the formulation described in this appendix, exploits the basic form of our parabolic equations. Consider the streamwise momentum equation:

$$\frac{\partial}{\partial x}(\rho u^2 + \omega p) = \frac{\partial}{\partial y}\left(\frac{\nu_{eff}}{U}\frac{\partial(\rho u^2)}{\partial y}\right) \tag{E.1}$$

Now, further assuming that the mass and energy fluxes are both constant: ρu=constant and ρuH=constant (this assumption could be relaxed in favor of the full transport equations for energy and mass, but the eigenvalue problem that would be need to be resolved is much more complex) and rewriting state:

$$p = \rho RT \tag{E.2}$$

in terms of energy yields:

$$p = \frac{\gamma - 1}{\gamma}\left(\rho H - \frac{1}{2}\rho u^2\right) \tag{E.3}$$

At this point, it is desirable to introduce the ω parameter as a "marker" on the static pressure, since it is the static pressure modeling which will control the eigenvalue consistency. Additionally, it is possible to factor the constant mass flux to yield:

$$\frac{\partial}{\partial x}\left((1 - \frac{\omega(\gamma - 1)}{\gamma})u + \frac{\omega(\gamma - 1)}{\gamma}\frac{H}{u}\right) = \frac{\partial}{\partial y}\left(\frac{\nu_{eff}}{U}\frac{\partial(u)}{\partial y}\right) \tag{E.4}$$

Re-writing, equation (E.4) in terms of u only, one obtains:

$$\left((1 - \frac{\omega(\gamma - 1)}{\gamma})u - \frac{\omega(\gamma - 1)}{\gamma}\frac{H}{u^2}\right)\frac{\partial u}{\partial x} = \frac{\partial}{\partial y}\left(\frac{\nu_{eff}}{U}\frac{\partial(u)}{\partial y}\right) \tag{E.5}$$

For a well posed diffusion problem (i.e. one with a positive eigenvalues or alternatively a positive "viscosity") the term in the brackets of equation (E.5) must be greater than zero:

$$\left((1 - \frac{\omega(\gamma - 1)}{\gamma})u - \frac{\omega(\gamma - 1)}{\gamma}\frac{H}{u^2}\right) \geq 0 \tag{E.6}$$

The similarity of this analysis with the model equation discussed in Section 2.4.3.3 is, of course, not coincidence. Inequality (E.6) may be simplified by recognizing that:

$$\frac{H}{u^2} = \frac{1}{(\gamma - 1)M^2} - \frac{1}{2} \tag{E.7}$$

Combining equations (E.6) and (E.7) and solving the inequality for the threshold value of ω that provides a physical eigenvalue, yields:

$$\omega = \frac{\gamma M^2}{1 + (\gamma - 1)M^2} \tag{E.8}$$

Which is, of course, the expected value for the Vigneron parameter.

REPORT DOCUMENTATION PAGE

Form Approved
OMB No. 0704-0188

1. AGENCY USE ONLY (*Leave blank*)	2. REPORT DATE	3. REPORT TYPE AND DATES COVERED
	April 1998	Final Contractor Report

4. TITLE AND SUBTITLE

Combined Numerical/Analytical Perturbation Solutions of the Navier-Stokes Equations for Aerodynamic Ejector/Mixer Nozzle Flows

5. FUNDING NUMBERS

WU–537–09–20–00
NGT–51244

6. AUTHOR(S)

Lawrence Justin De Chant

7. PERFORMING ORGANIZATION NAME(S) AND ADDRESS(ES)

Texas A&M University
College Station, Texas 77843

8. PERFORMING ORGANIZATION REPORT NUMBER

E–11166

9. SPONSORING/MONITORING AGENCY NAME(S) AND ADDRESS(ES)

National Aeronautics and Space Administration
Lewis Research Center
Cleveland, Ohio 44135–3191

10. SPONSORING/MONITORING AGENCY REPORT NUMBER

NASA CR—1998-207406

11. SUPPLEMENTARY NOTES

Project Manager, Shari Nadell, Propulsion Systems Analysis Office, NASA Lewis Research Center, organization code 2400, (216) 977–7035.

12a. DISTRIBUTION/AVAILABILITY STATEMENT

Unclassified - Unlimited
Subject Categories: 07 and 64 Distribution: Nonstandard

This publication is available from the NASA Center for AeroSpace Information, (301) 621–0390.

12b. DISTRIBUTION CODE

13. ABSTRACT ***(Maximum 200 words)***

In spite of rapid advances in both scalar and parallel computational tools, the large number of variables involved in both design and inverse problems make the use of sophisticated fluid flow models impractical. With this restriction, it is concluded that an important family of methods for mathematical/computational development are reduced or approximate fluid flow models. In this study a combined perturbation/numerical modeling methodology is developed which provides a rigorously derived family of solutions. The mathematical model is computationally more efficient than classical boundary layer but provides important two-dimensional information not available using quasi-1-d approaches. An additional strength of the current methodology is its ability to locally predict static pressure fields in a manner analogous to more sophisticated parabolized Navier Stokes (PNS) formulations. To resolve singular behavior, the model utilizes classical analytical solution techniques. Hence, analytical methods have been combined with efficient numerical methods to yield an efficient hybrid fluid flow model. In particular, the main objective of this research has been to develop a system of analytical and numerical ejector/mixer nozzle models, which require minimal empirical input. A computer code, DREA Differential Reduced Ejector/mixer Analysis has been developed with the ability to run sufficiently fast so that it may be used either as a subroutine or called by an design optimization routine. Models are of direct use to the High Speed Civil Transport Program (a joint government/industry project seeking to develop an economically viable U.S. commercial supersonic transport vehicle) and are currently being adopted by both NASA and industry. Experimental validation of these models is provided by comparison to results obtained from open literature and Limited Exclusive Right Distribution (LERD) sources, as well as dedicated experiments performed at Texas A&M. These experiments have been performed using a hydraulic/gas flow analog. Results of comparisons of DREA computations with experimental data, which include entrainment, thrust, and local profile information, are overall good. Computational time studies indicate that DREA provides considerably more information at a lower computational cost than contemporary ejector nozzle design models. Finally, physical limitations of the method, deviations from experimental data, potential improvements and alternative formulations are described. This report represents closure to the NASA Graduate Researchers Program and Grant NGT–51244. Versions of the DREA code and a user's guide may be obtained from the NASA Lewis Research Center grant monitor, Shari Nadell.

14. SUBJECT TERMS	15. NUMBER OF PAGES
Nozzle design; Mixers; Mixing layers; Jet propulsion; Aeronautical engineering; Fluid mechanics; Ejectors; System analysis	225
	16. PRICE CODE A10

17. SECURITY CLASSIFICATION OF REPORT	18. SECURITY CLASSIFICATION OF THIS PAGE	19. SECURITY CLASSIFICATION OF ABSTRACT	20. LIMITATION OF ABSTRACT
Unclassified	Unclassified	Unclassified	